

**DEVELOPMENT OF HOLLOW FIBER-BASED BIOREACTOR SYSTEMS FOR 3D
DYNAMIC NEURONAL CELL CULTURES**

by

Candace A. Brayfield

Bachelor of Science, University of Rochester, 2003

Submitted to the Graduate Faculty of
Swanson School of Engineering in partial fulfillment
of the requirements for the degree of
Doctor of Philosophy

University of Pittsburgh

2008

UNIVERSITY OF PITTSBURGH
SWANSON SCHOOL OF ENGINEERING

This dissertation was presented

by

Candace A. Brayfield

It was defended on

November 24, 2008

and approved by

Kacey G. Marra, Assistant Professor, Departments of Surgery and Bioengineering

X. Tracy Cui, Assistant Professor, Department of Bioengineering

John P. Leonard, Assistant Professor, Department of Mechanical Engineering and Materials
Science

Dissertation Director: Jorg C. Gerlach, Assistant Professor, Departments of Surgery and
Bioengineering

Copyright © by Candace A. Brayfield

2008

DEVELOPMENT OF HOLLOW FIBER-BASED BIOREACTOR SYSTEMS FOR 3D DYNAMIC NEURONAL CELL CULTURES

Candace A. Brayfield, PhD

University of Pittsburgh, 2008

Adult central nervous system tissue does not retain the ability to regenerate and restore functional tissue lost to disease or trauma. The peripheral nervous system only has the capacity to regenerate when tissue damage is minor. Most *in vitro* research investigating the neurobiological mechanisms relevant for enhancing nerve regeneration has focused on culture of neuronal cells on a 2D surface under static conditions. We have performed studies enabling development of an advanced *in vitro* culture model based on hollow fiber-based bioreactors to allow high density neuronal cell networking with directed axonal outgrowth.

The model neuronal-like PC12 cell line was initially used to compare neurite outgrowth after nerve growth factor stimulation between cultures under either static or dynamic conditions with 2D or 3D configurations. High density PC12 cell cultures with extensive neurite outgrowth in three dimensional collagen gels were only possible under the dynamically perfused conditions of a hollow fiber-based bioreactor. Analysis of neurite networking within cultures demonstrated enhanced active synapsin I⁺ synaptic vesicle clustering among PC12 cells cultured within the 3D dynamic bioreactor compared to cells cultured statically on a 2D surface. We further used two different hollow fiber-based bioreactor designs to investigate primary mouse neural stem cell differentiation within different injectable extracellular matrix hydrogel scaffolds cultured under dynamic conditions. HyStem, a cross-linked hyaluronan hydrogel, allowed structure formation with improved neuronal differentiation compared to collagen and Matrigel hydrogels.

We have made further developments in order to create a new hollow fiber-based bioreactor device for controlling directed axonal growth. Excimer laser modification was utilized to fabricate hollow fiber scaffolds allowing control over axonal outgrowth from neurons within a 3D space. Incorporation of these scaffolds into a novel hollow fiber-based bioreactor design will produce a device for high density neuronal tissue formation with axonal outgrowth in a 3D configuration. Such a device will provide an advanced research tool for more accurate evaluation of neurobiological events and development of therapeutic strategies useful for enhancing nerve regeneration.

TABLE OF CONTENTS

NOMENCLATURE

PREFACE.....	XVI
1.0 INTRODUCTION.....	1
1.1 DISEASES/DISORDERS OF THE NERVOUS SYSTEM.....	2
1.1.1 Diseases of the brain	3
1.1.2 Spinal cord injuries.....	5
1.1.3 Peripheral nerve injuries.....	7
1.2 NEURAL ENGINEERING.....	9
1.2.1 Cell therapies for enhancing nerve regeneration.....	9
1.2.2 Chemotropic factors	14
1.2.3 Substrates for directing axonal outgrowth.....	15
1.2.4 Nerve guide conduits.....	16
1.3 PREVIOUS NOVEL NEURONAL CULTURE SYSTEMS	18
1.3.1 3D dynamic bioreactors.....	18
1.3.2 Directed neurite/axonal outgrowth models	24
2.0 HIGH DENSITY NEURONAL CELL GROWTH AND NEURITE NETWORK FORMATION IN A 3D DYNAMIC HOLLOW FIBER-BASED BIOREACTOR COMPARED TO 2D AND 3D STATIC CULTURES	27
2.1 INTRODUCTION	27
2.1.1 Non-neuronal tissue formation within 3D dynamic cultures.....	27

2.1.2	Potential limitations of traditional 2D cell culture.....	29
2.1.3	Model neuronal PC12 cell line with NGF stimulation.....	30
2.1.4	Hollow fiber-based bioreactor for PC12 cultures	31
2.1.5	Synapsin I as a marker for synaptogenesis in neurons	32
2.2	METHODS	34
2.2.1	PC12 cell cultures with NGF stimulation	34
2.2.1.1	2D static cultures.....	34
2.2.1.2	3D static collagen gel cultures.....	35
2.2.1.3	3D dynamic hollow fiber-based bioreactor cultures.....	36
2.2.2	Metabolic measurements.....	42
2.2.3	Fluorescent immunohistochemistry visualized with confocal microscopy	43
2.2.4	Quantitative RT-PCR gene expression analysis.....	45
2.2.5	Western Blot protein analysis.....	46
2.3	RESULTS	49
2.3.1	Metabolic activity of 3D cultures.....	49
2.3.1.1	3D static gel cultures.....	49
2.3.1.2	3D dynamic bioreactor cultures	51
2.3.2	Comparison of cell morphology and neurite outgrowth	56
2.3.3	Comparison of neuronal network formation	65
2.3.3.1	Synapsin I protein localization	65
2.3.3.2	Synapsin I quantitative gene expression.....	72
2.3.3.3	Synapsin I protein quantification.....	74
2.3.3.4	Phosphorylated Synapsin I localization.....	77
2.3.3.5	Phosphorylated Synapsin I protein quantification.....	81
2.4	DISCUSSION	85

2.5	CONCLUSIONS.....	96
3.0	TESTING ECM SCAFFOLDS FOR ENHANCING NEURAL STEM CELL SURVIVAL AND DIFFERENTIATION WITHIN HOLLOW FIBER-BASED BIOREACTORS	98
3.1	INTRODUCTION	98
3.1.1	Neural stem cells (NSCs)	98
3.1.2	Obstacles using neural stem cells <i>in vivo</i> for potential therapy development.....	106
3.1.3	Biomaterials for enhancing neural stem cell survival and differentiation	109
3.2	METHODS.....	114
3.2.1	Mouse neural stem cells and culture conditions	114
3.2.2	Preparation of mNSC-ECM 3D hydrogel constructs.....	116
3.2.3	Hollow fiber-based bioreactor cultures	119
3.2.3.1	8 mL laboratory scale bioreactors.....	119
3.2.3.2	Four chamber analytical scale bioreactors.....	121
3.2.4	Bioreactor metabolic measurements.....	126
3.2.5	Fluorescent immunohistochemistry visualized with fluorescent microscopy	127
3.2.6	Quantitative RT-PCR gene expression analysis.....	129
3.3	RESULTS	130
3.3.1	Properties of mouse neural stem cells	130
3.3.2	Light microscopic analysis of mNSC differentiation on 2D and 3D ECM hydrogel cultures.....	137
3.3.3	mNSC neuronal and astrocytic differentiation on 2D ECM coated plate cultures.....	140
3.3.4	mNSC neuronal and astrocytic differentiation within 3D ECM hydrogel cultures.....	144
3.3.5	Metabolic activity of bioreactor cultures.....	149

3.3.6	Live cell imaging during four chamber bioreactor culture	151
3.3.7	mNSC neuronal and astrocytic differentiation within bioreactor cultures	158
3.3.8	Quantification of neuronal and astrocytic differentiation within ECM hydrogels.....	162
3.4	DISCUSSION.....	166
3.5	CONCLUSION	175
4.0	LASER MODIFIED HOLLOW FIBER SCAFFOLDS TO COMPARTMENTALIZE <i>IN VITRO</i> NEURONAL CELL CULTURE SYSTEMS FOR 3D DIRECTED AXONAL OUTGROWTH.....	177
4.1	INTRODUCTION	177
4.1.1	Significance of compartmentalization of axons from cell bodies <i>in vitro</i>	177
4.1.2	Excimer laser ablation in tissue engineering.....	178
4.2	METHODS.....	181
4.2.1	Laser modification of PES flat sheet membranes and hollow fibers....	181
4.2.2	Surface characterization of laser modified PES flat sheet membranes	183
4.2.2.1	Contact angle measurements	183
4.2.2.2	Quantification of laminin adsorption on PES flat sheet membranes.	184
4.2.2.3	PC12 cell adhesion assay on PES flat sheet membranes	185
4.2.3	Primary rat neural progenitor cell differentiation on modified hollow fibers.....	185
4.2.4	Scanning electron microscopy	187
4.2.5	Statistical analysis	187
4.3	RESULTS	188
4.3.1	Peak fluence of KrF excimer laser pulse at PES surface	188
4.3.2	Optimization of laser created channels in PES hollow fibers	188

4.3.3	PES flat sheet membrane surface wettability varying laser fluence	192
4.3.4	Laminin adsorption on laser modified PES flat sheet membrane surfaces	193
4.3.5	PC12 cell adhesion to PES flat sheet membrane surfaces varying laser fluence	194
4.3.6	Primary rat NPC differentiation on laser modified PES hollow fibers	196
4.4	DISCUSSION.....	198
4.4.1	Channel creation in PES hollow fibers via excimer laser ablation	198
4.4.2	Significance of laser modification to PES hollow fiber/membrane surface	201
4.5	CONCLUSIONS.....	203
5.0	FUTURE EXPERIMENTS.....	204
5.1	MOUSE NEURAL STEM CELL 4 CHAMBER BIOREACTORS	204
5.2	PRIMARY RAT CORTICAL NEURON BIOREACTORS	207
5.3	DESIGN AND DEVELOPMENT OF NEURONAL CELL SPECIFIC BIOREACTOR INCLUDING FIBER SCAFFOLDS FOR DIRECTED AXONAL OUTGROWTH	209
APPENDIX A		212
APPENDIX B		214
APPENDIX C		217
BIBLIOGRAPHY.....		222

LIST OF TABLES

Table 1. Example bioreactor designs used for in vitro cell cultures with dynamic conditions	23
Table 2. List of hollow fiber-based kidney and liver bioreactor systems entering clinical trials.	24
Table 3. Cell inoculation information for PC12 bioreactor experiments.....	42
Table 4. Contact angle measurements on laser modified PES flat sheet membranes.....	193

LIST OF FIGURES

Figure 1. 8 mL hollow fiber-based bioreactor: a) diagram; b) photograph	37
Figure 2. Photograph of perfusion system used for 8 mL bioreactor experiments.....	38
Figure 3. Diagram of tubing circuit for medium and gas perfusion through 8 mL bioreactor	39
Figure 4. Equation for bioreactor daily glucose consumption or lactate production values.....	43
Figure 5. 3D static gel culture metabolic data plotting daily glucose and lactate concentration..	51
Figure 6. Photograph of 8 mL bioreactor housing opened to obtain tissue samples	52
Figure 7. Metabolic data for all six PC12 bioreactor experiments	53
Figure 8. Bioreactor metabolism plots of actual daily measurements of PC12 bioreactors.....	56
Figure 9. Cell morphology of 2D control PC12 cells	57
Figure 10. Cell morphology of 3D static controls of PC12 cells.....	60
Figure 11. Confocal images of immunostained PC12 cells from bioreactor samples	63
Figure 12. Cell morphology of 3D dynamic bioreactor cultures of PC12 cells	64
Figure 13. Synapsin I immunostaining in a rat cortical brain section with DAPI.....	66
Figure 14. Synapsin I immunostaining of 2D positive control PC12 cell cultures.....	67
Figure 15. Synapsin I immunostaining of RNS-1 and RNS-2 bioreactor cultures.....	70
Figure 16. Synapsin I immunostaining of RNS-5 and RNS-6 bioreactor cultures.....	71
Figure 17. Synapsin I immunostaining of RNS-5 bioreactor culture (magnification 1000X).....	72
Figure 18. Quantitative RT-PCR results for synapsin I among different PC12 cell cultures.....	73

Figure 19. Western blot for synapsin I among different PC12 cell cultures.....	76
Figure 20. Western blot for synaptophysin among different PC12 cell cultures.....	77
Figure 21. Immunostaining for phospho-synapsin I (site Ser553) of 2D static PC12.....	79
Figure 22. Immunostaining of phospho-synapsin I (site Ser553) of bioreactor cultured PC12 ...	80
Figure 23. Western blot for phospho-synapsin I (site Ser553) among PC12 cultures.....	83
Figure 24. Quantification of Western blot for phospho-synapsin I (site Ser553).....	84
Figure 25. Western blot for phospho-synapsin I (Ser 9 site) among PC12 cultures.....	84
Figure 26. Diagram describing differences between 3D static and 3D dynamic cultures.....	86
Figure 27. Immunostaining for synapsin I for bioreactor cultured PC12 cells.....	93
Figure 28. Bloom et al. a 3D reconstructed diagram of a synaptic vesicle cluster.....	94
Figure 29. Diagram describing neural progenitor cell populations	101
Figure 30. Photograph of four chamber analytical-scale hollow fiber-based bioreactor.....	122
Figure 31. Diagram describing design of four chamber hollow fiber-based bioreactor.....	122
Figure 32. Diagram of tubing circuit used for four chamber bioreactor.....	123
Figure 33. Diagram of MNS-3 and MNS-5 bioreactor experiment chambers.	124
Figure 34. Photograph of perfusion system used for four chamber bioreactor experiments.....	126
Figure 35. Equation for bioreactor daily glucose consumption or lactate production values.....	127
Figure 36. Immunostaining for nestin of p9 mouse neurospheres.....	131
Figure 37. Differentiation of mNSCs on 2D laminin coated plates.....	135
Figure 38. Immunostaining of differentiated mNSCs for O4.....	136
Figure 39. Differentiation of mNSCs varying seeding density and dissociation methods.....	136
Figure 40. Culture day 8 mNSCs on 2D collagen coated cultures.	137
Figure 41. Mouse neurospheres differentiating on 2D Matrigel coated dishes.	138

Figure 42. Light microscopic images of mNSCs in 3D static ECM hydrogels	139
Figure 43. Differentiation of mNSCs on 2D collagen coated plates.	141
Figure 44. Differentiation of mNSCs with the addition of bFGF.....	143
Figure 45. Differentiation of mNSCs on 2D Matrigel coated plates.	144
Figure 46. Differentiation of mNSCs within 3D collagen hydrogels cultured statically.....	145
Figure 47. Differentiation of mNSCs within 3D collagen hydrogels with laminin of bFGF	146
Figure 48. Differentiation of mNSCs within 3D Matrigel hydrogels cultured statically.	147
Figure 49. Nestin immunotaining of mNSCs within 3D Matrigel hydrogels.....	148
Figure 50. Differentiation of mNSCs within 3D HyStem hydrogels cultured statically.....	149
Figure 51. Plots of glucose and lactate metabolism of mNSC bioreactor cultures.....	150
Figure 52. Live cell light microscopic imaging of mNSC bioreactor experiment MNS-3.....	153
Figure 53. Live cell light microscopic imaging of mNSCs in HyStem of MNS-3.....	154
Figure 54. Live cell light microscopic imaging of mNSC bioreactor experiment MNS-5.....	155
Figure 55. Light microscope images of mNSC testing PVC vs. Tygon tubing circuits.....	158
Figure 56. Differentiation of mNSCs within 8 mL bioreactors with ECM hydrogels.	159
Figure 57. Differentiation of mNSCs in four chamber bioreactor experiment MNS-3.....	161
Figure 58. Differentiation of mNSCs in HyStem of four chamber bioreactor MNS-3.	162
Figure 59. Quantitative RT-PCR results for β -III-tubulin and GFAP of mNSC cultures	165
Figure 60. Quantitative RT-PCR results for MBP of mNSC cultures.....	166
Figure 61. Diagram describing design concept neuronal cell bioreactor.....	180
Figure 62. Diagram of design for simplified neuronal cell bioreactor	181
Figure 63. Schematic view of excimer projection irradiation system.	182
Figure 64. SEM images of channel creation in PES fibers with excimer laser ablation	190

Figure 65. SEM images of channels in PES fibers used in cell culture experiments	191
Figure 66. Quantification of laminin adsorption on laser modified PES.....	194
Figure 67. PC12 cell adhesion on laser modified PES flat sheet membrane	196
Figure 68. Differentiation of adult rat neural stem cells on laser modified PES fibers	197
Figure 69. Photograph of prototype for novel 2 chamber neuronal cell bioreactor.....	210
Figure 70. Histology for original PC12 cell line bioreactor experiments.....	213
Figure 71. Bioreactor test chamber used for testing collagen gel compatibility	215
Figure 72. Photographs of perfusion fibers with aniline blue collagen staining after gel testing	216
Figure 73. Two compartment static single fiber culture model	220
Figure 74. Bioactivity of NGF diffusion through single fiber culture models	221

PREFACE

I would like to especially thank both of my advisors Dr. Jörg C. Gerlach and Dr. Kacey G. Marra. This project first began because of their desire to collaborate together and I was fortunate enough to be chosen as the student to conduct the work. I am so grateful to them to have been able to perform this research with them in their laboratories. They have also been truly great people to work for. I would like to thank Dr. Marra for the knowledge I have learned from her and her laboratory in the field of biomaterials. I will always continue to have a special interest in the field because of it. Equally, I would like to thank Dr. Gerlach for the opportunity to work with bioreactors that I have admired since college. I am so fortunate to have had that experience and hope to be able to continue within the field of 3D dynamic cell culture due to its significance.

I also would not have been able to conduct this research without the other members of my committee, Dr. Tracy X. Cui and Dr. John P. Leonard. The work within Chapter 4 was only possible with a significant collaboration working in Dr. Leonard's laboratory. I have greatly appreciated the skills and experience from performing the work within his lab. As well, the work within Chapter 3 would not have been possible without Dr. Cui. She was very generous to let me work within her laboratory to train me to perform neural stem cell cultures. Without this training I could have never continued with all the work that I have performed with the neural stem cells and am so fortunate to have been able to challenge into this field. I am so grateful to

have had an exceptional committee that has cared so much to be a part of the research within this dissertation. I have greatly benefitted from having the opportunities of learning from all of their different expertise.

I would particularly like to thank the Department of Bioengineering and the University of Pittsburgh for allowing me to have any of these opportunities. The McGowan Institute for Regenerative Medicine and the Bioengineering Department made me believe Pitt would be the best place for me for graduate school and I have never thought differently throughout my time there.

I would also like to thank all of the students and fellows I have been fortunate to work with within the Plastic Surgery Research Lab and the Bioreactor Group. Everyone has been so helpful and thoughtful and made working within these labs a wonderful experience. I would especially like to thank Alicia DeFail PhD, Lauren E. Kokai, Christina Lee, and Alexander Ring. They all have helped make my research possible as well as supported me tremendously throughout the years. Lauren has become one of the best friends I can imagine and have loved being able to also work with her. I would also like to acknowledge and thank all of my other friends who have been able to support me. I would especially like to thank Michael Jones for being my best friend and always being there for me.

I have to ultimately thank my parents whom always raised me to have the confidence in myself that I could achieve anything I desired. Their continuous belief in me has allowed me to believe in myself in order to accomplish what I have. My mother has showed me how strong and caring a woman can be together, and I continue to aspire to that because of her. I have achieved so much in my life only because of the drive and determination my father has instilled

in me. He has always been my biggest fan and I will always challenge myself knowing how proud he is of me.

I would also like to acknowledge and thank the following at the University of Pittsburgh, Pittsburgh, PA for their support, training, and use of equipment: J. Eric Kline M.S. for help with excimer laser system setup, Glenn T. Gobbel Ph.D. for supplying neural progenitor cells and training, William Stauffer B.S. for neural progenitor cell training, Dan McKeel for tremendous help with bioreactor fabrication and knowledge designing novel systems, and Univ. of Pittsburgh Center for Biologic Imaging who provided the microscope facility and training for me to be able to take amazing images within my work and am so grateful to Dr. Simon Watkins for allowing this facility to be open to other researchers, the Materials Science Dept. for use of SEM equipment, Dr. Toshio Miki for support and training for qRT-PCR work, and Dr. Han Li for support and training for Western Blot.

I would like to acknowledge both the National Institutes of Health (NIH) CATER University of Pittsburgh Pre-Doctoral Fellowship (NIH 5 T32 EB001026-03) and the University of Pittsburgh Provost Development Fund for providing me funding to be able to conduct this research. I would also like to acknowledge the Wymard Foundation, Pittsburgh, PA for their tremendous generosity for funding supporting this work.

1.0 INTRODUCTION

Recent trends for studying neurobiological mechanisms *in vitro* have been to develop substrates that can control specific arrangements of neuronal axon growth and synaptic connectivity in neuronal networks. Advantages of these neuronal cell cultures lie in the ability to separate multiple interactions in order to study single events. Information gathered from studying these cultures could permit synthetic manipulation of events such as directed axonal regeneration. For example, Aguayo et al. demonstrated that central nervous system neurons retain the ability to regenerate after damage given the proper environment [1, 2]. An *in vitro* system for neuronal cell cultures allowing controlled growth and signaling in a three-dimensional space could be used as a diagnostic tool for unveiling the permissive environments for nerve regeneration. The system could specifically be used to test diffusible molecules such as drugs and therapeutic proteins on their effects on directed neurite outgrowth for nerve regeneration. The responses of these 3D neuronal cell cultures could translate better from the *in vitro* models to animal models and clinical applications for deriving therapeutic strategies enhancing nerve regeneration.

Much research has been performed to investigate the mechanisms involved in nerve regeneration in order to derive clinical solutions to these problems. However, most of this research has focused on culturing neuronal cells on 2D surfaces without any compartmentalizing features specifically directing axonal growth. It is likely that primary neuronal cell types cultured on conventional 2D plates will not maintain growth, differentiation, and synaptic

formation characteristics similar to that *in vivo*. These unnatural culture environments might generate neuronal cell cultures that give atypical responses to therapeutic drugs or proteins and could increase the chance of failure with these therapies in patients. The same problems apply to tests of these reagents in animal models where different species might respond entirely different than humans. An optimal system for accurately testing therapies consisting of therapeutic drugs or proteins on the enhancement of nerve axonal regeneration would be one permitting use of human neuronal cell cultures in an environment mimicking the *in vivo* one.

1.1 DISEASES/DISORDERS OF THE NERVOUS SYSTEM

There are many diseases, disorders, and injuries affecting the nervous system that could benefit from a culture system allowing more accurate investigations of neurobiological mechanisms of these events and testing of potential novel treatments. The nervous system provides control over vital functions of the body and damage to this system can result in a large range of devastating effects. The potential diseases and injuries experienced within the nervous system with less than optimal current treatment strategies are discussed below. These clinical problems could benefit from advanced research methods such as using 3D dynamic *in vitro* neuronal culture systems. The advanced models could allow neuronal cell cultures that mimic brain or nerve tissue in order to further manipulate the cultures to study natural neurobiological events or induction of disease pathologies allowing testing of new therapies on their resolution of these states.

1.1.1 Diseases of the brain

Many disorders within the brain could be reversed if regeneration of the brain tissue could be enhanced to correct the affected regions. Many disorders do not have a cure and have only few treatment options available for relieving symptoms. Traumatic brain injuries (TBI) result in destruction of the brain tissue leaving loss of function according to the location of the injury within the brain [3]. Many diseases such as Parkinson's and Alzheimer's diseases cause neurodegeneration within the adult brain and also require regeneration of neurons to restore function. There are more than one million people in North America diagnosed with Parkinson's disease and two to four million people with Alzheimer's disease [3-5]. There are also diseases of the brain caused by disruption beginning within the vascular supply to the brain such as stroke, where thromboembolism or hemorrhage causes ischemic conditions leading to death of neuronal cells [3]. Strokes are the third most common cause of death in the United States and the most common cause of disability [6, 7]. Some diseases are genetically inherited, such as Batten's disease or neuronal ceroid lipofuscinosis (NCL), a rare and fatal lysosomal storage disease due to mutations in genes encoding necessary enzymes produced by neurons [3]. Multiple sclerosis (MS) is an autoimmune disease caused by demyelination and degeneration of neurons within the brain caused by cells of the immune system attacking oligodendrocytes, the cells within the brain that myelinate and insulate neurons [3]. Brain tumors are relatively rare in occurrence (1.4% of all cancers), but can be extremely invasive with poor prognoses. The American Cancer Society estimates 20,000 people within the United States will be diagnosed with a brain tumor each year [8].

All of these disorders of the brain could benefit from advanced research methods able to investigate new therapies for either enhancing endogenous brain tissue regeneration or therapies

able to replace dysfunctional cell products or lost tissue. Current treatments for Parkinson's disease (PD) include a drug called Levodopa which allows neurons to make and replenish the decreased dopamine neurotransmitter lost in this disease [3]. However, late stage PD continues to have a poor outcome in patients and newer treatment strategies should not focus only on dopamine deficiency [9]. There are currently no treatments to slow the progression of Alzheimer's disease (AD), but there are four FDA-approved medications able to treat symptoms [3]. Many novel therapies in clinical trials have moved forward due to their positive outcomes treating transgenic mouse models of AD [10]. Strokes occur with relation to poor cardiovascular conditions in which there are many preventative measures possible to prevent strokes and therapies after strokes revolve around the prevention of further strokes. The most promising therapies for stroke aim to protect further damage to neurons from the ischemic conditions created by stroke or to replace the lost tissue due to these conditions. Currently, there are many clinical trials for neuroprotective reagents such as nitric oxide [11]. However, some of the most promising trials involve use of autologous adult stem cells, mostly bone marrow derived, in order for the transplanted cells to facilitate neuroprotection [7]. There are no effective therapies for Batten's disease and are fatal after a long period of disability [12]. Although in March 2006 the company Stem Cells Inc. initiated a clinical trial treating Batten's disease with human fetal brain-derived neural stem cells [13]. The most popular treatment currently for MS is doses of the immunomodulatory therapeutic protein interferon-beta, but the response to this therapy is only partial and dosing has not fully been optimized [14]. Newer treatments in clinical development include monoclonal antibodies that deplete or inhibit immune cells [15]. However, there are concerns that these long-term therapies will have serious complicating side-effects where protective and regenerative therapies are still desired [16].

1.1.2 Spinal cord injuries

According to the National Spinal Cord Injury Database, disabling spinal cord injuries occur in around 11,000 Americans yearly. Approximately 250,000 Americans are already living with spinal cord injuries (SCI) [17]. Contusions are the most common type of injury due to mechanical damage to nerve tissue with following cell necrosis [18]. Inflammation following the injury can further lead to secondary injuries such as oligodendrocyte apoptosis. The gap created within the spinal cord at the site of injury fills with a fluid-filled cyst associated with secondary complications. Eventually glial cells migrate through and contribute to scar formation within this gap creating a barrier preventing nerve regeneration [18]. These events contribute to a hostile environment created at the site of injury that inhibits regeneration of the spinal cord. The current theory holds that the central nervous system has the ability to regenerate with axonal outgrowth from the proximal spinal cord reconnecting with the distal ends, but is only inhibited by the glial scar, inflammatory conditions, and inhibitory molecules. Research has been focused on better understanding this environment and factors contributing to inhibition of spinal cord regeneration.

The only way for functional restoration to occur is for treatments to result in proximal cut nerve ends reconnecting with their distal targets between the gap created from the injury. Immune and glial cells secreting molecules inhibitory to axonal regeneration has led traditional research to investigate drugs or therapeutic proteins that block or overcome these molecules in order to treat SCI. Regenerative medicine with tissue engineering has taken the approach to research engineered biomaterial scaffolds for enhancing axonal growth, controlled local release of neurotrophic factors, or transplantation of cellular therapies within animal models of SCI. The environment created after the spinal cord injury *in vivo* most likely requires optimal therapies to

be a combination of strategies that neutralize the inflammatory environment and allow neurons to reconnect in order to restore function of the spinal cord.

Despite the overwhelming difficulties of a new therapy to achieve functional recovery in spinal cord injuries, it has been noted that injuries leaving only 10-15% of spinal cord white matter results in significant functional sparing [18]. This small amount of tissue preservation gives hope that even a small degree of nerve regeneration from a new therapy could be a valuable treatment. Over half of the SCI cases since 2000 have been reported as functionally incomplete due to some sparing of the spinal cord tissue after injury [17, 18]. The secondary injuries resulting from inflammation and cascading events following injury can damage the conserved functioning tissue. According to Becker et. al., these secondary injuries are the current primary goals of any SCI treatments including a cellular therapy [19]. There are many basic benefits to using a cell therapy to treat SCI than the more complicated goal of creating functional integrated neurons. These benefits could be the neuro-protection or facilitation of re-growth of existing neurons by trophic support from transplanted cells with the secretion of anti-apoptotic factors, growth factors, angiogenic factors, inflammatory inhibitors, or deficient neurotransmitters [18, 20, 21]. Some associated symptoms/complications with SCI are spasticity of muscles, post-traumatic syringomyelia (PTS), autonomic dysreflexia, chronic pain, loss of bowel and bladder control, and sexual dysfunction [18]. Since 2000 the leading cause of death of patients with SCI surviving the first 24 hours after injury are due to respiratory diseases, mainly pneumonia [17]. The cause being due to the functional loss of a simple cough reflex [18]. If any improvements with new treatments could prevent any of these secondary complications it would be a tremendous clinical gain. The current treatments for SCI are high

dose corticosteroids, spine stabilization, and rehabilitation which usually help prevent further problems [22].

1.1.3 Peripheral nerve injuries

Unlike the central nervous system (CNS), the peripheral nervous system (PNS) has the ability to regenerate and repair small segments of damaged nerve tissue. The mediators involved in nerve regeneration after an injury is very different within peripheral nerves. First, there are different cell types within the CNS and PNS. Astrocytes are the reactive cells within the CNS that contribute to the inhibitory glial scar formation within the CNS. Also, oligodendrocytes are the myelinating cells of the CNS, but have been shown to deposit myelin-associated glycoproteins that are some of the inhibitory molecules deposited after CNS injuries. Within the PNS, there are no astrocytes because the normal immune system cells are able to assume the role of scavengers aiding in repair. Furthermore, Schwann cells are the myelinating cell types of the PNS instead of the CNS, which significantly contribute to the ability of the PNS to regenerate [23]. Peripheral nerves have the ability to regenerate at a rate of 1-5 mm per day. However, damage of peripheral nerves leaving gaps greater than 4 mm long surgical intervention is required for repair. Approximately 100,000 patients undergo surgical procedures for correction of the peripheral nervous system each year [24]. The standard technique in plastic surgery for reconstruction of very short nerve gaps is to surgically reconnect the severed nerve ends together, but if the gap is too long this will create tension and instead an autologous nerve graft is used to bridge the gap [25]. The autologous nerves used for these grafts are typically sensory nerves that leave donor site sensory loss and morbidity. Therefore, engineered strategies have been developed to create implantable nerve guidance channels made from either natural matrices

or biodegradable synthetic polymers. There are currently four different FDA approved nerve guidance channels available for use in reconstruction of peripheral nerve gaps up to 4 cm in length [25].

Initial studies of peripheral nerve regeneration events have been performed with transection of rat sciatic nerves with following connection to synthetic nerve guidance channels in order to observe the regenerating tissue within the channels at different time points. The sciatic nerve within the rat is the largest peripheral motor neuron and has been utilized by many researchers to study events related to peripheral nerve regeneration. In the first few days after injury the process of Wallerian degeneration occurs where distal axons degenerate, Schwann cells break down their myelin sheath, and macrophages remove debris [26]. Studies using impermeable channels (mostly made from silicone), preventing external factors from affecting the sciatic nerve regeneration, have observed no nerve regeneration if the distal nerve stump is placed at a distance greater than 10 mm from the proximal nerve ending or if the distal end of the channel is capped demonstrating the importance of the distal nerve ending in enhancing regeneration [27, 28]. However, Aebischer et al. discovered some tissue regeneration in semi-permeable channels in blind-ended tubes [29]. Also, the molecular weight cutoff of the channel significantly affected the ability of the regenerated tissue to have healthy myelinated axons where this was inhibited using channels with a higher molecular weight cutoff. Some have demonstrated that contribution of factors and cells influencing the axonal regeneration from the proximal nerve stump is equal from both nerve ends [30]. Many groups have observed the sequence of events that occur within impermeable silicone tubes forming a connection between the proximal and distal nerve stumps. Temporal changes of the events differ according to the length of gap created between the two nerve stumps, but the following describes events in a

shorter <6 mm gap. Within the first few days after transection and tube connection, a fibrin matrix is secreted within the tube to be used as a scaffold for infiltrating cells [31]. After one week perineurial cells migrate along the fibrin matrix through the tube and form a perineurial tube. Next, multiple cell types infiltrate the tube such as endothelial cells, pericytes, fibroblasts, and most importantly Schwann cells [31, 32]. Schwann cells and fibroblasts can secrete multiple factors of neurotrophins, neurokines, and growth factors to enhance the axonal growth through the tube [33-35]. After a few weeks within short gap distances, regenerated nerve fascicles can be seen with blood vessels and myelinated axons.

1.2 NEURAL ENGINEERING

Section 1.1 described major disorders and injuries experienced within the central and peripheral nervous system. Also included were the current treatments available for these disorders where almost none of the diseases mentioned have therapies providing complete long-term cures or allowing restoration of complete functional recovery of the brain or nerve tissue. This section further discusses current research areas focusing on development of novel therapies for nerve regeneration.

1.2.1 Cell therapies for enhancing nerve regeneration

Many of the neurological disorders result in functional impairments of either sensory or motor nerve tissue. One possible strategy for restoring nerve tissue function is to completely replace the lost tissue with transplantation of exogenous cells or tissue. Stem cell research has allowed

development of many potential therapeutic sources for cell therapies for nerve regeneration and tissue restoration.

In 1997 clinical trials began testing the the safety and feasibility of intraspinal transplantation of human fetal spinal cord (huFSC) tissue in a small number of patients in Gainesville, FL, Sweden, Denver, CO, and Russia [18]. Animal experiments leading to these trials showed extensive filling of cavitation in contusion injuries with injections of dissociated fetal CNS cell suspensions [18]. The patients used in the trial had previously suffered post-traumatic syringomyelia (PTS) so the goal was to observe improvements in decreasing cyst formation [18]. Several showed prevention of cyst formation with one patient having gait performance improvement. These clinical trials, however, came to a close after the FDA released a new memorandum in November 30, 2000 stating that Investigational New Drug applications were required for the use of fetal cells and tissues in human subjects [18]. Fetal tissue still could lead to a successful treatment for certain complications of SCI and should not be left behind. However, the disadvantages of this cell source are the non-uniformity in different tissue samples and the low availability of obtaining such grafts.

Embryonic stem cells (ESCs) can be derived from the inner cell mass of cultured embryos at the blastocyst stage [20]. These cells have the ability to divide into a self-renewed pluripotent parent cell and lineage-specific progenitor that may further divide into a specific differentiated cell type. The most advantageous feature of ESCs for creating a cell therapy for nervous system disorders is that the neuronal lineage is the default differentiation pathway of these cells. This might allow the easiest method for obtaining functional neurons that may integrate into the damage area after transplantation. The major disadvantage to ESCs are that the major requirement of the cells being designated as stem cells lies in their ability to form multi-

lineage cell teratocarcinomas after injection into mice, which means a significant chance for this same outcome in patients if the cells are transplanted in their undifferentiated state. The disadvantage again of having to transplant the ESCs as already differentiated neuronal cell types is that they will be post-mitotic and the amount of cells added to the injured site will be the maximum number of cells that will need to fill the lesion and recreate all of the functional circuitry. Also, mature neurons are fragile which limits their capacity for surviving after transplantation into the hostile diseased or trauma environment.

Despite these disadvantages, many researchers have shown promising results with *in vitro* differentiation and *in vivo* animal model experiments. *In vitro* differentiation of ESCs has shown that specific protocols can easily differentiate the cells into a specific neuronal cell type. Tang et. al. were able to develop a protocol for differentiating ESCs specifically into astrocytes [36]. Astrocytes could be beneficial in treatments because these cells can secrete many different desirable trophic factors, however they also have the ability to secrete undesirable factors that might further hinder nerve regeneration like Interleukin-6 (IL-6) [37]. A more relevant neuronal cell type in treating demyelinating diseases is the oligodendrocyte. These cells provide the myelin sheath necessary to insulate and protect the neurons spared after injury. Billon et. al. were able to develop a protocol for differentiating ESCs into oligodendrocytes [38]. Liu et al. were able to treat ESCs *in vitro* to make ‘oligospheres’ that contributed to myelination of neurons in the spinal cords of *shiverer* mice that lack the ability to form mature myelin [39]. The most important work to date with ESCs in treating SCI is the ability of these cells to differentiate into functional motor neurons that integrate with the host spinal cord. As early as 1999, McDonald et al. showed mouse ESCs survived and differentiated into astrocytes, oligodendrocytes, and neurons after transplantation into injured rat spinal cords [40]. These rats

showed hindlimb weight support and partial hindlimb coordination. In vitro differentiation of ESCs into motor neurons can be achieved using retinoic acid and Shh [20]. Most recently, Deshpande et. al. published experiments showing recovery of paralysis in rats from transplantation of motor neuron-committed ESCs with the evidence of hundreds of axons extending from the spinal cord to peripheral nervous system [20, 41]. Recently, Geron Corporation announced they are initiating a Phase I clinical trial treating patients with spinal cord injuries using their product of human embryonic stem cell-derived oligodendrocytes (www.geron.com).

Another source of cells useful in treating nervous system disorders via cell therapy are olfactory ensheathing cells (OECs) isolated from the adult olfactory bulb and possibly a patient biopsy of the olfactory mucosa [42]. An advantage of OECs is that serum-free media containing FGF2, forskolin, and heregulin-beta1 conditioned by astrocytes will allow significant growth of the OECs into a large amount of cells [42]. Amazingly, over 400 people with SCI throughout China, Portugal, and Australia have undergone fetal OEC transplantations [18]. However, there are no significant published results from these trials and the follow-up examinations only went out to 8 weeks post-transplantation [18]. Hopefully future clinical trials will allow collection of more useful data. ProCord, developed by the company Proneuron Biotechnologies, is a product created by culture of a patient's autologous macrophages that are specifically activated by culturing with the patient's skin biopsy. This product is currently FDA approved and in Phase II clinical trials throughout the world, including the United States, for treating acute spinal cord injuries.

Another major cell source for treatment of nervous system disorders is bone marrow-derived mesenchymal stem cells. Clinical trials by Sykova et. al. in Prague were initiated in 2003 using MSC intravenous delivery into 9 patients with SCI [18]. 6 patients seem to have some improvement, but still within the range of spontaneous recovery. One patient had significant recovery with the reappearance of motor-evoked potentials. There are currently multiple clinical trials using bone marrow-derived adult autologous stem cells for treating stroke. There are also a few using these cells to treat multiple sclerosis.

The most promising cell source for treating nervous system diseases and injuries are human neural stem/progenitor cells isolated from human fetal or adult central nervous system tissue. These cells retain the ability to specifically differentiate into neurons, astrocytes, or oligodendrocytes directly applicable to restoring function to nervous system tissue. The work performed in Chapter 3 has focused on research using mouse neural stem cells demonstrating the need to elaborate on the properties and capabilities of these cells in order to optimize therapeutic strategies for transplantation of human neural stem cells. Further details on the potentials and previous research using these cells are described in the introduction of Chapter 3. We have used the hollow fiber-based bioreactor systems for testing mouse neural stem cell differentiation under 3D dynamic conditions, mimicking the environment observed by the cells after transplantation *in vivo*. We believe the bioreactor systems provide an advanced research tool replacing traditional 2D cell culture or animal experiments allowing eventual culture of human neural stem cells for further elaboration on optimizing protocols for transplantation of these cells.

1.2.2 Chemotropic factors

During embryonic nervous system development many chemical factors are secreted in the surrounding areas to properly pattern the nervous system by either attracting or repelling neuronal cell migration or axonal growth to form the proper functional synapse connections between neurons throughout the body [43]. More specifically, gradients of factors can attract or repel the cells or axons in order to lead them to the proper final special destination throughout the developing tissue. The ends of growing axons, or axonal growth cones, express multiple receptors that enable sensitivity to these factors for directing the growth of the axon to the proper target. The protein family of neurotrophins includes chemotropic factors such as nerve growth factor (NGF), glial derived neurotrophic factor (GDNF), brain-derived neurotrophic factor (BDNF), ciliary neurotrophic factor (CNTF), and others such as NT3 that are present in the developing nervous system to act as attractive molecules directing axonal growth [44-47]. Other protein families involved in axonal attraction are netrins and slits [48]. Gradients of these molecules exist during development and can direct the axonal growth cones and migratory neural progenitor cells towards the higher concentrations. Semaphorins are a group of proteins that act as inhibitory molecules to axonal growth cones [49]. Other major inhibitory molecules include ephrin-A5, wnts, and repulsive guidance molecule (RGM) proteins [49]. These molecules also act by binding to receptors on axonal growth cones, but initiate signal cascades that encourage growth cone collapse and retraction [49]. They also can act to inhibit axonal growth by lining the surroundings of the desired path [48]. Chondroitin sulfate proteoglycans (CSPGs), Nogo-A, myelin-associated glycoprotein (MAG), and oligodendrocyte myelin glycoprotein (OMGp) are repulsive molecules present in adulthood with upregulation after injury to the CNS [49]. These molecules aid in the prevention of nerve regeneration within the damaged CNS tissue.

These natural mechanisms have initiated development of drug or protein therapies for enhancing nerve regeneration by applying gradients of these factors to attract the axons towards their distal targets for enhancing nerve regeneration. A small clinical trial consisting of three patients with Alzheimer's disease in Sweden in the 1990s were given intracerebral doses of NGF. Some results in cognitive tests were improved, but was associated with side-effects of weight loss and pain [47]. Also, animal studies testing rhNGF doses revealed non-malignant Schwann cell hyperplasia [47]. There have been some early trials of BDNF administration to patients with amyotrophic lateral sclerosis (ALS) showing possible improvements [47]. A preclinical trial has been recently implemented involving NT-3 administration to patients with Charcot-Marie-Tooth type 1A (CMT1A), a demyelinating syndrome [50]. However, direct administrations of these neurotrophic growth factors have the ability to stimulate neuronal plasticity in undesirable ways. Further research is necessary for fully understanding effects of the amounts and combinations of these factors on neuronal plasticity in order to benefit clinical therapies.

1.2.3 Substrates for directing axonal outgrowth

The topography of biomaterial surfaces used for directing neurite outgrowth is currently a useful topic in nerve tissue engineering in order to devise methods for improving nerve regeneration *in vivo*. Hirono et al in 1988 was one of the first groups to realize patterned substrates could control axonal outgrowth in neuronal cell cultures *in vitro* [51]. Many groups since then have studied different methods for creating structured biomaterial surfaces for controlling axonal guidance. One extensively studied method in generating these structured surfaces has been the microfabrication technology of photolithography. This method can be used to create different

topographical structures on a surface to construct grooved pathways for specific axonal growth [52-56]. Another attractive method for surface patterning has been the technique of microcontact printing. Wheeler et al. used microcontact printing to direct hippocampal neuronal growth on lysine and laminin patterned surfaces [57]. Others have created microcontact printed surfaces with even more complex patterns using adhesive proteins and molecules [58-62]. Thiebaud et al. have combined photolithography and microcontact printing in order to create a microfluidic device for continued *in vitro* growth of specific neuronal cell arrangements [63]. Using these two methods to pattern substrates in more than two dimensions can be very complex. It is possible to stack layers of the modified surfaces to create three-dimensional scaffolds, but this has not yet been achieved for neuronal cell culture scaffolds with the exception of creating a tube out of the layer for use as *in vivo* peripheral nerve guide conduits [52, 64, 65]. A technique that could also be scaled up to achieve three-dimensional neuronal *in vitro* scaffolds is that of polymer/extracellular matrix protein ink-jet printing [66]. These studies will all help lead to the establishment of scaffolds used for improving neural engineering strategies for either *in vitro* studies controlling axonal growth or *in vivo* nerve regeneration therapies.

1.2.4 Nerve guide conduits

Nerve guides are typically hollow tubes used to enhance regeneration of damaged peripheral nerve segments. The proximal and distal cut nerve stumps are sutured into the ends of the tube. The lumens of the nerve guides provide the mechanical contact guidance cues for directing the proximal nerve end to regenerate towards its distal target. There are currently five FDA approved commercially available nerve guides used clinically for peripheral and cranial nerve

repair [24, 25]. NeuraGen and NeuroMatrix NeuroFlex are two of these nerve guides comprised of collagen type I. Neurotube and Neurolac are the other two of these nerve guides which are composed of synthetic degradable polyester polymers. SaluBridge is a nerve guide consisting of a polyvinyl alcohol hydrogel [24]. Clinical use of these nerve guides is limited by the gap distance between damaged nerve endings, ranging from less than 2.5-4 cm in length for the different guides. Neurotube is currently the preferred guide used clinically because it is offered with the longest length of 4 cm, is the least expensive, and has more clinical data available.

Even with the availability of these products for short peripheral nerve gaps, surgeons often still prefer correction with a second surgery removing a sensory autologous nerve for use as a graft bridging the defect gap. The nerve guides have not been able to demonstrate results superior to the autologous nerve use and are also a much more expensive solution. Further research and development of novel advanced nerve guides has therefore been necessary to create a product allowing enhanced functional restoration after nerve regeneration when compared to autologous nerve grafts. Aspects investigating in creating a more superior nerve guide have ranged from varying the nerve guide conduit material properties, dimensions, and configurations [29, 67-74]. Methods to further improve functional nerve regeneration within these conduits have ranged from surface modifications or natural matrix incorporation (collagen or fibrin gels) to enhance cell adhesion, growth factor immobilization to conduit walls or microcarrier incorporation, and use of novel biomaterial surfaces i.e. electrically conducting polymers [75-90].

In order for us to develop an *in vitro* culture model used for analyzing directed neurite outgrowth, we have capitalized on the nerve guide concepts. In Chapter 4 we have developed a scaffold able to be incorporated into a hollow fiber-based bioreactor device in order to control

and manipulate directed neurite outgrowth within the device. The scaffold is based on a nerve guide consisting of a porous, cylindrical polymer conduit where contact guidance directs axon growth through the lumen.

1.3 PREVIOUS NOVEL NEURONAL CULTURE SYSTEMS

1.3.1 3D dynamic bioreactors

The ultimate goal of tissue engineering is to synthetically re-create tissues *in vitro* that are useful in clinical transplantation for reconstructing or replacing damaged tissue in the body lost to trauma or disease. However, creating a tissue implies a thick composite of cells and matrix in a 3D configuration instead of the monolayers achieved with traditional cell culture methods with cells grown on a 2D surface. These traditional methods rely on nutrition of cells with medium nutrients and oxygenation via passive diffusion of molecules such as glucose, amino acids, and O₂ with a thin layer of medium stagnantly covering the monolayer of cells on the bottom of the culture dish with allowing the diffusion of gas. However, as the layers of cells increase in order to build the cells into a tissue, under static culture conditions diffusion of nutrients to the inner layers of cells becomes limited by the cells on the outer layers consuming these products before they are able to diffuse to the inner cell layers. This could partially be solved by the addition of more medium to the culture, but a thicker layer of medium will begin to prevent diffusion of gas transport of O₂ and CO₂ to and from the cells. Therefore, advanced culture methods have been implemented in order to improve nutrition and oxygenation conditions for creating tissues *in vitro*.

An efficient method for improving nutrition conditions is to surpass static conditions relying on diffusive transport by adding features allowing dynamic pressure-driven convective transport with flow of medium in the cultures. Advanced culture systems controlling dynamic flow of medium have been termed bioreactors. One of the first groups to develop a mammalian cell culture system with dynamic medium flow through the system was Kruse et al. in 1963 [91, 92]. These authors also coined the term “perfusion” to indicate continuous medium flow through the cell culture system with mechanical pumps. The perfusion system within this work consisted of tubing connected to a traditional cell culture flask in which medium perfusion was performed through the flask via pumping. The perfusion enabled culture of tumor cells up to 17 monolayers thick [92].

The term bioreactor has been used because initial bioreactors were based on traditional designs of reactors used for chemical engineering. One of the most commonly used bioreactors still used today are spinner flask devices. Spinner flasks are based on the traditional reactor design for continuous stirred tank reactors (CSTRs) used for batch processing of chemical reactions. These systems require culture of cells suspended within a large volume of medium contained in a closed glass beaker (flask). The convective transport of medium nutrients is provided by an impeller extending into the flask able to mechanically be rotated to stir the suspended cells cultured within the medium. Typically adherent cell types are cultured on microcarrier beads that are also cultured in suspension within the spinner flasks. In 1983 Butler et al. described culture of fibroblasts attached to microcarriers in a spinner flask device with incorporation of connected tubing used to additionally perfuse medium through the flask [93].

Researchers investigating development of scaffolds useful in tissue engineering allowing tissue formation within these scaffolds have utilized direct perfusion bioreactors. These systems

are typically based on a single compartment supporting and immobilizing a cylindrical shaped cell seeded scaffolds with connections on the top and bottom for tubing used to pump medium flow through the compartment for direct perfusion of the scaffold. The cells seeded on scaffolds cultured in direct perfusion bioreactors observe shear forces from the flow directly around the cells. Bone tissue engineering has benefitted from the use of these bioreactor designs because cultured osteoblasts have been demonstrated to increase their bone matrix secretion with the shear flow of direct perfusion bioreactor cultures compared to static cultures [94-97]. The concept of direct perfusion bioreactors has been further adapted for culture of tissue engineered vascular grafts, where medium is perfused with pulsatile flow through the lumen of a hollow tube scaffold resembling a blood vessel with blood flow. Niklason et al. have been able to develop this type of bioreactor in creating superior tissue engineered vascular grafts [98].

A table listing some examples of different bioreactor designs and constructions is shown in Table 1. Another well-established bioreactor design is a rotating wall vessel bioreactor. These bioreactor designs were first developed by NASA to culture cells on microcarriers in suspension experiencing microgravity environments [99]. Saini and Wick have developed a similar bioreactor consisting of rotation of concentric cylinders containing medium with immobilized constructs on the inner walls observing shear flow from the rotation of the cylinders useful for creating cartilage tissue engineered constructs [100, 101]. A more complex bioreactor design useful for small scale hepatocyte cultures have been developed by Griffith et al. to be used as a diagnostic tool for toxicology and drug screening [102, 103]. Fabrication of these bioreactors have utilized the concepts of photolithography and micropatterning to achieve channels through a substrate creating control over directional flow through the device [104].

Advanced bioreactor designs achieve control over both medium perfusion and gas exchange through the cell compartment of the system. Most of the bioreactor designs focusing on perfusion of medium rely on the use of silicone tubing which is permeable to gas and require maintenance of these bioreactors in a humidified incubator with oxygenation of the medium by diffusion of gas into the medium reservoir and tubing to dissolve in the medium. Also, some designs incorporate an additional source of gas able to bubble into the medium reservoir to dissolve oxygen into the medium. Bioreactor designs based on woven sets of semi-permeable hollow fibers compared to direct perfusion and rotating wall vessel suspension designs have the advantage of providing both uniform nutrient and uniform gas exchange to the entire cell compartment volume. Medium and gas can be perfused through the hollow fibers running through a cell compartment where flow exchange through the porous walls of the fibers delivers nutrients and O₂ to the cells within the surrounding compartment and removes waste products and CO₂. These bioreactors offer a homogeneous environment with uniform nutrition and oxygenation for sustained long term cultures of cell types not requiring mechanical stimuli.

There have been many reports on the use of hollow fiber bioreactor designs used for hepatocyte cultures [105-110]. These hollow fiber bioreactors were first developed to be used as bioartificial livers or bioartificial kidneys with either hepatocyte cultures or kidney epithelial cultures with clinical use for extracorporeal organ support bridging patients with liver or kidney failure until supplied with a transplanted organ [111-114]. Hollow fiber-based bioreactors are preferable to other designs for the culture of soft tissues due to transport of medium via hollow fibers creating lower shear stresses compared to direct perfusion systems. The cell cultures within these devices have often shown improved tissue formation and structure by the inoculated

cell types compared with 2D cultures [115-118]. A table of bioreactor systems that have reached clinical trials for use in bioartificial kidney or liver support of patients is listed in Table 2.

Table 1. Listing of some examples of publications describing different bioreactor designs used for in vitro cell cultures with dynamic conditions. Literature citations for these publications are as follows [104, 119-151].

Table: Examples of Bioreactor Constructions Tested <i>in Vitro</i>		
Technology	Cell Type	Citation
Early perfusion chambers	Chick heart fibroblasts, human malignant epithelial cells, Chinese hamster cells, hybridomas	Christiansen et al. 1953; Rose, 1954; Freed, 1963; Katinger, 1985
Commercially available perfusion chambers	Bone marrow-derived osteoblasts	Minucells (Minucells and Minutissue Vertriebs GmbH).
Commercially available systems for non-adherent cells	Hybridomas	VectraCell gas-permeable bags (Diagnostic Chemicals, Ltd.), Rotary Cell Culture System (Synthecon, Inc.), Wave Bioreactor (Wave Biotech General Electric, Ltd.), CELLline (Integra Biosciences AG), miniPERM Bioreactor (Sartorius AG), CellMax (Spectrum Laboratories, Inc.), Tecnomouse (Integra Biosciences AG)
Commercially available system for bone marrow expansion	Hematopoietic stem cells	AstromReplCell (Astrom Biosciences, Inc.)
Hollow fiber-based bioreactors	Mouse fibroblasts, human chorioncarcinoma cells, Reuber hepatoma cells, human hepatocytes	Knazek et al. 1972; Wolf et al, 1975; Hager et al, 1978, 1983
Hollow fiber-based bioreactor with integral oxygenation	Human leukemic cell lines	Gloeckner et al, 2001
Coaxial hollow fiber-based bioreactor with integral oxygenation	Rat hepatocytes	Macdonald et al, 2001
Hollow fiber-based bioartificial liver with integral oxygenation (Gerlach CellModule)	Porcine and human liver cells	Gerlach et al, 1994, 1998, 2003; Sauer et al, 2002
Flat sheet and hollow fiber-based bioartificial liver with integral oxygenation	Porcine hepatocytes	Flendrig et al, 1997
Hollow fiber-based renal tubule assist device (Humes RAD)	Porcine renal tubule cells	Humes et al, 1999
Flat membrane bioreactor with integral oxygenation	Porcine hepatocytes	De Bartolo et al, 2000
Flat plate bioartificial liver with integral oxygenation	Porcine hepatocytes	Shito et al, 2001
Micropatterned borosilicate wafers	Rat hepatocytes and 3T3 fibroblasts	Bhatia et al, 1997
Biodegradable polymer bioreactor constructed via 3D printing	Rat liver cells	Kim et al, 1998
Microfabricated bioreactor constructed via ion etching of silicon wafers	Rat hepatocytes	Powers et al, 2002
Titanium mesh bioreactor	Rat bone marrow stromal osteoblasts	Bancroft et al, 2003
Bioreactor containing hydrated polyester fibers and porcine autologous biomatrix	Porcine hepatocytes (10^{10})	Ambrosino et al, 2002
Bioreactor containing nonwoven polyurethane matrix with integral oxygenation	Rat or pig hepatocytes	Linti et al, 2002

Table 2. List of hollow fiber-based bioreactor systems used for kidney or liver support systems that have entered clinical trials. Literature references cited are the following [107, 114, 152-158].

Table listing Bioreactors for Hybrid Kidney Support and Bioartificial Liver Support, Tested in Clinical Trials				
Bioreactor Technology	Additional Therapeutic Components	Perfusate	Cell Type	Literature
Hollow fiber-based renal tubule assist device			Human renal tubule cells	Humes et al, 2002
Hollow fiber-based, two compartments (Vital Therapies ELAD®)		Plasma	Human hepatoblastoma cell line (C3A)	Sussman et al. 1992
Hollow fiber-based, two compartments, with hepatocytes attached to dextran microcarriers (Arblos Systems HepatAssist®)	Charcoal perfusion chamber	Plasma	Porcine hepatocytes	Watanabe et al. 1997
Hollow fiber-based, two compartments (Excorp Medical BLSS®)		Blood	Porcine hepatocytes	Mazariegos et al. 2002
Hollow fiber-based, four compartments, with integral oxygenation (Gerlach MLS CellModule)	MLS concept may involve dialysis and artificial detoxification	Plasma	Porcine and human liver cells	Mundt et al. 2002; Irgang et al, 2003; Sauer et al. 2003
Perfused scaffold with oxygenation fibers (two compartment system)		Plasma	Porcine cells	Van de Kerkhove et al.

1.3.2 Directed neurite/axonal outgrowth models

Suspension bioreactors have already been used to culture neuronal precursor cells, neural progenitor cells, or neuronal like cell lines to achieve tissue-like structures that more closely resemble natural neuronal tissues compared to 2D cultures [159-161]. Lelkes et al. have demonstrated enhanced neuronal like differentiation of the PC12 cell line within the NASA designed rotating wall vessel bioreactor [162]. Lin et. al. recently demonstrated synapsin I+ staining in differentiated neural progenitor cells growing within collagen constructs suspended in the NASA designed rotating wall vessel bioreactor [163]. These stirred tank and rotating wall vessel systems can easily allow manipulation of the culture environment to change important features such as cell aggregate size and viability, but are unable to address the functional

neuronal property of directed neurite outgrowth [161, 164, 165]. 3D *in vitro* neuronal culture work in the past was mainly dedicated for preliminary testing of implantable tissue engineered constructs, but not for the goal of long term *in vitro* neuronal cultures [166-169].

Recently some groups have begun developing *in vitro* culture models as a first step toward producing long-term 3D neuronal cell interactions *in vitro*. Microfluidic devices with channels for directed neuronal culture growth have been investigated as initial devices for establishing long term 3D neuronal interactions *in vitro* [63, 170, 171]. Some other 3D neuronal cell cultures have been based on the incorporation of collagen hydrogels or synthetic 3D matrices [54, 172-174]. All of this work will significantly contribute to creating long term 3D *in vitro* neuronal cell culture devices used as tools for studying neurobiological mechanisms.

The hollow fiber-based bioreactors used in the work presented within this thesis are current versions of those described in Table 1 and Table 2 by Gerlach et al. We have used laboratory scale versions of these four compartment hollow fiber-based bioreactors in order to culture both the PC12 cell line and mouse neural stem cells. The bioreactors have allowed high density cultures of the PC12 cells with continuous tissue formation throughout the cell compartment. The bioreactors have also provided a tool for testing behavior of mouse neural stem cell differentiation with 3D dynamic conditions similar to the *in vivo* environment in order to facilitate development of strategies using these cells clinically.

Further developments have been made to modify the hollow fibers used for perfusion in the bioreactors to be used also as scaffolds for directing neurite/axonal outgrowth. These fiber scaffolds can be incorporated into novel hollow fiber-based bioreactor systems that can achieve cultures of high density of neuronal cells into tissue like structures with the additional feature of directing axonal growth in a 3D space through the high density cultures. We believe this will

allow an advanced culture model as a diagnostic tool for enhancing assessment of neurobiological mechanisms such as screening for therapeutic factors for nerve regeneration and for observing behavior of neural stem cells in a 3D dynamic environment.

2.0 HIGH DENSITY NEURONAL CELL GROWTH AND NEURITE NETWORK FORMATION IN A 3D DYNAMIC HOLLOW FIBER-BASED BIOREACTOR COMPARED TO 2D AND 3D STATIC CULTURES

2.1 INTRODUCTION

2.1.1 Non-neuronal tissue formation within 3D dynamic cultures

The field of tissue engineering has endeavored to create either improved tissue culture models for *in vitro* studies or functional tissue constructs that may be used clinically in humans to replace lost or damaged tissue. This field has necessitated advanced methods beyond traditional 2D static cell culture methods in order to overcome diffusion limitations when scaling up in the z-direction in addressing tissue functionality. Many reports have documented the inability to generate tissue constructs *in vitro* with thicknesses greater than 100 μm having continuous viable cellular content by static culture methods that allow transport of nutrients and gas by diffusion alone [175-182]. There are two possible solutions to this problem for generating tissues *in vitro*. The most desirable goal in order to produce transplantable tissues for clinical therapies is to achieve a vascularized tissue for blood perfusion that permits incorporation into the surrounding host tissue and continued survival. However, this solution is tremendously complicated due to the ability to first tissue engineer viable and stable blood vessels that are composed of multiple

cell types and matrix components and second to achieve integration into the host blood circulation after transplantation. The earliest resolutions to overcoming the diffusion limitations in static cultures were to create systems with dynamic environments that sustain convective transport, termed bioreactors. Many different bioreactor designs with different flow patterns exist today and were elaborated previously in section 1.3.1. Bioreactors allow the most effective solutions for generating thick 3D tissue constructs. Bioreactor systems can especially be designed for creating and sustaining better *in vitro* models to more accurately study the desired tissues.

There are numerous previous demonstrations of enhancing tissue formation among non-neuronal cell types within bioreactor systems having a 3D culture space under dynamic flow conditions. Carrier et al. in 1999 were one of the first groups to systematically compare bioreactors (with different methods of creating dynamic flow by stirring) to static control cultures for cardiac tissue engineered constructs [176]. They were able to show dynamically created tissues had higher cellular content where convective transport allowed more aerobic metabolism than the static cultures limited to transport by diffusion resulting in anaerobic metabolism. Kim et al. have demonstrated increased elastin and collagen production from smooth muscle cells seeded on polyglycolic acid (PGA) scaffolds when cultured in spinner flasks having dynamic flow versus control cultures under static conditions [183]. Chondrocyte growth rates on PGA scaffolds have been shown to stop at 3 weeks of culture whereas well-mixed bioreactor cultured constructs maintained high growth rates over 7 weeks with normal tissue cell densities [180, 181]. Many groups have seen enhanced tissue-like growth of cell bodies among tumor cells when cultured in 3D matrices [184, 185]. Bone tissue engineering has

benefitted from direct perfusion bioreactors stimulating better osteoblast growth and matrix production on 3D scaffolds compared to statically cultured scaffolds [94-97].

2.1.2 Potential limitations of traditional 2D cell culture

Traditional neuronal cell culture systems only allow axonal projection and synapse formation between cells on the two dimensional culture plate surfaces. However, in an *in vivo* environment neuronal cells have the ability to organize and form connections in three dimensions. This difference might be crucial when observing how axonal growth cones migrate and connect with their distal target cells. Some groups have begun investigation into the differences in organization of neuronal cells cultured in 3D fibrin and collagen matrices compared to 2D surfaces [85, 186-190]. O'Shaughnessy et. al. have demonstrated 3D synapse formation between rat cortical neurons in 3D collagen gel matrices [172]. The significance of the 3D environment for the neuronal cell bodies is the ability for the cells to form high density cultures with tight tissue-like configurations. This close proximity of cell bodies in three dimensions is more similar to that *in vivo* and could result in more precise cell functioning. A 3D environment for this axonal growth might enable differential spatial reorganization of multiple axons due to responses in changes applied to the culture environment, especially concerning testing of drugs and therapeutic proteins and their potential for enhancing axon regeneration for clinical therapies. We have therefore performed studies comparing neurite outgrowth and synapse formation of the model neuron-like cell line PC12 cells within cultures maintaining 3D configurations at high densities.

2.1.3 Model neuronal PC12 cell line with NGF stimulation

The PC12 cell line was first derived from a pheochromocytoma in the medullary part of a rat adrenal gland in 1976 by Greene and Tischler [191, 192]. These cells have the ability to undergo changes when stimulated with nerve growth factor (NGF) that extend processes resembling that of sympathetic neurons. These neurite-like processes have been demonstrated by voltage patch clamp studies to produce Na⁺-dependent action potentials, while the unstimulated PC12 cells cannot sustain action potentials [193, 194]. PC12 cells can be used as model neurons because their normal non-neoplastic counterparts are chromaffin cells of the adrenal gland that are derived from the same primitive stem cell of neural crest origin during embryogenesis that gives rise to many types of neurons, especially sympathetic neurons [195]. It is thought that the neoplastic PC12 cells act more like this primitive stem cell and the stimulation of NGF differentiates them towards the sympathetic neuronal phenotype. Many researchers have consequently used the PC12 cell line to investigate many aspects modeling real neurons, specifically such as the mechanisms involved in neurite outgrowth to better understand axonal growth of real neurons [196-198]. The PC12 cell line has also been significantly used to study neurotoxicology of reagents [199, 200]. Recently, these cells have also been used as model neurons with neurite outgrowth to assess treatments useful for nerve regeneration using tissue engineering [75, 201]. PC12 cells have also been useful in developing tissue engineering strategies for enhancing nerve repair and regeneration because the neurite outgrowth from these cells is dependent on increasing NGF concentrations where neurites are longer with increased concentrations as well as being gradient dependent with neurites growing towards the source of NGF [75, 89, 202-204].

Our initial work utilized the PC12 cell line, but the growth of these cells is not contact dependent allowing these cells to remain within aggregates during proliferation. This complicates analysis of neurite outgrowth from individual cells. Therefore, we have performed most of the work presented here using the cell line Neuroscreen-1 (Cellomics Inc., Pittsburgh, PA). This line was created by subcloning a population of the PC12 cell line that had superior properties. This line of cells exhibits the property of contact inhibition, preventing the cells from aggregating with each other allowing observation of neurite outgrowth from single cells.

2.1.4 Hollow fiber-based bioreactor for PC12 cultures

In order to create high density neuronal-like cell cultures in more physiologically relevant arrangements we have cultured the PC12 cell line with nerve growth factor (NGF) stimulation in a hollow fiber-based bioreactor consisting of a three-dimensional culture space under homogeneous nutrient and gas perfusion. Our group has previously developed this hollow fiber-based bioreactor system for high density 3D hepatocyte cell culture [118]. We have used this system here to demonstrate 3D neuronal-like cell growth and neurite networking using the PC12 cell line. We have been able to demonstrate improved growth and 3D neurite networking when compared to 3D static collagen gel cultures at high densities in order to form tissue-like structures. In order to more accurately assess the neuronal networking between the cells in these cultures, we have examined synapsin I expression within the PC12 cells.

2.1.5 Synapsin I as a marker for synaptogenesis in neurons

Synapsins are abundant brain proteins involved in regulation of neurotransmitter release from synaptic vesicles in nerve terminals [205, 206]. There are three synapsin genes that are highly conserved with several protein isoforms due to alternative splicing [207]. The dominant isoforms in the mature nerve terminal are synapsins Ia, Ib, IIa, and IIb. It is currently unknown the exact distinct functions each of the synapsin gene products have in relation to each other [207]. Synapsins in neurons are exclusively localized to peripheral membrane proteins coating synaptic vesicles [205, 206, 208, 209]. The function of synapsin proteins is to tether the synaptic vesicles to each other and the actin-based cytoskeleton creating synaptic vesicle clusters (SVCs) in reserve pools within nerve terminals [205]. Upon changes in intraterminal Ca^{2+} concentrations due to excitation of a nerve terminal, the synapsin proteins are phosphorylated to their active form that decreases the affinity for synaptic vesicles to release them from the reserve pools, allowing them to leave the presynaptic nerve ending for neurotransmitter release from the synapse [205, 206, 210-212].

Many researchers in the fields of neurobiology and neuroscience have used Synapsin I as markers for synapses between neurons. De Camilli, Cameron, and Greengard first demonstrated that Synapsin I protein is present in all neuronal synapses *in vivo* using immunohistochemical light microscopy [213]. The immunohistochemical staining in nervous tissue sections from this work revealed Synapsin I staining as bright fluorescent dots or puncta. It is likely these bright puncta display where the Synapsin I is clustered, tethering the synaptic vesicles together in SVCs. Gitler et al. have demonstrated this same punctate staining localized to only mark presynaptic terminals in cultured hippocampal neurons [212]. Using transmission electron microscopy Bloom et al. studied synapsin I staining in presynaptic terminals explicitly showing

the staining within the SVCs at the presynaptic terminals of the giant synapse of the lamprey [207].

Furthermore, Lohmann et al. demonstrated that synapsin I appearance correlated with synapse formation during development [214]. DeGrenaro et al. as well as Lu et al. have showed synapsin I is greatest at the time of maximal synaptogenesis in the developing rat brain [214, 215]. Also, researchers have shown a reduction in synapsins leads to delayed neuronal differentiation, axonal outgrowth, and synaptogenesis [216-218]. Kao et al. demonstrated a role for synapsin with increased neurite outgrowth in *Xenopus laevis* embryonic neuronal cultures expressing a mutation mimicking constitutive phosphorylation of site I (Ser9) on synapsin. In human brain samples it has been shown that there is a reduction of synapsin proteins by Western blot in patients having bipolar disorder and schizophrenia relating the importance of maximal synapsin expression and synaptogenesis [219]. Romano, Nichols, Greengard, and Greene (co-developer of PC12 cell line) first characterized the effects of NGF on synapsin I in PC12 cells [214]. They specifically showed by Western Blot a significant increase of synapsin I in PC12 cells stimulated with NGF for 14 days, with a low detection in the nontreated cells. Das et al. described neurite outgrowth with increasing levels of synapsin I and growth associated protein 43 (GAP-43) in PC12 cells reaching maximal levels and plateau at 6 days of NGF stimulation [220]. We therefore proceeded to investigate synapsin I expression by immunostaining, Western blot, and quantitative RT-PCR among the NGF stimulated PC12 cells in this work between 2D static, 3D static, and the 3D dynamic perfusion bioreactor culture system.

2.2 METHODS

2.2.1 PC12 cell cultures with NGF stimulation

Two initial experiments used the original rat pheochromocytoma-derived PC12 cell line (ATCC; Manassas, VA). However, due to cell aggregation, neurite observation of individual cells was not possible and these experiments are described in Appendix A. All further experiments utilized the Neuroscreen-1 cell line (Cellomics Inc.; Pittsburgh, PA), which is an expansion of a sub-cloned population of the PC12 cell line having the beneficial property of contact inhibition. The Neuroscreen-1 cells (all Neuroscreen-1 cells now referred to as PC12 cells) enable direct visualization of individual neurites from all cells in order to demonstrate the 3D neurite outgrowth.

All cultures were carried out for a total of 6 days with the first day consisting of cell seeding and serum starvation without NGF following with continued low serum plus NGF for 5 days. Medium formulation included RPMI-1640 (containing L-glutamine and HEPES, Lonza; Allendale, NJ) including 0.5% HS (heat-inactivated horse serum; Invitrogen Corp., Grand Island, NY), 1000 IU/ml penicillin, and 1000 µg/ml streptomycin (Invitrogen Corp.). Neurite process outgrowth was stimulated in all cultures using a concentration of 75 ng/ml nerve growth factor (NGF; Invitrogen Corp.). This protocol achieved superior neurite outgrowth among PC12 cells in a 2D culture compared to other medium regimens and therefore was used in all culture types.

2.2.1.1 2D static cultures

2D static control cultures were maintained in tissue-culture treated 100 mm Petri dishes (BD Biosciences; San Jose, CA). Dishes were first coated with 5µg/mL collagen type I (from rat tail

sterile filtered solution; BD Biosciences) dissolved in 0.02 N acetic acid for 1 hour in 5 % CO₂ humidified incubator at 37°C. Dishes were then washed with Dulbecco's phosphate buffered saline solution (PBS; Invitrogen Corp). 1x10⁶ PC12 cells were plated in each dish at a density of 127 cells/mm² in low serum medium without NGF. Throughout rest of culture period medium with NGF was replaced once daily. N= 5 dishes were seeded for each experiment. These 2D static cultures were replicated in triplicate.

2.2.1.2 3D static collagen gel cultures

3D static control cultures were possible using collagen type I (rat tail, BD Biosciences) hydrogels (gels). Collagen gels were fabricated and cultured within tissue culture-treated 12 well plates with a 1 mL volume gel within each well. Collagen gels were prepared using the following components quickly added in the given order: 100 uL 10X PBS (Invitrogen Corp.), PC12 cells with 500-600 uL RPMI medium containing 0.5% HS and 1% Pen/Strep (enough to bring final volume to 1 mL), 250-350 uL collagen type I sterile solution (amount varied with manufacturer stock concentration, final concentration of collagen in gel 1 mg/mL), and 6 uL 1 N NaOH. Collagen gel solutions can then undergo fibrillation and gel formation after addition of NaOH for final pH approximately 7.4 and plates placed in 5% CO₂ humidified incubator at 37°C. Collagen gel formation completed within 15 minutes and 1.5 mL RPMI with low serum was added to each well. Collagen gels were detached from the well edges using a sterile scalpel in order to maintain gel cultures as "free-floating" to improve nutrient exchange from fresh medium on entire surface area of gels. Collagen gel dimensions within the 12 well plates resulted approximately in 20 mm diameters and 2 mm in height. Gel plus liquid medium layer height never exceeded 6 mm from bottom of well in order to not further limit gas diffusion into gel constructs. Medium was completely replaced in each well once daily (every 24 hours).

During each experiment a total of 9 collagen gels were made within a 12 well plate for $n = 3$ gels at each of three densities: 1×10^3 cells/mm² (1×10^6 total cells), 2.5×10^3 cells/mm² (2.5×10^6 total cells), and 5×10^3 cells/mm² (5×10^6 total cells). These 3D static collagen gel cultures were replicated in triplicate.

2.2.1.3 3D dynamic hollow fiber-based bioreactor cultures

The hollow fiber-based bioreactors used in this work are the laboratory scale devices previously designed and used by our lab as described by Gerlach et al. [116-118, 137, 221-223]. The bioreactor contains four separate compartments as shown in Figure 1. Two woven bundles of porous, hydrophilic polyethersulfone hollow fiber membranes with molecular weight cutoff of 400 kD and maximum pore size $0.5 \mu\text{m} \pm 0.1 \mu\text{m}$ (Membrana, Wuppertal, Germany) compose two of the compartments which are arranged to allow countercurrent medium perfusion. The third compartment is composed of a bundle of hydrophobic polypropylene hollow fibers (MHF; Mitsubishi, Tokyo, Japan) used for integral gas exchange of oxygenation and CO₂ removal within bioreactor. These three separate fiber bundles are inter-woven layer by layer throughout compartment 4 of the bioreactor forming the volume used to culture cells. Cells are able to fill the 3D volume within this extra-fiber compartment and use the perfusion fibers as scaffolds to form tissue around. The medium perfusion and oxygenation fibers therefore mimic the *in vivo* configuration of blood supply through capillary network beds in order to maintain dynamic homogeneous nutrition and gas exchange in order to allow tissue formation.

Figure 1b shows a photograph of the actual 8 mL lab scale bioreactors used here that have been fabricated and produced at the company Stem Cell Systems (Berlin, Germany). The hollow fiber bundles are embedded in a fiber-compatible two component polyurethane (Pur 725,

Morton, Bremen, Germany) utilizing dialyzer potting techniques to seal the ends of the bundles and retain the inner cell compartment to have an extra-fiber volume of approximately 8 milliliters. This polyurethane housing creates flow heads at the ends of the fiber bundles that each lead to their own ports. There are nine ports total: two for medium inlet tubing connections leading to each PES fiber bundle, two for medium outlet tubing connections leading from each PES fiber bundle, two ports connect the inlet and outlet flow through the gas polypropylene fiber bundle, two ports sit directly at the top and bottom of the housing that directly connect to the cell compartment (used for pre-cell inoculation degassing), and the last port used for cell inoculation which leads into small diameter silicone tubes that allow distribution of cells throughout the extra-fiber cell compartment.

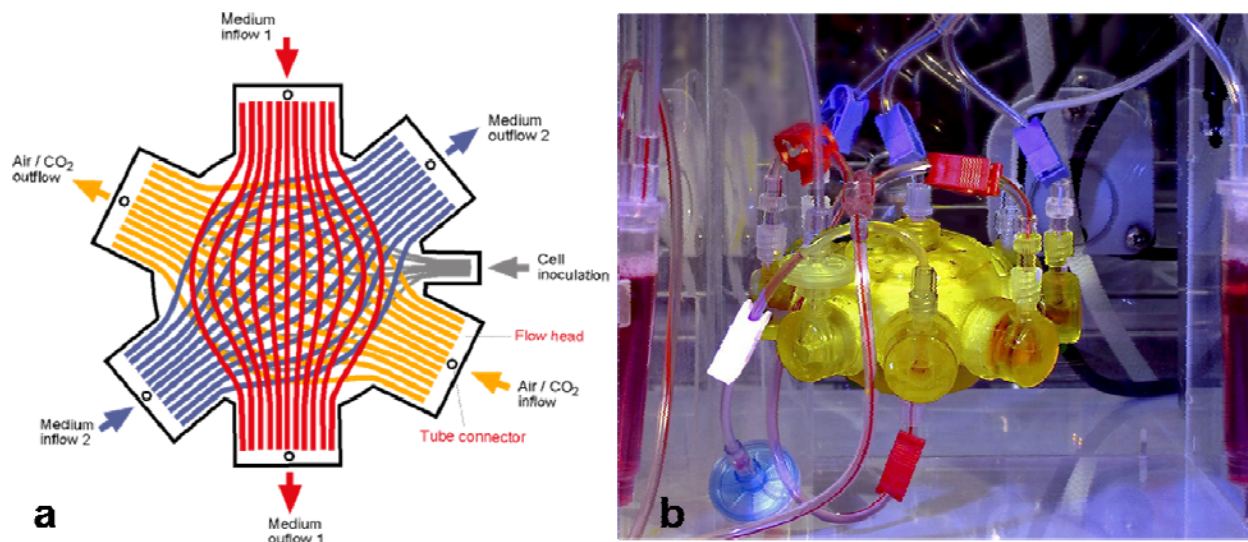


Figure 1. 8 mL hollow fiber-based bioreactor: a) diagram of displaying three separate fiber bundles running through inner cell compartment; b) photograph of 8 mL bioreactor placed in heating chamber with perfusion tubing circuit connected at each flow head port.

The bioreactor becomes a dynamic system when the ports are connected to the tubing circuits used to perfuse medium and gas with pump systems. The 8 mL hollow fiber-based

bioreactor is shown in Figure 2 within the perfusion system used for these experiments. The pump on the bottom left is a roller style pump that enables pulsatile flow through the recirculation loop of the medium perfusion circuit through the perfusion fibers of the bioreactor. The perfusion circuits used here in these experiments used tubing made of medical-grade polyvinyl chloride (PVC; B. Braun Medical Inc., Melsungen, Germany). The medium and gas perfusion tubing circuits are shown in the diagram of Figure 3.

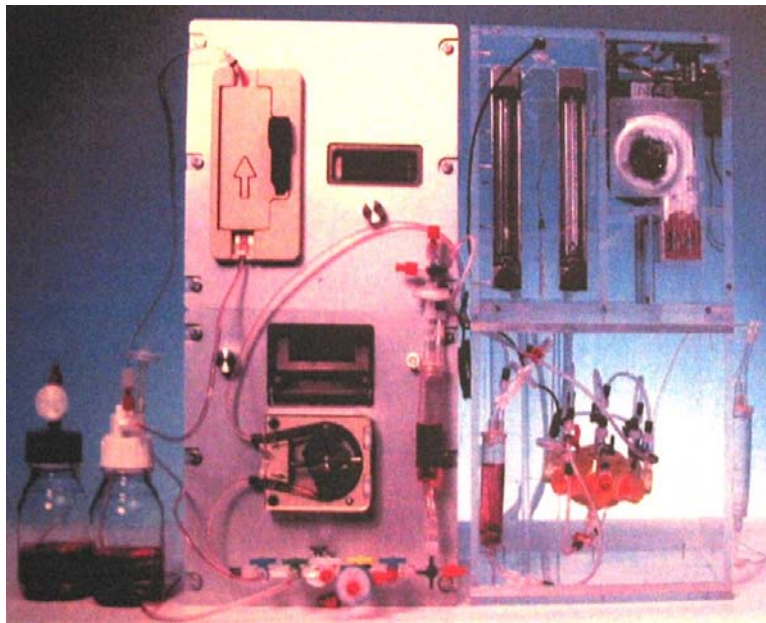


Figure 2. Photograph of bioreactor system used for 8 mL hollow fiber-based bioreactor experiments with bioreactor connected to tubing circuit within heating chamber. Shown on the top right are the rotameters used to control air and CO₂ gas flow rates. The top left shows the feed pump and bottom left the recirculation roller pump. The feed and waste bottles are shown connected to the medium perfusion tubing circuit. However, the feed medium bottle is kept within a mini-fridge above the system at 4°C.

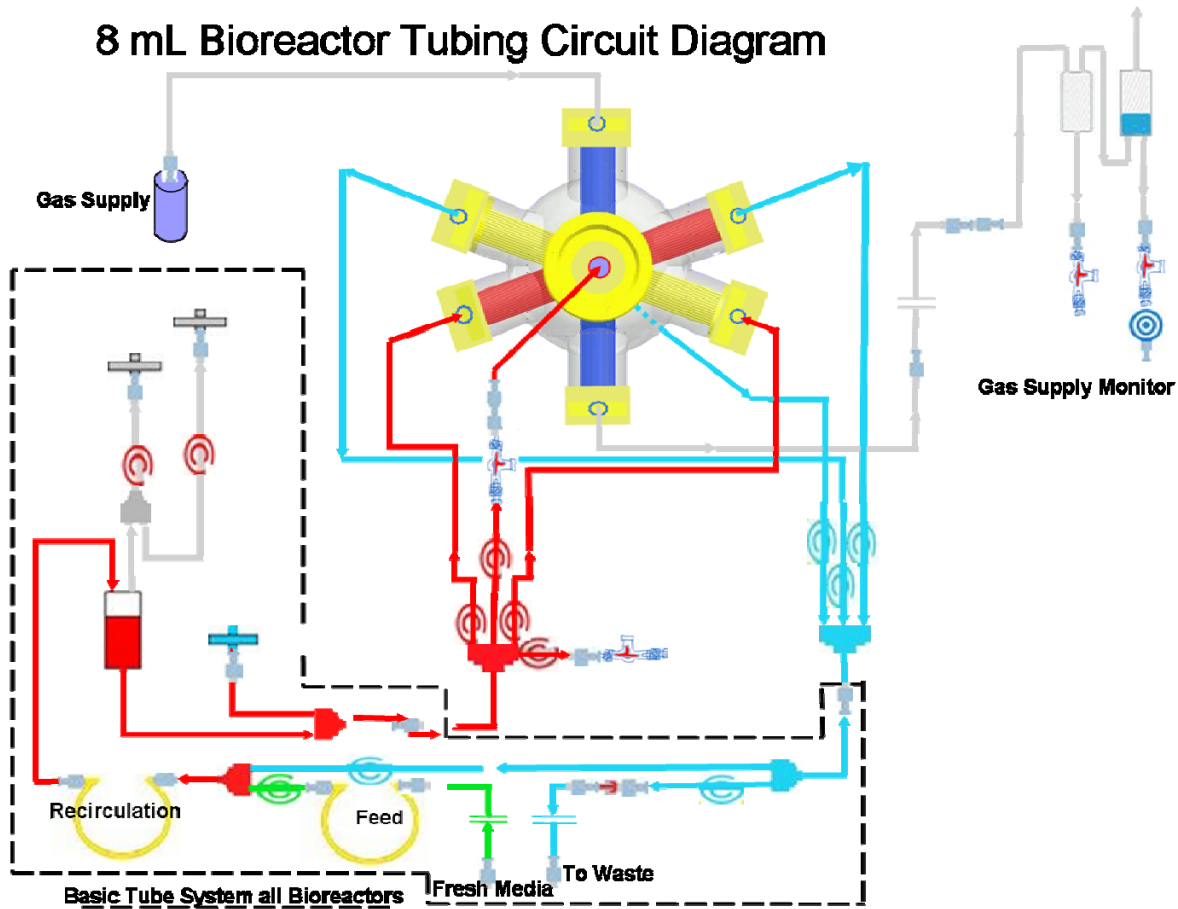


Figure 3. Diagram of tubing circuit used for medium and gas perfusion through 8 mL hollow fiber-based bioreactor. Red lines indicate arterial side tubing with medium flow leading into bioreactor. Blue lines indicate venous side tubing with medium flow leading out of bioreactor. This diagrams the tubing connections allowing medium flow in through the feed line, through the bioreactor in the recirculation loop, and out through the waste line. Yellow lines indicate pump tube segments connected to roller pumps. The sample port for recirculation medium daily samples is shown as the blue filter.

A total of six PC12 cell (Neuroscreen-1 cell line) bioreactor experiments were completed. Notation used to identify each bioreactor experiment in an abbreviated form with the example of the first experiment noted by RNS-1; where the first initial is the species being rat, the second and third initial correspond to the cell type (in this case Neuroscreen-1), and the number giving

the order within the six experiments (RNS-1 through RNS-6). All six RNS bioreactor experiments included inoculation of the bioreactor with PC12 cells suspended in a collagen gel solution. Two separate 10 mL collagen gel solutions were made; one including all cells and one for flushing behind to further disperse cell solution throughout bioreactor. A 10 mL collagen solution was made similarly to the 3D static gel cultures by adding the following components to a 50 mL conical tube in the given order: 1 mL 10X PBS, 5-6 mL media (RPMI 1640 with 10% HS and 1% Pen/Strep) (including cells in first solution), 2.5-3.5 mL collagen type I (amount to achieve final 1 mg/mL concentration; BD), and 40 μ L 0.2 N NaOH. Solutions were withdrawn into two separate 20 mL syringes for inoculation into bioreactor through the cell injection ports. The syringe containing cells plus gel solution was first connected to cell injection port. Media was first withdrawn from bioreactor into syringe to remove any air bubbles from line. Solution plus cells was then slowly injected into bioreactor cell compartment. Finally, the second 10 mL gel solution-containing syringe was connected and injected to further distribute cells in collagen solution throughout cell compartment volume.

The extra-fiber cell compartment volume is only 8 mL, but the 20 mL collagen solution allows for an approximate 1 mg/mL final concentration of collagen within the formed gel due to the solution mixing first with the medium initially in the compartment before injection. Also, any excessive collagen injected into the cell compartment can penetrate the medium perfusion fiber walls and be diluted into the circuit volume without any detrimental effects. In all experiments, cells were injected with gel solution with recirculation flow rate being kept on to prevent collagen gel formation within lumens of fibers. Also, tubing connecting top and bottom cell compartment ports remained clamped (closed) during inoculation and entire culture period to

confine the cells and gel to the bioreactor cell compartment (compartment can be opened to flush debris, but this was never performed in these experiments using the gel system).

RNS-1 was the first Neuroscreen-1 PC12 bioreactor experiment performed (original PC12 bioreactors: RPC-1 and RPC-2). Using the original PC12 cell line, cells were only maintainable even with NGF under high serum conditions (not below 10% HS). Therefore, when continuing to the Neuroscreen-1 cell line a high serum of 10% HS was also used for the RNS-1 bioreactor experiment throughout the culture period. However, serum levels were then tested on control Neuroscreen-1 2D cultures and found that cells achieved maximal neurite outgrowth with 0.5% HS concentrations and bioreactor experiments RNS-2 through RNS-6 were continued using this low serum level. It was not possible to maintain any of these lines with no serum present in the medium. RNS-2 through RNS-6 bioreactors were cultured using the medium regimens described in section 2.2.1 for the six day culture period.

The numbers of cells inoculated into each bioreactor are listed below in Table 3. Cell numbers were increased initially and varied among bioreactor experiments in order to optimize cell density within the bioreactor to have high density neurite network formation and subsequent increased synapse formation between cells. Due to the contact inhibition properties of these PC12 cells, bioreactors were not able to be repeated exactly even with RNS-5 and RNS-6 having the same initial cell inoculation number. Therefore, we have instead completed a series of experiments varying this cell density to see the effects on synapsin I expression.

Table 3. Cell inoculation information for PC12 bioreactor experiments

Bioreactor #	Cell Number (x10⁶)	Pellet Volume (mL)	Bioreactor Density (cells/mm³)
RNS-1	700	2.5	8.75x10 ⁴
RNS-2	200	1	2.5x10 ⁴
RNS-3	1000	3	1.25x10 ⁵
RNS-4	700	2.5	8.75x10 ⁴
RNS-5	300	1	3.75x10 ⁴
RNS-6	300	1	3.75x10 ⁴

2.2.2 Metabolic measurements

Medium samples were infused into single use CG4+ cartridges or G Glucose cartridges to measure the following metabolic parameters: lactate, pH, pCO₂, pO₂, and glucose; using the i-STAT[®] clinical blood analyzer system (Abbott, East Windsor, NJ). 3D static gel cultures were maintained each day during culture period by collecting 1.5 mL of culture medium (previously replaced 24 hours earlier) and analyzing metabolic parameters. Medium from bioreactor cultures was collected via syringe withdrawal from the sample port within the recirculation segment of the tubing circuit (medium flowing through recirculation tubing and bioreactor perfusion fibers at flow rate 30 mL/min). Bioreactor glucose and lactate concentrations have been inserted into formulas incorporating feed medium flow rate to give consumption and production values averaged between two measurements. The formula used is shown below in Figure 4.

$$\text{Glucose or Lactate Metabolism} = - \left[\frac{24 * Q_{\text{feed}}}{1000} \right] \left[\frac{(C_i + C_{i+1})}{2} - C_B \right]$$

Metabolism = glucose consumption (mg/day) or lactate production (mmol/day)

Q_{feed} = feed medium flow rate (mL/hr)

C_i = metabolite concentration at indicated culture day (mg/L)

Figure 4. Equation used to obtain daily glucose consumption or lactate production values of samples taken from the recirculation medium perfusion circuit during bioreactor culture experiments.

2.2.3 Fluorescent immunohistochemistry visualized with confocal microscopy

Static control cultures used for immunohistochemistry were first washed with PBS three times and fixed with 4% paraformaldehyde for 30 minutes and then washed with PBS again 3 times. Bioreactor fiber layer samples were transferred immediately after opening to tissue cassettes and placed in 4% paraformaldehyde for 1 hour. Samples were then washed with PBS three times, 15 minutes each.

Immunostaining procedure was first carried out by blocking in a 5% horse serum/PBS solution containing 0.3 % triton X-100 (LabChem Inc., Pittsburgh, PA) for 1 hour. All samples were first stained with mouse monoclonal primary antibody against class III neuronal specific β -tubulin (Covance CRP Inc.; Princeton, NJ) 1:500 dilution in 3% HS/PBS solution containing 0.3% triton-X for 1.5 hours. Samples were then washed five times with PBS each for 10 minutes. Goat-anti-mouse secondary antibody Alexa Fluor 488 (Molecular Probes, Invitrogen Corp.) was then added at dilution 1:1000 in 3% HS/PBS solution containing 0.3% triton-X for 1.5 hours. Samples then received washes five times with PBS each for 10 minutes. Double immunostaining was carried out on all samples with the same previous protocol but with one of

the following antibodies: anti-Synapsin I polyclonal rabbit primary antibody (Covance CRP Inc.) 1:200 dilution, anti-phosphorylated Synapsin I (site Ser 553) polyclonal rabbit primary antibody (Santa Cruz Biotechnology, Inc.; Santa Cruz, CA) 1:200 dilution, and anti-phosphorylated Synapsin I (site Ser 9) rabbit polyclonal primary antibody (Cell Signaling Technology, Inc.; Danvers, MA) 1:200 dilution. Goat-anti-rabbit secondary antibody Cy3 (Molecular Probes, Invitrogen Corp.) was then added at dilution 1:1000 in 3% HS/PBS solution containing 0.3% triton-X for 1.5 hours. Samples then received final washes five times with PBS each for 10 minutes. All samples were counterstained with DAPI (Sigma Aldrich, St. Louis, MO) for nuclear localization. Two 3D static gel and 3D dynamic bioreactor samples were used as immunostaining controls by performing the above staining protocol with deletion of primary antibody step with addition of Cy3 secondary antibody to check for residual secondary antibody within the gel or tissue samples.

Fluorescent confocal microscopy was used to visualize the immunohistochemical staining of all samples (inverted Olympus Fluoview 1000; Center Valley, PA). 2D samples cultured on tissue culture treated dishes were imaged by cutting the bottom surface out of the dish and sealing with gelvatol and glass coverslip. 3D gel and bioreactor samples were imaged by wet mounting with directly placing the sample onto a glass coverslip in order to image both sides of sample. To image cell morphology and neurite outgrowth images were taken using a 20X oil objective (final magnification 200X) and a 40X or 100X objective for imaging Synapsin staining (final magnification 400X or 1000X, respectively). All images were taken as z-stacks with 0.5 μm or 1 μm thick sections at 10 μm depth for 2D samples and approximately 50 μm depths for 3D gel and bioreactor samples. Stacked section images were reconstructed into maximum intensity projection representations in a single image or avi movie file to demonstrate

30 degree rotation showing 3D characteristics using Metamorph software (Molecular Devices; Downington, PA). When imagining synapsin I-Cy3 staining, microscope laser and imaging software settings were changed to optimize actual staining and minimize background noise (laser intensity and gain were minimized with offset set to 40%).

2.2.4 Quantitative RT-PCR gene expression analysis

3D static gel and 3D dynamic bioreactor samples for RNA collection were immediately immersed in RNA Protect reagent (QIAGEN, Valencia, CA) and stored at 4°C for less than two weeks before RNA collection. For RNA collection, samples were first centrifuged to pellet cell, gel, and/or fiber material with removal of supernatant. Total RNA was isolated from all samples with an mRNA isolation kit including on-column DNase digestion (QIAGEN, Valencia, CA). The first step was carried out by placing the samples in the first buffer solution of the kit and using a disposable pestle the sample was ground to mechanically digest the collage gel tissue. cDNA was synthesized by a conventional reverse transcription process (Promega, Madison, WI). The master mixture contained 5 mmol/L MgCl₂, 1x Reverse Transcription Buffer, 1 mmol/L deoxynucleotide triphosphate mixture, 1unit/μL recombinant RNasin® ribonuclease inhibitor, 0.75U/μL AMV reverse transcriptase, and 1μg of random hexamer Primers. Two micrograms of total RNA were prepared in sterile H₂O to a final volume of 20μL. The reaction mixture was incubated at 42°C for 60 minutes, followed by heat inactivation of the enzyme at 95°C for 5 minutes. After cooling on ice for 5 minutes, the cDNA was stored at -20°C until analysis. Quantification of mRNAs using real-time polymerase chain reaction (qRT-PCR) analysis was performed using an ABI PRISM 7000. The pre-designed TaqMan

probe and primer sets for Syn1 (Rn00569468_m1), Gap43 (Rn00567901_m1), and GAPDH (Rn99999916_s1) were selected from TaqMan Gene Expression Assays (Applied Biosystems, Foster City, CA).

2.2.5 Western Blot protein analysis

Protein collection from samples was first attempted by digestion of collagen gel from 3D static gel and 3D bioreactor samples using 30 units/ mL collagenase type II (Worthington Biochemical Corp.; Lakewood, NJ) for 1 hour at 37°C. Digestion was then stopped using RPMI 1640 medium with 10% HS and samples centrifuged to pellet cells. Cells were resuspended in 300 µL MPER cell lysis buffer (Pierce Biotechnology; Rockford, IL) including 3 µL protease inhibitor cocktail (Sigma Aldrich) and heavily vortexed. The samples were kept in lysis buffer on ice for 30 minutes with repeated vortexing to completely lyse cells. Samples were finally centrifuged to pellet membrane protein fractions and keep the supernatant containing the cytoplasmic protein fraction. These supernatants and pellets were stored separately at -80°C. The standard protein quantification method using a BCA Protein Assay kit (Pierce Biotechnology) was implemented to measure protein concentrations of each sample. Using this protein collection method, Western blots were performed to determine ability to collect synapsin proteins from PC12 cells efficiently within the supernatant fraction only.

After the bioreactor experiment RNS-2, a second protein collection method was then applied on further bioreactor experiments as well as completely restarting control 2D static and 3D static gel cultures in order to preserve the synapsin proteins in their active phosphorylated states. This method was executed using a cell lysis buffer solution of 300 µL TGN cell lysis buffer (50 mM Tris-HCl pH 7.5, 150 mM NaCl, 50 mM NaF, 1% Tween 20, 0.2% NP-40)

containing 3 μ L protease inhibitor cocktail. For the 2D static cultures this method was executed by directly placing the lysis buffer solution onto the 2D plate and collecting lysate using a cell scraper. Protein was collected from the 3D samples by placing the entire cell containing gel (plus fibers in the case of the bioreactor samples) into a 50 mL conical tube containing the TGN lysis buffer solution. Gels were first disrupted mechanically with disposable pestle. Then protein collection method was completed as above with samples on ice for 30 minutes with intermittent vortexing. Supernatants after centrifugation were then collected from each sample and stored at -80°C . This protein collection method differs from the first method by excluding collagen gel digestion, which results in some collagen proteins contaminating the final collected cell lysate protein sample. The BCA assay was implemented before Western blotting to give an estimate of cell lysate protein concentration (since the BCA assay used recognizes both the cell proteins and collagenous proteins from collagen gel matrix). Western blots were performed multiple times in order to optimize loading of all nine sample types via trial and error to achieve final blot containing all samples together with equal loading (according to control protein bands).

Western blots were performed using the Bio-Rad Mini Trans-Blot cell system with SDS-PAGE (Bio-Rad Laboratories Inc.; Hercules, CA). Collected protein samples at 10-20 μg were loaded into wells of 7.5% Tris-HCL Ready Gel (Bio-Rad Laboratories). Precision Plus Protein Kaleidoscope standard ladder was used (Bio-Rad Laboratories). Samples were run through gel with constant voltage of 125V for 75 minutes in Ultra Pure Tris/Glycine/SDS running buffer (National Diagnostics; Atlanta, GA). Protein was transferred onto trans-blot transfer membrane (Bio-Rad Laboratories) from gel using Bio-Rad system at constant current of 250A for 90 minutes in Ultra Pure Tris/Glycine transfer buffer. Membrane was then blocked with 5% milk solution (5% dry milk powder in 1X PBS with 0.1% Tween 20) with shaker for 2 hours. Primary

antibodies used were: synapsin I polyclonal rabbit primary antibody (Covance CRP Inc.) 1:2000 dilution, anti-phosphorylated Synapsin I (site Ser 553) polyclonal rabbit primary antibody (Santa Cruz Biotechnology, Inc.; Santa Cruz, CA) 1:1500 dilution, anti-phosphorylated Synapsin I (site Ser 9) rabbit polyclonal primary antibody (Cell Signaling Technology, Inc.; Danvers, MA) 1:1000 dilution, and anti-synaptophysin monoclonal mouse primary antibody (Covance CRP Inc.) 1:1000 dilution. Membrane was incubated with primary antibody in 1% milk/PBS/0.1% Tween 20 solution with shaking overnight at 4°C. Membrane was washed several times with PBS/Tween 20. Secondary antibody goat-anti-rabbit HRP or goat-anti-mouse HRP (Jackson ImmunoResearch Laboratories Inc., West Grove, PA) was incubated on membrane at dilution in 1% milk/PBS/Tween 20 solution for one hour with shaking. Antibody was washed off several times with PBS/Tween 20 for 30 minutes. Protein detection was carried out by blotting membrane with ECL Plus western blotting detection system (GE Healthcare Amersham; Piscataway, NJ) and X-ray film developing system using Hyper film ECL (GE Healthcare). Loading for cell protein among all samples was checked by stripping membrane (1 hour at 37°C) and re-blotting for control GAPDH protein (using primary anti-GAPDH antibody; Santa Cruz Biotechnology) which is an abundant house keeping gene product present at same levels in all cells. Dilution used for GAPDH primary antibody was 1:8000 incubated only for one hour on membrane and then with a secondary antibody goat-anti-mouse HRP.

2.3 RESULTS

2.3.1 Metabolic activity of 3D cultures

2.3.1.1 3D static gel cultures

Figure 5 shows the results of measuring daily glucose and lactate concentrations throughout the period of culturing PC12 cells at three different densities in 3D collagen gels cultured under static conditions. Media on these cultures was replaced entirely each day, so that the daily readings measure concentration produced over the past 24 hours within the culture. The baseline concentrations are shown on Day 0 at 1900 mg/L glucose and 0 mmol/L lactate. The curves to the left on Figure 5 represent the metabolic data for 1 million PC12 cells cultured in a 1 mL gel (density is 1×10^3 cells/mm³). These curves for 1 million cells/gel culture show steadily increasing glucose consumption and lactate production over the six day culture period. Also, the pH within this culture remained between 7.3 – 7.4 with p_{CO_2} ranging 17-25 mmHg and p_{O_2} ranging 140-150 mmHg. These values are within normal limits of desired and baseline values of pH 7.4, p_{CO_2} 17 mmHg, and p_{O_2} 140 mmHg.

The curves in the middle of Figure 5 represent the glucose and lactate concentrations measured from the culture of 2.5 million PC12 cells in 1 mL collagen gel. There is a large decline in glucose concentration to 0 mg/L by culture day 3, where the cells proliferated enough to consume all the glucose before the media could be replaced again for the rest of the culture period. The lactate for this culture did steadily increase, but the pH dropped to 7.0 by culture day 3 and reached as low as 6.7 at the end of the culture period. The p_{CO_2} values of this culture reached a maximum on day 3 of 30 mmHg, but remained between 15-20 mmHg for the rest of

the culture period. The p_{O_2} also reached a minimum of 106 mmHg on day 3, but remained above 120 mmHg for the rest of the culture period.

The curves on the right of Figure 5 show the results of glucose and lactate concentrations measured from the culture of 5 million PC12 cells in 1 mL collagen gel under static conditions. Within this culture there is a rapid decrease of glucose to 0 mg/mL and a high lactate accumulation by culture day 2 with a corresponding pH value of 6.8. The lactate concentration sustained a plateau between 15-16.6 mmol/L for the duration of the culture period. Even with the pH measuring 7.0 and 6.8 on the first two culture days the p_{CO_2} remained within the baseline limits of 16-17 mmHg.

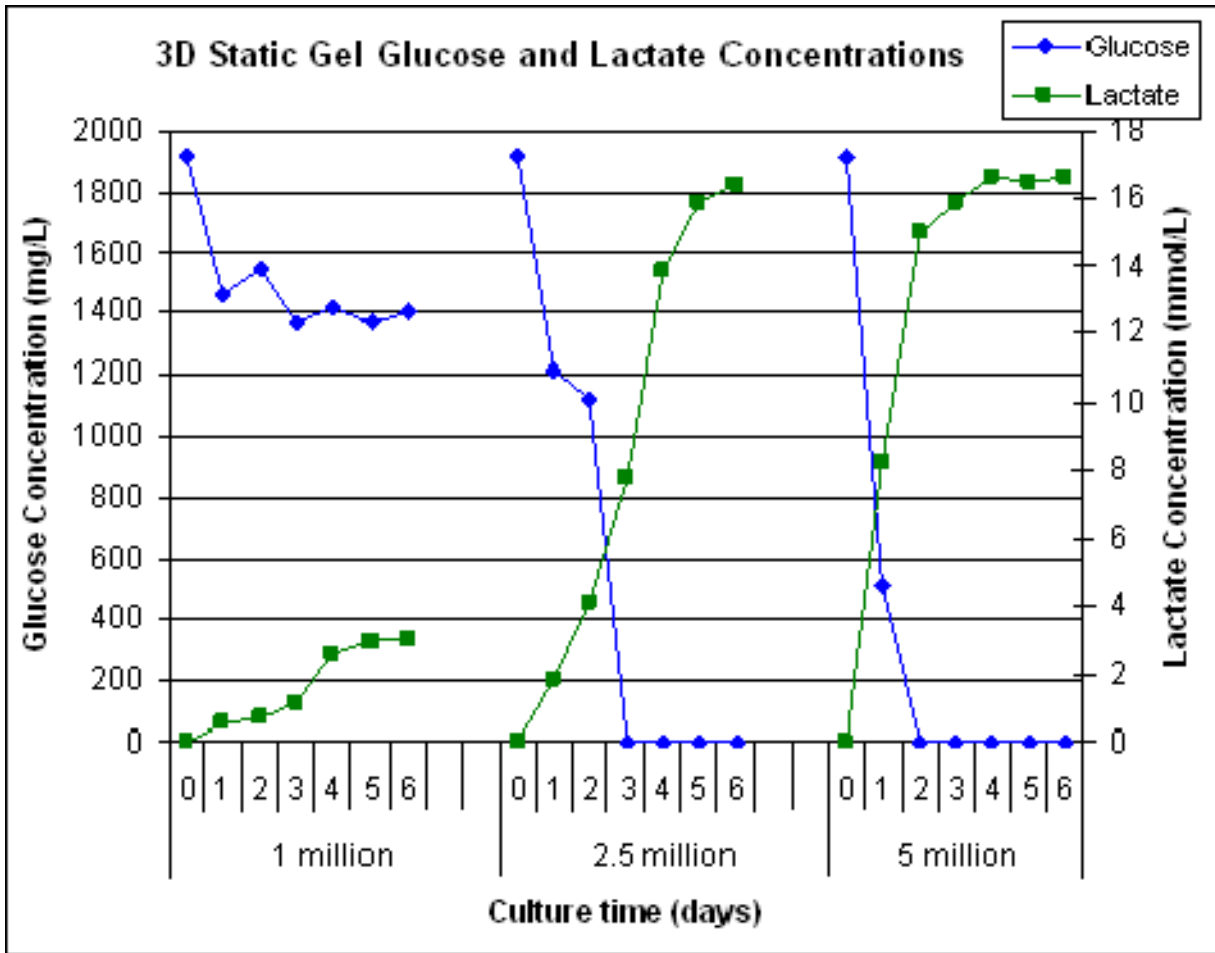


Figure 5. 3D static gel culture metabolic data plotting daily glucose and lactate concentration measurements over culture period for each density of cells cultured in 1 mL collagen gels.

2.3.1.2 3D dynamic bioreactor cultures

With all bioreactor experiments, however, the PC12 cells experienced significant proliferation as evidenced by increasing glucose consumption and lactate production during bioreactor culture described in the plots of Figure 7 and macroscopic tissue formation seen in Figure 6 below. Figure 7 plots the glucose consumption and lactate production according to averaging the daily concentration measurements between two days with subtracting the baseline concentration value and multiplying by the amount of fresh medium supplied due to the feed flow rate over the

previous 24 hours. These plots heavily relying on the feed flow rate, which was increased differently throughout all experiments, shows similar trends for metabolic activity of all bioreactors (except RNS-4 where there was a clear significant drop in activity after Day 3). Therefore, it is more interesting to observe the trends shown in Figure 8 with the plots of actual glucose and lactate measurements taken each day over the culture period. It is only in these plots that the glucose concentration reaching zero is observable, which occurred in RNS-3 on culture day 3.

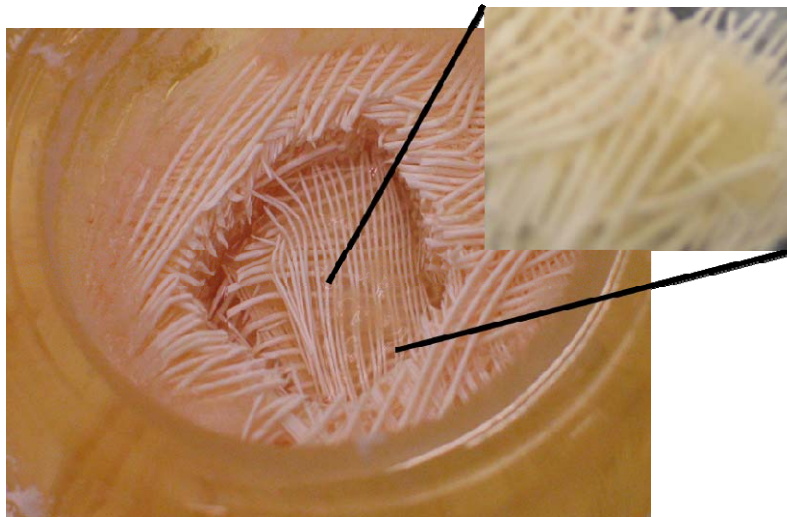


Figure 6. Photograph of 8 mL bioreactor housing opened to obtain tissue samples including fiber layers; shown here is RNS-1 with macroscopic tissue formation within collagen gel between fibers.

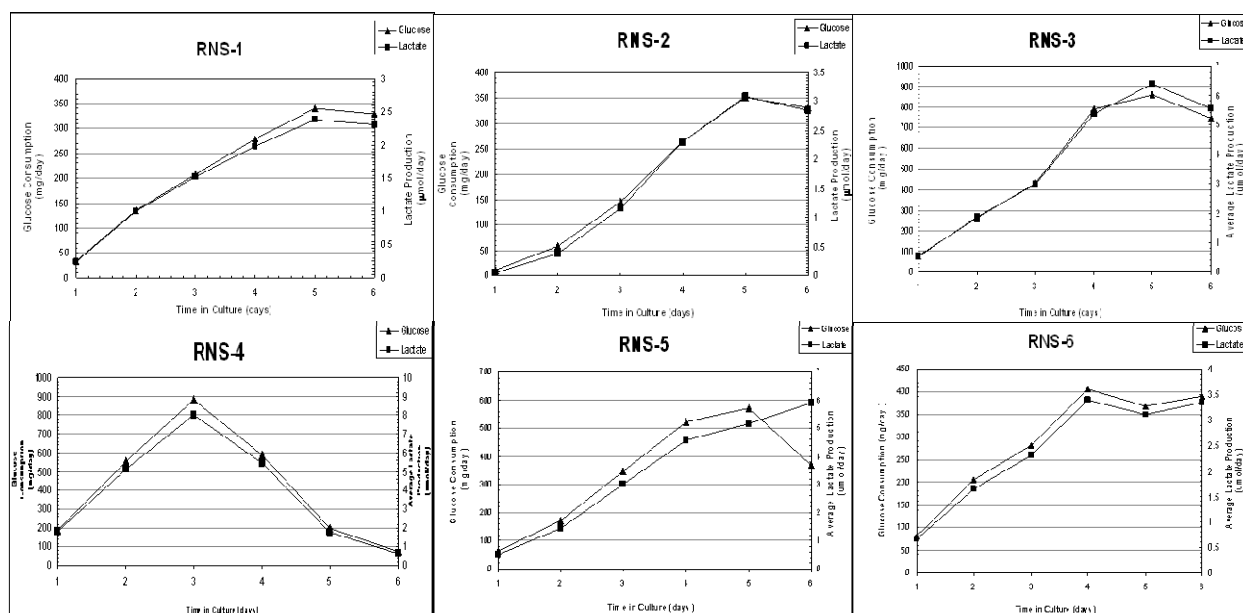


Figure 7. Metabolic data for all six bioreactor experiments plotting glucose consumption on the left axis and lactate production on the right axis averaged between each daily measurement including dilution due to change in feed flow rate.

The glucose and lactate concentration plots shown in Figure 8 demonstrate that for RNS-1, with high serum conditions, there was an immediate increase of lactate concentration above 10 mmol/L within the first 24 hours of culturing. The lactate concentration maintained a plateau of 10-12 mmol/L for the duration of the culture period. Unlike the 3D static gel cultures, this plateau of lactate concentration (and therefore possibly cell number) was not due to limitations of nutrition or medium acidity. The RNS-1 bioreactor maintained glucose concentrations above 200 mg/L and a pH above 7.275. This result (along with the description of the more rounded cell morphology of RNS-1 samples in section 2.3.2) necessitated the change in medium regimen to using very low serum concentrations. RNS-2 was then cultured with medium containing only 0.5% HS while also lowering the inoculation cell number to only 200×10^6 cells. The glucose and

lactate concentrations for RNS-2 both slowly decreased and increased, respectively, representing a more gradual proliferation of PC12 cells within the bioreactor.

Cell morphology within samples from RNS-2 showed healthy and adequate neurite outgrowth from the PC12 cells, but cell density throughout the bioreactor was not uniform. There were regions varying between high and low densities (seen below in section 2.3.2). This and other results from Western blot analysis of RNS-2 (described in section 2.3.3.3) lead to the continuation of RNS-3 with a higher initial cell inoculation number with low serum conditions to achieve a maximum density of cells and therefore neurites within the bioreactor to obtain the highest possible capacity for synapse formation between cells. However, lactate concentrations for RNS-3 did quickly plateau at only culture day 2. These PC12 cells do hold the property of contact-inhibition, where the cells will not proliferate past confluent densities, and therefore RNS-3 is suspected to have reached a maximum density. The cell morphology within RNS-3 showed confluent clusters of rounded cells, therefore the density for inoculation of RNS-4 was decreased to 700×10^6 cells. Also, to avoid the possibility of complete glucose depletion during the culture period, the baseline glucose concentration of the medium was doubled to 4000 mg/L. Most other bioreactor experiments performed by our group uses the control of CO₂ flow rate through the gas perfusion to maintain a healthy pH values, whereas RNS bioreactors are maintained already with 0 mL/min CO₂. The pH has to instead be regulated in these experiments by increasing the feed flow rate in order to flush the high accumulation of lactate. This method unfortunately makes it hard to predict ability to accurately predict the necessary increase in feed flow rate to maintain a healthy pH value. Including the higher glucose concentration in the baseline medium for RNS-4 made it even hard to predict the needed increase in feed rate. Culture day 1 and 2 for RNS-4 had feed flow rates already at 10 and 13 mL/hour, respectively,

while most other RNS bioreactors the feed flow rate was under 6 mL/hour for those culture days. However, the lactate concentration for RNS-4 on culture day 2 reached 17.9 mmol/L, which created a pH value of 6.8. The feed flow rate was then increased to 20 mL/hour to attempt to maintain the pH on culture day 3, but for the duration of the experiment the lactate concentration decreased possibly due to death of the cells based on the unacceptable environment. Upon opening of RNS-4 there seemed to be a significant amount of tissue formation, but again with the cells attaining rounded and clustered cell morphology (data not shown).

The cell inoculation numbers for RNS-3 and RNS-4 were then concluded to be too high for the cells to not reach confluency during the six day culture period, but the optimal density desired within the bioreactor by the end of the culture still was believed to be higher than the inoculation number for RNS-2 of 200×10^6 cells. Therefore, the next experiment of RNS-5 was inoculated with 300×10^6 , only a slight increase in cell number compared to the increase used for RNS-3 and RNS-4. Seen Figure 7 and Figure 8 the trends in glucose and lactate concentration are much more gradually increasing, similarly to that of RNS-2. Also, the pH values for RNS-5 were maintained between 7.2-7.4. The morphology of RNS-5 samples consequently had extensive neurite outgrowth with a high density throughout the volume of the cell compartment in the bioreactor (discussed below in section 2.3.2). Therefore, RNS-6 was performed to attempt replication of RNS-5 with a cell inoculation number of 300×10^6 cells. However, RNS-5 seemed to reach a plateau of lactate concentration on culture day 2 instead of day 3 for RNS-6.

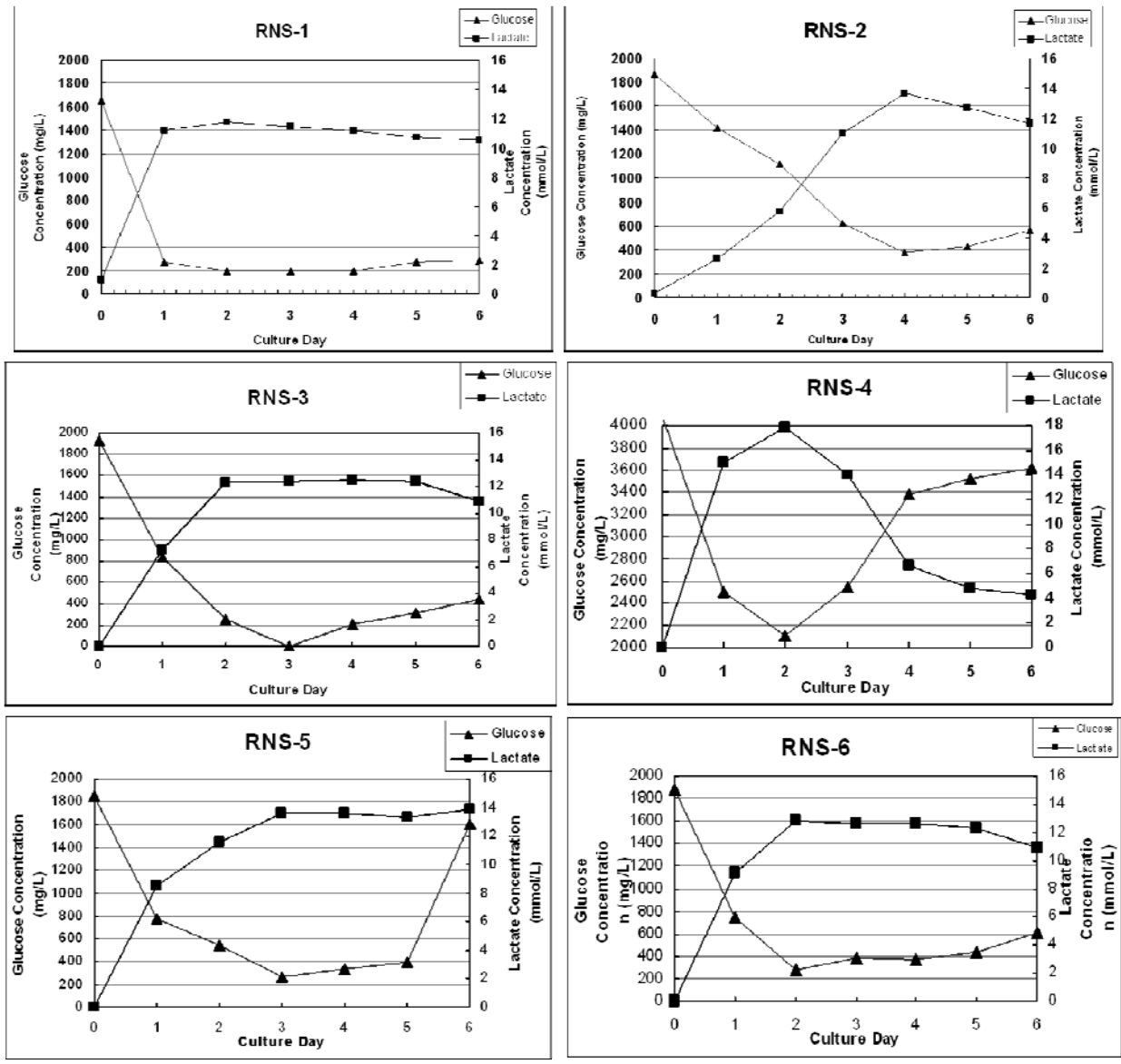


Figure 8. Bioreactor metabolism plots of actual daily measurements taken for glucose and lactate concentrations not accounting for feed flow rate.

2.3.2 Comparison of cell morphology and neurite outgrowth

PC12 cells are used as model neurons in tissue engineering specifically due to their ability to generate substantial neurite outgrowth when stimulated with NGF. The 2D control cultures of PC12 cells were traditionally plated on 2D tissue cultured treated polystyrene plates coated with

collagen type I at $5 \mu\text{g}/\text{cm}^2$ with 0.5% horse serum (HS) starvation for one day and then NGF supplementation at $75 \text{ ng}/\text{mL}$ for 5 days. These PC12 cells cultured for six days are shown in Figure 9 with immunocytochemical staining of neuronal class III β -tubulin (Tuj1 clonal antibody) with AlexaFluor 488 secondary antibody (green) and counterstained with DAPI for nuclear staining (blue) at magnification of 200X. β -III-tubulin within the PC12 cells shows up throughout the entire cytoskeleton of these cells and is a good marker representing the cell morphology and neurite outgrowth. Figure 9 demonstrates the ability of the PC12 cells to generate extensive neurite outgrowth within the control 2D culture and represents the motivation for use of these cells as a model neuron.

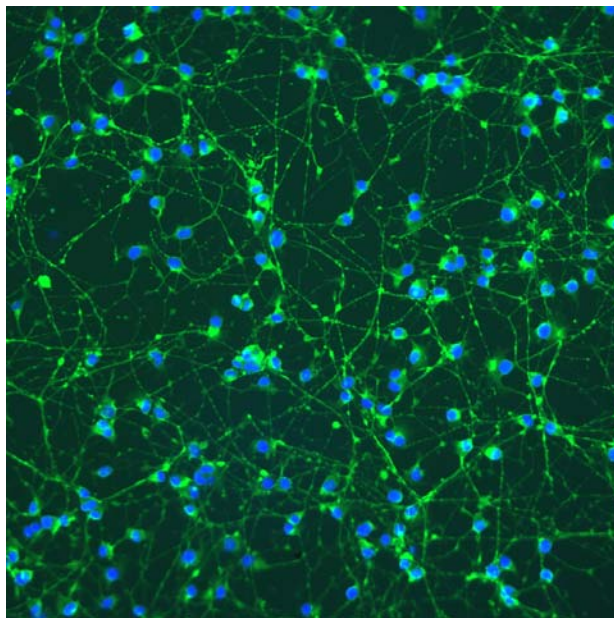


Figure 9. Cell morphology of 2D control PC12 cells cultured for 6 days on collagen coated dishes at a density of $127 \text{ cells}/\text{mm}^2$ with NGF stimulation showing β -III-tubulin neurite staining (green) and DAPI nuclear staining (blue) (confocal z-stack single image reconstructions $10 \mu\text{m}$ depth at magnification 200X).

3D static control cultures consisted of PC12 cells encapsulated in collagen type I hydrogels, where the cells are mixed with the 1 mL collagen solution and gelled in traditional

12-well tissue culture plates. The gels take the shape of the well with the approximate dimensions of 20 mm diameter and 2 mm height. The gels are kept in the 12 well plates, but free-floating in the culture media so that diffusion of nutrients can occur through all surfaces of the gel. The gels have a final collagen concentration of 1 mg/mL, which is the lowest possible collagen type I concentration in order to maintain a cohesive hydrogel. Gels made with lower collagen concentrations either do not completely form a hydrogel or degrade before the end of the necessary six day culture period (data not shown but these concentrations have been tested). Also, the lowest possible collagen concentration was used so that the PC12 cells are able to sprout their neurites throughout the porous gel and not be inhibited by a dense collagen matrix. Krewson et al. demonstrated that lower density collagen gels allow better neurite outgrowth from PC12 cells stimulated with NGF [224].

Figure 10 shows confocal fluorescent images representing the cell morphology of PC12 cells stimulated with NGF encapsulated in collagen type I hydrogels cultured with static conditions in a tissue culture plate in a 5% CO₂ humidified incubator with immunostaining of β -III-tubulin and DAPI. Figure 10a is representative of the growth of PC12 cells seeding 1×10^6 cells in the 1 mL gel volume with density 1×10^3 cells/mm³ after culture for six days. This density according to metabolic data in Figure 5 allows steady growth of the cells within the gel also with healthy conditions of pH and gas partial pressures. The image demonstrates the ability of these cells under adequate conditions to sprout long neurites in 3D throughout the collagen gel. Also demonstrated is the sparse final cell density with cells far apart in the representative image with seeding at the low 1×10^3 cells/mm³ initial density which prevents cells having close neighboring cells in all three directions for potential synapse formation.

Figure 10b is a representative image of the PC12 cells in the 3D static collagen gel with an initial seeding density of 2.5×10^6 cells for a density 2.5×10^3 cells/mm³. This image, however, does not demonstrate an increased number of cells present at this region of the gel compared to the lower density gel. It does demonstrate the decreased neurite outgrowth from the cells at this lower local density. The image in Figure 10b only represents a region of the gel near the edge where the best neurite outgrowth occurred, due to increased nutrient and gas diffusion for improved culture conditions. Figure 5 demonstrated that the metabolic activity of this density culture was high, but created unfavorable conditions with acidic pH values. The center of the gel had an increased local density, but the images shown in Figure 10 demonstrate representative images of the best neurite outgrowth within each culture.

Figure 10c represents the PC12 cell growth and neurite outgrowth of the cells seeding 5×10^6 cells in the 1 mL gel with initial density 5×10^3 cells/mm³. This image demonstrates the increased cell density within the gel compared to the other cultures where cells have neighboring cells in all three surrounding dimensions. However, due to the poor environment occurring from culturing this high density of cells under static conditions in the gels, as revealed in Figure 5, the representative image here shows little neurite outgrowth from the cells with most cells obtaining a rounded morphology instead. With the high density culture depleting its glucose every day and lactate accumulation producing a very acidic pH the effects are shown by preventing healthy neurite outgrowth from the cell.

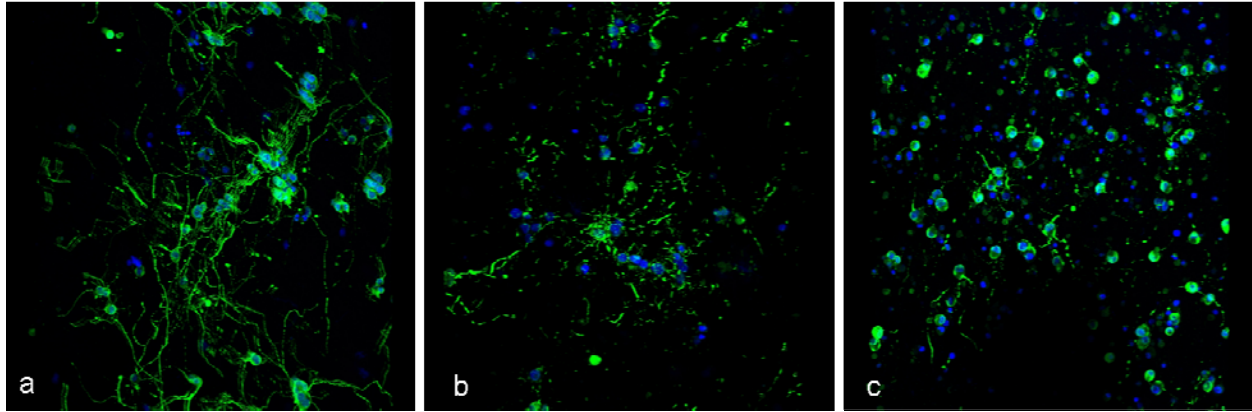


Figure 10. Cell morphology of 3D static controls of PC12 cells cultured for 6 days within 1 mg/mL collagen gels with NGF stimulation showing β -III-tubulin neurite staining (green) and DAPI nuclear staining (blue) at different densities: a) 1×10^3 cells/mm³, b) 2.5×10^3 cells/mm³, c) 5×10^3 cells/mm³ (all confocal z-stack single image reconstructions approximately 50 μ m depths at magnification 200X).

Six experiments were performed culturing the PC12 cells in the hollow-fiber based bioreactor maintaining dynamic flow conditions with decentralized oxygenation. Medium supplemented with 75 ng/mL NGF was circulated through the PVC tubing circuit, which perfused through the hollow fibers of the bioreactor to allow convective transport of nutrients to the cell compartment. Figure 11 illustrates the PC12 cells encapsulated in the collagen gel surrounding the extra-fiber space of the cell compartment of the 8 mL bioreactor of experiment RNS-2. The images demonstrate considerable neurite outgrowth from the PC12 cells throughout the collagen gel of the 3D cell compartment including dynamic homogeneous nutrition and oxygenation. Confocal fluorescent images representing cell morphology of the cells in regions with the best neurite outgrowth of most of the bioreactor cultures are shown in Figure 12. Images of RNS-3 and RNS-4 are not shown here, but look similar to the morphology shown in Figure 12a for experiment RNS-1 with most cells having a rounded morphology. RNS-1, RNS-3, and RNS-4 due to their high initial cell inoculation number (all over 700×10^6 total cells)

resulted in poor neurite outgrowth from the cells due to the contact inhibition that these cells maintain. RNS-3 and RNS-4 both reached deficient conditions of either glucose depletion or acidic pH values during the culture period and could be the reason for the rounded cell morphology within these experiments, however RNS-1 never achieved unfavorable culture conditions and the medium even contained higher serum content. It is likely that the reduced neurite outgrowth of these bioreactors is due to their overpopulation within the cell compartment with the contact inhibition properties preventing further overlap of the cells with neurites.

The bioreactor experiments RNS-2, RNS-5, and RNS-6 with the lower initial cell inoculation densities (fewer than 400×10^6 cells) were able to maintain substantial neurite outgrowth under the 3D dynamic perfused culture environment within the hollow fiber-based bioreactor. Figure 12b, c, and d represent the morphology of the PC12 cells in regions of these bioreactors, respectively, with the maximal neurite outgrowth. Throughout the culture period of RNS-2 there was a steady increase in metabolic activity from the cells. The image of Figure 12b demonstrates the morphology within a region of the bioreactor samples that had a moderate local density; however this was approximately representative of one third of the entire cell compartment. The other two-thirds of the cell compartment volume were at slightly lower and higher local densities (with the lower local density regions shown in Figure 11). Therefore the density within the bioreactor cell compartment for RNS-2 was not uniform and lead to increasing the initial inoculation cell number for the subsequent experiments. Conversely, the image shown in Figure 12c is representative of the morphology of the PC12 cells throughout the entire bioreactor culture space for RNS-5 with remarkable neurite outgrowth from cells in close proximity to each other. All images within this section for the 3D cultures are single images of z-stack reconstructions where the image shown is a compilation of the maximum intensity

projection of 50 images taken in the z-direction to represent the cells within the 50 μm depth of the 3D space imaged. Therefore, the images do represent the substantial 3D neurite outgrowth from the PC12 cells achieved under dynamic perfusion conditions with the hollow fiber-based bioreactor. The culture of RNS-5 and RNS-6 allowed sustainment of very high density PC12 cell cultures with extensive neurite outgrowth between cells. RNS-6 attempted to repeat the experiment of RNS-5 with the same initial conditions, but the cells within this bioreactor did not distribute evenly throughout the cell compartment and resulted in dispersed macroscopic tissue masses with low cell densities in between. The image shown in Figure 12d is representative of the cell morphology within one of the large tissue masses, but not representative of the entire cell compartment of the RNS-6 culture. Therefore, the overall cell morphology with extensive neurite outgrowth from PC12 cells maintained at a uniform high density was only achievable in the bioreactor culture of RNS-5.

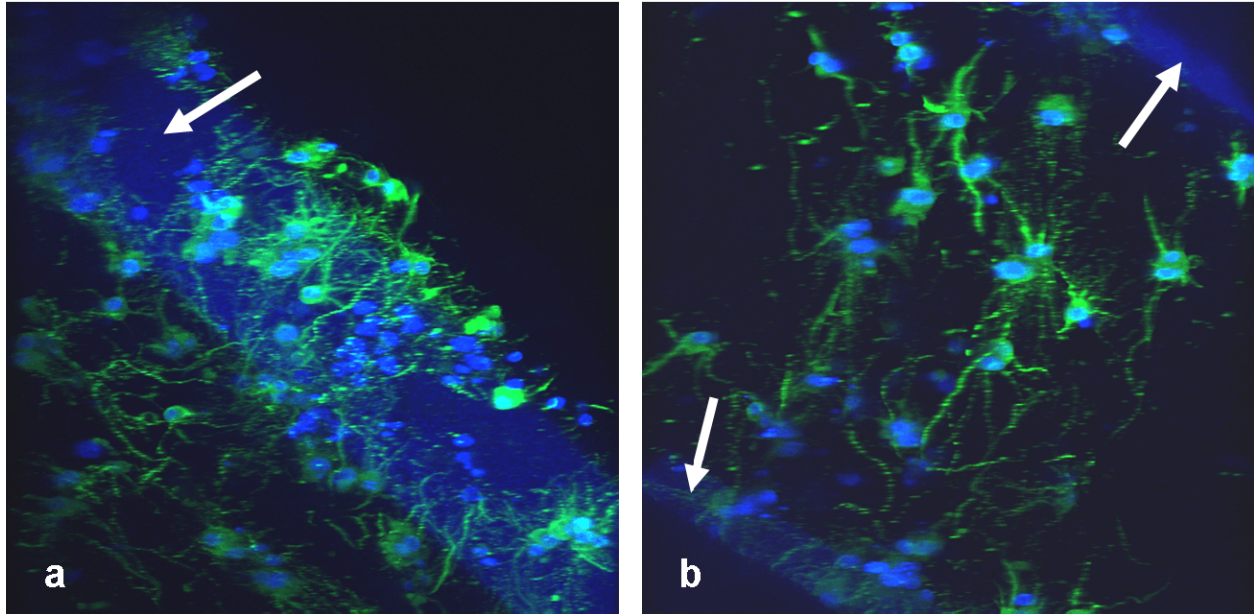


Figure 11. Confocal images (z-stack single image reconstructions with approximate 50 μm depths) of fluorescently immunostained PC12 cells (with antibodies against β -III-tubulin-green and DAPI-blue) at end of six day culture period within hollow-fiber based bioreactor (RNS-2) demonstrating neurite outgrowth from cells within collagen gel a) around medium perfusion hollow fiber and b) between two medium perfusion hollow fibers (arrows point to fibers; magnification 200X).

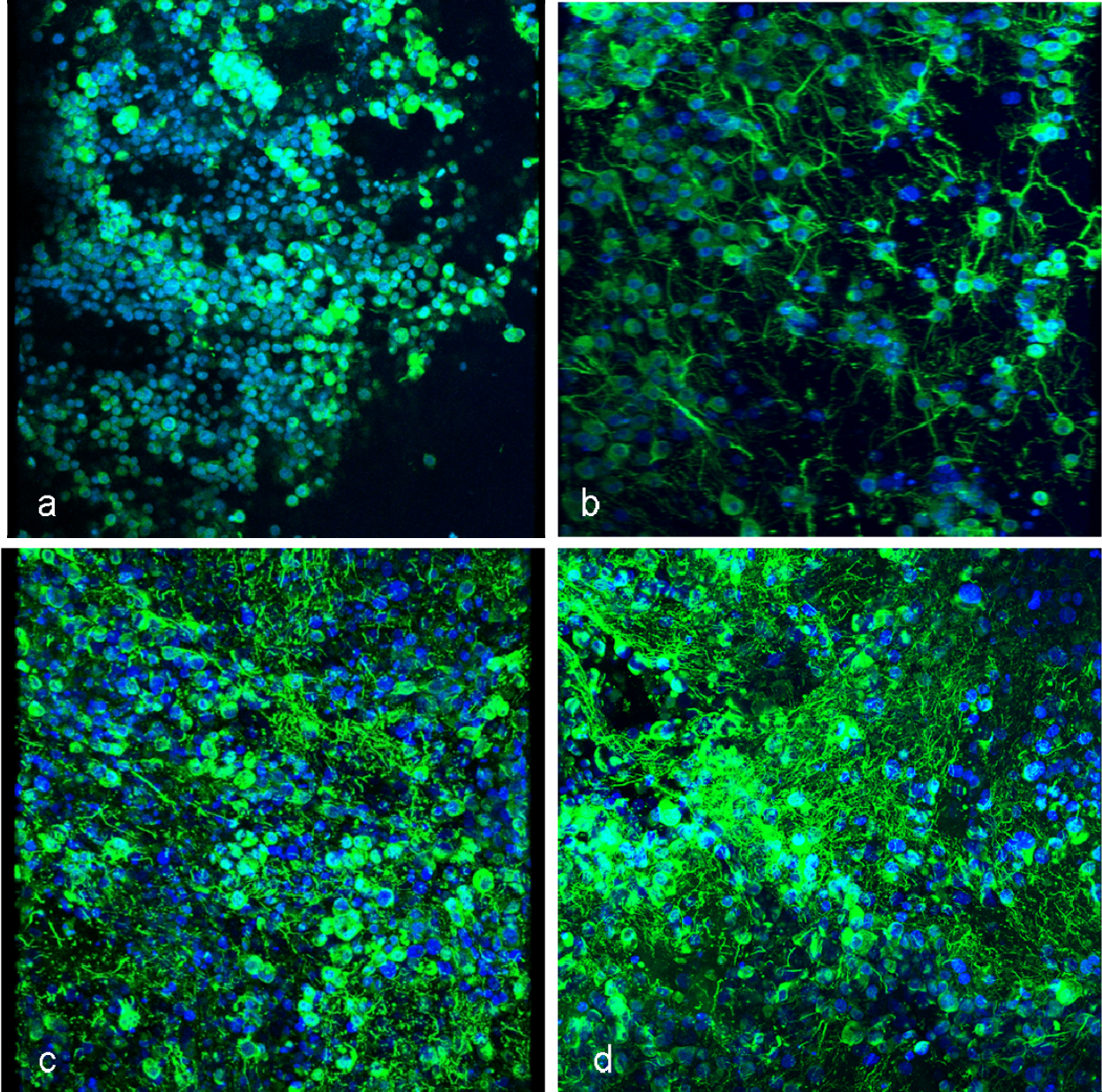


Figure 12. Cell morphology of 3D dynamic bioreactor cultures of PC12 cells with NGF stimulation showing immunostaining with antibodies against β -III-tubulin neurite staining (green) and DAPI nuclear staining (blue) for four of the different bioreactor experiments: a) RNS-1, b) RNS-2, c) RNS-5, d) RNS-6 (all confocal z-stack single image reconstructions approximately 50 μ m depths at magnification 200X).

2.3.3 Comparison of neuronal network formation

2.3.3.1 Synapsin I protein localization

Due to the significant neurite outgrowth achieved within the PC12 cells cultured with dynamic conditions in the 3D culture space of the bioreactor as well as in the 2D static control cultures we have further investigated the properties of the neurite networks formed. In order to observe synapse formation between PC12 cells after stimulation with NGF that have undergone neurite outgrowth after six days, we have detected synapsin I protein within the cells. Synapsin I localization within cells was observed using immunohistochemical staining with anti-synapsin I antibodies and visualized with confocal fluorescence microscopy. An example of synapsin I staining within a 10 μm thick section of a rat cortical brain slice is shown in Figure 13. Figure 14 displays the synapsin I (red) immunostaining throughout the 10 μm thick layer of cells with neurite networking cultured on the 2D collagen coated plate. Figure 14a displays the staining at low magnification where most cells stain positively for synapsin I, but the staining shows up mostly as diffuse speckles throughout the cell bodies. In Figure 14b at a higher magnification, the synapsin I in the PC12 cells cultured on 2D plates reveals more about the localization of the synapsin I protein. Both diffuse staining throughout the cell body can be seen as well as more clustered brighter staining within some nerve terminals and presynaptic terminal forming a synapse on a neighboring cell (white arrows in figure). This localization reveals the control cultures on traditional 2D plates have synapsin I not just localized the nerve terminals and therefore is not just a marker for synapse formation within 2D PC12 cell cultures.

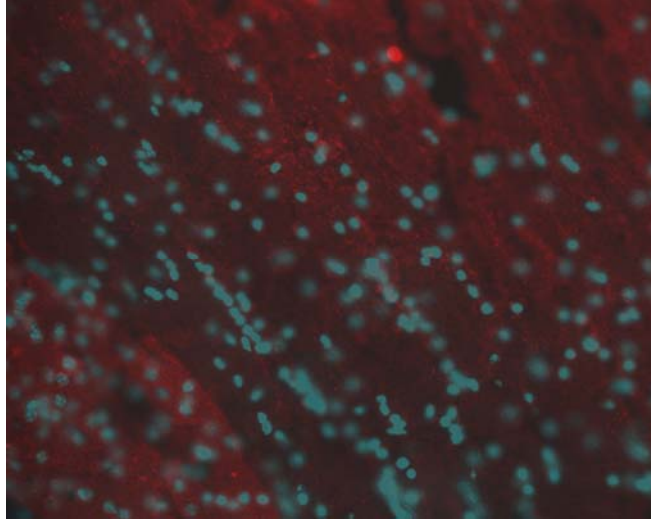


Figure 13. Fluorescent microscopic image of synapsin I immunostaining with Cy3 (red) in a rat cortical brain section with DAPI nuclear counterstaining (blue) at magnification 200X. Image depicts abundant red punctate staining with synapsin I staining in the brain.

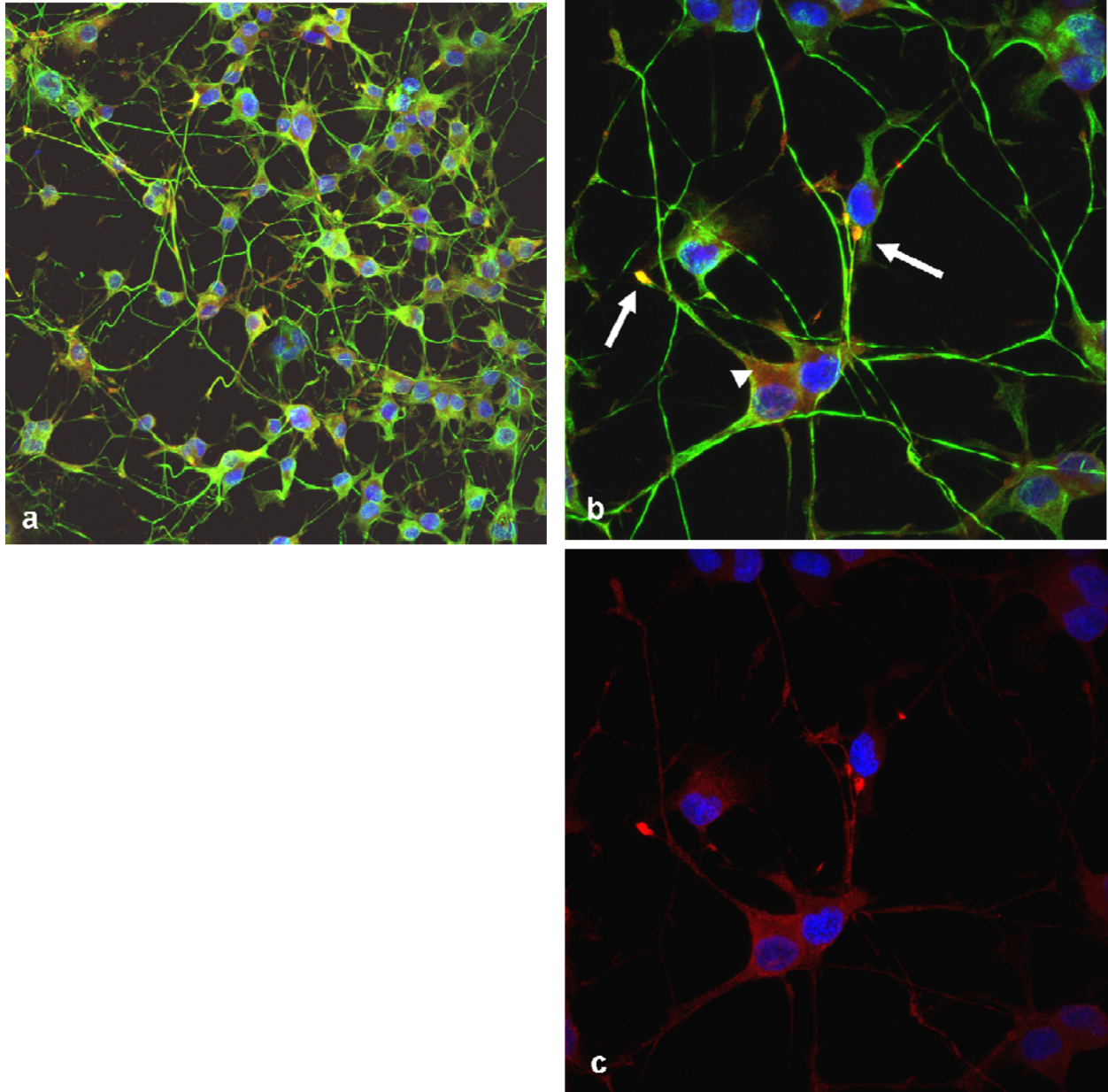


Figure 14. Confocal fluorescent images representative of 2D positive control PC12 cell cultures stimulated with NGF at the end of the six day culture period immunostained with antibodies against Synapsin I with Cy3 (red), β -III-tubulin with AlexaFluor 488 (green), and nuclear DAPI (blue) at magnifications of a) 400X, b) 1000X, and c) same image as b without green channel. In b, arrows point to brighter punctuate staining of Synapsin I clustered at nerve terminals while arrowhead points to diffuse Synapsin I staining throughout cell somata (single image z-stack reconstructions throughout entire 10 μ m depth of 2D culture).

Immunostaining of samples from PC12 cells cultured in 3D collagen gel within the dynamically perfused bioreactor environment of the hollow fiber-based bioreactor reveals different staining patterns than the 2D cultured cells. Figure 15-16 display confocal fluorescent images of regions within the successful bioreactor cultures with the best synapsin I staining (the images are not necessarily representative of the entire culture space). Figure 15a-b depicts the synapsin I staining in bioreactor experiment RNS-1 which is representative of regions in these samples where there was more neurite outgrowth. As described earlier, RNS-1 was cultured with high serum containing medium which lead to an increased proliferation of the cells over more neurite outgrowth, with Figure 12a showing many cells with a rounded morphology. However, where there was substantial neurite outgrowth from the PC12 cells within RNS-1, there was significant synapsin I staining as multiple bright puncta in many cells (revealed in Figure 15b). In bioreactor experiment RNS-2, the density of PC12 cells was lower and variable throughout the cell compartment. Figure 15c-d is an example of synapsin I staining in regions of RNS-2 where there was a higher cell density with increased neurite networking. This high density neurite networking within these regions of the bioreactor culture created numerous synapsin I⁺ puncta. In control samples testing for residual secondary fluorescent antibody within the sample by performing staining with deletion of primary antibody, no signal was seen throughout the samples with the 594 nm laser excitation (red signal for Cy 3 secondary antibody).

Subsequent bioreactor experiments were conducted to increase the cell density and therefore neurite networking density in order to achieve higher synapsin I expression within the 3D dynamic bioreactor cultures. Images of synapsin I staining within the cultures of bioreactors RNS-5 and RNS-6 are shown in Figure 16-16. RNS-5 culture samples achieved extensive

neurite outgrowth throughout the entire cell compartment. As a result synapsin I staining as bright puncta was observed throughout these samples. However, there were a few cells detected with diffuse synapsin I staining throughout the cell body as seen in one cell of Figure 16a. Most importantly, confocal fluorescent images of Figure 17 were taken immediately after the images seen in Figure 14b with the exact same laser intensity and image software settings. However, even with increasing signal intensities for synapsin I staining in the RNS-5 bioreactor samples, diffuse speckle pattern staining could not be found in most cells. This is demonstrated by there being only one cell within Figure 16a showing diffuse staining within the cell body with all other cells only possibly containing punctate staining.

PC12 cells cultured in bioreactor experiment RNS-6 experienced significant high densities and neurite outgrowth within certain distinct regions of the bioreactor where cells seemed to not distribute well upon cell inoculation. Despite the increased neurite outgrowth within these accumulated areas there was not as much bright punctate staining of synapsin I and instead more cells were seen with the diffuse synapsin I patterning as demonstrated in Figure 16d.

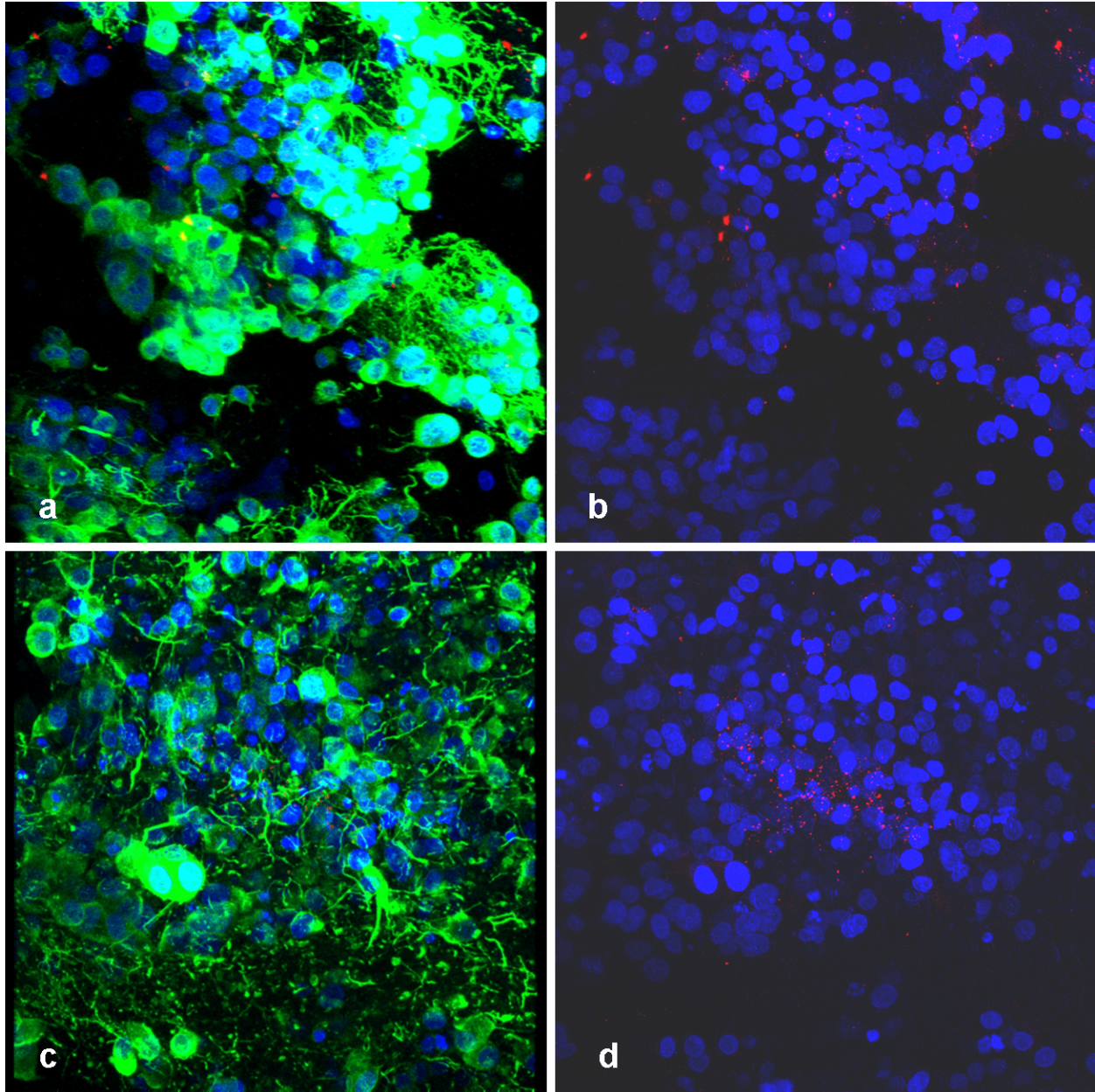


Figure 15. Confocal fluorescent images of 3D dynamic bioreactor cultures of PC12 cells stimulated with NGF at the end of the six day culture period for experiments RNS-1 in a and RNS-2 in c immunostained with antibodies against Synapsin I with Cy3 (red), β -III-tubulin with AlexaFluor 488 (green), and nuclear DAPI (blue) at magnifications of 400X; b and d repeats the images of the first column without the green layers of β -III-tubulin revealing all Synapsin I staining in red (single image z-stack reconstructions throughout a 50 μ m depth of the 3D samples).

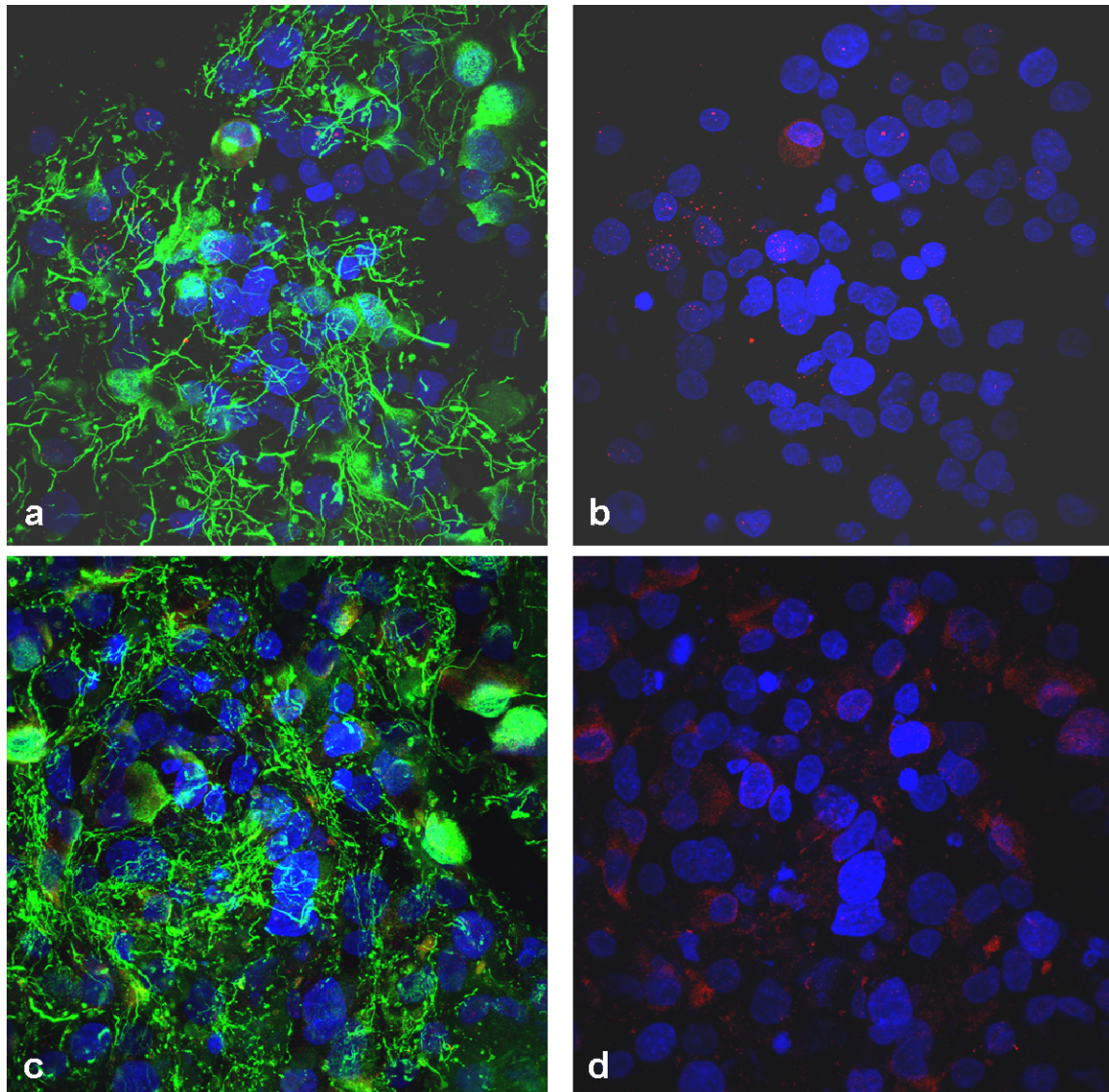


Figure 16. Confocal fluorescent images of 3D dynamic bioreactor cultures of PC12 cells stimulated with NGF at the end of the six day culture period for experiments RNS-5 in a and RNS-6 in c immunostained with antibodies against Synapsin I with Cy3 (red), β -III-tubulin with AlexaFluor 488 (green), and nuclear DAPI (blue) at magnifications of 600X; b and d repeats these images of the first column without the green layers of β -III-tubulin revealing all Synapsin I staining in red (single image z-stack reconstructions throughout a 50 μ m depth of the 3D samples).

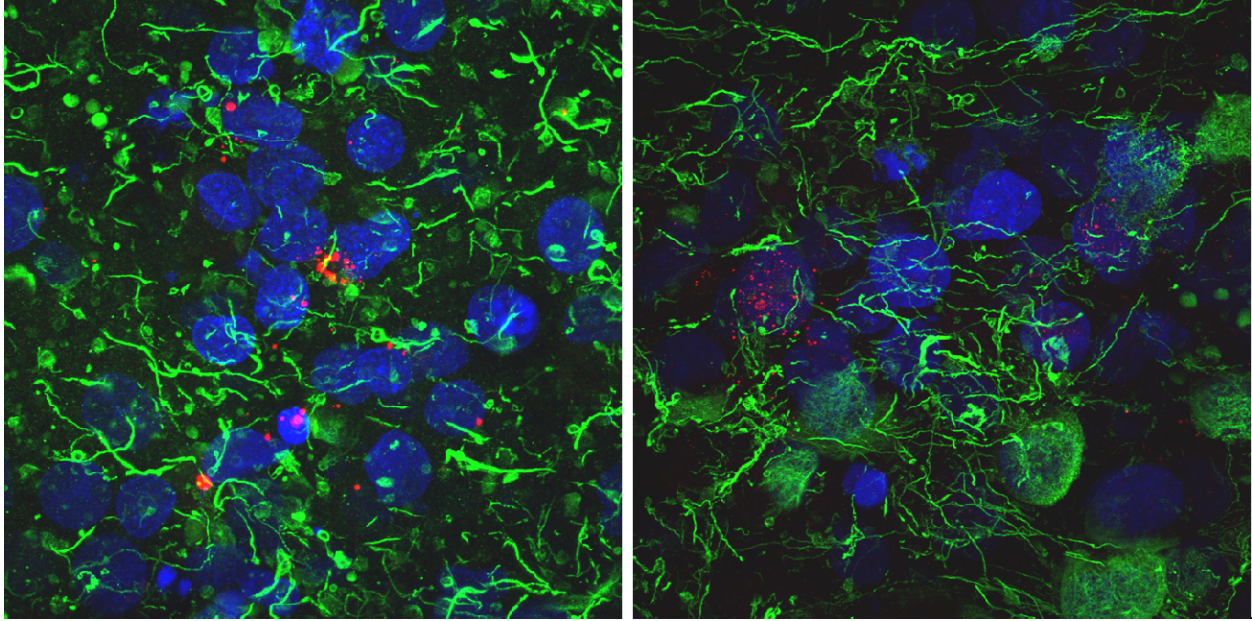


Figure 17. Confocal fluorescent images of 3D dynamic bioreactor cultures of PC12 cells stimulated with NGF at the end of the six day culture period for experiment RNS-5 immunostained with antibodies against Synapsin I with Cy3 (red puncta), β -III-tubulin with AlexaFluor 488 (green), and nuclear DAPI (blue) at magnification of 1000X (single image z-stack reconstructions throughout a 50 μ m depth of the 3D samples).

2.3.3.2 Synapsin I quantitative gene expression

Immunostaining with anti-synapsin I antibodies allowed localization of this protein, but further analysis was conducted to quantify this synapsin I expression in PC12 cells across culture methods. Gene expression data for PC12 cells cultured in bioreactor experiments RNS-1 through RNS-4 was not performed because RNA was not collected from these cultures. Figure 18 displays the results of quantifying Synapsin I gene expression using quantitative RT-PCR (reverse transcriptase polymerase chain reaction, quantifies mRNA transcripts produced in cells corresponding to the activity of synapsin I genes being transcribed). The first two bars on the graph show the difference in Synapsin I gene expression from PC12 cells in their normal chromaffin phenotype untreated with NGF compared to the neuronal phenotype after NGF

stimulation for five days during the culture period. Synapsin I gene expression between the PC12 cells cultured in 3D static collagen gels shows no significant differences between the cells cultured at the three different densities. There is a significant difference of Synapsin I gene expression of PC12 cells cultured at the low density in the 3D static collagen gels compared to the cells cultured on a 2D surface with NGF stimulation (p -value <0.05). The Synapsin I gene expression of cells cultured in the bioreactor RNS-5 is approximately equal to the 2D cultured cells with NGF stimulation. The expression within the RNS-6 bioreactor culture was, however, substantially lower.

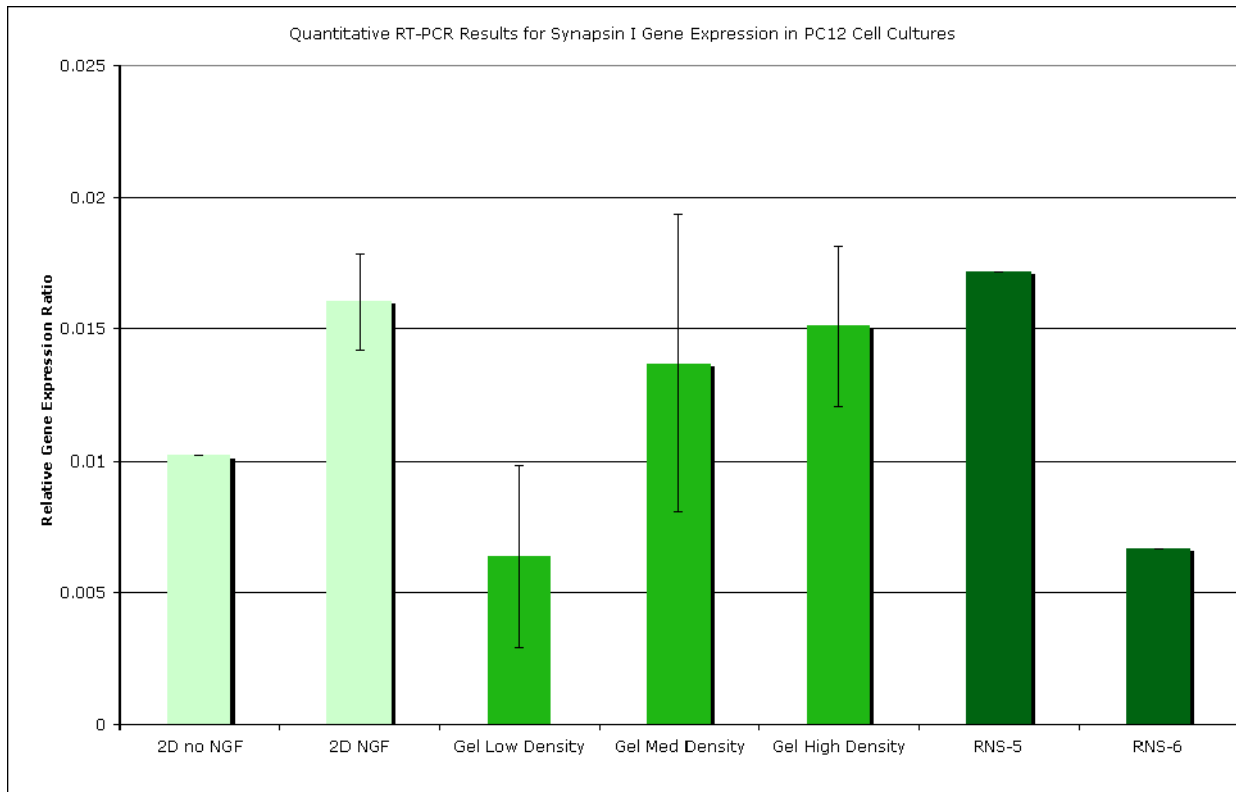


Figure 18. Quantitative RT-PCR results comparing gene expression ratios for synapsin I among different PC12 cell culture types (for 2D and gel cultures bars represent means $n = 3$ replicate cultures with error bars representing standard deviation).

2.3.3.3 Synapsin I protein quantification

We have implemented the Western blot assay in order to further quantify detection of the synapsin I proteins within the different culture methods of PC12 cells. The Western blots were carried out using the same anti-synapsin I antibody used for immunostaining results of section 2.3.3.1. Samples for bioreactor experiment RNS-1 were not possible because protein from this experiment was not collected from the cells. Western blots for samples from bioreactor experiments RNS-3 and RNS-4 were performed and showed no band for synapsin I detection since these bioreactors did reach unhealthy culture conditions (data not shown). Figure 19 shows the results of blotting for synapsin I as well as the loading control protein GAPDH with all samples run on the same gel and developed together with the same exposure time for each antibody. The control rat cortical brain whole cell lysate is shown on the farthest right lane loading only 1.5 µg protein. Even with this small amount of brain protein loaded synapsin I is so abundant in brain tissue that the blot shows up as a smear down the lane. The second to last lane contained a control ladder with known molecular weight standards showing that the synapsin I bands close to the 75 kDa marker. Synapsin I should be present as a 77-80 kDa molecular weight protein, which it does here as well in the PC12 cell samples. However, normal rat brain synapsin I shows up as a doublet at 77 and 80 kDa representing synapsin Ia and Ib isoforms. Within the PC12 cells it shows up as a singlet around these molecular weights.

The differences in protein detection between PC12 cells cultured on 2D plates without and with NGF stimulation are seen in the first and second lanes, respectively. Again, along with the results of qRT-PCR quantification of synapsin I expression in these two groups shows only a small increase due to NGF stimulation. There is a high level of protein already existing within the untreated non NGF-stimulated 2D cultured control PC12 cells of the chromaffin phenotype.

Lanes 3-5 represent the synapsin I protein detection of PC12 cells cultured statically in a 3D collagen gel at the low density of 1×10^3 cells/mm³, medium density of 2.5×10^3 cells/mm³, and high density of 5×10^3 cells/mm³. Protein collected from PC12 cells cultured in the 3D dynamic bioreactor of experiments RNS-2, RNS-5, and RNS-6 are shown in lanes 6-8, respectively. The bands detecting synapsin I for all NGF treated samples (which only excludes the first lane with control untreated PC12 cells) display approximately the same quantities of synapsin I protein within the samples. However, some samples such as the 2D NGF stimulated samples and all bioreactor samples display darker bands of lower molecular weights. These bands correspond to the banding pattern similar to synapsin IIa, IIb, and III. The sample for RNS-2 shows an increase of the band possibly correlating with synapsin IIa compared to the 2D NGF stimulated cultured cells.

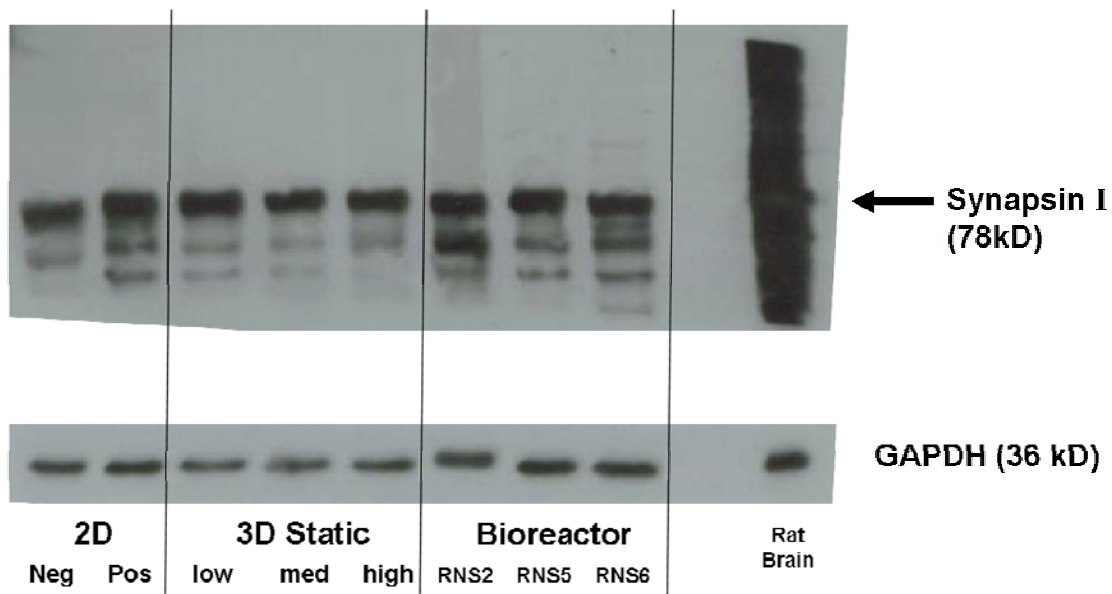


Figure 19. Western blot of all samples detecting synapsin I (~78 kDa). Samples include 2D cultured PC12 cells without (Neg) and with (Pos) NGF stimulation, 3D static collagen gel samples (3D Static) at the three different densities tested, bioreactor experiment samples from RNS-2, RNS-5, and RNS-6, and control rat cortical brain lysate. Some samples display multiple bands with a banding pattern similar to the lower molecular weights for Synapsin IIa, IIb, and III. Cortical rat brain lysate displays smearing of detection through the lane due to the abundance of synapsin I within the brain at the same sample loading as the PC12 cells. Also, with loading control GAPDH (36 kDa).

We have also detected synaptophysin by Western blot with the protein collected from the different PC12 cell cultures. The same Western blot above is shown in Figure 20 with re-blotting for synaptophysin. Synaptophysin is present as a synaptic vesicle associated protein within normal nerve tissue. However, for the PC12 cells synaptophysin is highly present within the normal untreated chromaffin phenotype cells. Upon NGF stimulation within the 2D cultures there is a decrease in synaptophysin expression, as shown in lane 2 compared to lane 1. The intensity of the bands for the PC12 cells cultured in the 3D static collagen gels shows an increase in synaptophysin with increasing density of cells cultured within the gels under static conditions.

The sample collected from bioreactor experiment RNS-2 displays very little synaptophysin detection, whereas the samples collected from bioreactor experiments RNS-5 and RNS-6 display a high detection of synaptophysin.

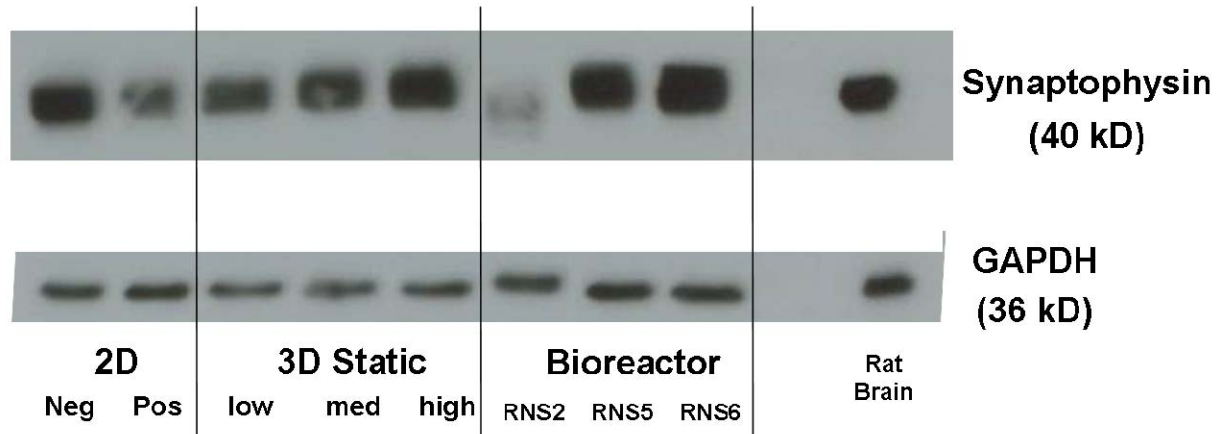


Figure 20. Western blot of all samples detecting synaptophysin (40 kDa). Samples include 2D cultured PC12 cells without (Neg) and with (Pos) NGF stimulation, 3D static collagen gel samples (3D Static) at the three different densities tested, bioreactor experiment samples from RNS-2, RNS-5, and RNS-6, and control rat cortical brain lysate. Also, with loading control GAPDH (36 kDa).

2.3.3.4 Phosphorylated Synapsin I localization

In order to further investigate synapsin I within PC12 cells with different culture methods we have continued by attempting to look at the phosphorylated active form of synapsin I. Synapsin I can be phosphorylated at least at six different sites, which are at serine residues and is the active form when phosphorylated. We have used antibodies specifically detecting synapsin I that is under current phosphorylation at two different sites. The first antibody used detected synapsin I phosphorylated serine 553 residue (Ser 553). The results of localization of this phosphorylated synapsin I and PC12 cells cultured on collagen coated 2D plates stimulated with NGF after the six day culture period is shown in Figure 21. These images represent areas within the 2D sample of the most significant staining detected. Within 2D cultured PC12 cells stimulated with NGF,

the phosphorylated synapsin I is detected mostly as small red puncta correlating with nerve terminals. However, there is still some phosphorylated synapsin I staining shown as diffuse speckling pattern throughout parts of the cell bodies in some of the cells. Therefore, this antibody more accurately shows active synapsin I within the PC12 cells, but is still not an exclusively specific marker for only synaptic transmission of a nerve terminal.

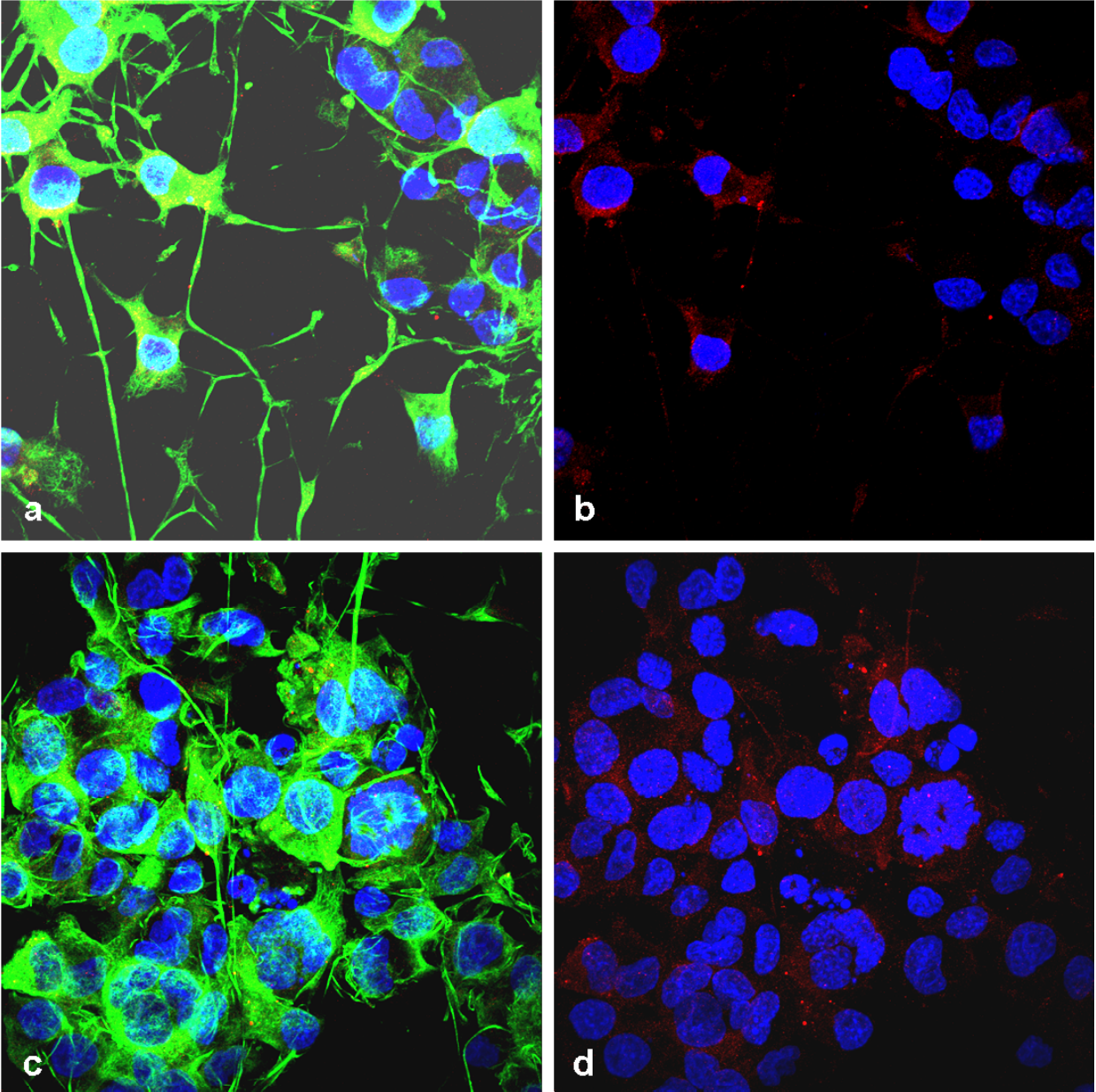


Figure 21. Confocal fluorescent images of 2D static cultures of PC12 cells stimulated with NGF at the end of the six day culture period immunostained with antibodies against phosphorylated-Synapsin I (site Ser553) with Cy3 (red puncta), β -III-tubulin with AlexaFluor 488 (green), and nuclear DAPI (blue) at magnification of 1000X (single image z-stack reconstructions throughout the 10 μ m depth). Images shown on right are same images on left excluding green channel allowing visualization of all phosphorylated synapsin I (Ser 553) staining.

Figure 22a represents a region within a sample from bioreactor experiment RNS-5 with significant phosphorylated synapsin I immunostaining. The image in Figure 22b is representative of staining seen throughout most of the RNS-5 tissue samples. Again, the staining for synapsin I phosphorylated at the serine 553 residue is detected as strong bright punctate staining with no diffuse speckle patterns throughout the cytoplasm. Later phosphorylated synapsin I staining was not performed on samples from bioreactor cultures RNS-1 and RNS-2 because all samples were already previously stained. Since synapsin I staining in samples from bioreactor culture RNS-5 were superior to that of RNS-6, these RNS-6 samples were not continued to be stained for phosphorylated synapsin I antibodies.

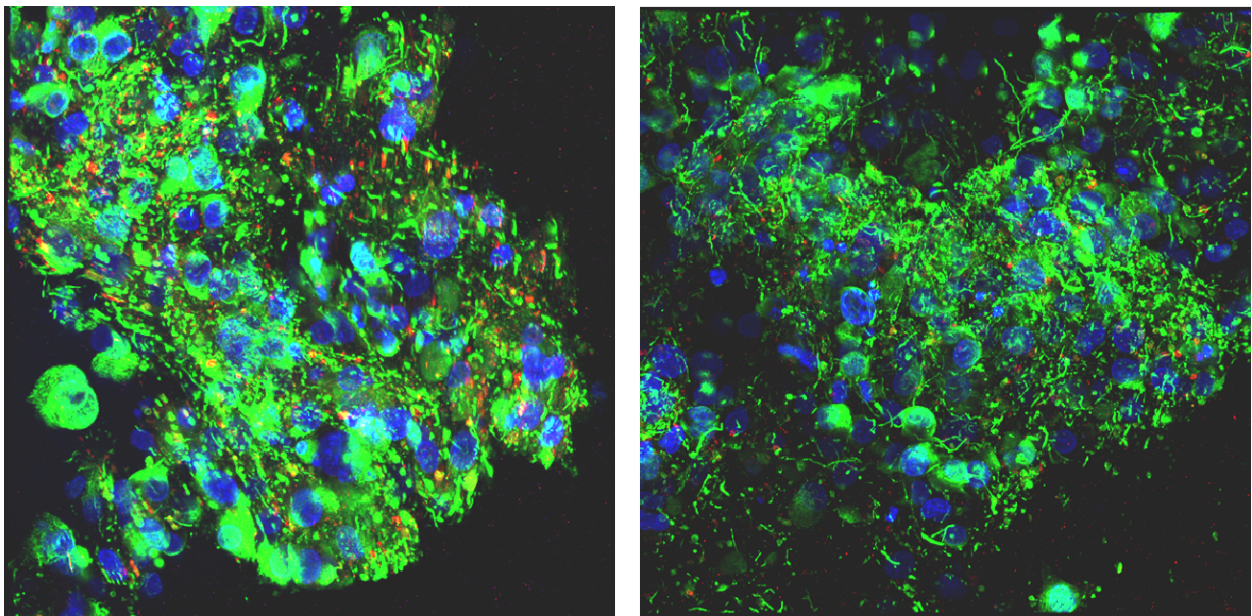


Figure 22. Confocal fluorescent images of 3D dynamic bioreactor cultures of PC12 cells stimulated with NGF at the end of the six day culture period for experiment RNS-5 immunostained with antibodies against phosphorylated-Synapsin I (site Ser553) with Cy3 (red puncta), β -III-tubulin with AlexaFluor 488 (green), and nuclear DAPI (blue) at magnification of 400X (single image z-stack reconstructions throughout a 50 μ m depth of the 3D samples).

2.3.3.5 Phosphorylated Synapsin I protein quantification

It was not possible to accurately detect phosphorylated synapsin I in RNS-2 bioreactor samples due to the protein collection method using a first step of collagenase digestion and lysis buffer not compatible with preserving phosphorylated protein states. Protein from PC12 cells was first collected using collagenase digestion step in order to remove collagenous proteins from samples leaving protein samples with mostly cell lysate. However, Synapsin I has a collagenase sensitive tail and digestion with collagenase might not allow complete recovery of cells with extensive neurite processes intact during centrifugation before the cell lysis step [213]. Control 3D static collagen gels were repeated in order to test the Ser 553 phosphorylated synapsin I antibody on the two different collection methods used. The first being collagenase digestion and cell lysis with MPER buffer and the second using TGN buffer added directly to entire collagen gel-cell construct treated like tissue. The results of this experiment are not shown, but proved that using the 3D static collagen gel cultures with protein collected via collagenase digestion and MPER lysis buffer were not able to detect phosphorylated synapsin due to no bands up for the western blot. However, we decided to include the RNS-2 protein sample the Western Blot shown in Figure 23 detecting phosphorylated synapsin I (Ser 553).

Figure 23 depicts the results of the Western blot detecting site Serine 553 phosphorylated synapsin I among samples from different culture methods of PC12 cells. In the last lane to the far right, a positive control sample of cortical brain lysate is shown marking the accurate molecular weight of approximately 80 kD for this protein. All protein samples used for this Western Blot, except for that of RNS-2, were collected immediately at end of culture with the lysis buffer preserving phosphorylated proteins. Therefore, the intensity of the band for the

RNS-2 bioreactor culture sample is not accurately accessible because the actually phosphorylated protein within this sample could have been higher.

The loading for this Western blot was not exactly equal across all samples as shown by different intensities of some GAPDH bands. Quantification of the intensities of the bands of Figure 23 was performed using free NIH Image J software. The results of expressing the relative intensity of the bands for p-synapsin I (Ser 553) to their respective GAPDH bands is show in Figure 24. Plotting this data shows an increase in phosphorylated synapsin I (Ser 553) found in samples from 2D PC12 cell cultures stimulated with NGF over the untreated non-NGF stimulated PC12 cells. The relative intensities for the 3D static collagen gel cultures demonstrate lower amounts of active phosphorylated synapsin I than either 2D NGF stimulated cultures or RNS-5 3D bioreactor culture with a further decrease among the 3D static cultures with increasing cell density. The 3D static gel with the highest initial cell density of 5×10^3 cells/mm³ contains the lowest amount of active phosphorylated synapsin I (Ser 553) demonstrating a large increase in cell density of cultures under static conditions does not allow increased active synapsin I. However, when comparing the samples of 2D cultured PC12 cells with NGF stimulation to the samples of 3D dynamic bioreactor cultures of RNS-5 and RNS-6 show equal detection of phosphorylated synapsin I (Ser 553).

Figure 25 demonstrates the Western blot using an antibody specific for site I phosphorylation on synapsin I on the serine 9 residue (Ser 9). The antibody used here was raised against a synthetic human phosphorylated synapsin I peptide. The antibody detected phosphorylation at site I of all isoforms of synapsin, including synapsin I, IIa, IIb, and III, corresponding to the four top bands appearing in Figure 25. This is only an example of the

banding pattern for p-synapsin Ser 9 and cannot be used to directly compare the 2D PC12 cell culture and bioreactor culture RNS-5 because loading was not checked with GAPDH.

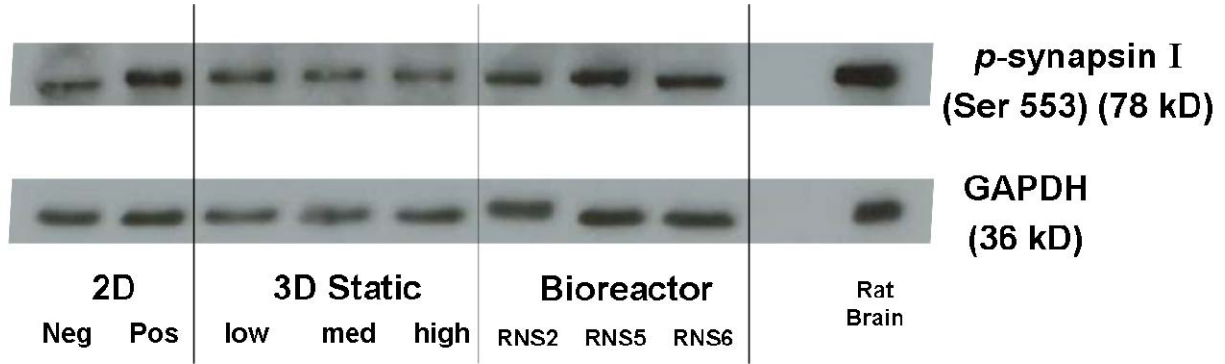


Figure 23. Western blot of all samples detecting Synapsin I phosphorylated at the Ser 553 site (~78 kDa). Samples include 2D cultured PC12 cells without (Neg) and with (Pos) NGF stimulation, 3D static collagen gel samples (3D Static) at the three different densities tested, bioreactor experiment samples from RNS-2, RNS-5, and RNS-6, and control rat cortical brain lysate. Also, with loading control GAPDH (36 kDa).

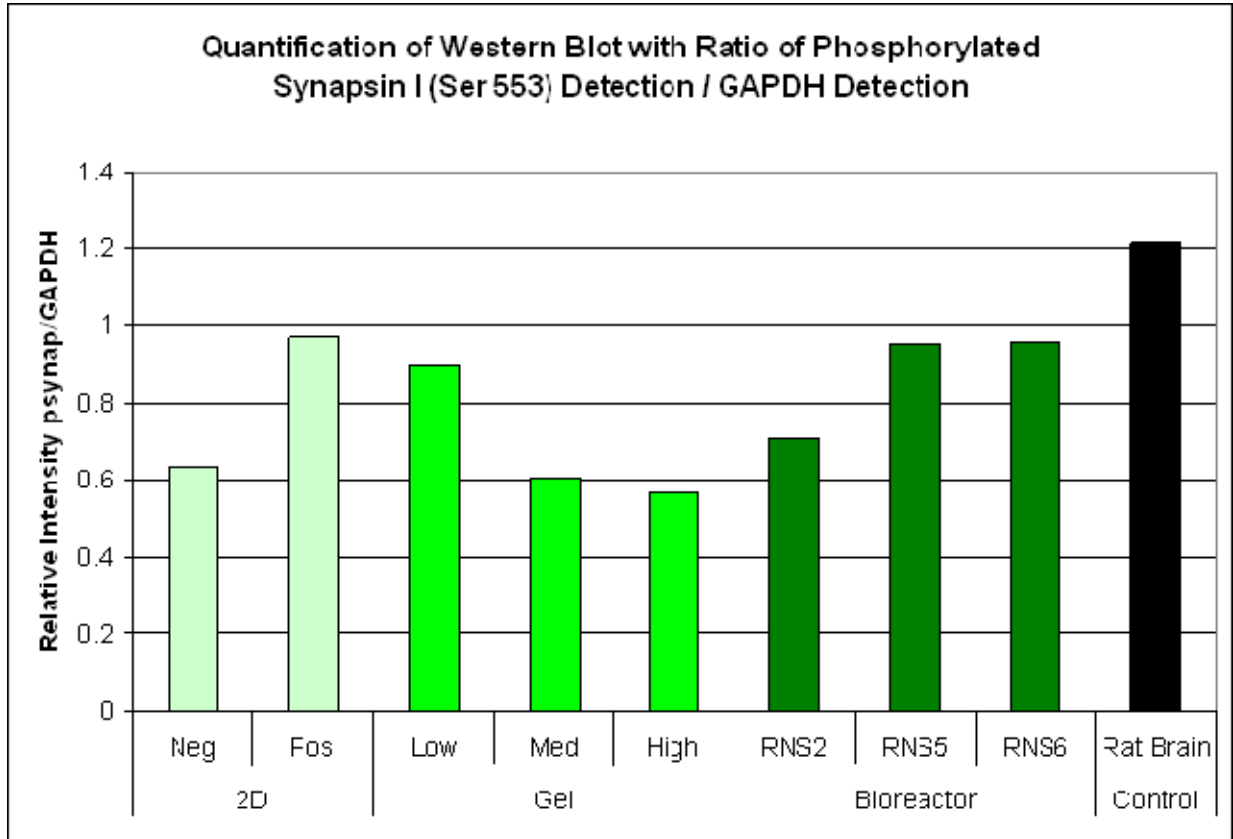


Figure 24. Quantification of Western blot for synapsin I phosphorylated at serine 553 (Ser 553) by measuring band intensities with NIH software ImageJ and plotting ratio of p-synapsin I (Ser 553) to GAPDH to normalize samples accounting for unequal loading (Gels are shown labeled as the three different densities tested).

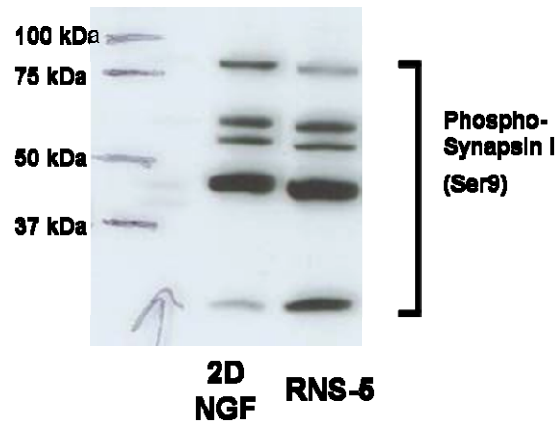


Figure 25. Example of Western blot using antibody detecting Synapsin I phosphorylated at the Ser 9 site; this antibody should be specific but instead shows a multiple band pattern similar to that of all four synapsin proteins at their respective molecular weights (MW ladder shown on left).

2.4 DISCUSSION

For PC12 cells cultured under static conditions within 3D collagen gels, only very low densities were effectively able to be maintained. The culture of 2.5×10^6 cells/1 mL gel was not able to maintain sufficient nutrition and acceptable pH values. The culture of 5×10^6 cells/1 mL gel reached conditions of depleted glucose as soon as culture day 2 also with pH levels mostly below 7.0. Cell morphology visualized with confocal fluorescence microscopy revealed only cultures at low density within static 3D collagen gels provided conditions necessary for extensive neurite outgrowth from the cells. This metabolic data seems to indicate that the acidity of the culture medium is due to the lactate accumulation rather than the limitations on gas diffusion within the static culture. Cullen et al. describe cultures of rat embryonic cortical neurons with postnatal astrocytes at densities above 5×10^3 cells/mm³ under static conditions in 3D had significantly reduced viability of cells [225]. They also observed delayed cell death at low density cultures, possibly due to the lack of available neuron-neuron interactions. This work along with the literature demonstrates the need for dynamic conditions in order to sustain high density neuronal cell cultures in thick 3D configurations. Also, very thick 3D tissue formation will eventually also be limited by gas transport through a tissue maintained in a scaffold only having dynamic perfusion of medium. This problem is as easily solvable as increasing medium flow rates using the hollow fiber-based bioreactor designs used here. These limitations are outlined in the below diagram of Figure 26 and how the design of the hollow fiber-based bioreactor is able to resolve these issues.

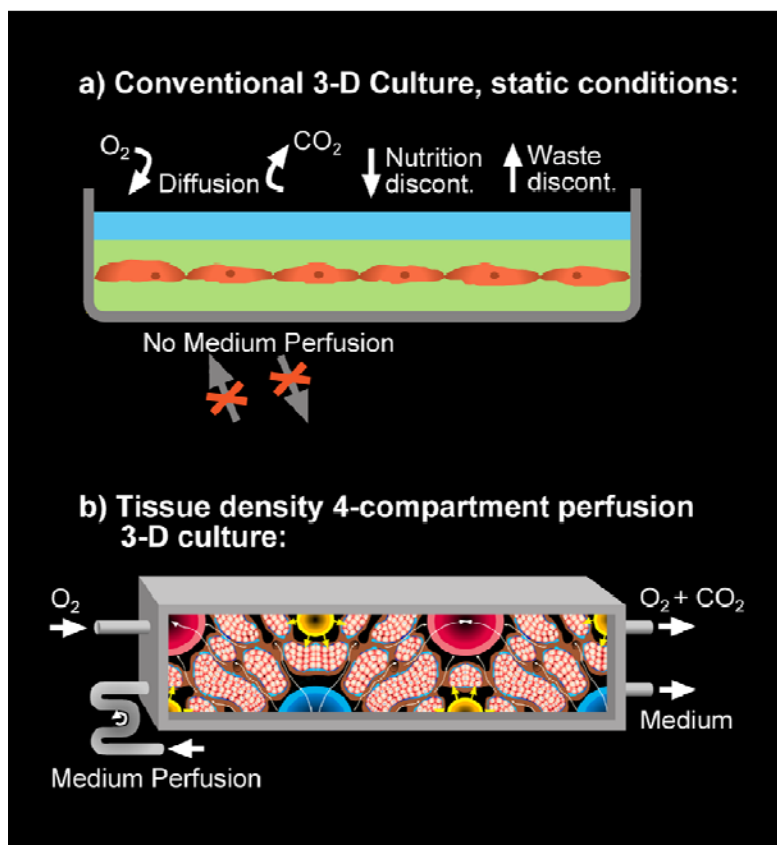


Figure 26. Diagram describing differences in culture conditions between a) 3D static conditions with cells encapsulated within an ECM hydrogel scaffold maintained in a Petri dish and b) 3D dynamic conditions with cells within the cell compartment of the 8 mL hollow fiber-based bioreactor (yellow tubes indicating gas perfusion fibers and red and blue tubes indicating counter-current flow through medium perfusion fibers).

Using lactate concentration as an indicator of cell number, the metabolic data from 3D static and 3D dynamic bioreactor cultures demonstrates the ability of the PC12 cell line to proliferate at different rates depending on the surrounding cell density. The lactate curve for the 1×10^6 cells/gel culture only reaches a maximum of 3 mmol/L by the end of the culture which is approximately only 20% of the concentration reached by the other density cultures, which both reach the same concentration at 16.5 mmol/L. This is in contrast to initial reports of NGF effects on PC12 cultures where proliferation ceases upon NGF stimulation and neurite outgrowth

begins[191, 192, 226, 227]. It is only under higher serum conditions that PC12 cells have a doubling time of 48-96 hours [227].

The culture of PC12 cells within the hollow fiber-based bioreactor maintaining dynamic flow conditions with perfusion of the cell compartment allowing homogeneous and decentralized nutrition and oxygenation allowed significant neurite outgrowth in three dimensions throughout the collagen gel. In bioreactor experiments such as RNS-5, significant neurite outgrowth was visualized throughout the entire 8 mL cell compartment of the bioreactor. Macroscopic tissue formation was seen in all bioreactor experiments. Traditional two dimensional culture plates allow extensive neurite outgrowth between PC12 cells, but the only method able to produce extensive neurite outgrowth especially at high densities throughout 3D collagen gels was using dynamic conditions in the hollow fiber-based bioreactor.

We have observed synapsin I expression in PC12 cells among the different culture types using immunohistochemical staining visualized with confocal fluorescence microscopy, Western blot, and qRT-PCR. Within control 2D static PC12 cell cultures, Western blot and qRT-PCR revealed an initially high level of synapsin I expression within untreated non-NGF-stimulated PC12 cells. Also, the qRT-PCR data presented here revealed a very small increase in synapsin I gene expression in NGF treated PC12 cells over untreated. Romano et al. described a low level of synapsin I expression detected with Western blot from untreated PC12 cells, with a significant increase in detection of NGF treated PC12 cells [214]. Das et al. plotted a curve representing a significant increase in synapsin I over the course of 6 day NGF stimulation in PC12 cells [220]. We expected a higher increase in synapsin I expression in the control 2D cultures between non-NGF stimulated cells and NGF stimulated cells in order to see a range of expression according to increased neuronal phenotype of the PC12 cells over their non-neuronal phenotype. However,

the cells used in these studies are Neuroscreen-I cells, a sub-cloned population of the original PC12 cell line used in other previous studies and could be the reason for discrepancies between our results with previous reports. Other inconsistencies have arisen using the PC12 cell line between initial cell line use and more recent reports including PMNT activity and epinephrine synthesis [228]. Eaton et al. purport discrepancies to be due to lack of cell line subcloning to achieve homogeneous populations and that initial reports were most likely using a very heterogeneous population of cells [228].

The lower increase in synapsin I expression demonstrates an inadequacy of the PC12 cell line to perfectly model real neurons. As described earlier, real neurons of the developing nervous system display an increase of synapsin I expression correlating with neurite outgrowth and synaptogenesis. Romano et al. also claims synapsin I detection by Western blot was independent of cell density [214]. If synapsin I quantification is not density dependent within PC12 cells, it cannot correlate with synaptogenesis. This implies synapsin I is not a useful marker to delineate the stage of the chromaffin phenotype of the PC12 cell to the neuronal phenotype after NGF stimulation, especially referring to synaptogenesis. Therefore, our results of Western blot quantification and qRT-PCR do not necessarily show that the 3D dynamic bioreactor cultures of PC12 cells are only equal in synapse formation compared to control 2D static cultures based on comparing synapsin I expression.

Normal non-neoplastic cells of the medullary regions of the adrenal gland are chromaffin cells. The normal function of chromaffin cells in the adrenal gland is to store catecholamines, including dopamine and epinephrine, and release them upon stimulation by the sympathetic nervous system directly into the blood and not through typical synapses [228]. These chromaffin cells do not express synapsin I, but the neoplastic aspect of the PC12 cell line makes them very

different from their non-transformed chromaffin cell counterparts [214, 228]. The chromaffin cells secrete the catecholamines via abundant membrane-bound dense granules which are only transported along microtubules to the cell surface [228]. The functions of chromaffin cells closely resemble that of neurons, which have the same function of neurotransmitter secretion except via specialized synapses. PC12 cells potentially very closely resemble neurons even at the untreated chromaffin like phenotype without NGF stimulation. Again, use of this cell line to specify enhanced neuronal phenotypes comparing treated vs. nontreated controls may not allow enough change expression of proteins useful in synaptic transmission due to the similarities of vesicle transport and catecholamine secretion in both phenotypes with and without NGF stimulation. It is possible that the subcloned population available as the Neuroscreen-I line of the PC12 line, is already a more neuronal-like phenotype population than the original PC12 line and a reason for the increase in synapsin I expression.

Localization of synapsin I with immunohistochemistry and confocal fluorescent microscopy revealed that NGF stimulated static 2D cultures had diffuse staining throughout the cell bodies of cells and brighter clustered staining only at nerve terminals, especially those forming synapses with neighboring cells as seen in Figure 14. The results of Foster-Barber and Bishop display synapsin I staining in PC12 cells stimulated with NGF as bright diffuse staining throughout the entire cytoplasm of all cells [229]. It is possible that the non NGF-stimulated PC12 cells maintain diffuse levels of synapsin I throughout the cytoplasm and after NGF stimulation the synapsin I partially relocates to the nerve terminals and presynaptic endings of the neurites formed. This theory would imply the importance of synapsin I localization using immunostaining with fluorescence microscopy instead of whole cell lysate protein collection and quantification by Western blot.

Surprisingly, immunostaining of samples from 3D dynamic bioreactor cultures for synapsin I mostly showed bright punctate staining. It was only in some cells of samples from experiment RNS-6, where qRT-PCR synapsin I expression was lower, that diffuse synapsin I staining throughout a cell body was ever seen in bioreactor samples. Images shown in Figure 15 and Figure 17 display this staining as bright red puncta of varying sizes. Brigadski et al. discusses secretion of neurotrophins from synapsin I positive presynaptic terminals in hippocampal neurons displaying immunostaining for synapsin as similar bright immunoreactive dots [230]. Results of Gitler et al. also show similar fluorescent punctate staining of synapsin I in neurons as bright varying sized dots [212]. Unfortunately, here in our work the confocal microscopic images display a substantial amount of broken neurites. This is due to the sample retrieval methods after opening the bioreactor, where the samples including the hollow fibers are cut out using a scalpel as seen in Figure 6. Therefore, it is difficult to precisely localize the bright punctate staining of synapsin I in the bioreactor samples only to nerve terminals and synapses.

However, it is possible that this punctate staining does express a significant difference in synapsin I of PC12 cells cultured with dynamic conditions in three dimensions within the bioreactor over the 2D static control cultures. Z-stacks of confocal images displayed as rotating 3D reconstructions among only some images where the neurites are more intact, especially from samples of RNS-1, reveals the bright red punctate staining can be localized to nerve terminals. This is only observable by 30 degree rotation of the 3D reconstructed image to demonstrate the synapsin I red puncta around the surface of a cell membrane. An example of this staining in an image from bioreactor experiment RNS-1 is shown in Figure 27 below. The variable size of the immunoreactive red puncta can be explained with varying sizes of synaptic vesicle clusters

(SVCs). Bloom et al. demonstrated with transmission electron microscopy the localization of synapsin I to SVCs as individual dots within the clusters of vesicles at a very high magnification [207]. Figure 28 is a diagram from this report demonstrating the visualization of an SVC by reconstructing the TEM serial sections. This depicts the bright red puncta in immunostained images with our work to correspond to a collection of synapsin I proteins throughout an SVC, so the brighter the puncta the larger the SVC is containing more vesicles. The larger, brighter synapsin I puncta staining within the 3D dynamic bioreactor cultures of PC12 cells over the 2D control cultures possibly infers there are larger SVCs generated within some of the PC12 cells cultured with dynamic 3D perfusion conditions. Also, due to the lack of diffuse synapsin I staining throughout the cell bodies of the 3D bioreactor samples it is likely that these cells have further matured and undergone complete synaptogenesis with present synapsin I collecting in SVCs to function more like real neurons for synaptic vesicle trafficking instead of the more chromaffin like phenotype of granule secretion directly through the cytoplasm.

Tao-Cheng et al. have demonstrated very similar results comparing synapsin I and synaptic vesicle clustering comparing 2D cultured NGF treated PC12 cells with both NGF stimulation and K-ras oncogene overexpression [231]. These authors demonstrated with electron microscopy that synapsin I⁺ synaptic vesicles clustered with larger numbers of synaptic vesicles and at higher frequencies with the additional treatment of ras overexpression. Even with these differences observed the two treatment groups from imaging synapsin I expression they observed no difference when quantifying synapsin I with Western Blot. The doubly treated cells had the same overall quantification of synapsin I compared with the NGF treated cells. Therefore, these results support our hypothesis that the increased punctate immunostaining of synapsin I within the PC12 cells cultured within the 3D dynamic bioreactor correlates with more synaptic vesicle

clustering compared to the 2D cultures. Also, these authors discuss synaptophysin expression among the PC12 cells explaining that with electron microscopy synaptophysin is localized not just to synaptic vesicles within normal untreated PC12 cells, but as well as other organelles such as Golgi apparatus. They demonstrate that there is a re-localization of synaptophysin within PC12 cells after NGF stimulation to the synaptic vesicles of the nerve terminals. However, there is an overall decrease in synaptophysin expression within normal 2D cultured samples. Here, we see this increase in synaptophysin among the 3D statically cultured collagen gels with higher densities, correlating with the poor differentiation of these cells to the neuronal phenotype. However, the increase of synaptophysin within the RNS-5 bioreactor sample could correlate with an increase in the synaptophysin that is localized to the nerve terminals. Further work to clarify this with synaptophysin immunostaining and confocal fluorescent microscopy could therefore demonstrate further possible differences between the 2D cultures and 3D dynamic bioreactor cultures.

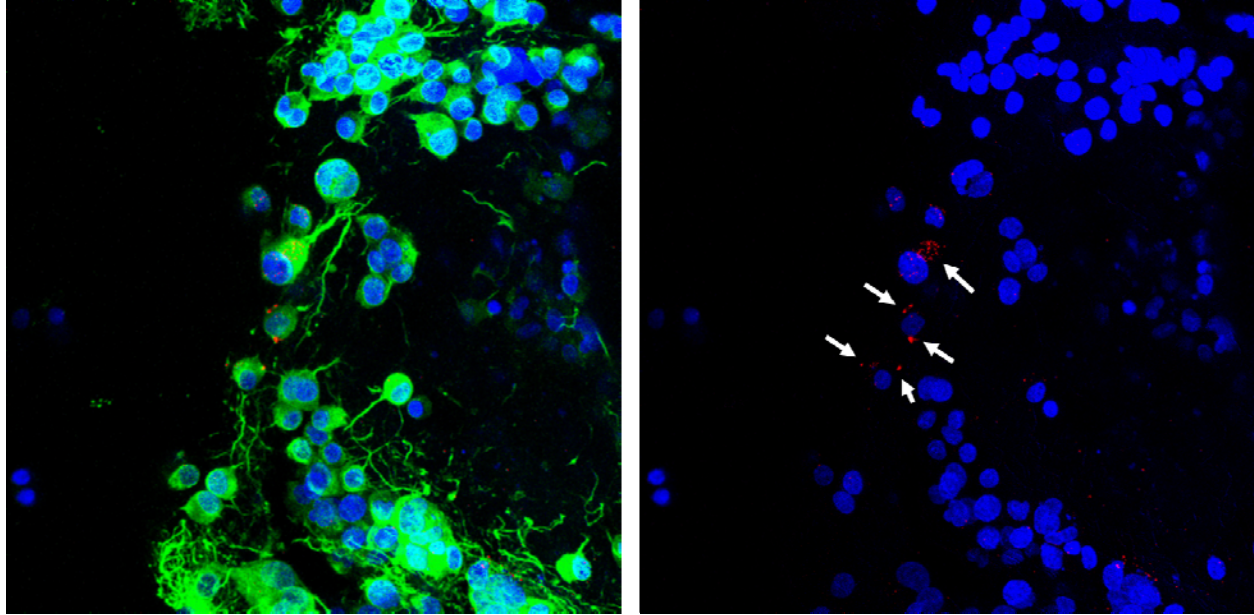


Figure 27. Confocal fluorescent images of 3D dynamic bioreactor cultures of PC12 cells stimulated with NGF at the end of the six day culture period for experiments RNS-1 immunostained with antibodies against synapsin I with Cy3 (red), β -III-tubulin with AlexaFluor 488 (green), and nuclear DAPI (blue) at magnification 400X. Image to right is duplicate of image on left without the green layers of β -III-tubulin revealing all Synapsin I staining in red (single image z-stack reconstructions throughout a 50 μ m depth of the 3D samples). Arrows point to red punctate staining of synapsin I that localizes to the surface of the PC12 cells shown, which is further demonstrated by rotation of 3D reconstructed images.

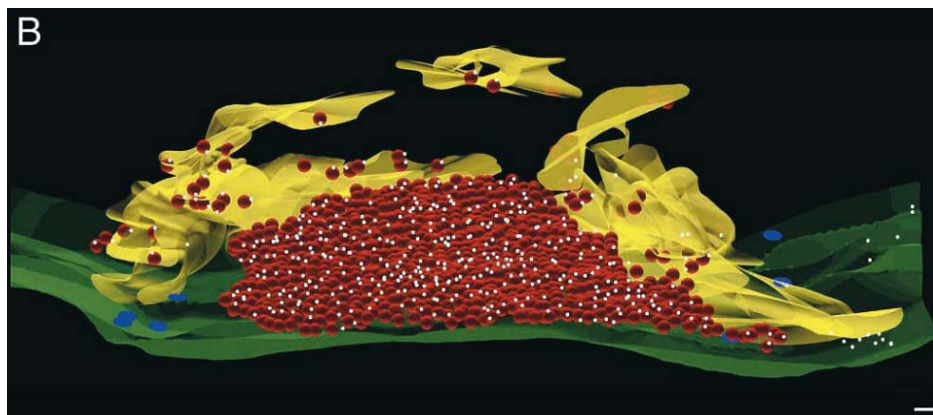


Figure 28. From Bloom et al. a 3D reconstructed diagram of a synaptic vesicle cluster. Synaptic vesicles are shown as red spheres with white dots representing synapsin I tethering the vesicles in the cluster. The plasma membrane marking the border dividing the presynaptic cleft at the top portion and postsynaptic dendrite to the bottom is shown in green. An actin rich cytomatrix is shown in yellow surrounding the SVC.

In order to further investigate synapsin I within PC12 cells with different culture methods we have continued by attempting to look at the phosphorylated active form of synapsin I. Synapsin I can be phosphorylated at least at six different sites, which are at serine residues. The protein undergoes conformational changes after phosphorylation that decreases the binding affinity for tethering the synaptic vesicles together. Hosaka et al. demonstrated that phosphorylation of the synapsins at site I or serine residue 9 dissociates synapsins from synaptic vesicles and shows this site phosphorylation significance for participating in synaptic transmission within normal neurons [206]. However, Romano et al. and Hall et al. discovered that NGF stimulation of PC12 cells phosphorylated synapsin I at a novel specific site, that of serine residue 553 [209, 232]. We have therefore used antibodies directed towards both phosphorylation sites in order to investigate active synapsin I protein within the PC12 cells among the different culture methods. The Western blot using the site I Ser 9 antibody detected

this site within all four synapsin isoforms and therefore made it unable to easily quantify this detection.

Since the site Ser 553 is more relevant within NGF stimulated PC12 cells, we have focused on the use of the antibody directed towards this site. Immunostaining results with this antibody showed very few bright puncta of active synapsin I within control 2D cultured PC12 cells with NGF stimulation. Immunostaining with this antibody on bioreactor cultured PC12 cells for experiment RNS-5, however, contained numerous bright puncta throughout the tissue samples. However, again quantification with Western Blot of the phosphorylated synapsin I at Ser 553 evidenced in Figure 24 showed approximately equal levels of active protein within the PC12 cells cultured in the 3D dynamic conditions of the bioreactor in RNS-5 compared with the control 2D cultured NGF stimulated cells. This Western blot also showed a decrease in active synapsin I of the PC12 cells cultured at a high density within 3D statically cultured collagen gels that underwent poor culture conditions due to accumulating lactate concentrations.

Only confocal imaging has been able to reveal significant differences of synapsin I expression between PC12 cells cultured on 2D surfaces compared to 3D dynamic bioreactor culture. Imaging revealed larger synaptic vesicle clustering within some of the PC12 cells cultured with 3D dynamic conditions in the bioreactor, but with some cells showing no positive staining for synapsin I. Almost all PC12 cells cultured on 2D surfaces demonstrate synapsin I immunostaining, however most of the staining is displayed as diffuse speckled pattern throughout the cytoplasm. This explains why the quantification of synapsin I of samples containing collection of protein or mRNA from all cells shows no overall differences between 2D and 3D dynamic bioreactor cultures.

Results of Xue et al. revealed diffuse immunostaining pattern of synapsin I with site I Ser 9 phosphorylation within untreated non-NGF stimulated control PC12 cells [233]. Also, here using the antibody for phosphorylated synapsin I (Ser 553) also still detects some diffuse synapsin throughout the cell bodies as active phosphorylated proteins and therefore again makes it impossible to accurately quantify synapse formation among the PC12 cell cultures. This implies that the untreated chromaffin phenotype of PC12 cells have active synapsin I participating in vesicle transport through their adrenal-type movement directly through the cytoplasm instead of through the neuronal synaptic transport of vesicles. Immunostaining of our treated NGF stimulated 2D cultured PC12 cells shows bright puncta at active nerve terminals indicating synaptic vesicle transmission, but some diffuse speckling throughout the cytoplasm with this synapsin participating in the non-neuronal vesicle transmission. Immunostaining of the PC12 cells cultured in the 3D dynamic bioreactor reveals only bright punctate staining implying a more mature neuronal phenotype participating in vesicle transport only through typical synaptic transmission.

2.5 CONCLUSIONS

Initial experiments demonstrated the original PC12 cell line forms large tissue aggregates within high density 3D cultures under dynamic conditions. However, the Neuroscreen-1 subcloned cell line allows superior observation of the neurite outgrowth within the different culture types. The data presented using the Neuroscreen-1 cell line with NGF stimulation among different culture conditions leads to the conclusion that in order to maintain high density neurite networking of Neuroscreen-1 cells with active synaptic transmission in three dimensions, a dynamic culture

system like that demonstrated here of the hollow fiber-based bioreactor is necessary. It is also likely that the 3D dynamic culture described here allowed enhanced synaptic transmission among the Neuroscreen-1 cells with larger synaptic vesicle clusters containing active synapsin I at nerve terminals. Within the optimized bioreactor culture in experiment RNS-5 it is possible that some of the Neuroscreen-1 cells were able to differentiate into a more mature neuronal phenotype with only synaptic transport of vesicles compared to the 2D cultured NGF stimulated cells. This work has initiated discussion of improving synapse formation among *in vitro* neuronal cultures to more accurately reflect the *in vivo* situation. However, significant differences comparing 2D statically cultured Neuroscreen-1 cells to those cultured in a 3D dynamic situation were difficult due to the Neuroscreen-I cell line used here maintaining the property of contact inhibition. This work leads to the hypothesis that it might be possible to achieve more significant synapse formation using primary neurons cultured within the 3D dynamic environment able to form neuronal tissue structures compared with traditional culture methods on 2D surfaces.

3.0 TESTING ECM SCAFFOLDS FOR ENHANCING NEURAL STEM CELL SURVIVAL AND DIFFERENTIATION WITHIN HOLLOW FIBER-BASED BIOREACTORS

3.1 INTRODUCTION

3.1.1 Neural stem cells (NSCs)

Proliferating neural cells were discovered in the adult rat brain in the late 1960s [37]. Reynolds and Weiss, in 1992, were the first to demonstrate that neural stem cells could be isolated from the adult and embryonic mouse brain able to clonally self-renew or differentiate into the three major cell types of the central nervous system (neurons, astrocytes, and oligodendrocytes) [234, 235]. Today, neural stem/progenitor cells can be isolated from both fetal central nervous system (CNS) ganglionic eminence(s) in the embryo and adult CNS locations at the subventricular zone (SVZ) of the lateral ventricles or the subgranular zone (SGZ) of the hippocampal dentate gyrus (DG), and throughout areas of the spinal cord [37, 236].

Protocols for expanding these cells in culture have been refined to allow significant expansion of the neural progenitors while maintaining their “stemness” or ability to self-renew producing many progeny and differentiate into the three major central nervous system cell types [237]. The cells are usually grown as cell clusters termed neurospheres in serum-free media

containing epidermal growth factor (EGF) and basic fibroblast growth factor (bFGF/FGF2) [37]. Adult mouse neurospheres can easily be expanded in suspension culture whereas adult rat neurospheres are grown in 96 well plates utilizing the walls of the wells for attachment. Adult NSCs have been shown to divide less frequently than the embryonic/fetal NSCs leaving a possible advantage to the fetal derived NSCs [20]. Therefore, we have continued the work in this chapter utilizing the commercially available source of mouse neurospheres obtained from the striatum of the embryonic mouse brain from the company Stem Cell Technologies Inc. (Vancouver, B.C., Canada). Neural stem/progenitor cells isolated from these regions can differentiate into astrocytes, oligodendrocytes, and neurons after withdrawal of EGF and addition of serum [37]. The neurospheres in culture are a combination of progenitor cell populations capable of differentiating into all three lineages to neurons, astrocytes, and oligodendrocytes. Lobo et al. has described rat neurospheres generated *in vitro* to consist of at least two different cell types [238]. Figure 29 depicts the relationships between these different progenitor cell populations and their progeny of terminally differentiated neuronal cell types [37, 239-241].

The final terminal differentiation of a neural stem cell through the progenitor cell types leads to a neuron, astrocyte, or oligodendrocyte. Neurons are the primary functioning cell type of the nervous system allowing signal propagation and communication within the brain and the rest of the body. Neurons are therefore the most desired cell type with neural stem cell differentiation to enable replacement of functional tissue within the damaged or diseased nervous system. Astrocytes were thought to only perform supporting roles to neurons acting as scavengers and forming the blood brain barrier to maintain and regulate a healthy environment in the nervous system tissue [242]. Reactive astrocytes are major contributors to the glial scar formed after spinal cord injury, preventing nerve regeneration, but recent investigations have

shown astrocytes can also provide support and guidance for neurons during regeneration [243]. Davies et al. have demonstrated glial restricted progenitor cells treated with different neurotrophic factors have differential effects on spinal cord injury repair [244]. Therefore the control over improving nerve regeneration by addition of astrocytes could be beneficial, but needs refining in order to have a positive outcome. Oligodendrocytes are the cells of the central nervous system that create insulation of signal propagation through neurons by wrapping their cytoplasmic processes around the axons of neurons forming a myelin sheath, a dielectric phospholipid layer. It is this myelin sheath of oligodendrocytes that is damaged in the disease multiple sclerosis, contributing improper signal transduction and further degeneration of axons. Therefore, the oligodendrocytes are also a highly sought after population of cells derived from neural stem cell differentiation.

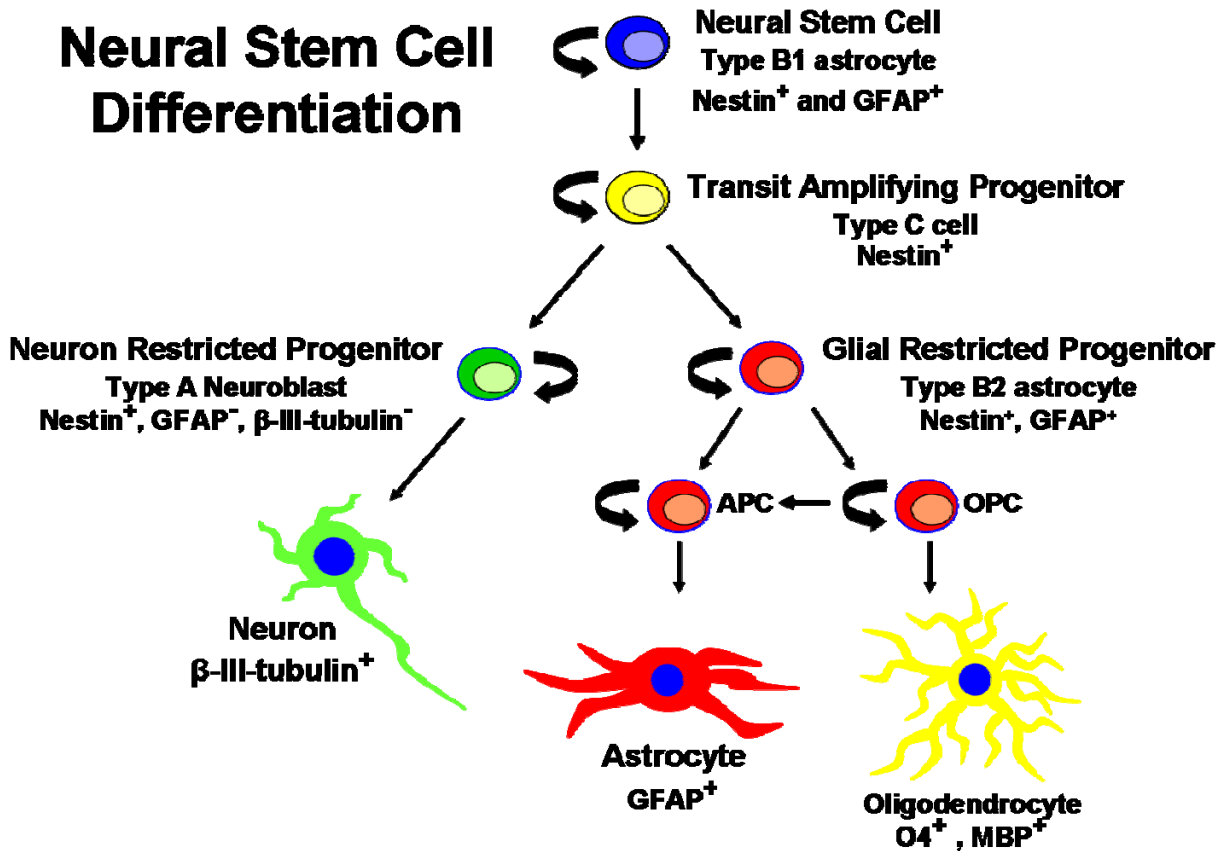


Figure 29. Diagram describing neural progenitor cell populations arising from the astrocytic neural stem cells found in the neurogenic regions of the brain. The transit amplifying nestin positive progenitor cells are the EGF responsive cell type able to generate neurospheres in culture. All progenitor populations of the neural stem cells are able to terminally differentiate into the post-mitotic three major cell types of the central nervous system: neurons, astrocytes, and oligodendrocytes. Looped arrows imply cell type can symmetrically divide to self-renew itself. Straight arrows imply cells can asymmetrically divide into the specified more differentiated cell type.

Neural stem cells *in vivo* have very specific niches within the brain. These neural stem and progenitor cell niches are distinct regions having specific cellular, molecular, and structural components in order to maintain both long term preservation of the stem cell populations and regulation of differentiation for neural cell repopulation. Embryonic neural stem cells, used in this work instead of adult derived cells, are derived from the entire embryonic striatum which

includes the adult subventricular zone (SVZ). Doetsch et al. first described the cellular organization of neural progenitor cells within the SVZ niche of the adult mammalian brain [245]. This group demonstrated that the progenitor populations reside inside the lateral wall ependymal cell lining of the lateral ventricles. Within this layer, the type A neuroblast populations reside in migratory tracts lined by type B1 and B2 stem cells with intermittent clusters of the transit-amplifying progenitor type C cells. Multiple groups have described that the neural stem cell population within the SVZ are actually a specific type of astrocytes [239, 246]. In 2003, Doetsch described that the quiescent type B1 astrocytes are the actual stem cells of the SVZ which give rise to the more rapidly proliferating type C cells which undergo asymmetric division into neuroblasts [241]. Recently, Mirzadeh et al. discovered that the B1 astrocytic neural stem cells have a pinwheel organization with direct apical endings touching the ventricle plus a long basal process reaching throughout the subventricular zone ending on blood vessels [247]. Doetsch et al. also describes the location of neural stem cells of the SGZ in the hippocampal formation of the adult mammalian brain [241]. The same type B1 astrocytes reside within this niche lining blood vessels and give rise to type D immature dividing cells that can asymmetrically divide into polysialylated neural cell adhesion molecule, PSL-NCAM, positive granule neurons. Doetsch et al. have also demonstrated that it is the type C transit amplifying population of neural progenitor cells within the SVZ *in vivo* that give rise to the EGF responsive population able to generate neurospheres *in vitro* [240]. Ependymal cells from the SVZ region have been demonstrated by Capela et al. to not be the cell population able to generate neurospheres *in vitro* [248].

Mercier et al. have investigated the ECM components of the SVZ niche for neural stem and progenitor cells of the adult mammalian brain [249, 250]. They describe fractal patterned extensions of capillary basal laminae, termed fractones, folding throughout the sub-ependymal

layer tracts of neuroblast type A cells bounded by type B stem cell astrocytes. These basal lamina fractions were distinguished with laminin immunoreactivity. Also, there were specific random regions within the fractions containing collagen type I. More recently, these fractions of adult rat, mouse, and human SVZ regions have been shown to contain laminin $\beta 1$ and $\gamma 1$, collagen IV, nidogen, and perlecan, but not laminin- $\alpha 1$ [251]. This work also demonstrated that proliferative cells specifically localized with regions of fractions containing heparin sulfate proteoglycans (HSPG) binding FGF2. The interconnection of the basal laminae within this neurogenic SVZ region is possible because there is a rich plexus of capillaries throughout where the cells are highly organized around the blood vessels [252, 253]. As described above, the type B1 astrocytic neural stem cells have a basal process extending from the ventricle to capillaries surrounded by the fractions extensions from these capillaries. Tenascin-R has been found to inhibit neural stem cell-derived neuroblasts *in vitro* and surrounds the neuroblast migratory tracts *in vivo* [254, 255].

Cell surface receptors able to bind laminins are integrins (especially integrin subunits $\alpha 6$ or $\beta 1$), dystroglycan, and syndecans [247]. The type B1 neural stem cells have been shown to highly express the $\alpha 6\beta 1$ integrin heterodimer just like many other non-neural stem cell types [247]. These integrins on the NSCs allow the cells to bind and interact with the laminins of the basal lamina fractions *in vivo*. Neurospheres generated from transgenic mice with subsequent $\beta 1$ integrin knockout contained fewer nestin positive cells with decreased proliferation and increased apoptosis, but was partially recovered with addition of exogenous growth factors [256]. Within the *in vivo* neurogenic niche, growth factors are able to be captured and stored by the basal lamina fractions reaching from SVZ capillaries and CSF of the ventricles. Cell surface receptors on neural stem cells for soluble growth factors, cell-cell contacts (especially E-

cadherins), and cell-ECM contacts (especially $\alpha6$ or $\beta1$ integrins) interacting with the niche microenvironment allow control over the fate of neural stem cells *in vivo*. It is currently hypothesized that disruption of the cell-ECM contacts of $\beta1$ integrins and laminins may lead to changes in the state of the neural stem cells in directing them to either proliferate, migrate, or differentiate [257, 258]. Integrins can also regulate growth factor signaling to further control stem cell fate [257]. In a review by Campos, the changing neurogenic niche over development is described in terms of laminin, fibronectin, and expressed integrins [258]. Laminin $\alpha2$ is abundant throughout a thick layer of the ventricular zone during embryonic development. Further into development, this laminin $\alpha2$ layer becomes thinner and eventually is confined to only a small lining of the ventricle with the rest of the subventricular zone containing mostly fibronectin. Tate et al. has demonstrated that blocking $\alpha6\beta1$ integrins prevents migration of neural stem cells *in vitro* on laminin and blocking $\alpha5\beta1$ prevents migration on fibronectin [259]. Yoshida et al. have demonstrated a decrease in $\alpha5\beta1$ integrin expression with neuronal differentiation of neural progenitor cells [260]. Therefore, these integrins play special roles in the ability of the neural progenitor cells to be maintained *in vivo* and properly migrate away from the subventricular zone, but further clarification is still needed on the exact temporal expression of these receptors for enhancing neural stem cell proliferation and differentiation *in vitro*.

Other important ECM components involved in neural tissue development and present within adult neural tissue are glycoconjugates, including proteoglycans, glycoproteins, and glycolipids. The ECM of the neural stem cell niche was described above to be comprised significantly of basement membranes. Large components of basement membranes within tissues are proteoglycans. The chains of proteoglycans are present throughout the laminin and fibronectin components. Heparan sulfate proteoglycans (HSPG) is a major contributor within

many tissues, including neural tissue, which regulates growth factor binding and presentation to cells within the ECM. Specifically within the neural stem cell niche, HSPG can bind bFGF for regulating neural stem cell proliferation [251, 261]. Another proteoglycan important in regulating growth factor presentation within the neural stem cell niche is nerve/glial antigen 2 (NG2) [261]. Chondroitin sulfate proteoglycans (CSPG) are a group of proteoglycans extremely important in regulating neural tissue function. Some important CSPGs within neural tissue are neurocan, brevican, versican, aggrecan, and phosphacan [262]. CSPGs have been demonstrated to be highly synthesized by astrocytes within the CNS [262]. Kabos et al. have demonstrated the increase of CSPGs synthesized by neural stem cells during proliferation and neurosphere formation with a decrease in CSPG expression during differentiation in culture [263]. CSPGs have been shown to be present within both embryonic and adult neural stem cell niches of the ventricular and subventricular zones [262]. Also, CSPGs have been demonstrated to directly affect neural stem cell proliferation and decreased neuronal differentiation in culture [262]. However, CSPGs have also been demonstrated as a major component of the glial scar within adult CNS tissue after injury preventing axonal regeneration [262]. Some forms of CSPGs are also present within the developing nervous system as inhibitory molecules that line tracts guiding neuroblast migration and axonal growth pathways [262].

Another important glycosaminoglycan present throughout developing tissues, including the central nervous system, is hyaluronic acid (or hyaluronan; HA). HA is present within the developing mouse brain diffusely in gray matter and along axonal tracts in white matter. It has also been detected as present lining the migratory tracts of neuroblasts allowing migration of these cells [262]. In culture, HA has been shown to inhibit astrocyte proliferation and injection of hyaluronidase *in vivo* causes proliferation of astrocytes within the spinal cord [262]. HA

along with CSPGs have been shown to be overexpressed within the site of CNS injuries and glial lesions. Reactive astrocytes staining positive for GFAP within CNS lesions highly express CD44, a specific receptor for cell attachment to HA. It is possible that HA is upregulated within the tissue of the lesion formed after a CNS injury for the ability of reactive astrocytes, with HA receptors, to migrate throughout the site to perform their functions of protecting and maintaining the spared neural tissue [262].

3.1.2 Obstacles using neural stem cells *in vivo* for potential therapy development

Neural stem cells (NSCs) hold the foremost potential to be used as a cell source for treating various nervous system injuries and diseases with cell therapies. Some of the major nervous system diseases and disorders able to potentially be corrected with neural stem cell transplantation were described earlier in section 1.1. Transplantation of NSCs has been demonstrated to be free of tumor growth after long-term engraftment *in vivo*, unlike embryonic stem cells. Progress in reaching this goal has been hindered by a number of factors. Many *in vivo* reports of testing NSC types for cell therapy transplantation in animal models have encountered significant problems of low cell survival rate with poor neuronal differentiation.

Cao et al. demonstrated that transplantation of neurospheres into normal adult rat spinal cords led to high survival and neuronal differentiation, but when transplanted into rats with injured spinal cords differentiation was inhibited resulting in very few neurons [264]. The significance of this particular study was that the neurospheres used for transplantation were pre-treated and induced to become neuronal restricted progenitor cells. Most previous studies show a high degree of astrocyte differentiation of transplanted neural stem cells into injured spinal cord animal models [264-266]. Human NSC neurospheres were demonstrated by Cummings et

al. to survive and differentiate into oligodendrocytes and neurons with few astrocytes, contribute to locomotor recovery, and form synapses with mouse host neurons after transplantation into spinal cord-injured NOD-scid mice [266]. They specifically showed that the neurons created by the NSCs directly contributed to the functional recovery by selective destruction of these cells and subsequent loss of the recovered function. This report shows the promise of using neural stem cells to treat spinal cord injuries, but the lack of positive outcomes using rodent derived NSCs within rodent spinal cord injury models might illustrate a larger problem using immunodeficient animals for accurately assessing human neural stem cells *in vivo*. As described above in section 1.1.2, the injured spinal cord possesses a very hostile environment with a reactive immune response contributing to glial scar formation. Ricci-Vitiani et. al. have hypothesized that it is the inflammatory environment of spinal cord injuries that pushes the NSCs to differentiate into astrocytes by showing *in vitro* differentiation of the cells into the astrocytes after stimulation with tumor necrosis factor-alpha (TNF-alpha), interleukin-1beta (IL-1beta), and interferon-gamma (IFN-gamma) [267]. To date there has only been a handful of successful reports on functional recovery in rodent models of acute spinal cord injury treated by transplantation of neural stem cells [266, 268-271]. Cummings et al. have been the only group to prove neural stem cell incorporation into the host neural circuitry, while most of these reports cite functional improvement due to the “bystander effect” where the neural stem cells provide trophic support and prevent worsening due to secondary complications in SCI [37].

In a review by Martino and Pluchino, the authors hypothesize that recruitment of endogenous neural stem cells in the brain to repair diseased cells and tissue is limited by the addition of inflammatory conditions with many nervous system diseases and injuries [37]. Multiple sclerosis (MS) is a specific nervous system disease that is caused by autoimmune

reactivity. Lesions in patients with MS are frequently seen as wedge-shaped with a broad base along the ventricular lining. These lesions most likely occur from infiltration of immune cells through the rich blood supply to the SVZ. This emphasizes the poor surrounding conditions the endogenous neural stem cells have to overcome in order to repopulate brain tissue within lesions due to MS. However, in 2003 these same authors reported their results of mouse neural stem cell transplantation abolishing functional impairment of mouse MS model, experimental autoimmune encephalomyelitis (EAE) [272]. Jeong et al. have demonstrated improvement in rats with an experimental stroke model with transplantation of human neural stem cells into the brain [273]. Zhang et al. have demonstrated an increase in neural stem cell repopulation of the brain after induction of stroke within rat brains [274]. Some groups have been able to demonstrate improved outcomes from fetal or adult neural progenitor cell transplantation into animals having an experimental model of Parkinson's disease [275-278]. However, it is likely that the positive outcomes of these studies have occurred considerably by the mechanism of the neural stem cells acting through immune modulation and neuroprotection by trophic factor secretion instead of differentiation and integration for functional cell replacement.

There are a number of ongoing clinical trials for the treatment of different CNS diseases such as stroke, multiple sclerosis (MS), lupus erythematosus, cancer, and traumatic brain injury using transplant cell therapies, but these so far have focused on adult autologous stem cells such as bone marrow-derived cells (www.clinicaltrials.gov). Stem Cells Inc. has been the first company to generate a human fetal brain-derived neural stem cell product (HuCNS-SC) used for transplantation cell therapies [13]. The first clinical trial using the HuCNS-SC cells was initiated in 2006 in order to test the safety of the cells transplanted into patients with neuronal ceroid lipofuscinosis or Batten's disease, where the complications arise from the lack of specific

enzyme production from neurons. The HuCNS-SCs have been demonstrated to produce the enzymes lacking in Batten's disease after transplantation into pre-clinical animal models. The company hopes to prove the safety of the neural stem cell transplantations in order to continue with future clinical trials using the cells for other nervous system diseases such as SCI, demyelinating disease, stroke, and Alzheimer's disease.

3.1.3 Biomaterials for enhancing neural stem cell survival and differentiation

Compatibility and control of neural stem cells using biomaterials has only recently been studied within the past few years. This is due mostly to the fact that protocols for long-term culture of neural stem cells were only developed in 1996, but it has only recently been recognized that improvements are needed to produce a more promising strategy for clinical use of these cells [279]. It is known that *in vitro* neural stem cells have the ability to differentiate into functional neurons on a two dimensional surface coated with laminin, but the ability to achieve this differentiation in a 3D organization has recently been of interest. Laminin is a protein component of the extracellular matrix within tissues highly present within basal lamina basement membranes in a thin layer. Laminin has multiple active domains useful in binding other ECM proteins like fibronectin in order to form a matrix, however currently it is not possible to form a 3D hydrogel completely from natural unmodified laminin molecules. The neural stem cells differentiate very well on laminin due to functional domains on laminin able to enhance neuronal survival and neurite outgrowth [280, 281]. The whole laminin molecule has binding domains for many integrin receptors (especially $\beta 1$ integrins), which include the sites on laminin having the amino acid sequence RGD and YIGSR [281]. The IKVAV peptide sequence found in laminin has been able to mimic the neurite outgrowth enhancing activity of laminin [281].

However, we have been interested in culture of the neural stem cells within a 3D matrix instead of the traditional 2D laminin coated surface.

Martinez-Ramos et al. examined neuronal differentiation of adult rat neural stem cells on different polymeric biomaterials, but described the increase in neuronal differentiation on some of the materials due most likely to the increased ability of the material to adsorb laminin [282]. Ma et al. have described functional synapse formation between embryonic rat neural precursor cells within 3D collagen hydrogels *in vitro* [283]. Very recently these authors described further differentiation of the rat neural precursor cells within collagen gels maintained in a rotating wall vessel bioreactor [284]. Some groups have described testing of biomaterial compatibility with neural stem cells using printing of the materials in arrays for screening NSC behavior on multiple materials [285]. The results of this work showed an increase in neuronal differentiation on fibronectin and ProNectin L, a recombinant polymer consisting of multiple fibronectin RGD (arginine-glycine-aspartic acid amino acid sequence) cell attachment domains.

Most *in vivo* studies incorporating biomaterial enhancement of neural stem cell transplants have been used in spinal cord regeneration. Prang et al. have developed an alginate based hydrogel scaffold allowing incorporation of NSCs for transplantation for improvement in recovery of spinal cord injury models [286]. Wu et al. have attempted to improve spinal cord regeneration with the implantation of rat fetal hippocampal neural progenitor cells encapsulated by delivery within an alginate hydrogel, but most cells still differentiated into astrocytes rather than neurons [287]. Another study investigating improvement of rat spinal cord injuries by spinal cord-derived NSC transplantation including a hydrogel, has been performed by Vacanti et al. [288]. These authors demonstrated coordinated hindlimb movements with recovery in animals transplanted with the NSCs with hydrogel scaffold while the animals receiving only the

NSCs had scar formation with little behavioral improvement. These reports comprise the majority of the papers described in a comprehensive review published very recently by Little et al. entitled “Engineering Biomaterials or Synthetic Neural Stem Cell Microenvironments” [289]. This demonstrates the need for more investigation on the proper biomaterials for enhancing control and manipulation on the neural stem cell environment either *in vitro* or *in vivo*.

The *in vivo* neural stem cell niche is highly organized including a variety of ECM molecules and growth factors for controlling neural stem cell behavior and therefore poses the difficulty in attempting to recreate the proper environment to permit NSC survival and neuronal differentiation. There are two major clinical goals for research involving neural stem cells. The first goal has been to use these cells as a cell therapy as described in the previous section. However, due to the limited success of neural stem cell transplantation to replace lost functional neurons from disease and trauma, investigation into additional factors enhancing the environment and delivery of these cells used as cell therapies is relevant for improving the neural stem cell survival and differentiation after transplantation. The other goal is to better understand the endogenous neural stem cell niche and its control over the cell behavior. Information from understanding the natural mechanisms and environment for NSCs might allow further manipulation to enhance endogenous neural stem cell repopulation in central nervous system injuries and diseases rather than transplantation of engineered non-autologous neural stem cells.

The research necessary in achieving both of these goals can be pursued with the ability to recreate a synthetic neural stem cell niche *in vitro*. Attempting to achieve this goal could enable insight into the natural mechanisms for controlling neural stem cell behavior. Once a reproducible *in vitro* system is available, allowing high density tissue configurations, the application of such a system for *in vitro* studies for therapeutic development can be expected.

We have initiated the work here in order to develop such a 3D dynamic *in vitro* system allowing manipulation of the microenvironment for optimizing neuronal differentiation of mouse embryonic neural stem cells. Our initial studies in achieving this goal have focused on testing different injectable extracellular matrix (ECM) hydrogel-based scaffolds allowing assessment of neurosphere differentiation within a 3D configuration. Further work included use of hollow fiber-based bioreactors as tools for recreating an *in vivo*-like dynamic environment allowing investigation of neuronal differentiation within this environment after delivery of neural stem cell neurospheres suspended within the different injectable hydrogels.

The ECM hydrogels investigated here consist of commercially available products: collagen type I (BD Biosciences), high concentration growth factor-reduced Matrigel (BD Biosciences), and HyStem (cross-linked hyaluronan; Glycosan Biosystems Inc.). There are many FDA approved collagen products currently used clinically as dermal fillers for cosmetic or reconstructive purposes [290]. There are also many hyaluronan or hyaluronic acid products used clinically as either dermal fillers or joint fillers for osteoarthritis [291-293]. Matrigel, however, is not a synthetic material useful for actual cell therapies in clinical treatments, but is an injectable hydrogel with naturally occurring endogenous ECM proteins that can provide an initial framework for analyzing scaffolds to modulate neural stem cell behavior. Matrigel contains 60% laminin and could prove useful in directing neural stem cell differentiation in 3D. Laminin is a large component of the natural basement membrane matrix present in many tissues, and highly present within the nervous system tissue, but it is only an adhesive protein able to link other proteins of the basal lamina together forming a matrix [294]. It is not currently possible to form a hydrogel purely out of whole unmodified laminin molecules and therefore we have specifically investigated Matrigel which has a very high percentage of laminin.

Our objectives within this chapter were to begin studies of mouse neural stem cell cultures within 3D dynamic *in vitro* culture systems. The ultimate desired goal is to develop an *in vitro* culture system allowing studies of neural stem cell expansion, migration, and differentiation within a 3D configuration under dynamic conditions. Such a system could allow pursuit of the two goals mentioned above: synthetic recreation of the *in vivo* neural stem cell niche to further elaborate on the environment naturally allowing control of endogenous neural stem cells and using the system as a tool mimicking the *in vivo* 3D dynamic environment for testing strategies improving development of cell therapies using neural stem cells. In order to obtain this system we have initially investigated the three injectable hydrogel scaffolds allowing a 3D space for neural stem cell cultures. We have also investigated the use of these scaffolds within two different hollow fiber-based bioreactor systems for further culture of the neural stem cells under dynamic conditions within the 3D scaffolds. These studies have allowed further understanding of the behavior of mouse neural stem cells *in vitro* under 3D dynamic conditions. We have been able to achieve differences in neuronal differentiation with modulation of the 3D scaffold used. Also, we have demonstrated the complexity of the environment necessary for manipulating neural stem cell behavior, which includes further investigations of soluble factors within the medium formulations in order to further control the cells. We believe the system being developed here could enhance *in vitro* studies for improving neural stem cell research.

3.2 METHODS

3.2.1 Mouse neural stem cells and culture conditions

Mouse neural stem cells were purchased as passage 1 neurospheres isolated from the striata of embryonic day 14 (E14) mouse brains from Stem Cell Technologies (Stem Cell Technologies Inc., Vancouver, B.C., Canada). Cells were expanded according to Stem Cell Technologies protocols using Neurocult[®] Basal Media with Neurocult[®] Proliferation Supplements (Stem Cell Technologies, Inc.) and the addition of 20 ng/mL recombinant human epidermal growth factor (rhEGF; Stem Cell Technologies Inc.) within Costar 162 cm vented cap flasks (40 mL medium in each flask). Basic fibroblast growth factor (bFGF) was not included in the proliferation medium, because mouse embryonic neural stem cells do not require the growth factor for expansion. Neurospheres were expanded until sphere size was quite large and passaging was carried out by mechanical dissociation by trituration 5-15 times using a fire-polished glass Pasteur pipette. The fire-polishing narrows pipette tip opening. Trituration consists of aspirating cells into pipette and holding tip angled at bottom of conical tube cells and expelling neurospheres through narrow tip to dissociate into smaller clusters. Trituration 20-30 times creates single cell suspensions with this method and initial sphere size. Cells used in all experiments were expanded 8 times to reach passage 9 neurospheres in order to obtain enough cells for entire experiment including bioreactor culture (except in initial testing of different cell differentiation protocols).

Initial testing of different neural stem cell differentiation protocols on 2D laminin coated surfaces included testing neurosphere dissociation methods, single cell suspension vs. whole neurospheres, and seeding density effects on differentiation. All differentiation protocols were

tested on laminin coated tissue culture treated dishes. Dissociation methods tested were the traditional mechanical trituration method as described above and chemical dissociation (kit from Stem Cell Technologies Inc.). Chemical dissociation kit was performed according to manufacturer's protocol. These methods were used to dissociate neurospheres into a single cell suspension. These cells were also compared to differentiation of whole neurospheres. Also, mechanical trituration was utilized to partially dissociate neurospheres resulting in smaller diameter neurospheres. Later, partially triturated smaller neurosphere differentiation was tested at varying sphere seeding densities of 0.1×10^3 cells/mm², 0.25×10^3 cells/mm², 0.5×10^3 cells/mm² (Stem Cell Technologies Inc. recommended density), 1×10^3 cells/mm², 2.5×10^3 cells/mm², and 5×10^3 cells/mm².

Traditional differentiation protocols using neural stem cells require cells seeded onto laminin (extracellular matrix protein with properties enhancing neurite outgrowth) coated 2D tissue culture dishes. Most of these protocols, including that of Stem Cell Technologies Inc., describe initial coating of culture dish with poly-L-lysine to improve laminin adsorption. Therefore, positive control mNSC 2D static cultures were performed within 6 well tissue culture treated plates first coated with 50 µg/mL poly-L-lysine (Sigma Aldrich) for one hour and then coated with 20 µg/mL laminin (Invitrogen) overnight at 37°C in a humidified 5% CO₂ incubator. There is currently no commercially available product able to obtain a 3D hydrogel matrix made of 100% laminin. We have therefore proceeded to test commercially available hydrogels for the 3D differentiation of mNSCs. We have also included 2D static control cultures of the three hydrogel matrices tested, which included either an adsorbed diluted layer of the ECM molecule or a thin gel coating.

3.2.2 Preparation of mNSC-ECM 3D hydrogel constructs

Each ECM 2D coating and 3D hydrogel was prepared according to the manufacturer's standard protocol. 2D static control cultures were maintained in tissue-culture treated 12 or 6 well plates (BD Biosciences; San Jose, CA). For 2D cultures, cells were seeded as partially triturated neurospheres at either 0.5×10^6 cells/well in a 12 well plate or 1×10^6 cells/well in a 6 well plate for a density of 1.5×10^3 cells/mm² (including laminin coated positive control cultures). 2D cultures were seeded and maintained with Neurocult Differentiation medium with medium being replaced every other day for the 14 day cultures. Dishes used for 2D collagen cultures were first coated with 5µg/mL collagen type I (from rat tail sterile filtered solution; BD Biosciences) dissolved in 0.02 N acetic acid for 1 hour in 5 % CO₂ humidified incubator at 37°C. Dishes were then washed with Dulbecco's phosphate buffered saline solution (PBS; Invitrogen). Matrigel (high concentration growth factor reduced; BD Biosciences) 2D cultures were prepared by first thawing the Matrigel vial overnight on ice at 4°C. Matrigel was handled by keeping on ice to avoid hydrogel solidification. 2D coatings were prepared by diluting high concentration Matrigel 1:10 with ice cold Neurocult Differentiation medium and was aliquoted 1 mL into each well of a 6 well plate or 0.5 mL into each well of a 12 well plate. Dishes were then placed in a 5 % CO₂ humidified incubator at 37°C for 30 minutes. Excess solution was then aspirated off and fresh medium was replaced. 2D cultures on HyStem (cross-linked hyaluronic acid (HA); Glycosan Biosystems Inc., Salt Lake City, UT) were performed using two different methods. 2D coatings were prepared by diluting the HA component of HyStem in PBS 1:1 and using solution to completely cover wells of 12 well plate. Plates were placed in a 5 % CO₂ humidified incubator at 37°C for 1 hour. Also, 1 mm thick hydrogel layers were formed on 12 well plates adding 0.5 mL of the hydrogel solution into each well (cells were later seeded on top of the

hydrogel layer instead of encapsulated into the 3D gel). At least n=6 wells of 12 or 6 well plates were prepared each time for 2D mNSC cultures with each of the three ECM coatings tested and were replicated in triplicate.

3D ECM hydrogel cultures were performed by preparing 1 mL of each of the ECM hydrogel solutions with the addition of 1×10^6 neural stem cells (as partially triturated neurospheres) and placing the 1 mL solution plus cells into a well of a 12 well tissue culture plate. Collagen type I hydrogels were prepared using the following components quickly added in the given order: 100 μ L 10X PBS (Invitrogen Corp.), PC12 cells with 500-600 μ L RPMI medium containing 0.5% HS and 1% Pen/Strep (enough to bring final volume to 1 mL), 250-350 μ L collagen type I sterile solution (amount varied with manufacturer stock concentration, final concentration of collagen in gel 1 mg/mL), and 6 μ L 1 N NaOH. Collagen gel solutions can then undergo fibrillation and gel formation after addition of NaOH for final pH approximately 7.4 and plates placed in 5% CO₂ humidified incubator at 37°C. Collagen gel formation completed within 15 minutes and medium was placed on hydrogel construct.

Matrigel 3D ECM hydrogels were prepared by handling Matrigel on ice as described above to prevent early matrix gelation. 1 mL of undiluted high concentration (approximately 19 mg/mL) Matrigel solution was pipetted into each well of a 12 well culture plate. Neurospheres were then pipetted into the solution and quickly mixed into gel solution using pipette tip to create uniform cell suspension. Plates were then placed in 5% CO₂ humidified incubator at 37°C. Initial Matrigel used for neural stem cell cultures was the original 7-8 mg/mL concentration Matrigel product, but using this solution for the 3D hydrogel cultures even under static conditions for the 14 day culture period resulted in partial hydrolytic degradation of the gels preventing possible analysis of intact 3D cell-gel constructs. Therefore, all further experiments

utilized high concentration Matrigel product, which is recommended for *in vivo* studies having dynamic conditions.

HyStem 3D ECM hydrogels (Glycosan Biosystems Inc.) were prepared according to the manufacturer's protocol. The HyStem kit contains two components, thiol-modified hyaluronan (HA) and reactive polyethylene glycol diacrylate (PEG-DA) used to cross-link the hyaluronan molecules in order to form a hydrogel. In order to create 2.5 mL of hydrogel solution, sterile water, provided with HyStem kit, was used to reconstitute the two components by adding 1 mL of water to each of two HA component vials and 0.5 mL water to one PEG-DA vial. Then the vials are further reconstituted as liquid solutions by placing within 37°C water bath for 30 minutes. Finally, the solutions of the 3 vials (two HA vials and one PEG-DA vial) were combined together and quickly mixed with pipetting. 1 mL of solution was placed into each well of a 12 well culture plate and neurospheres were then added directly to gel solution within plate and the pipette tip was used to uniformly mix the cells into the gel solution. Plates were then placed in 5% CO₂ humidified incubator at 37°C.

3D hydrogel dimensions within the 12 well plates resulted approximately in 20 mm diameters and 2 mm in height. 1.5 mL Neurocult Differentiation medium was placed in each well after gelation of each ECM hydrogel was complete after 30 minutes within incubator. Gel plus liquid medium layer height never exceeded 6 mm from bottom of well in order to not further limit gas diffusion into gel constructs. Medium was completely replaced in each well once daily (every 24 hours). 12 well plates containing 3D ECM hydrogel plus cell constructs were maintained under static culture conditions within a 5% CO₂ humidified incubator at 37°C. At least n=6 wells of 12 or 6 well plates were prepared each time for mNSC cultures within each of the three 3D ECM hydrogels tested and were replicated in triplicate.

3.2.3 Hollow fiber-based bioreactor cultures

A total of five bioreactor experiments testing mouse neural stem cell differentiation were completed. Notation used to identify each bioreactor experiment in an abbreviated form with the example of the first experiment noted by MNS-1; where the first initial is the species being mouse, the second and third initial correspond to the cell type (in this case neural stem), and the number giving the order among the five experiments (MNS-1 through MNS-5). MNS-1, 2, and 4 were conducted using the 8 mL laboratory scale hollow fiber-based bioreactor. MNS-3 and 5 were conducted using the four compartment analytical scale bioreactor. All five bioreactor experiments included inoculation of the bioreactor with mouse neural stem cells suspended in one of the three extracellular matrices (ECM) gel solutions investigated. These ECM gel solutions were prepared with the same methods described above in section 3.2.2 for making gel solutions used for 3D static control cultures. All bioreactor experiments were maintained for the entire 14 day culture period necessary for differentiation of mouse neural stem cells.

3.2.3.1 8 mL laboratory scale bioreactors

There were a total of three 8 mL hollow fiber-based bioreactor experiments performed to differentiate mouse neural stem cells in a 3D space under dynamic conditions. One 8 mL bioreactor was used for each of the three ECM hydrogels tested. These experiments were performed similarly to those described in section 2 using the 8 mL hollow fiber-based bioreactor and perfusion systems shown in Figure 1-3. Each ECM hydrogel solution was prepared exactly as specified in the above section 3.2.2. Within each experiment, 1×10^8 mouse neural stem cells as passage 9 partially triturated neurospheres were suspended in 10 mL of the ECM hydrogel solution and inoculated into the bioreactor. Next, 5-10 mL of the ECM hydrogel was inoculated

to further distribute the neurospheres within the bioreactor. For these experiments, culture conditions were maintained with medium pH between 7.2-7.4 by varying the CO₂ flow rate through the gas perfusion system. Feed medium flow rate in all experiments was set to 2 mL/hr, which is the lowest possible flow rate using the pumps used. Medium used for entire bioreactor set up and culture was Neurocult Differentiation medium.

Perfusion tubing circuits used for these 8 mL bioreactor experiments were made from medical-grade PVC (circuit produced by Stem Cell Systems, tubing manufactured by B. Braun Medical Inc.). Poor outcome due to experiment MNS-1 necessitated testing of bioreactor and tubing material compatibility with neural stem cell cultures. Therefore, during setup of 8 mL bioreactor experiment MNS-2, Neurocult differentiation medium was used to pre-fill the bioreactor plus tubing circuit and circulated through the circuit for 24 hours and then collected. A second batch of medium then replaced into the circuit volume and circulated for a second 24 hour period. Both batches of medium were collected in order to test circulated medium on control mNSC cultures. This was performed to test if any detrimental particles/reagents leached into the medium during circulation from any of the materials used in the bioreactor or tubing circuit. For experiment MNS-2, these control cultures testing medium were performed by seeding neurospheres onto Matrigel coated plates with the collected medium from each time point and compared to mNSCs differentiating in control fresh medium. For experiment MNS-4 this material testing was performed again, but tested on control mNSC cultures differentiating on tissue culture plates coated with control laminin coatings (for optimal cell survival and differentiation).

3.2.3.2 Four chamber analytical scale bioreactors

A photograph of the four chamber analytical-scale hollow fiber-based bioreactor is seen in Figure 30. This bioreactor is a scaled down version of the 8 mL hollow fiber-based bioreactor containing only a single layer of parallel hollow fibers used for gas and medium perfusion. This allows a system providing dynamic conditions to the cell compartment, but allows visualization of the cultures using microscopy during the culture period. The hollow fiber layer is bounded on the top and bottom within each chamber by a plastic coverslip. This allows placement of the entire bioreactor onto the stage of an inverted microscope in order to image cells during bioreactor culture.

Four chambers are seen surrounded by the bioreactor polyurethane housing. Perfusion hollow fibers run horizontally through the polyurethane housing. Each of the four chambers is separated by the polyurethane housing sealing the fibers around each chamber. Each chamber has its own white cap port for cell and hydrogel solution inoculation into each chamber individually. Medium passing through each row of two chambers flows directly into the other, but medium is then ultimately diluted into the same perfusion circuit tubing volume (one tubing circuit for the entire bioreactor). Red ports at ends of fiber bundles are used to connect medium perfusion circuit tubing for medium flow through hollow fibers under counter-current flow through each chamber. White ports are at ends of gas fiber bundles used to connect the gas perfusion tubing circuit. A diagram of this perfusion tubing circuit used for the four chamber bioreactor experiments is shown in Figure 32. The perfusion systems used for these experiments is shown in Figure 34.

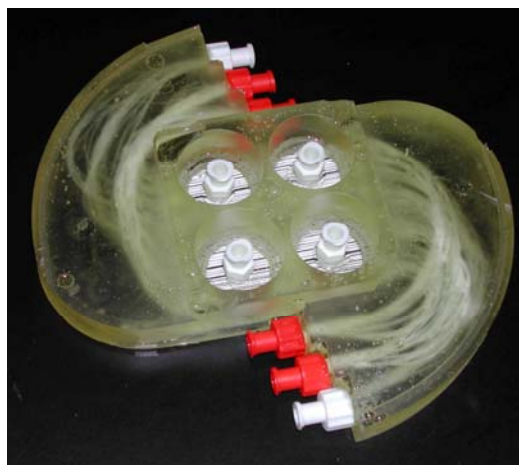


Figure 30. Photograph of four chamber analytical-scale hollow fiber-based bioreactor.

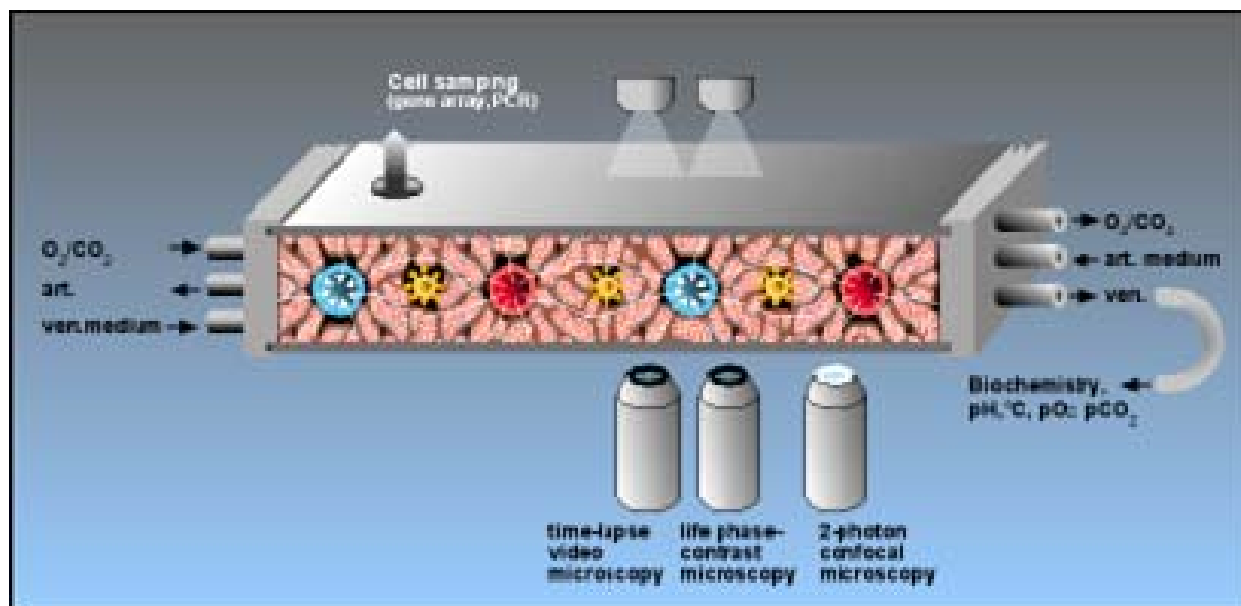


Figure 31. Diagram describing flow patterns through each chamber of the four chambered hollow fiber-based analytical scale bioreactor. Also shown are the analytical capabilities possible with microscopic visualization of the cell compartments with this bioreactor design.

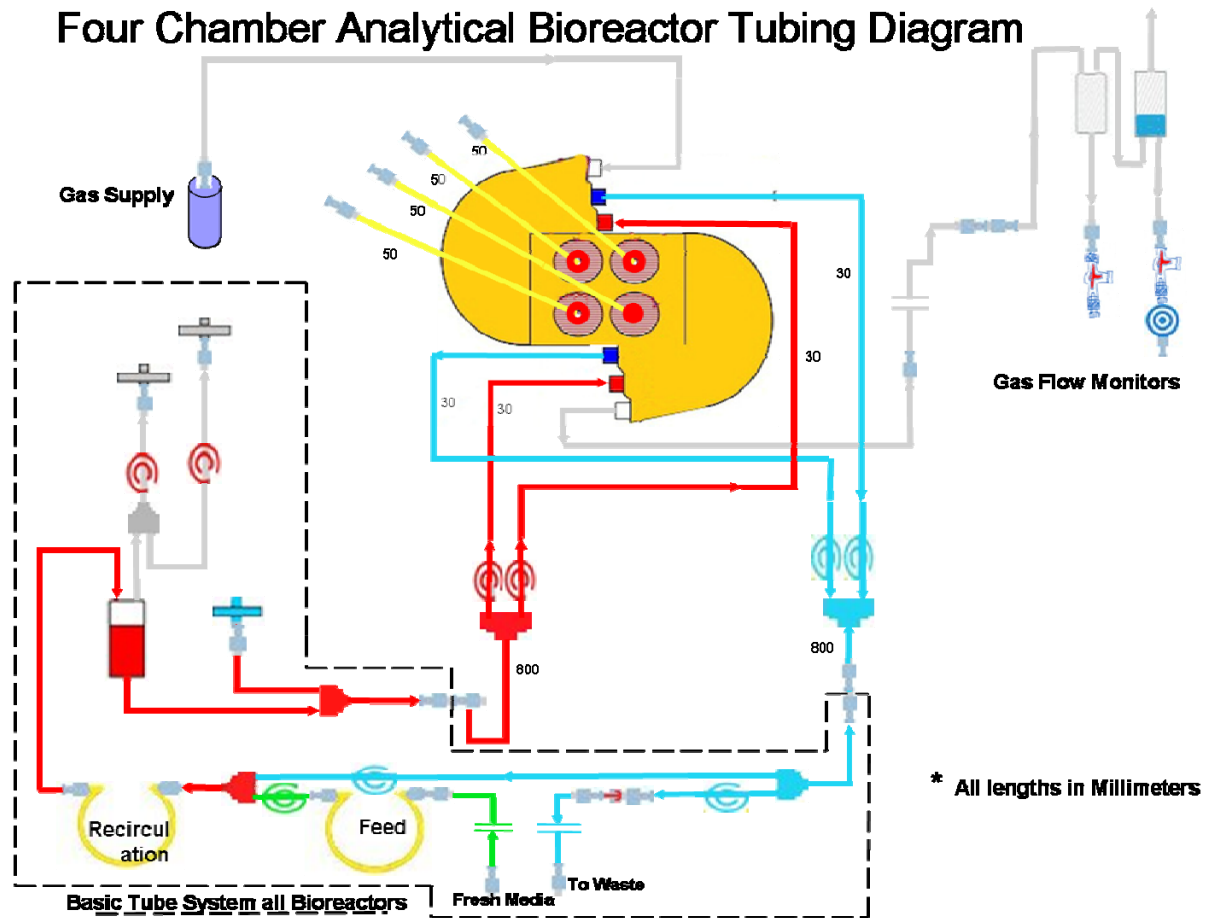


Figure 32. Diagram of tubing circuit used for medium and gas perfusion through four chamber analytical scale hollow fiber-based bioreactor. The tubing segments outlined in the dotted black box indicated the same circuit design used for the 8 mL bioreactor experiments. Differences in this tubing circuit are just the lengths of the segments leading to the bioreactor, which are longer allowing movement of the bioreactor to the microscope stage. Also, there are no tubing segments connecting the perfusion circuit to the cell compartments of the individual chambers within the bioreactor. Instead cells are inoculated through ports directly connected to each chamber.

MNS-3 and MNS-5 bioreactor experiments were performed using this four chamber analytical scale bioreactor design. The chambers within the bioreactor were inoculated with 5×10^6 mNSCs (as partially triturated neurospheres) in each chamber. Each chamber within the bioreactor was inoculated with a different ECM hydrogel out of the three different matrices

investigated within this work. All 5×10^6 mNSCs for each chamber were suspended into collagen, Matrigel, or HyStem solutions in a 1 mL volume of each gel solution. The orientation of chambers with different ECM hydrogels for each experiment is seen in Figure 33.

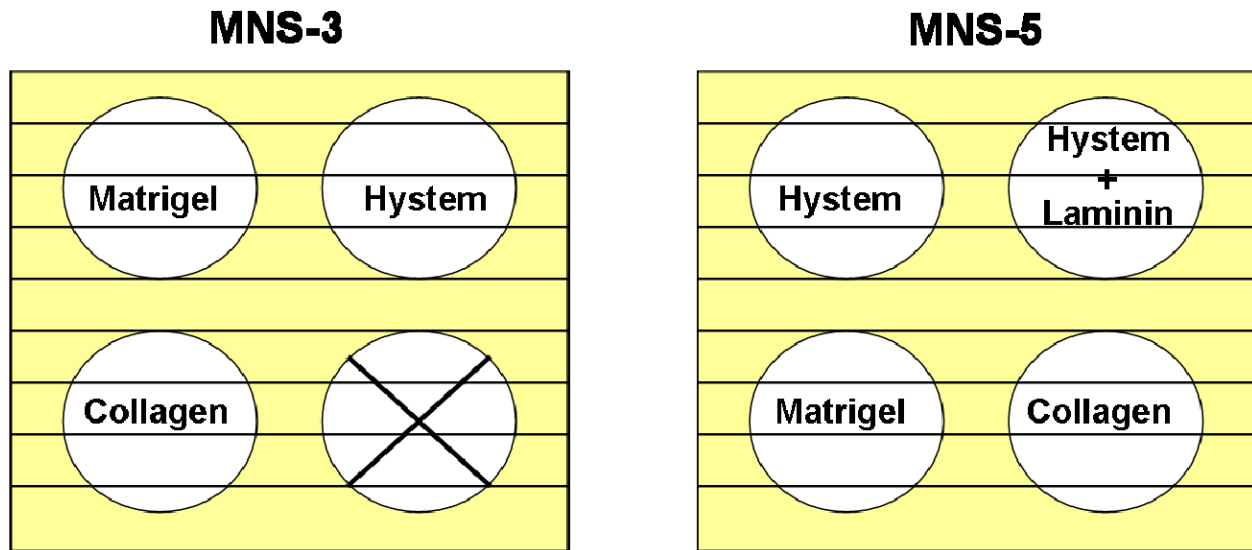


Figure 33. Diagram of orientation of mNSC plus ECM hydrogel solutions inoculated into the separate chambers of the four chambered bioreactor within each of the two experiments performed. Black lines indicate direction of perfusion hollow fibers through the chambers. The “x” through the bottom right chamber of MNS-3 indicates that this chamber was not used (the port connector leading to the inoculation tubing line of this chamber came off during bioreactor-tubing assembly).

MNS-3 and MNS-5 were maintained with a feed medium flow rate of 2 mL/hr and recirculation medium flow rate of 8 mL/hr. The pH of the medium was maintained between 7.2-7.4 by controlling the CO₂ and air flow rate mixtures. The gas perfusion flow rate through the gas perfusion circuit was maintained at 2.5 mL/min. Both of these experiments were performed using the newer version four rotameter perfusion systems from Stem Cell Systems (Berlin, Germany). A photograph of this perfusion system is seen in Figure 34. The tubing perfusion

circuit used for experiment MNS-3 used the original medical-grade PVC tubing used for all previous experiments.

Due to poor outcome of testing medium perfused through bioreactor and tubing circuit on control cultures, further tests were performed by testing only the tubing perfusion circuit. Perfusion tubing circuits were made including only a single loop of tubing with one pump tube segment and two three-way stopcock connectors. Two different tubing circuits were made for this test and sterilized with ethylene oxide gas. The first was comprised of the original medical grade polyvinyl chloride (PVC) tubing previously used in all bioreactor experiments and the second of Tygon 2275 (Saint-Gobain, Valley Forge, PA). For this test, Neurocult Differentiation medium was perfused through each tubing circuit for two consecutive 24 hour periods within the perfusion system at 37°C and then collected and tested on control laminin coated culture dishes seeded with mNSC neurospheres with the medium. Cultures were compared to control wells using fresh medium. Due to the outcome of this test MNS-5 was performed using the newer version of the tubing circuit made with Tygon 2275 tubing that was assembled within our laboratory.

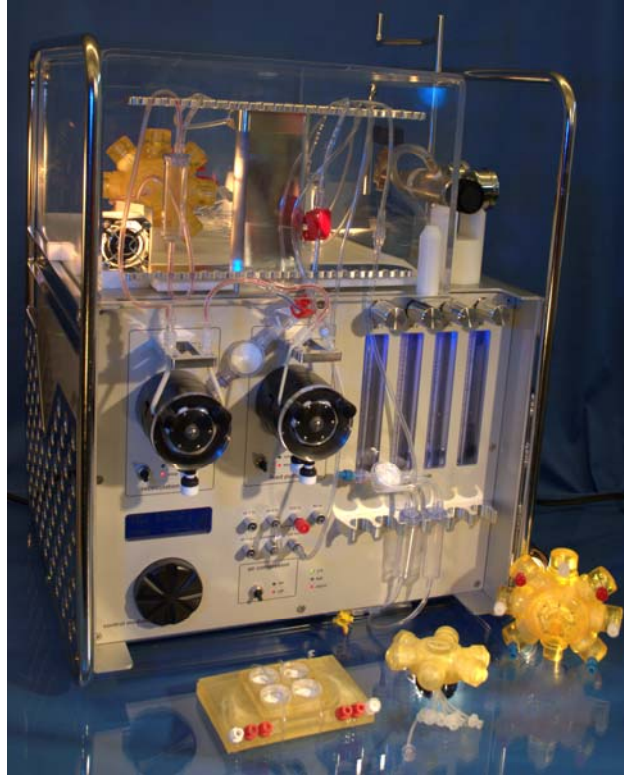


Figure 34. Photograph of latest version of perfusion system (from Stem Cell Systems) used for MNS-3 and MNS-5 four chamber bioreactor experiments. Shows an 8 mL bioreactor placed on the top within the plexiglass heating chamber with tubing circuit connected and configured within the two roller pumps. Chamber is heated using the light bulbs plus fans seen at the top left. Four rotameters to the right control the gas flow rates: gas mixture going into bioreactor and individual air, CO₂, and N₂ components (N₂ not used in these experiments).

3.2.4 Bioreactor metabolic measurements

Medium samples were infused into single use CG4+ cartridges or G Glucose cartridges to measure the following metabolic parameters: lactate, pH, pCO₂, pO₂, and glucose; using the i-STAT[®] clinical blood analyzer system (Abbott, East Windsor, NJ). 3D static gel cultures were maintained each day during culture period by collecting 1.5 mL of culture medium (previously replaced 24 hours earlier) and analyzing metabolic parameters. Medium from bioreactor cultures was collected via syringe withdrawal from the sample port within the recirculation segment of

the tubing circuit (medium flowing through recirculation tubing and bioreactor perfusion fibers at flow rate 30 mL/min). Bioreactor glucose and lactate concentrations have been inserted into formulas incorporating feed medium flow rate to give consumption and production values averaged between two measurements. The formula used for this is shown below in Figure 35.

$$\text{Glucose or Lactate Metabolism} = - \left[\frac{24 * Q_{\text{feed}}}{1000} \right] \left[\frac{(C_1 + C_{1+1})}{2} - C_B \right]$$

Metabolism = glucose consumption (mg/day) or lactate production (mmol/day)

Q_{feed} = feed medium flow rate (mL/hr)

C_1 = metabolite concentration at indicated culture day (mg/L)

Figure 35. Equation used to obtain daily glucose consumption or lactate production values of samples taken from the recirculation medium perfusion circuit during bioreactor culture experiments.

3.2.5 Fluorescent immunohistochemistry visualized with fluorescent microscopy

One sample was used to observe living cells versus dead cells using the Live/Dead Cell Viability Assay (Molecular Probes, Invitrogen) and these samples therefore were not fixed. This kit includes calcein AM staining live cells with a green fluorescent signal and ethidium homodimer-1 (EthD-1) staining dead cells with a red fluorescent signal. Samples were directly incubated with solutions at 2 μm calcein AM and 4 μm EthD-1 and imaged within 30 minutes.

Static control cultures used for immunohistochemistry were first washed with PBS three times and fixed with 4% paraformaldehyde for 30 minutes and washed with PBS again 3 times. Fiber layer samples from 8 mL bioreactor experiments were transferred immediately after opening to tissue cassettes and placed in 4% paraformaldehyde for 1 hour. Samples were then washed with PBS three times, 15 minutes each. For bioreactor experiment MNS-3, using the

four chamber analytical bioreactor, the entire four well compartments were used for immunohistochemical staining and therefore the entire bioreactor was perfused with 4% paraformaldehyde through the perfusion circuit and cell compartment for one hour followed by PBS washing. The bioreactor wells were opened by cutting through the bottom plastic coverslip of each well and removing the fiber-gel layer.

Immunostaining procedure was first carried out by blocking all samples in a 5% horse serum/PBS solution containing 0.3 % triton X-100 (LabChem Inc., Pittsburgh, PA) for 1 hour. All samples were first stained with mouse monoclonal primary antibody against class III neuronal specific β -tubulin (Covance CRP Inc.; Princeton, NJ) 1:500 dilution in 3% HS/PBS solution containing 0.3% triton-X for 1.5 hours. Some samples were instead stained with anti-nestin mouse monoclonal primary antibody (Stem Cell Technologies Inc.) at 1:100 dilution. Samples were then washed five times with PBS each for 10 minutes. Goat-anti-mouse secondary antibody Alexa Fluor 488 (Molecular Probes, Invitrogen Corp.) was then added at dilution 1:1000 in 3% HS/PBS solution containing 0.3% triton-X for 1.5 hours. Samples then received washes five times with PBS each for 10 minutes. Double immunostaining was carried out on all samples with the same previous protocol but with one of the following antibodies: anti-GFAP (glial fibrillary acidic protein) polyclonal rabbit primary antibody (Stem Cell Technologies Inc.) 1:400 dilution, anti-O4 polyclonal rabbit primary antibody (Stem Cell Technologies Inc.) 1:100 dilution. Goat-anti-rabbit secondary antibody Cy3 (Molecular Probes, Invitrogen Corp.) was then added at dilution 1:1000 in 3% HS/PBS solution containing 0.3% triton-X for 1.5 hours. Samples then received final washes five times with PBS each for 10 minutes. All samples were counterstained with DAPI (Sigma Aldrich) for nuclear localization.

2D samples cultured on tissue culture treated dishes were imaged by cutting the bottom surface out of the dish and sealing with gelvatol and glass coverslip. These 2D samples were imaged using an Olympus Provis light microscope with fluorescence capabilities (Olympus; Center Valley, PA) with a 40X oil objective for final magnification of 400X.

Fluorescent confocal microscopy was used to visualize the immunohistochemical staining of 3D static gel and 3D dynamic bioreactor samples (inverted Olympus Fluoview 1000; Center Valley, PA). These 3D samples were imaged by wet mounting with directly placing the sample onto a glass coverslip in order to image both sides of sample. All images taken to observe neural stem cell differentiation were taken using a 40X oil objective (final magnification 400X). All images were taken as z-stacks with 1 μm thick sections at approximately 50 μm depths for 3D gel and bioreactor samples. Stacked section images were reconstructed into maximum intensity projection representations in a single image or avi movie file to demonstrate 30 degree rotation showing 3D characteristics using Metamorph software (Molecular Devices; Downington, PA).

3.2.6 Quantitative RT-PCR gene expression analysis

3D static gel and 3D dynamic bioreactor samples for RNA collection were immediately immersed in RNA Protect reagent (QIAGEN, Valencia, CA) and stored at 4°C for less than two weeks before RNA collection. For RNA collection, samples were first centrifuged to pellet cell, gel, and/or fiber material with removal of supernatant. Total RNA was isolated from all samples with an mRNA isolation kit including on-column DNase digestion (QIAGEN, Valencia, CA). The first step was carried out by placing the samples in the first buffer solution of the kit and using a disposable pestle the sample was ground to mechanically digest the collagen gel tissue.

cDNA was synthesized by a conventional reverse transcription process (Promega, Madison, WI). The master mixture contained 5 mmol/L MgCl₂, 1x Reverse Transcription Buffer, 1 mmol/L deoxynucleotide triphosphate mixture, 1unit/μL recombinant RNasin® ribonuclease inhibitor, 0.75U/μL AMV reverse transcriptase, and 1μg of random hexamer Primers. Two micrograms of total RNA were prepared in sterile H₂O to a final volume of 20μL. The reaction mixture was incubated at 42°C for 60 minutes, followed by heat inactivation of the enzyme at 95°C for 5 minutes. After cooling on ice for 5 minutes, the cDNA was stored at -20°C until analysis. Quantification of mRNAs using real-time polymerase chain reaction (qRT-PCR) analysis was performed using an ABI PRISM 7000. The pre-designed TaqMan probe and primer sets for *Tubb3* (Mm00727586_s1), *Gfap* (Mm01253033_m1), *Mbp* (Mm01262037_m1), and *GAPDH* (Rn99999915_g1) were selected from TaqMan Gene Expression Assays (Applied Biosystems, Foster City, CA).

3.3 RESULTS

3.3.1 Properties of mouse neural stem cells

Mouse embryonic neural stem cells (mNSCs) were purchased as passage 1 neurospheres from Stem Cell Technologies Inc. Cells were expanded to passage 9 using Neurocult Proliferation medium including 20 ng/mL rhEGF in order to obtain enough cells for bioreactor experiments and therefore performed most experiments using neurospheres at passage 9. Only initial neurosphere differentiation tests were performed using lower passage cells. Figure 36 represents the nestin immunostaining of the passage 9 neurospheres after expansion demonstrating cells

could be expanded within our laboratory maintaining the cells in an undifferentiated state, correlating with high positive staining for nestin, while preventing too much spontaneous differentiation of the cells. When the neurospheres expand and reach a sphere size that is too large to be maintained, the cells will begin to spontaneously differentiate and attach to the bottom of the culture flask. A neurosphere in the initial stage of this process with low nestin staining is seen in the middle of the image on the right in Figure 36.

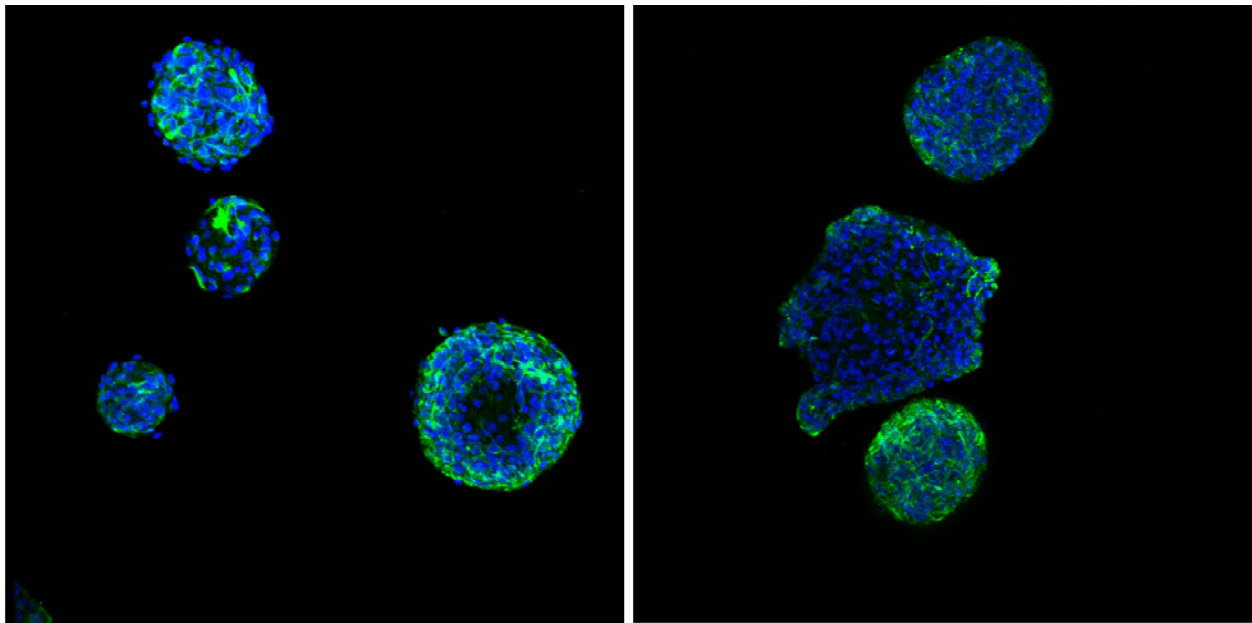


Figure 36. Confocal fluorescent images representative of mouse neural stem cell neurospheres expanded to passage 9; immunostained with antibody against nestin (neural stem cell marker) with AlexaFluor 488 (green) and nuclear DAPI (blue) at magnification 200X (single image z-stack reconstructions through 50 μm depth of neurospheres).

For differentiation of the neurospheres, cells are seeded on dishes coated with an adhesive surface for the neurospheres to attach and cultured using Neurocult Differentiation medium. Standard protocol for optimal neural stem cell differentiation is by seeding the cells onto laminin coated tissue culture plates. When mNSCs are seeded onto adhesive laminin coated

tissue culture plates as neurospheres, the neurospheres attach and begin to migrate away from the neurosphere in order to properly differentiate. After 24 hours of neurosphere seeding onto laminin coated plates, the cells completely attach and form a confluent layer on the surface of the laminin coated substrate with different morphologies (some cells already resemble neurons with phase bright bodies and multiple processes).

Other factors could contribute to determining enhanced differentiation conditions of the cells as well and therefore we tested the effects of neurosphere dissociation and seeding density on mNSC differentiation. The results of these tests are shown using passage 3 mNSCs in Figure 37. The top row of this figure depicts examples of seeding mNSCs as a single cell suspension by dissociating the neurospheres with two different methods: mechanical trituration or chemical enzymatic digestion. Both images demonstrate a low percentage of differentiation of the mNSCs into neurons (green β -III-tubulin staining). Therefore, all further experiments were performed by seeding mNSCs as neurospheres instead of in a single cell suspension. Also, cells were seeded as neurospheres so that autocrine factors produced by the cells could help maintain support of the cells especially after inoculation into the bioreactor. Most *in vivo* studies testing neural stem cell transplantation as cell therapy treatments use the cells as whole intact neurospheres for this same reason.

The bottom row of Figure 37 shows the results of varying the seeding density of the neurospheres and the effects on differentiation at the different densities. The images shown are the differentiated cells seeded at the two highest seeding densities tested of 2.5×10^3 cells/mm² and 5×10^3 cells/mm² after 14 days of differentiating (other densities not shown). The percentage of mNSCs differentiated into neurons did not appear to change, but a higher number of cells would seem to imply the ability to attain more neurons within a culture. However, at these

higher densities on a 2D surface, the cells did not have enough surface area to completely attach onto the surface from the neurospheres (as seen in the images as brighter GFAP (red) stained clusters). In order for the neurospheres to have the proper surface area to completely spread out from the spheres to confluency on the 2D surfaces, all 2D cultures were performed with an initial seeding density of 1.5×10^3 cells/mm².

The mNSCs have the ability to differentiate into neurons and astrocytes as well as oligodendrocytes. These cells are an important and desired lineage of differentiation for the mNSCs, but the percentage of cells differentiating within the control 2D laminin coated cultures towards the oligodendrocyte lineage was very low. An example of O4 immunostaining (immature oligodendrocyte marker) is shown in Figure 38 with cells differentiated for 14 days on a laminin coated dish. Since the detection of immature oligodendrocytes was observed to be very low under optimal differentiation conditions and ability to perform triple immunostaining on a single sample is complicated, differentiation on most samples was observed by double immunostaining for only β -III-tubulin labeling neurons and GFAP labeling astrocytes together. Also, a very high percentage of the mNSCs differentiate mostly into astrocytes even with the optimal culture conditions, and the desired goal was to vary culture conditions for improving neuronal differentiation which is also by preventing astrocyte differentiation.

Figure 39 is representative of the differentiation achieved in positive control cultures of mNSCs after 14 days in Neurocult Differentiation medium on laminin coated dishes. The cells were seeded in these cultures using the same neurosphere preparation protocol as all further experiments. Cells were expanded to passage 9 and neurospheres were mechanically dissociated by partial trituration to obtain smaller diameter neurospheres. All 2D cultures were seeded at the same density of 1.5×10^3 cells/mm², which is the same density for the cultures shown in Figure

39. This density was chosen because on the laminin coated surface, this density allows complete attachment and spreading of the cells from the neurospheres to attain a confluent monolayer of cells. The seeding of cells as partially triturated (5-10 times trituration) smaller diameter neurospheres allowed this complete migration of cells out onto the 2D surface from the spheres, and therefore cells were seeded in all experiments using this method.

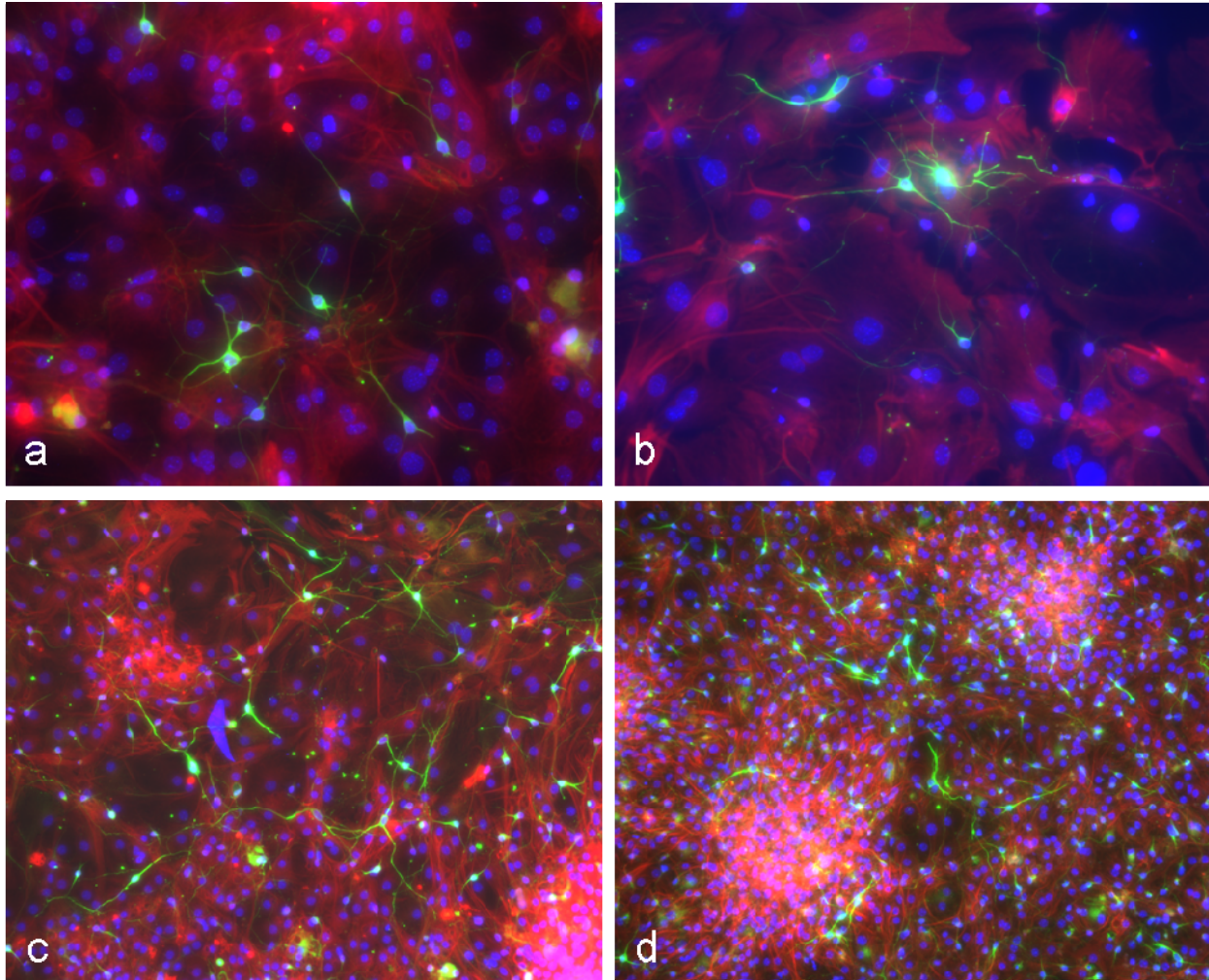


Figure 37. Fluorescent microscopic images of passage 3 mouse neural stem cells differentiated on 2D laminin coated tissue culture treated dishes for 14 days. Immunostaining with antibodies against β -III-tubulin (neuron specific) with AlexaFluor 488 (green), glial fibrillary acidic protein (GFAP; astrocyte specific), and nuclear DAPI (blue). Top row depicts neuronal differentiation after seeding single cell suspension testing neurosphere dissociation techniques: a) chemical dissociation (enzymatic kit from Stem Cell Technologies Inc.) and b) mechanical trituration with fire polished Pasteur pipette (magnification 400X). Bottom row depicts neuronal differentiation after seeding partially triturerated neurospheres testing seeding density effects on differentiation: c) 2.5×10^3 cells/mm² seeding density and d) 5×10^3 cells/mm² seeding density (magnification of 200X).

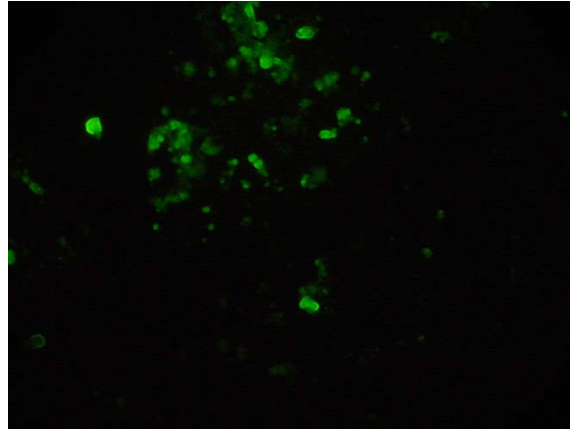


Figure 38. Example of fluorescent microscopic image detecting mNSC differentiation into oligodendrocytes by immunostaining with antibody against O4, an immature oligodendrocyte marker, with AlexaFluor 488 (green) (magnification 200X).

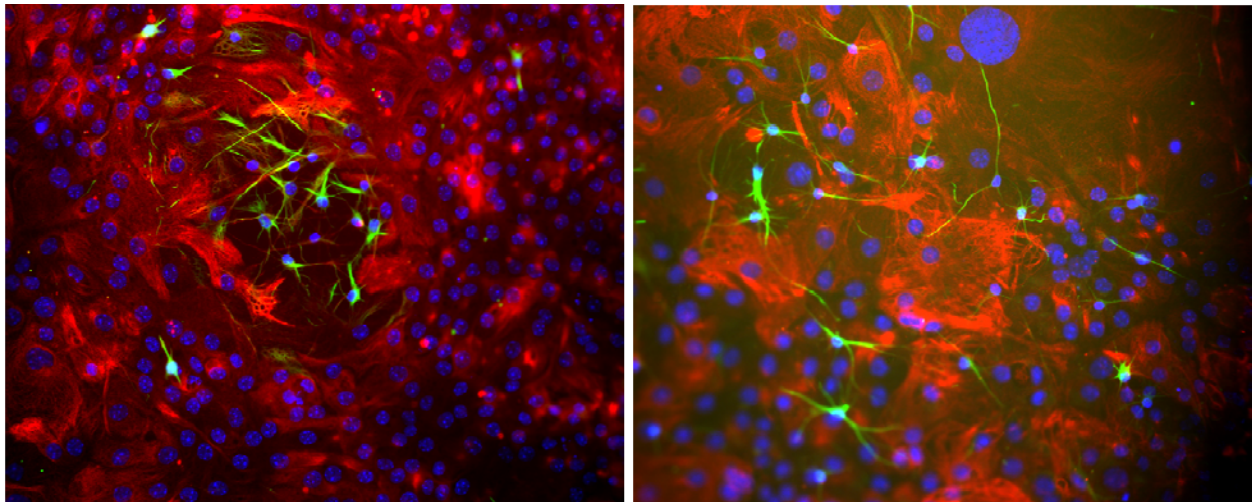


Figure 39. Fluorescent microscopic images of passage 9 mouse neurospheres differentiated on 2D laminin coated tissue culture treated dishes for 14 days. Immunostaining with antibodies against β -III-tubulin (neuron specific) with AlexaFluor 488 (green), glial fibrillary acidic protein (GFAP; astrocyte specific) with Cy3 (red), and nuclear DAPI (blue) (magnification 400X). Displays optimal differentiation of control mNSC cultures with cells expanded to passage 9 and seeded as semi-dissociated smaller neurospheres and differentiated with Neurocult Differentiation media.

3.3.2 Light microscopic analysis of mNSC differentiation on 2D and 3D ECM hydrogel cultures

Imaging of neural stem cells during the differentiation culture period testing the effect of varying the ECM was performed using an inverted light microscope. Figure 40a shows the results of mNSC neurosphere differentiation on collagen coated 2D tissue culture plates at day 5 of the differentiation culture period. The image shows spheres attached to the collagen coated surface with cells only forming structures between the attached spheres. However, many single cells migrated out from the neurospheres attaching to the collagen coated substrate throughout the entire surface area of the plate by culture day 1 (24 hours after neurosphere seeding) (image not shown), but these cells had died and lifted from the plate by culture day 3. Therefore, only the cells left by culture day 8 are the surviving cells that were able to attach onto each other within structures instead of attaching to the collagen coated surface. Images of Figure 40 b and c show the results of cell viability using a live/dead (green/red) staining on this same culture showing most of the cells remaining within the structures by culture day 8 were alive.

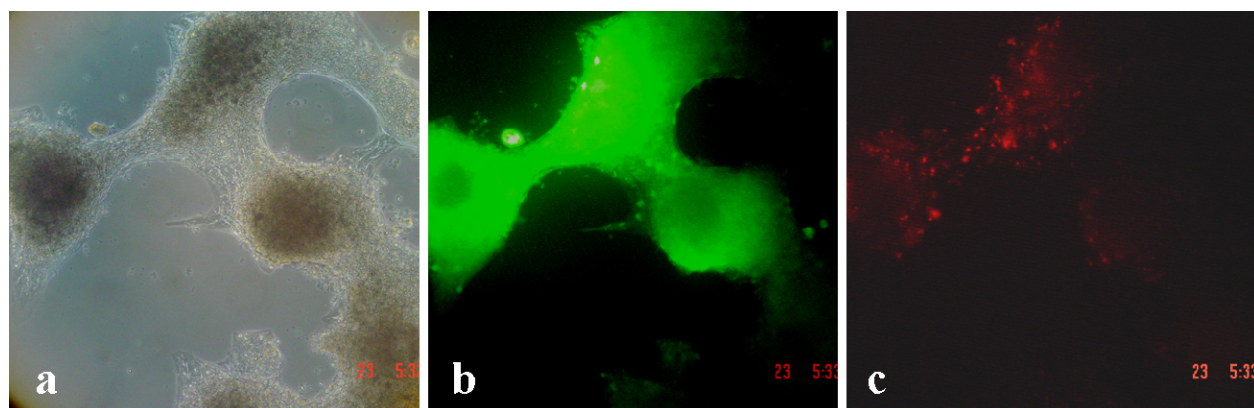


Figure 40. Mouse neurospheres differentiating for 8 days on 2D collagen coated dishes: a) light microscopic image showing neurosphere structure formation; b) cell viability staining of these structures showing live cells (green); and c) cell viability staining of these structures showing dead cells (red) (magnification 100X).

Figure 41a depicts the morphology of mNSCs differentiating on Matrigel coated tissue culture plates at culture day 5. Some single cells were able to attach from the spheres onto the Matrigel coated surface forming multiple processes from the cells out of the spheres and towards each other. However, by culture day 14 as shown in Figure 41b, many cells did not survive the full differentiation culture period when differentiating on the 2D Matrigel coated surfaces. Seeding neurospheres onto 2D coatings of HyStem, either as coatings of HA component or 1 mm thick hydrogel layer, resulted in no neurospheres attaching to this ECM substrate after 24 hours. This therefore prevented possible 2D cultures of mNSC differentiation on HyStem.

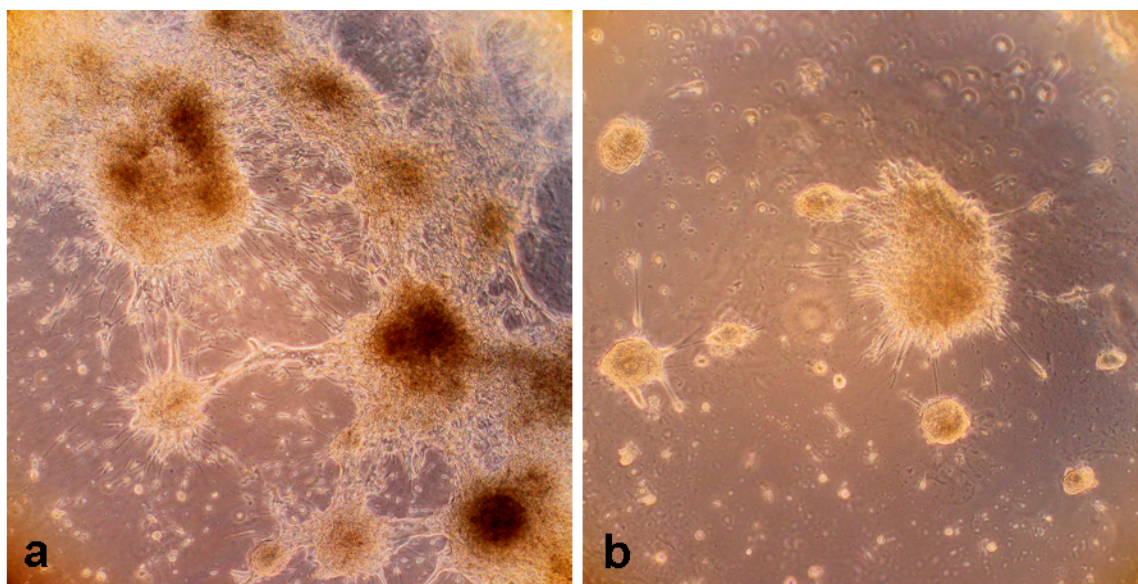


Figure 41. Mouse neurospheres differentiating on 2D Matrigel coated dishes: a) light microscopic image showing neurosphere differentiation on culture day 5, b) light microscopic image showing neurosphere differentiation on culture day 14 (magnification 100X).

Figure 42 depicts examples of light microscope imaging of mNSC neurospheres differentiating within the three different 3D ECM hydrogels maintained under static culture conditions at culture day 2. The first image (a) represents the neurospheres within the collagen type I hydrogel showing few processes protruding from neurospheres into the surrounding

collagen hydrogel. The image in (b) represents the morphology of mNSCs differentiating within the Matrigel hydrogels. Neurospheres within the Matrigel acquired multiple processes extending from the spheres within the first two days of culture. These processes and spheres stayed in tact within the Matrigel 3D hydrogels for the entire duration of the 14 day culture period.

When prepared with the manufacturer recommended ratio of HA component to PEG-DA cross-linker component, the HyStem product enables formation of a more rigid hydrogel when compared to the collagen and Matrigel hydrogels. The mNSC cultures using the 3D HyStem hydrogels cultured under static conditions led to an acidic medium pH of 6.9 after the first 24 hours of culture. The image in Figure 42c depicts the neurospheres encapsulated within the HyStem hydrogel at culture day 2. Most cells within the neurospheres are seen instead as individual rounded cells broken apart from the intact neurosphere, implying cells are dead. Cells continued to appear with this same morphology throughout the entire culture period. Also, morphology of mNSCs within 3D HyStem hydrogel cultures incorporating 100 $\mu\text{g}/\text{mL}$ laminin looked exactly the same as the image shown in Figure 42c for the unmodified 3D HyStem hydrogel cultures.

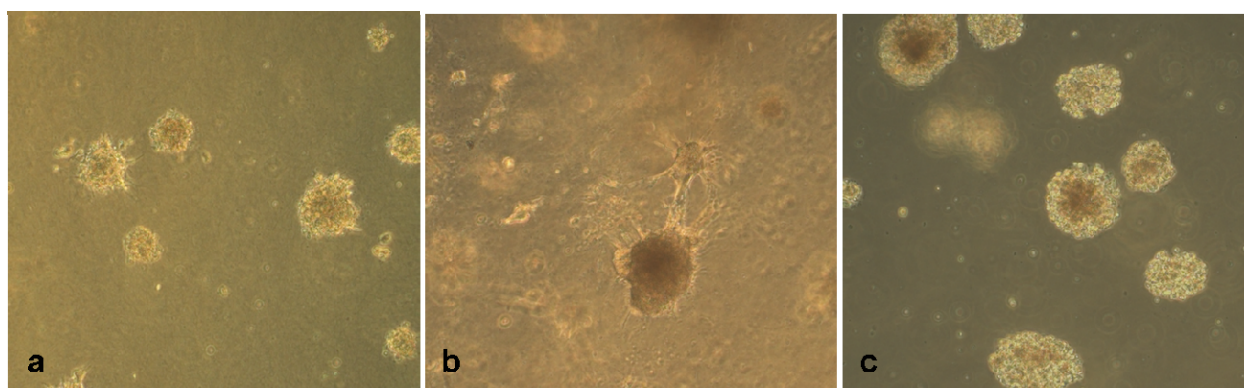


Figure 42. Light microscopic images of mouse neurospheres differentiating within 3D ECM hydrogels on culture day 2 under static conditions: a) collagen type I; b) high concentration growth factor-reduced Matrigel; and c) HyStem (cross-linked hyaluronic acid) (magnification 100X).

3.3.3 mNSC neuronal and astrocytic differentiation on 2D ECM coated plate cultures

Immunostaining for detection of neurons and astrocytes of the mNSCs cultured and differentiated for 14 days on the 2D ECM coated tissue culture plates are shown in Figure 43- Figure 45. Images in Figure 43 show examples of neuron and astrocyte differentiation of mNSCs on the 2D collagen coated surfaces. As described above the cells completely spreading out from the neurospheres and attaching to the coated plate died and lifted from the plate by the end of the 14 day culture period, but the cells left intact that were able to form structures and differentiate on top of each other were able to undergo substantial neuronal differentiation. More neurons are seen around the edges of intact neurospheres attached to the surface. It seems that this neuronal differentiation was possible where cells were able to attach on top of underlying astrocytes, as seen in the bottom right image.

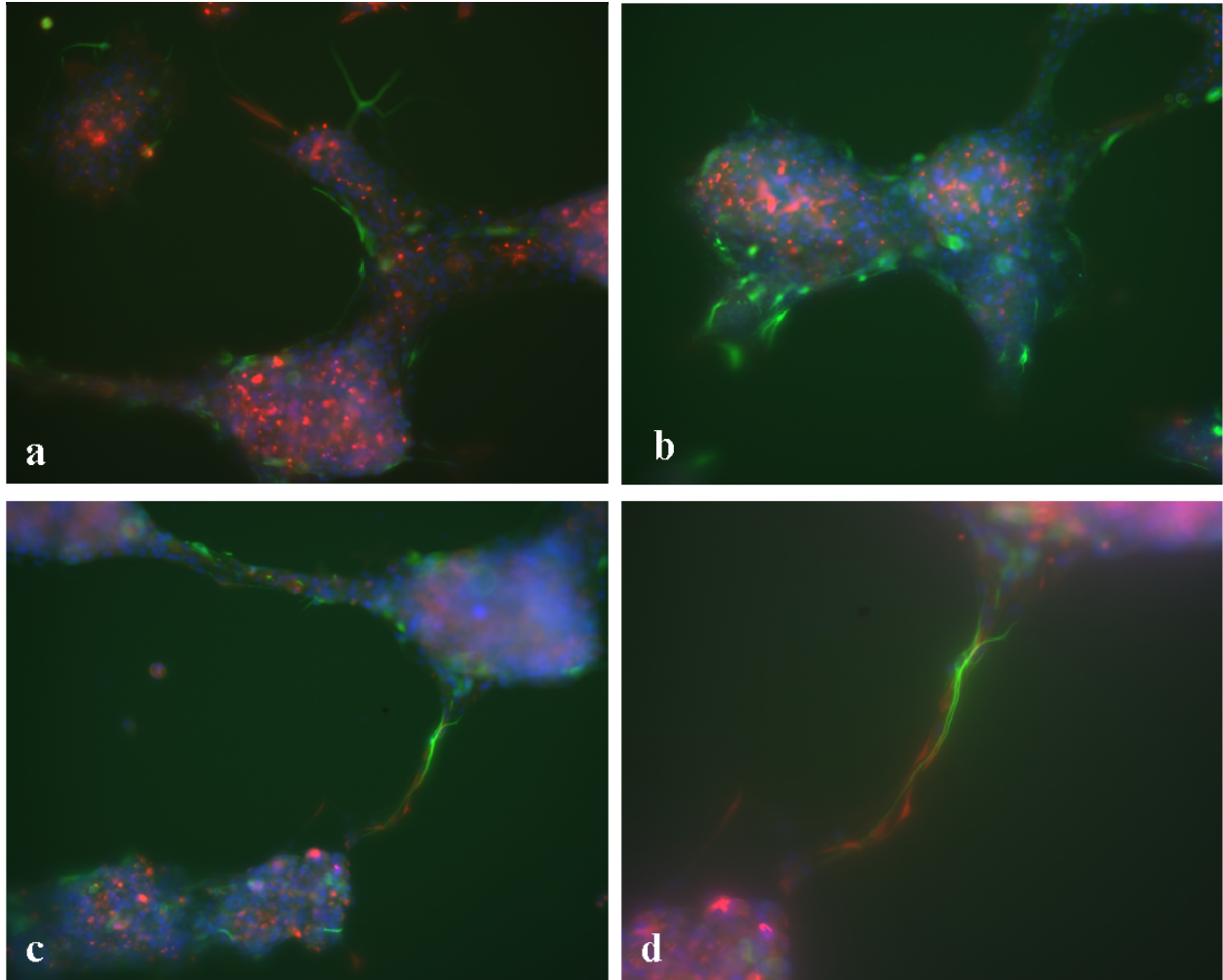


Figure 43. Fluorescent microscopic images of mouse neurospheres differentiated on 2D collagen coated tissue culture treated dishes for 14 days. Immunostaining with antibodies against β -III-tubulin (neuron specific) with AlexaFluor 488 (green), glial fibrillary acidic protein (GFAP; astrocyte specific) with Cy3 (red), and nuclear DAPI (blue) (a and c magnification 200X, b and d magnification 400X).

Since attachment and spreading of cells from neurospheres onto collagen coated 2D surfaces was poor, the culture medium was altered to include 20 ng/mL of bFGF (basic fibroblast growth factor) for enhancing cell survival. This growth factor was incorporated because Gobbel et al. demonstrated increased neuronal differentiation from rat neurospheres with the addition of bFGF at this concentration when kept in the differentiation medium [295]. Also, O'Shaughnessy

et al. achieved functional neuronal differentiation from rat neurospheres differentiating within 3D collagen hydrogels using a medium formulation including bFGF [172]. The results of our mouse neurospheres differentiating on either laminin or collagen coated 2D surfaces with incorporation of bFGF into the differentiation medium improved cell survival, but decreased neuronal differentiation of the cells especially on the collagen as seen in Figure 44. Therefore, bFGF was not further added to the differentiation medium in any further experiments.

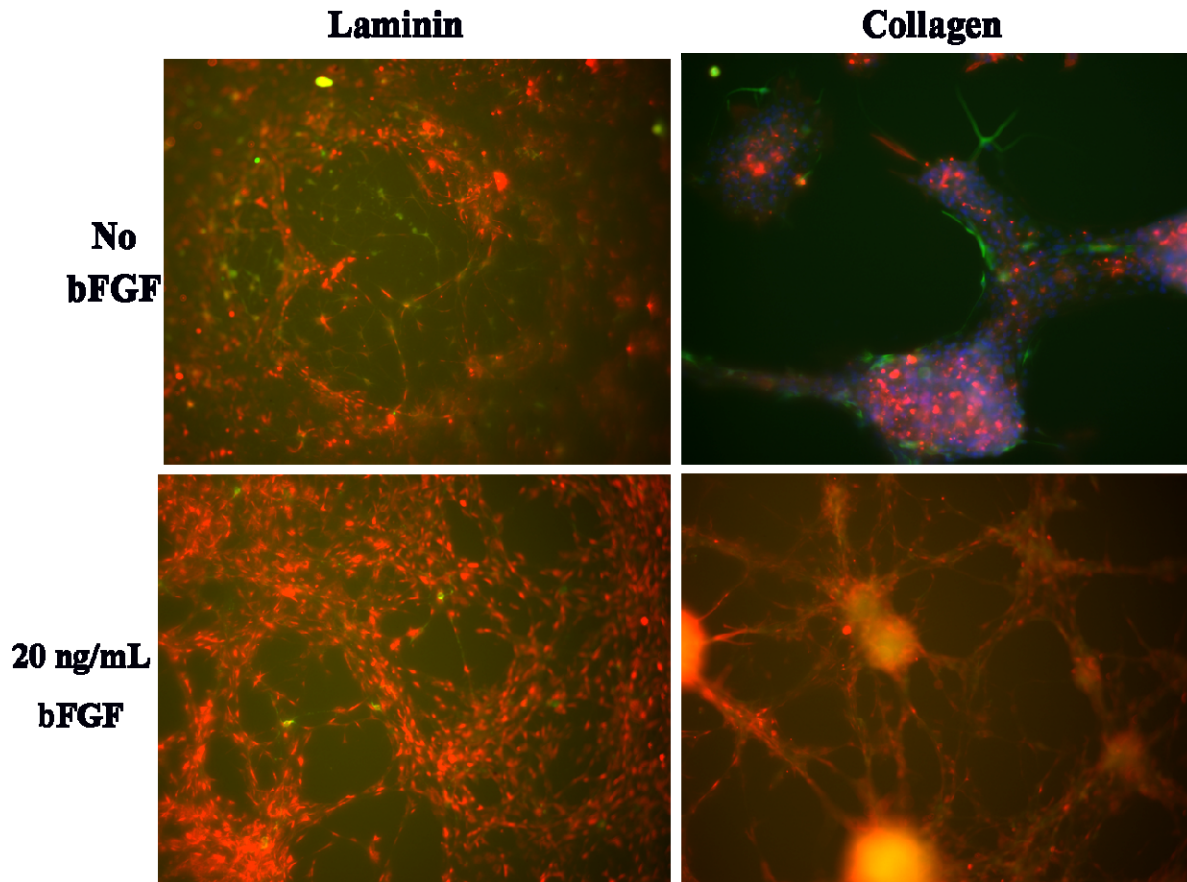


Figure 44. Fluorescent microscopic images of mouse neurospheres differentiated for 14 days testing effects of addition of 20 ng/mL bFGF on neuronal differentiation. Immunostaining with antibodies against β -III-tubulin (neuron specific) with AlexaFluor 488 (green), glial fibrillary acidic protein (GFAP; astrocyte specific) with Cy3 (red), and nuclear DAPI (blue, only in top right image) (magnification 400X). Left column shows neurospheres seeded on laminin coated dishes and right column shows neurospheres seeded on collagen coated dishes. Top row shows these cultures with no added growth factors while bottom row shows these cultures with the addition of 20 ng/mL bFGF to the Neurocult Differentiation media.

Differentiation of the mNSC neurospheres onto Matrigel coated 2D tissue culture plates resulted in more attachment of cells onto the Matrigel coated surface, but the differentiation of these cells resulted in mostly astrocytes as seen in Figure 45. Also, most of the cells that did stain positive for β -III-tubulin, indicating neuronal differentiation, also partially stained positive

for GFAP, usually indicating astrocyte differentiation. This double positive staining was never observed within any other mNSC cultures on other ECM substrates. The arrows of Figure 45 indicate these double stained cells.

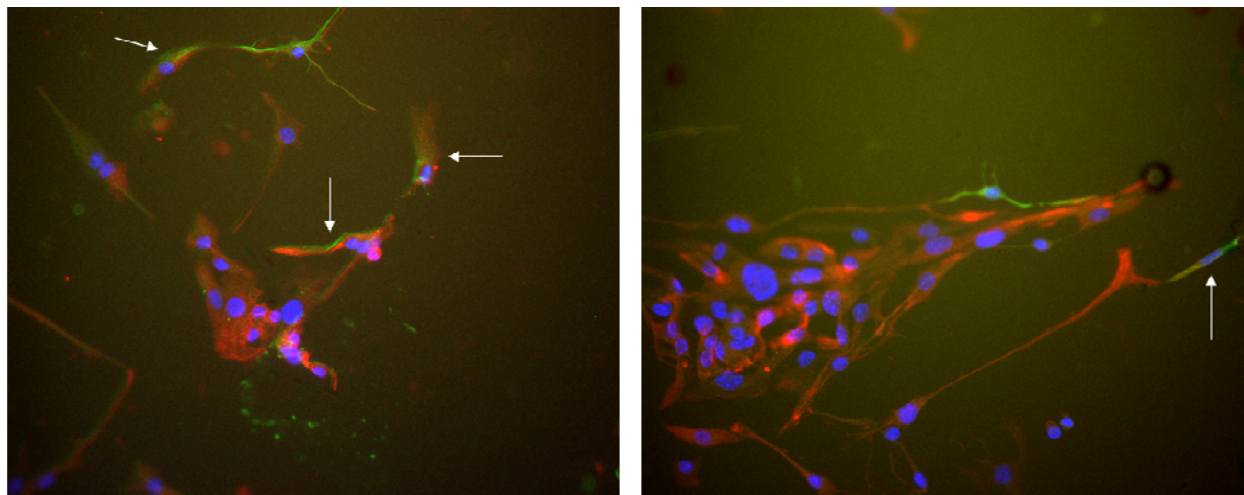


Figure 45. Fluorescent microscopic images of mouse neurospheres differentiated on 2D Matrigel coated tissue culture treated dishes for 14 days. Immunostaining with antibodies against β -III-tubulin (neuron specific) with AlexaFluor 488 (green), glial fibrillary acidic protein (GFAP; astrocyte specific) with Cy3 (red), and nuclear DAPI (blue) (magnification 400X). Arrows indicate cells staining positive for both β -III-tubulin and GFAP.

3.3.4 mNSC neuronal and astrocytic differentiation within 3D ECM hydrogel cultures

Confocal fluorescence imaging with immunostaining was used to observe differentiation of the mNSCs cultured within the different 3D ECM hydrogels tested. Figure 46 shows the results of confocal imaging of different stains of mNSCs differentiated within 3D collagen hydrogels cultured under static conditions. The image in Figure 46a represents the cell viability live/dead staining showing that most cells within the collagen hydrogels at the end of the 14 day culture period are alive. The image in Figure 46b shows the results of immunostaining these samples with nestin, the neural stem cell marker, indicating that most cells still located within the

neurospheres are still nestin positive and remain as undifferentiated stem cells. The image in Figure 46c shows that very few of the cells cultured within the collagen hydrogels differentiate either into neurons or astrocytes. Very few cells were stained positive with the β -III-tubulin or GFAP markers.

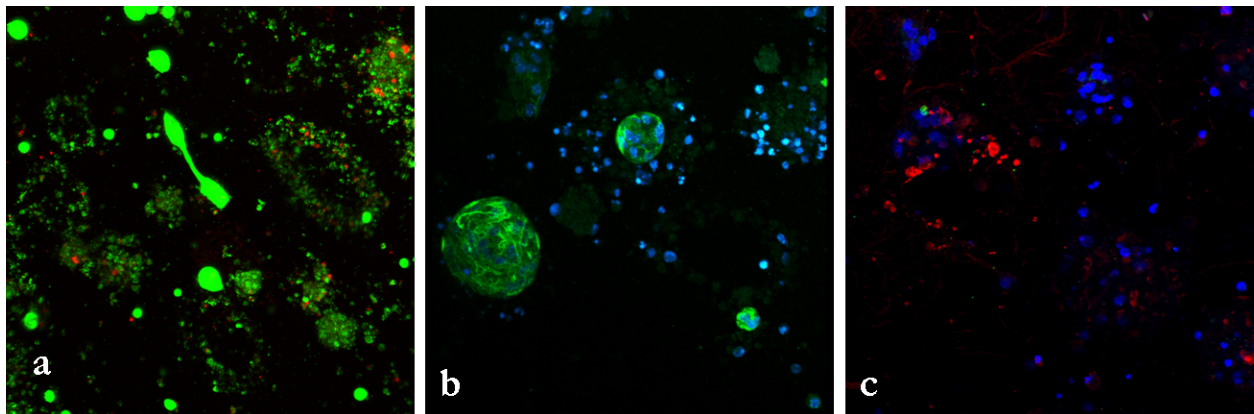


Figure 46. Confocal fluorescent microscopic images of mouse neurospheres within 3D collagen hydrogels after 14 days of differentiation under static conditions: a) cell viability staining with live cells (green) and dead cells (red) (magnification 200X); b) immunostaining with antibody against nestin (stem cell marker; green) and nuclear DAPI (blue) counterstaining (magnification 400X); and c) immunostaining with antibodies against β -III-tubulin (neuron specific) with AlexaFluor 488 (green), glial fibrillary acidic protein (GFAP; astrocyte specific) with Cy3 (red), and nuclear DAPI (blue) (magnification 400X).

Enhancement of neurospheres differentiated within 3D collagen hydrogels was attempted by modifications incorporating either bFGF into the medium or incorporation of laminin within the collagen hydrogel solution before gelation. The results of these cultures are shown in Figure 47. The image in Figure 47a depicts the results of culturing the neurospheres in the collagen hydrogel including bFGF in the medium, showing similar results as the 2D cultures with this modification where migration of cells out from spheres into the surrounding collagen hydrogel is not enhanced. However, the modification of adding laminin into the collagen hydrogel did

increase neuronal differentiation in these cultures substantially and in a dose-dependent manner. The images in Figure 47b-c demonstrate the increasing amounts of incorporated laminin further enhanced neuronal differentiation within the collagen hydrogels and imply the importance of the effects of laminin on the differentiation of mNSCs.

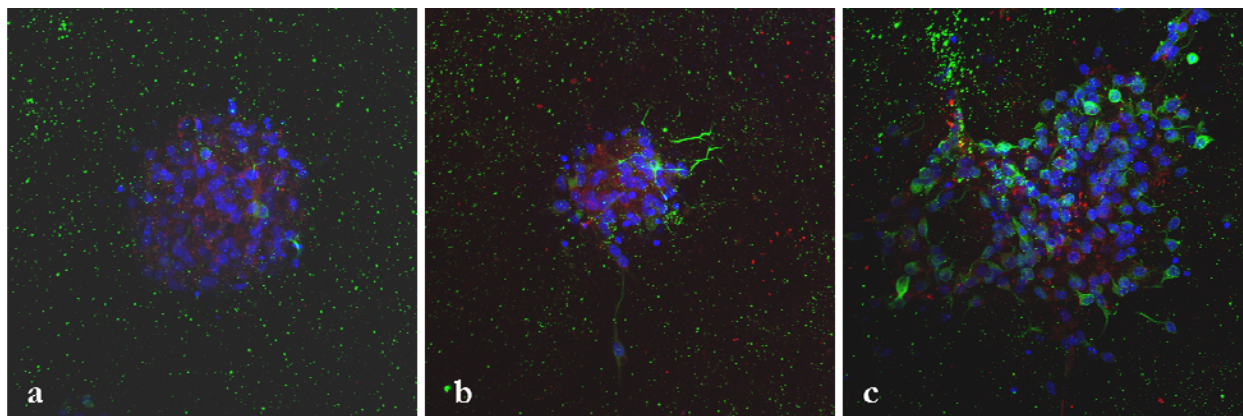


Figure 47. Confocal fluorescent microscopic images of mouse neurospheres within 3D collagen hydrogels including modifications after 14 days of differentiation under static conditions: a) 20 ng/mL bFGF included in medium; b) incorporation of 50 µg/mL laminin within collagen gel solution; and c) incorporation of 100 µg/mL laminin within collagen gel solution. Immunostaining with antibodies against β -III-tubulin (neuron specific) with AlexaFluor 488 (green), glial fibrillary acidic protein (GFAP; astrocyte specific) with Cy3 (red), and nuclear DAPI (blue) (magnification 400X). Staining protocol for these samples was modified to incubate with primary antibodies overnight at 4°C to improve neurosphere staining, but resulted in inability to completely wash out all excess antibody and therefore gave non-specific staining across entire samples.

Figure 48 show images of confocal fluorescent microscopy of immunostaining mNSCs differentiated within 3D Matrigel hydrogels cultured under static conditions. The images depict some astrocyte differentiation of the cells having processes extending from the neurospheres. Also, a higher number of β -III-tubulin positive cells are seen within these 3D Matrigel cultures as compared to the 2D Matrigel coated cultures. However, again these cells staining positive for the neuronal marker again are mostly also positive for the GFAP astrocyte marker, indicated in

the images with arrows. There are many cells within these cultures that do not stain positive for either neurons or astrocytes, but nestin immunostaining on the mNSCs cultured within 3D Matrigel hydrogels is shown in Figure 49. Few cells stained positive for nestin within this image indicating remaining stem cells within the Matrigel cultures is rarer than what is implied by the amount of cells not staining positive for the other markers, but these stains were performed on separate samples.

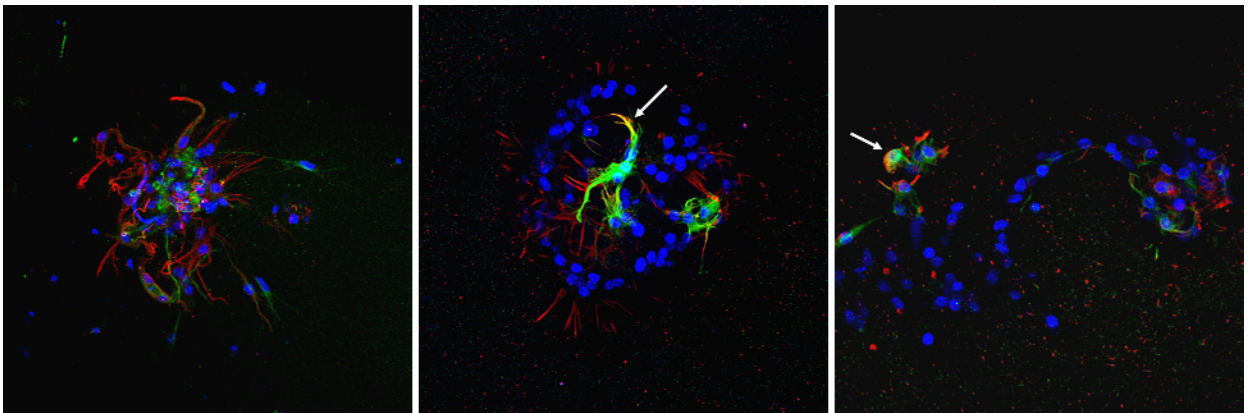


Figure 48. Confocal fluorescent microscopic images of mouse neurospheres within 3D Matrigel hydrogels after 14 days of differentiation under static conditions. Immunostaining with antibodies against β -III-tubulin (neuron specific) with AlexaFluor 488 (green), glial fibrillary acidic protein (GFAP; astrocyte specific) with Cy3 (red), and nuclear DAPI (blue) (magnification 400X). Arrows indicate cells staining positive for both β -III-tubulin and GFAP.

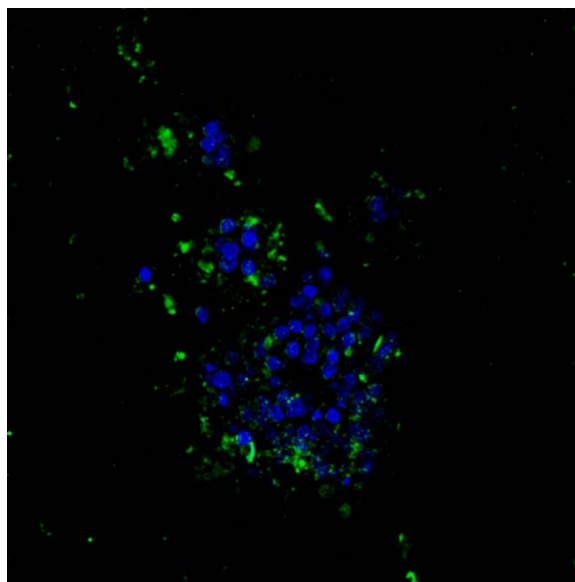


Figure 49. Confocal fluorescent microscopic images of mouse neurospheres within 3D Matrigel hydrogels after 14 days of differentiation under static conditions. Immunostaining with antibody against nestin (neural stem cell marker) with AlexaFluor 488 (green) and nuclear DAPI (blue) counterstaining (magnification 400X).

Even though light microscopic images of mNSC differentiation within HyStem cultures revealed possible cell death within this ECM hydrogel, samples were immunostained and imaged using confocal fluorescence microscopy. Figure 50 shows that there was no staining of the cells within these cultures for the differentiation markers. This image also shows very few intact nuclei with DAPI staining within a neurosphere with instead leftover fragments of the dead cell nuclei. This image is also representative of the mNSCs cultured within 3D HyStem hydrogels incorporating 100 $\mu\text{g}/\text{mL}$ laminin within the hydrogel solution before gelation where laminin was not able to enhance cell survival or differentiation within this hydrogel (specific image of this culture looks similar to Figure 50 with only some DAPI nuclear staining).

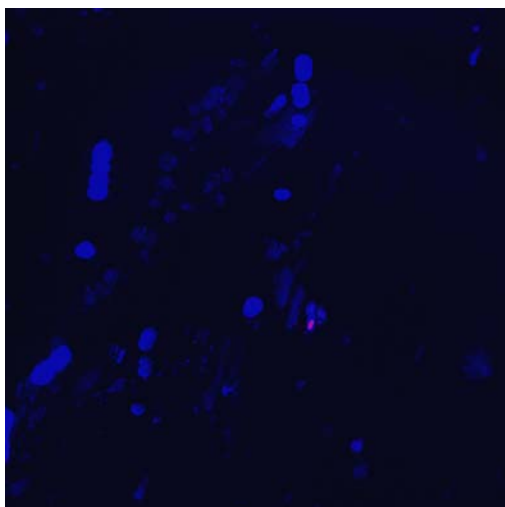


Figure 50. Confocal fluorescent microscopic image of mouse neurospheres within 3D HyStem hydrogel after 14 days of differentiation under static conditions. Immunostaining with antibodies against β -III-tubulin (neuron specific) with AlexaFluor 488 (green), glial fibrillary acidic protein (GFAP; astrocyte specific) with Cy3 (red), and nuclear DAPI (blue) (magnification 400X).

3.3.5 Metabolic activity of bioreactor cultures

Glucose and lactate measurements were taken daily during the culture of mNSCs within the 8 mL bioreactor experiments. The results of the glucose and lactate metabolism throughout these three cultures are shown in Figure 51. The three 8 mL bioreactor experiments were seeded with 1×10^8 neural stem cells as neurospheres in each of the three ECM hydrogel solutions. All three of these bioreactor cultures underwent a dramatic decrease in metabolic activity within the first five days in culture. The lactate concentrations dropped by the end of the culture period to 20-25% of the initial concentrations on culture day 1 for all of the 8 mL bioreactor experiments. Decreasing metabolic activity implies cell death within the bioreactor. Also, after shut down of these experiments and opening of the cell compartment it was apparent the many cells had not

survived the culture period and very few neurospheres were observed within the samples either by light microscopy or confocal fluorescence microscopy after immunostaining.

Metabolic data for experiment MNS-3 culturing mNSCs within the four chambered bioreactor was taken daily, but the results of this data showed no changes within the glucose concentrations and no detection of lactate throughout the entire culture period. The tubing circuit used for the 8 mL bioreactors was the same as that used for MNS-3, holding the same volume that the glucose and lactate concentrations are sampled from. However, the four chamber bioreactor was seeded with 20% of the total number of cells seeded within the 8 mL bioreactors experiments. This same circuit volume dilutes any observable changes within the concentrations measured within the circuit and therefore this data is not shown. The lactate concentrations for MNS-3 and MNS-5 were below the operable detection range of the i-Stat device used to measure these concentrations (range = 0.3 -20 mmol/L).

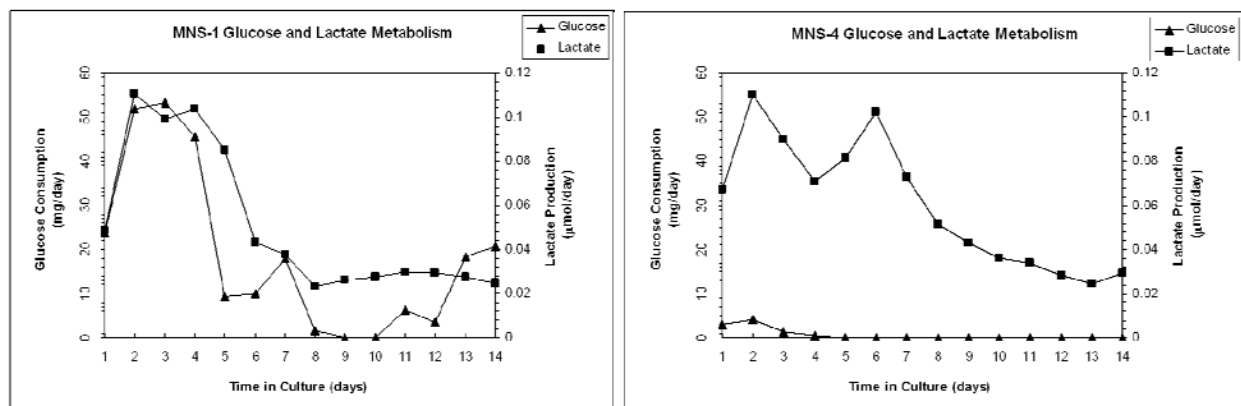


Figure 51. Plots of glucose and lactate metabolism of samples collected daily from the mNSC cultures within the 8 mL hollow fiber-based bioreactors. Only metabolic plots for experiments MNS-1 and MNS-4 are shown.

3.3.6 Live cell imaging during four chamber bioreactor culture

Unlike the larger 8 mL bioreactor, the four chamber bioreactor allows light microscopic visualization of the cells within the chambers during the culture period. The bioreactor perfusion systems for these experiments are placed adjacent to an inverted light microscope, with the tubing circuit used for these bioreactors having extensions long enough to maintain the tubing connected to the pumps while moving the bioreactor from the perfusion system to the microscope stage in order to image. Images were taken daily of each chamber throughout the culture periods of bioreactor experiments MNS-3 and MNS-5. A montage of the images taken in experiment MNS-3 is shown in Figure 52 demonstrating the morphology of the neurospheres on culture day 2, 6, and 14. The chamber with mNSCs encapsulated in collagen shows initial process outgrowth from the cells and attachment of cells from the neurospheres within the first 5 culture days, but by culture day 5 the cells that migrated out appear rounded resembling dying cells. By the end of the 14 day culture the neurospheres within the collagen appeared to have a halo formed around the spheres.

The neurospheres within the Matrigel chamber of experiment MNS-3 remained intact with no changes in morphology until culture day 6. It was only on this culture day that the cells within the spheres began to extend processes into the surrounding Matrigel hydrogel. Also, the Matrigel within this chamber seemed to detach between some of the fibers, as seen in the image for the Matrigel chamber at culture day 2 as the phase bright horizontal line. Imaging of the Matrigel and collagen containing chambers after culture day 6 revealed pulsatile movements of the neurospheres within the gel between fibers in coordination with the pulsatile flow of the recirculation pump. A time lapse movie was taken demonstrating this back and forth movement of some of the spheres, but not all neurospheres endured observable movements.

The chamber containing mNSCs encapsulated in the HyStem hydrogel of MNS-3 displayed dramatic morphological changes within 12 hours after bioreactor cell inoculation (as seen in Figure 53a). The cells began to migrate from the neurospheres forming structures throughout the HyStem hydrogel. By culture day 2 as seen in the image of Figure 52, these cells formed structures between neurospheres. By culture day 14 within the HyStem cells continued to spread throughout the hydrogel into morphologies that were hard to detect with the light microscope. Individual cells are then difficult to observe within the 3D hydrogels. However, there were some structures that deteriorated over the 14 day culture period within the HyStem chamber. The structures seen in the culture day 2 image of Figure 52 is the same structure at the end of the culture period shown in Figure 53c. The result of this deterioration is later elaborated on within the Discussion Section 3.4.

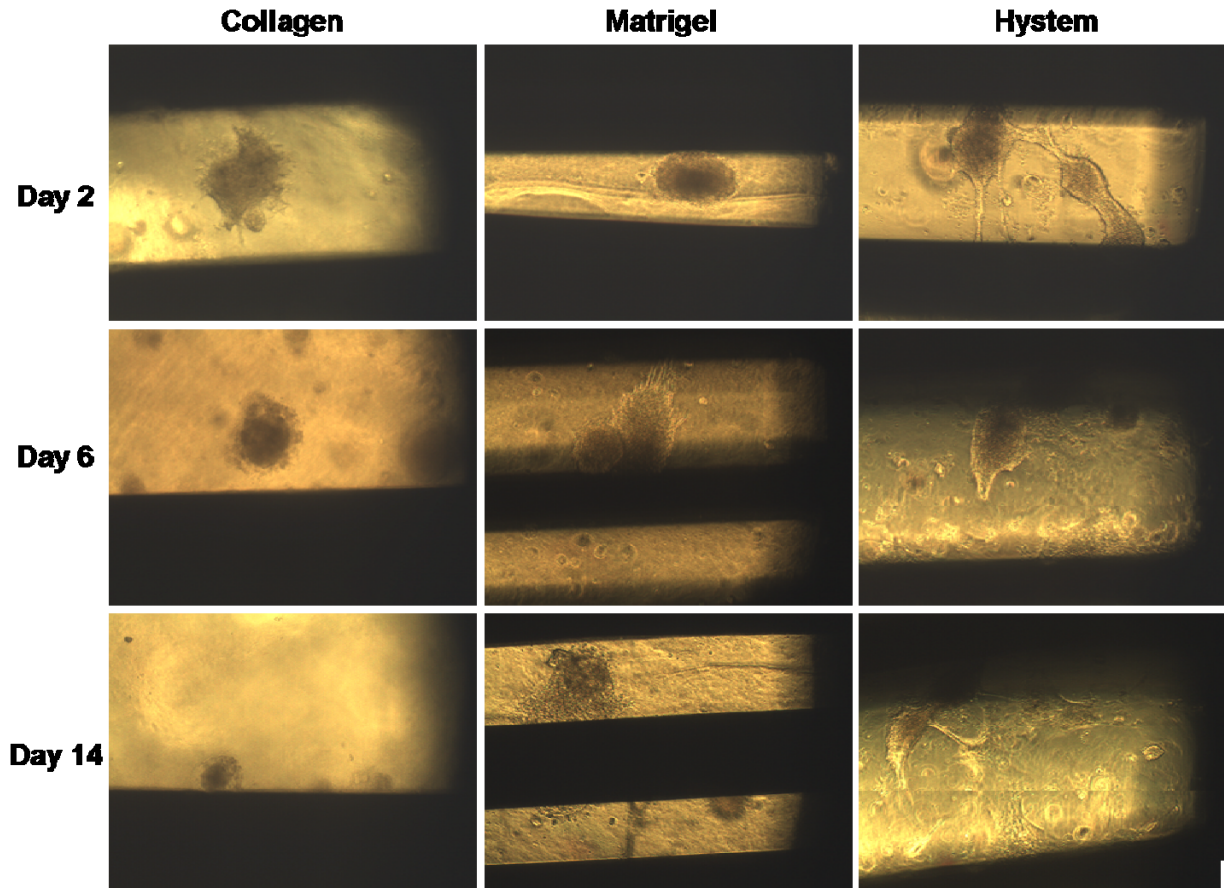


Figure 52. Live cell light microscopic imaging of experiment MNS-3 of neurosphere differentiation within 4 chamber bioreactor through different culture days within chambers containing ECM hydrogels. Top row shows neurospheres at culture day 2, middle row at culture day 6, and bottom row at culture day 14. Left column shows neurosphere within collagen type I, middle column within Matrigel, and within HyStem (cross-linked hyaluronic (magnification 100X). Neurospheres are seen within ECM gel between non-transparent medium perfusion hollow fibers (horizontal black lines).

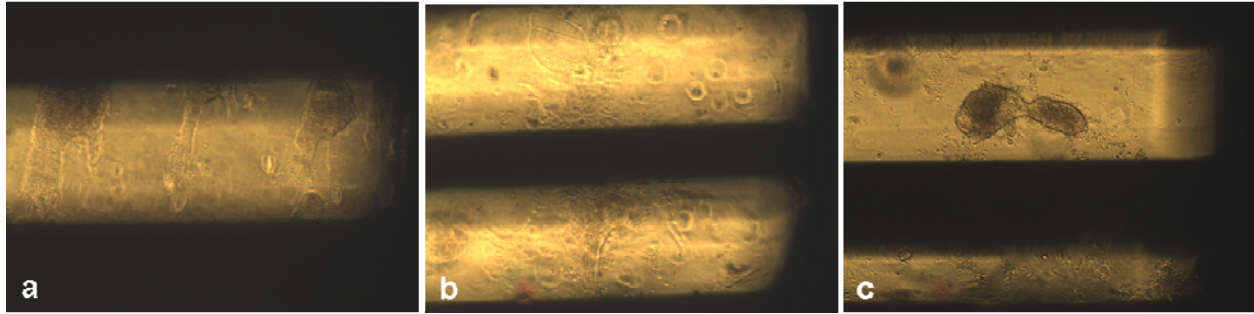


Figure 53. Live cell light microscopic imaging of neurosphere differentiation within chamber of MNS-3 bioreactor within HyStem cross-linked HA hydrogel through different culture days: a) neurospheres at 12 hours after seeding; b) culture day 6; c) culture day 14 (magnification 100X).

The bioreactor experiment MNS-5 was attempted to reproduce the results seen in experiment MNS-3. However, the arrangement of hydrogels within the chambers was changed, as described in Figure 33. MNS-5 included a new hydrogel with the combination of 100 $\mu\text{g}/\text{mL}$ laminin within the cross-linked HyStem hydrogel, where the two HyStem containing chambers were inline with each other. The collagen and Matrigel chambers were inline together on the bottom row of the bioreactor. The morphology of the cells within the HyStem chamber of experiment MNS-5 was dramatically different from what was observed in experiment MNS-3. Very few cells spread from the neurospheres within the first two culture days within the HyStem chamber. The neurospheres within this chamber resembled the morphologies of the cells within the collagen chamber, where the migrating cells appear rounded and dying by culture day 2. However, there seemed to be only a slight improvement of migration of cells from the neurospheres. The neurospheres through culture day 1-5 of the HyStem with laminin chamber appeared to have a more flattened morphology of the cells with the neurosphere attaching to the surrounding matrix. However, instead of further attachment throughout the hydrogel and differentiation from these cells within the HyStem with laminin chamber, by culture day 7 the

morphologies of these cells appeared similar to the cells in the HyStem chamber without added laminin. By culture day 14 within all chambers of bioreactor MNS-5 none of the cells were able to maintain any migration from the neurospheres into the surrounding ECM to acquire any structure formation.

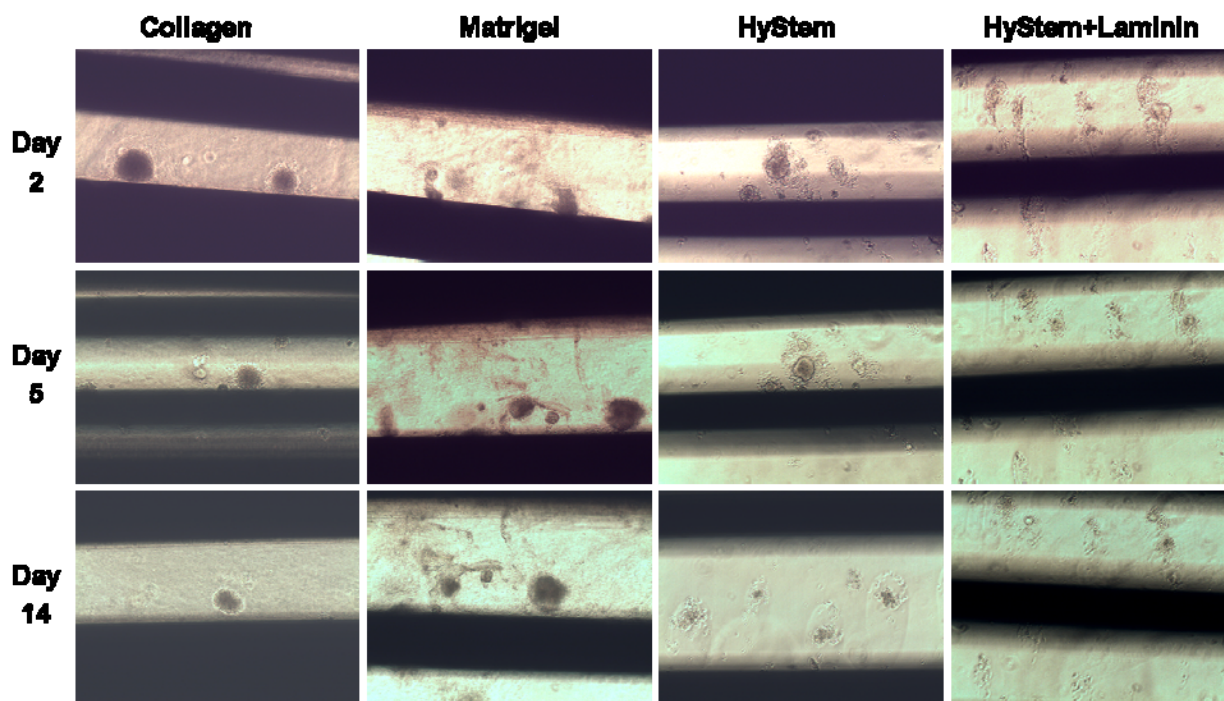


Figure 54. Live cell light microscopic imaging of experiment MNS-5 of neurosphere differentiation within 4 chamber bioreactor through different culture days within chambers containing ECM hydrogels. Top row shows neurospheres at culture day 2, middle row at culture day 5, and bottom row at culture day 14. Left column shows neurosphere within collagen type I, middle left column within Matrigel, middle right within HyStem (cross-linked hyaluronic, and right column within HyStem including 100 $\mu\text{g}/\text{mL}$ laminin (magnification 100X). Neurospheres are seen within ECM gel between non-transparent medium perfusion hollow fibers (horizontal black lines).

Due to less than desirable results of the 8 mL bioreactor experiments achieving poor cell survival within these devices, testing was performed to isolate the materials to test specifically the effects of the materials used within the tubing circuits. Previous tests included testing media

circulated through the tubing circuit including the connected 8 mL bioreactor prior to experiments MNS-2 and MNS-4. The results of testing media circulated for 24 hours of the bioreactor collected from experiment MNS-2 were tested on control cultures coated on Matrigel. The results of this test were misleading because cells did not survive well on the control Matrigel coated wells. This test was repeated with setup of experiment MNS-4 using mNSCs cultured on laminin coated plates using the collected media. Results are not shown here, but the neurospheres cultured in the bioreactor system collected medium appeared to attach and differentiate similarly to the control cultures on the first culture day, but by culture day 3 most of the cells had died and lifted from the plate. Therefore, further material testing was performed in order to isolate the compatibility of the materials used in the system. The only components of the 8 mL bioreactors are the perfusion hollow fibers (both microPES and polypropylene), the polyurethane housing, and silicone cell inoculation tubes. Results in Appendix B previously demonstrated substantial rat neural stem cell attachment to the microPES hollow fibers sealed to petri dishes using the housing polyurethane and therefore it was assumed that it was not the bioreactor materials that were detrimental to the circulating culture medium in the system.

An experiment was performed testing the perfusion of Neurocult differentiation medium through only two tubing circuits made of different materials. The tubing used was the medical-grade PVC that has been previously used as the tubing circuits for bioreactor cultures of our laboratory for many different cell types for many years. The other tubing material tested was Tygon 275 a more expensive medical grade product useful for many devices used clinically. The results of perfusing the differentiation medium through these two tubing circuits in two separate consecutive batches each for a 24 hour period and used to seed and culture mNSCs on laminin coated dishes is shown in Figure 55 compared to control cultures with fresh medium. The

control cultures showed excellent neurosphere attachment to the laminin coated dishes with multiple cells showing morphologies resembling neurons by culture day 2 (illustrated with arrows). The cultures maintained with medium circulated through the PVC tubing circuit resulted in very few neurospheres attaching to the laminin coated dishes. The second batch of medium perfused through the circuit for the second 24 hour period, seemed to have a slight increase in neurosphere attachment, but by culture day 2 most of the spheres were seen as detached and floating. The cells cultured in medium circulated through the Tygon 2275 tubing circuit, however, appeared to survive similarly to the control cultures achieving morphologies by day resembling multiple neurons with phase bright bodies and long processes (arrow point to group of neuronal like cells in image using medium perfused through 2275 circuit during the second 24 hour period).

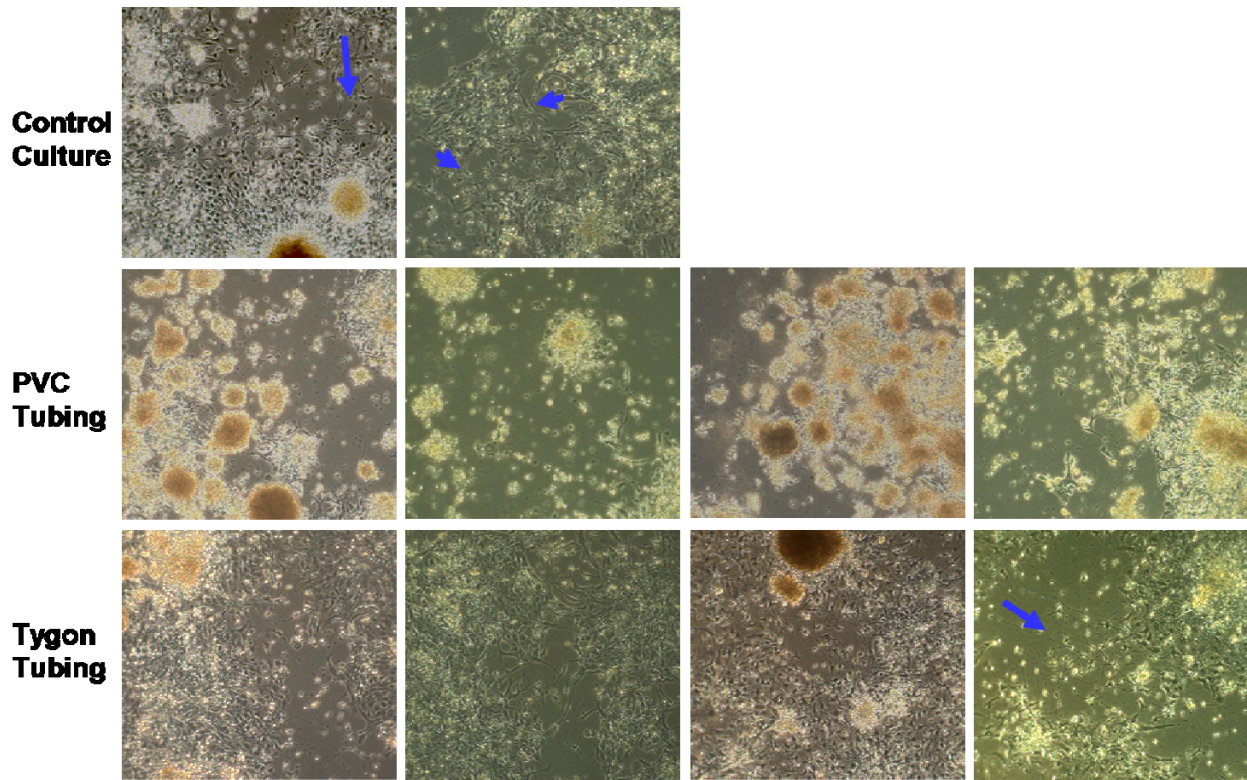


Figure 55. Light microscope images of mNSC cultures performed testing Differentiation medium perfused through either PVC or Tygon 2275 tubing circuits compared to control cultures with fresh Differentiation medium. The first column shows the mNSCs cultured for one day within the medium and the second column shows the same cultures after 2 days within culture; medium in this column for tubing types was the batch circulated for the first 24 hour period through the tubing circuits. The third and fourth column show the mNSCS at culture day 1 and 2, respectively with medium from the second batch circulated through the tubing circuits for the second 24 hour period. Phase bright neurospheres as seen in the PVC tubing cultures are unattached floating spheres. Arrows indicate clusters of cells having neuronal-like morphologies.

3.3.7 mNSC neuronal and astrocytic differentiation within bioreactor cultures

Example images of fluorescent confocal images of 8 mL bioreactor experiments MNS-1, MNS-2, and MNS-4 demonstrating immunostaining of samples with β -III-tubulin and GFAP staining are shown in Figure 56. The images shown in this figure are representative of the very few

neurospheres able to be located within these samples, revealing minimal cell survival within these experiments. The only neurospheres detected within MNS-1 within collagen hydrogel were found attached to the perfusion fibers, as seen in Figure 56a where the perfusion fiber is autofluorescent in blue. The culture within MNS-2 of Matrigel revealed a slightly better survival of neurospheres present within the 3D space of the hydrogel, but cells appeared to be dying, with staining of the cytoplasm present with no nuclear staining. The culture of MNS-4 revealed a slightly higher increase of neurospheres structures left intact within the samples, an example of the differentiation of these spheres is seen in the representative image.

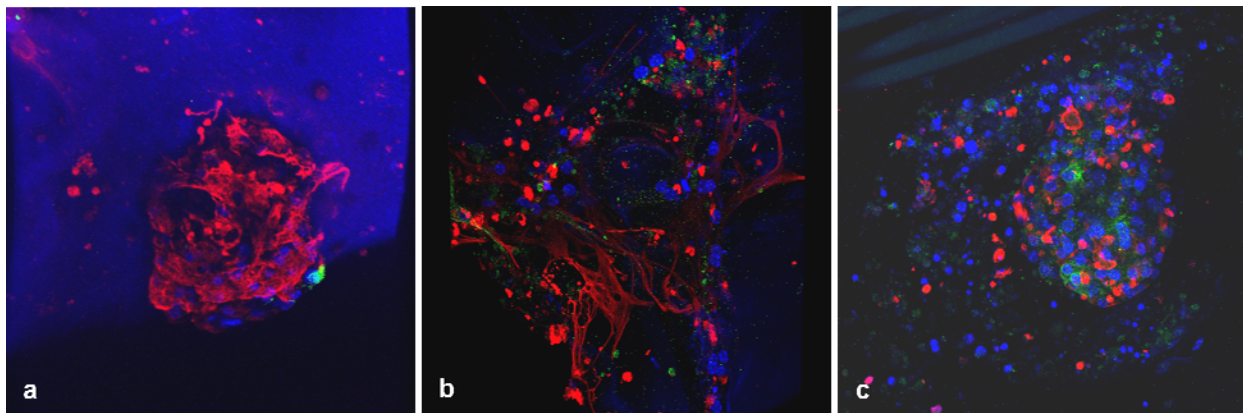


Figure 56. Confocal fluorescent microscopic images of neurosphere differentiation within 8 mL laboratory scale bioreactors containing 3D ECM hydrogels after 14 days of differentiation within the following experiments: a) MNS-1 mNSCs within collagen hydrogel (neurosphere attached to fiber which is autofluorescent in blue), b) MNS-2 mNSCs within Matrigel hydrogel, and c) MNS-4 mNSCs within HyStem hydrogel. Immunostaining with antibodies against β -III-tubulin (neuron specific) with AlexaFluor 488 (green), glial fibrillary acidic protein (GFAP; astrocyte specific) with Cy3 (red), and nuclear DAPI (blue) (magnification 400X).

Figure 57 and Figure 58 demonstrate representative images of the neurospheres detected from the four chamber bioreactor experiment MNS-3 in which the bioreactor was perfused with

paraformaldehyde at the end for the entire samples to be used for confocal fluorescence microscopy. The neurospheres within the collagen containing chamber reveal an increase in differentiated cells when compared to the 3D collagen hydrogels cultured statically. However, the spheres left intact completely encapsulated between fibers within the collagen gel were smaller in diameter compared to those in the statically cultured collagen hydrogels. The neurospheres within the Matrigel containing chamber also appeared smaller in diameter, but with most cells staining positive for GFAP associated with astrocyte differentiation. The processes from the neurospheres seen in the light microscopic images were not detected with the double staining fluorescence microscopic images. Immunostaining of the structures formed within the HyStem containing chamber of experiment MNS-3 revealed a substantial number of cells staining positive for β -III-tubulin depicting multiple neurons within these structures. Also, very few cells stained positive for GFAP representing low astrocyte differentiation within the structures. These images show the beneficial enhancement of neuronal differentiation over astrocytic differentiation from the neural stem cells cultured in HyStem hydrogels under dynamic conditions compared to all other conditions tested.

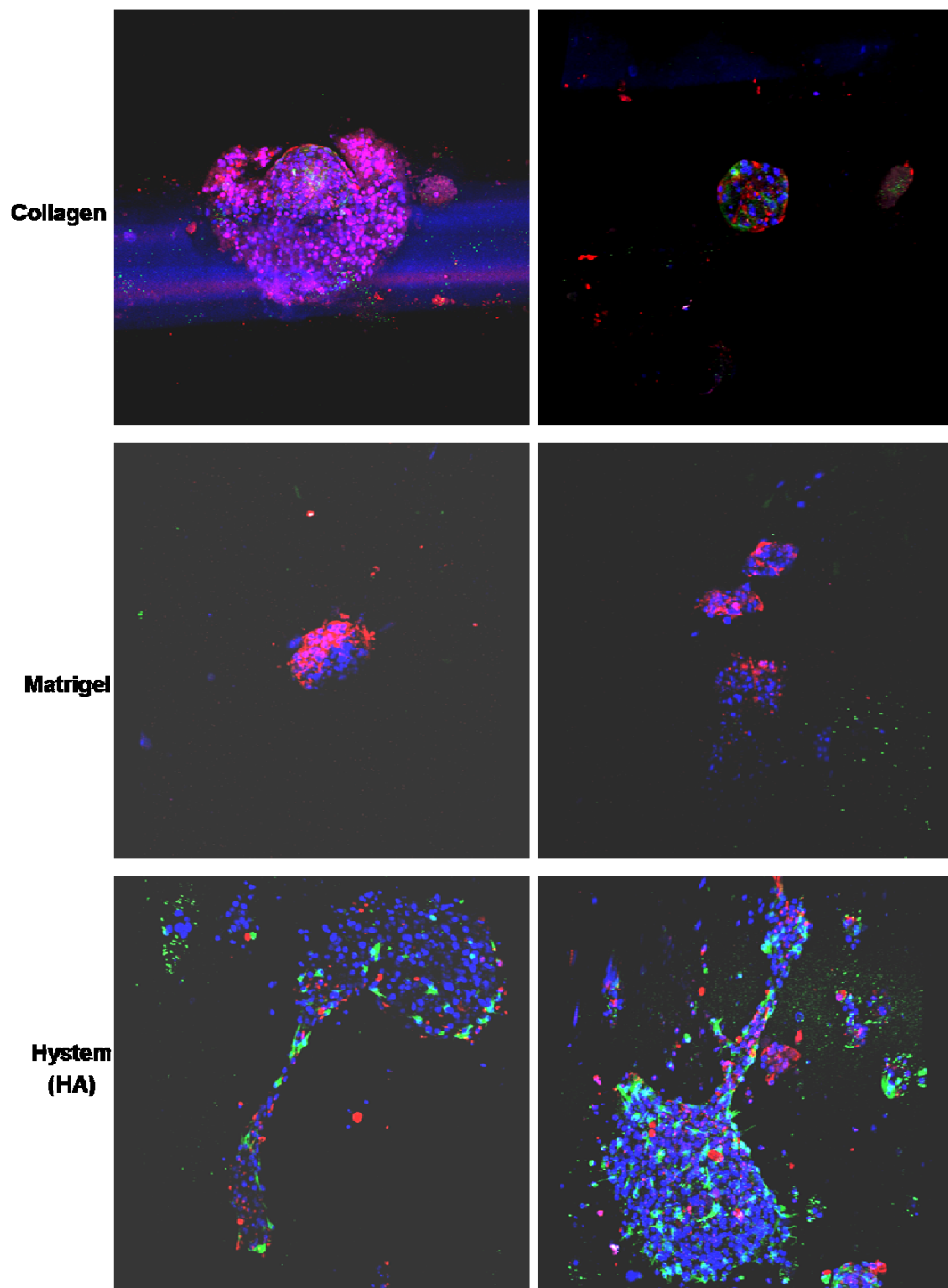


Figure 57. Confocal fluorescent microscopic images of experiment MNS-3 neurosphere differentiation within 4 chamber bioreactor containing 3D ECM hydrogels after 14 days of differentiation. Immunostaining with antibodies against β -III-tubulin (neuron specific) with AlexaFluor 488 (green), glial fibrillary acidic protein (GFAP; astrocyte specific) with Cy3 (red), and nuclear DAPI (blue) (magnification 400X).

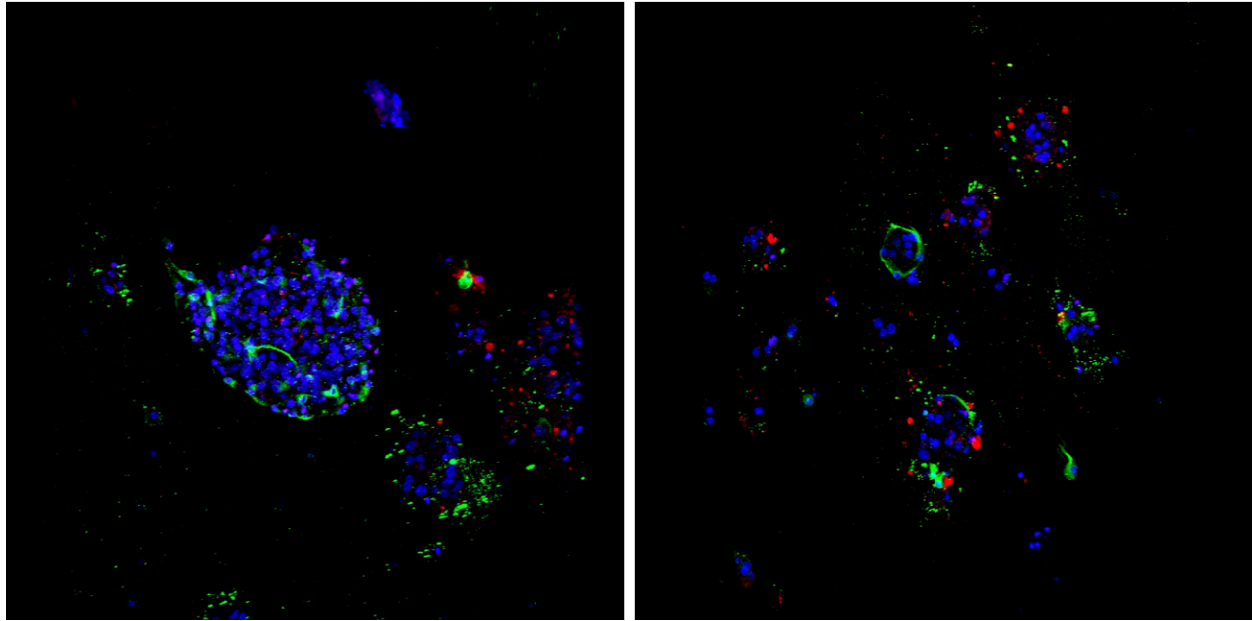


Figure 58. Confocal fluorescent microscopic images of experiment MNS-3 neurosphere differentiation within 4 chamber bioreactor containing HyStem (cross-linked hyaluronic acid) hydrogel after 14 days of differentiation. Immunostaining with antibodies against β -III-tubulin (neuron specific) with AlexaFluor 488 (green), glial fibrillary acidic protein (GFAP; astrocyte specific) with Cy3 (red), and nuclear DAPI (blue) (magnification 400X).

3.3.8 Quantification of neuronal and astrocytic differentiation within ECM hydrogels

We have further attempted to assess neuronal and astrocyte differentiation of the mNSCs cultured on and within the different ECM hydrogels using quantitative RT-PCR. RNA was collected from all samples and cDNA was synthesized and gene expression for β -III-tubulin, GFAP, and myelin basic protein (MBP) gene expression was quantified comparing to internal control of GAPDH gene expression. These results of the relative expression ratios of these two genes as differentiation markers compared to the internal GAPDH control for the same RNA samples are shown in Figure 59 and Figure 60. The data shown for the “2D” ECM coated plate cultures is representative of RNA collected from only one culture, except for the 2D Matrigel

including data from two separate cultures. The data for all “Gel” 3D static cultured hydrogel cultures are representative of the mean and standard deviation between three separate cultures of each ECM hydrogel tested. The “Bioreactor” samples within this data are from the RNA collected from the 8 mL bioreactor experiments MNS-1 (collagen), MNS-2 (Matrigel), and MNS-4 (HyStem).

There is a large variation of the β -III-tubulin expression within the 3D hydrogels cultured statically. Some of these samples had very low mRNA expression of β -III-tubulin when compared to the control GAPDH mRNA. Also, quantification of the RNA samples revealed very low amounts of RNA collected from all of the mNSC cultures. This was the case even with the 2D laminin coated positive control culture where many cells were present by the end of the 14 day culture period. RNA was collected at the end of the 14 day culture period only and therefore represents the gene expression only of the cells that survived until the end of this culture period. Therefore, some of these results are potentially misleading when quantifying percentage of cells differentiating into either neurons or astrocytes because the same number of cells do not survive the entire 14 day culture period among the different culture types. Many cells survive and differentiate on the 2D laminin coated plates, while within the 3D HyStem hydrogels barely any cells survived the culture within the first culture day (as described above with the imaging results of these static cultures). It is surprising that there was any β -III-tubulin gene expression detected within the 3D HyStem hydrogels cultured statically since imaging of these cultures revealed no immunostaining for this protein. However, the standard deviation for this group is very large because two of the 3D static HyStem culture samples detected no mRNA presence with only one sample having enough mRNA to analyze the gene expression. The results of this quantitative gene expression for differentiation of mNSCs on and within the

Matrigel hydrogels do correlate with the results observed by immunostaining and imaging of these cultures demonstrating that Matrigel enhances astrocyte differentiation among the mNSCs. In Figure 60, the results of some of the cultures are shown for myelin basic protein (MBP) gene expression, which is a marker for cells differentiating towards the oligodendrocyte lineage. The expression of MBP within the cultures compared to β -III-tubulin and GFAP is very low.

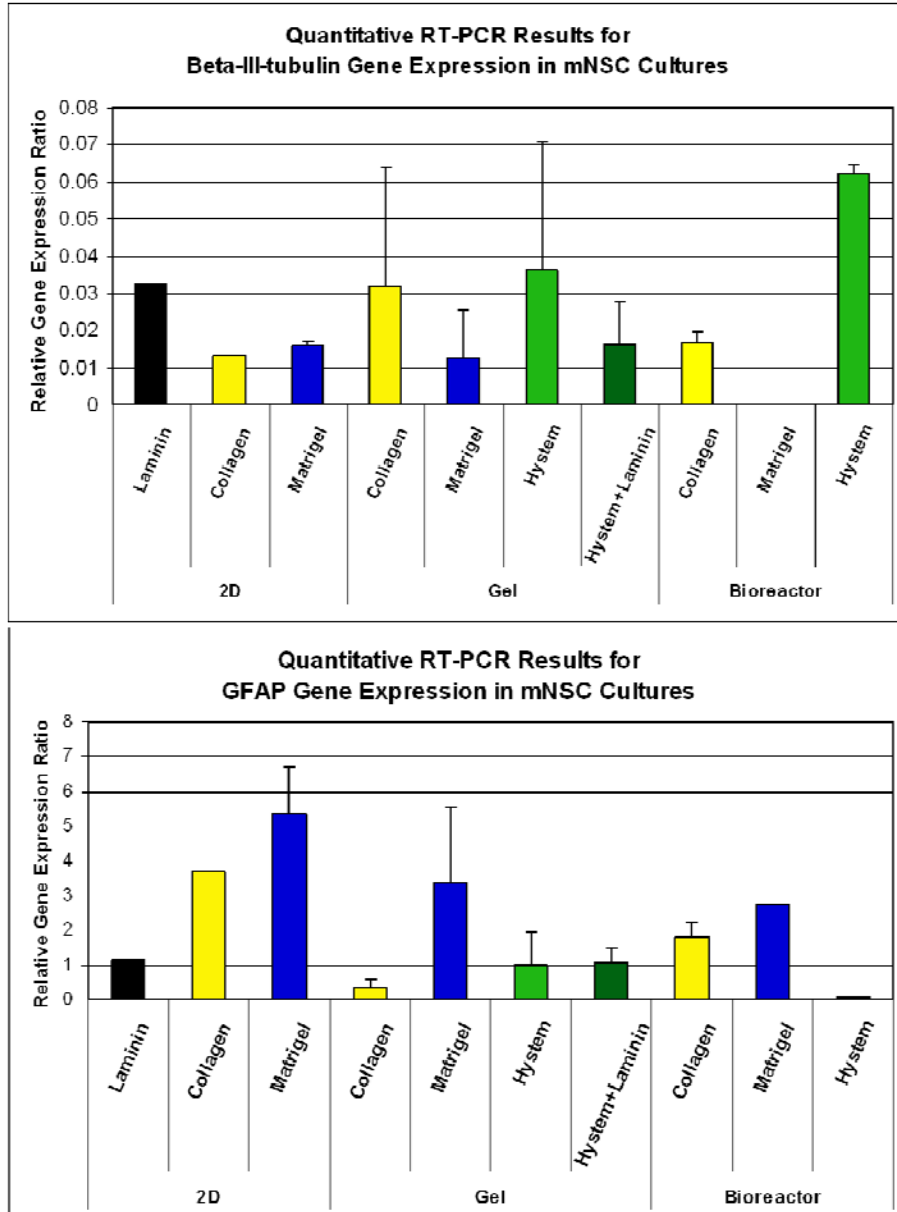


Figure 59. Quantitative RT-PCR results comparing β -III-tubulin (neuron marker) and GFAP (astrocyte marker) gene expression of mNSCs cultured with different ECM matrices under the different culture conditions. Data represents mean of n=3 samples for “Gel” cultures from 3D hydrogel static cultures. Error bars on “Gel” samples represent the standard deviation between the n =3 samples. Bioreactor data presented are the results from mRNA collected from MNS-1, MNS-2, and MNS-4 performed within the 8 mL bioreactors. Error bar on “Bioreactor Collagen” is the standard deviation between the two RNA samples collected from the 8 mL bioreactor experiment, but from the same experiment.

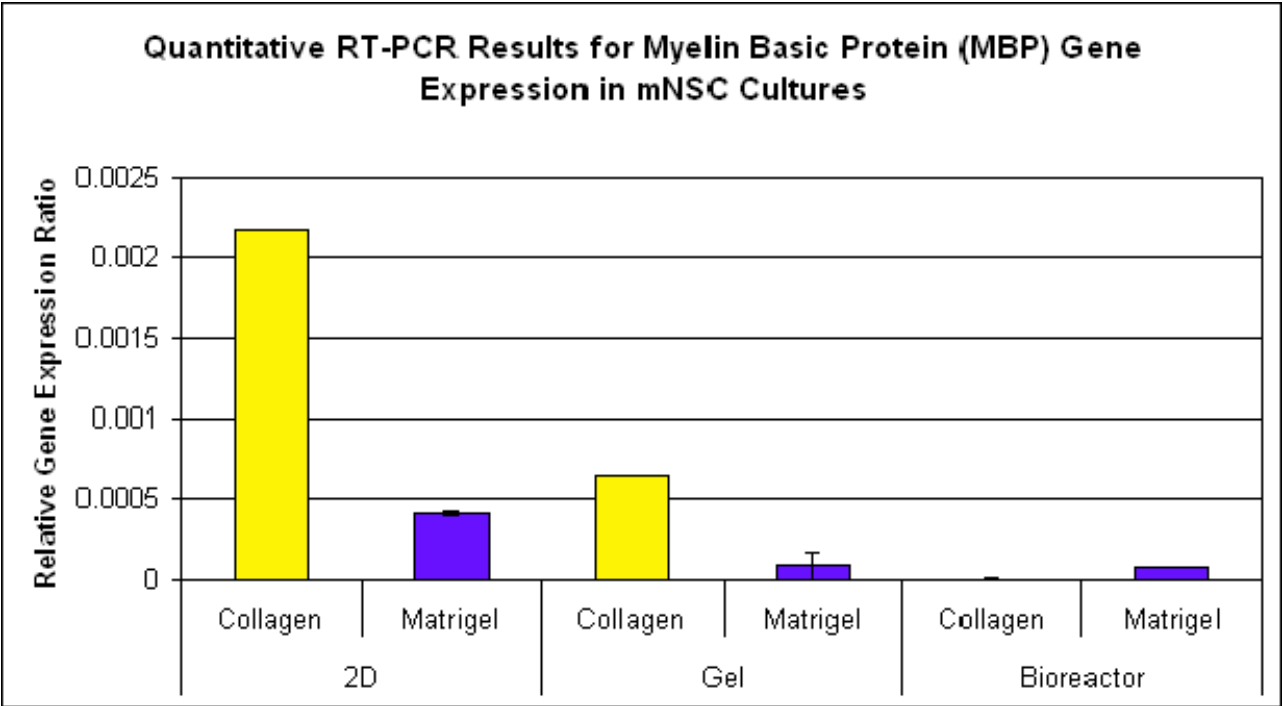


Figure 60. Quantitative RT-PCR results comparing β -III-tubulin (neuron marker) and GFAP (astrocyte marker) gene expression of mNSCs cultured with different ECM matrices under the different culture conditions. Data represents mean of n=2 samples only for samples with error bars. Bioreactor data presented are the results from mRNA collected from MNS-1 and MNS-2 performed within the 8 mL bioreactors.

3.4 DISCUSSION

We have tested the effects of varying ECM scaffolds on mouse embryonic neural stem cell differentiation *in vitro* in order to determine a suitable matrix for neural stem cell differentiation within three dimensions *in vitro*. As described in section 3.1.1, the *in vivo* adult neural stem cell niche has been well investigated in terms of the organization of cellular components, extracellular matrix components, and cell surface receptor expression. This organization very

specifically defines the cell-cell and cell-ECM interactions between the different neural stem and progenitor cell types. This entire *in vivo* niche is organized within three dimensions allowing the neural stem cells to have the proper morphology enabling growth factor modulation and regulation of neural progenitor cell expansion and migration. Therefore, culturing neural stem cells *in vitro* on a 2D substrate would not allow recreation of this same neural stem cell niche in order to investigate the properties that naturally allow neural stem cell migration and differentiation.

Unfortunately, the survival of the mNSCs was low within experiments using the large-scale 8 mL bioreactors culturing the mNSCs at high densities within the different ECM hydrogels under 3D dynamic conditions. The material testing of medium circulated through the PVC tubing circuit, similarly to the circuits used within the 8 mL bioreactor experiments, revealed the extremely poor compatibility of this tubing useful for bioreactor medium circulation for mouse neural stem cell cultures. We previously used tubing circuits comprised of this medical-grade PVC tubing because it is the same tubing used clinically for dialyzer tubing extensions for blood perfusion in patient applications. Also, this tubing material allowed easy production of our custom circuits by welding of the tubing at connection sites. These PVC tubing circuits have previously been used in bioreactor experiments within our laboratory culturing multiple stem cell types including mouse and human embryonic stem cells and primary human adipose-derived stem cells. The use of this PVC tubing circuit with the four chamber bioreactor of experiment MNS-3 did not produce results as extremely poor as the 8 mL bioreactor cultures. The mNSCs survived and experienced neuronal differentiation within the HyStem chamber of this experiment more superior to any other culture performed within this work. It is possible that within the 8 mL bioreactors the very large number of highly woven

perfusion fibers within the cell compartment creates a system similar to a filter. It is possible that perfusion in areas of the 8 mL bioreactor cell compartment are not as highly perfused as the cell chambers within the four chamber bioreactors and particles and materials leaching from the PVC tubing circuit get trapped within the cell chamber without exiting. For bioreactor experiment MNS-5 we produced our own newer version of the tubing circuit used for this four chamber bioreactor experiment with the tubing made from the more compatibility material Tygon 2275. We hope that future experiments using this Tygon 2275 tubing circuit will allow an increased cell survival and differentiation of the mNSCs within the 8 mL hollow fiber-based bioreactors.

Results from culture of mNSCs on 2D collagen coated surfaces revealed poor movement of cells from neurospheres and attachment onto the collagen substrate, but led to enhanced differentiation of cells attached to each other within the structures remaining at the end of the culture. The opposite occurred for mNSCs cultured within 3D collagen hydrogels with most cells remaining within the neurospheres still staining positive for the stem cell marker nestin. Mercier et al. described fractones of the SVZ mostly consist of the typical basal lamina protein laminin, but there were also random locations throughout the fractones where collagen type I was detected. The mNSCs cultured here in collagen type I hydrogels resulted in low attachment of cells to the collagen hydrogel with cells remaining within the neurospheres. In the 3D static collagen gel cultures, most intact neurospheres at the end of the two week differentiation period were still nestin positive. It is possible that collagen type I within the localized regions of fractones of the SVZ *in vivo* has a similar function to maintain proliferating progenitor cells and preventing differentiation within these locations. Therefore, collagen type I is not a suitable ECM scaffold useful for permitting extensive differentiation of mouse neural stem cells.

However, collagen type I hydrogels could be useful in maintaining proliferative populations for expansion of neural stem cells. This could be useful in transplant applications where neural stem cells are desired to be maintained in an undifferentiated state in order to act therapeutically as a source of neuroprotective factors, termed the “bystander effect” [296].

Conversely, Ma et al. have described production of functional neural circuitry among tissue generated from rat neural precursor cells encapsulated in collagen gels cultured in rotating wall vessel bioreactors with inclusion of bFGF in the culture media [284]. In our work we have shown that addition of bFGF to the Neurocult Differentiation medium (Stem Cell Technologies Inc.) used to culture mouse neural stem cells in collagen gels further inhibits neuronal differentiation of the cells. Differences therefore most likely exist within the pathways driving differentiation of neural stem cells across species. Also with our work, incorporation of laminin into the collagen gel solution before gelation resulted in increased neuronal differentiation within these hydrogels cultured under static conditions in a dose-dependent manner with increasing laminin concentrations. However, Guarnieri et al. have characterized collagen gels with incorporation of different laminin concentrations to find laminin forms concentrated aggregates within the collagen network instead of a continuous matrix throughout, which also decreases the mechanical properties of the hydrogel with increasing laminin concentrations [297].

Matrigel is a crude mixture of native basement membrane components isolated from cultured mouse EHS tumor cells, which produce these components in abundance [298]. The growth factor reduced Matrigel used in these studies consists of approximately 60% laminin, 30% collagen type IV, 7% entactin, as well as heparan sulfate proteoglycans (HSPG). Previously, Matrigel has been used to support neurite extension with primary neuronal cultures [299, 300]. Matrigel is the only commercially available 3D matrix composed of such a high

concentration of laminin. We utilized this product since laminin is traditionally preferred as the substrate for NSC differentiation on a 2D surface. However, results using this matrix both in 3D static cultures as well as bioreactor cultures showed enhanced astrocyte differentiation from the neural stem cells encapsulated in the Matrigel hydrogels. Original concentration Matrigel was first used, but this product was not able to sustain the 14 day culture period as an intact hydrogel even under the static culture conditions and therefore high-concentration Matrigel product was further used. Also, we have utilized the high concentration plus growth-factor reduced Matrigel product in order to minimize effects of the active growth factor components within the original Matrigel. We attempted to focus on varying only the ECM component of the cultures instead of growth factor variation. However, even this growth factor reduced product still contains low amounts of the known active growth factors within Matrigel: 0-0.1 pg/mL bFGF, <0.5 ng/mL EGF, 5 ng/mL IGF-1, <5 pg/mL PDGF (platelet-derived growth factor), <0.2 ng/mL NGF, and 1.7 ng/mL TGF- β .

Neural stem and progenitor cells are known to proliferate and differentiate in response to multiple growth factors *in vivo* [245, 301-305]. Further investigation of the ECM components of the SVZ *in vivo* has revealed the function of the permissive components, such as laminin and HSPG, is to regulate growth factor presentation to the specific cell types [251]. The fractones, basal lamina extensions, extend from blood vessels and the ventricle in order to capture growth factors from the blood and cerebrospinal fluid (CSF). Here we utilized a commercially available defined media for inducing neural stem cell differentiation (Neurocult, Stem Cell Technologies, Inc.). The specific component formulation of this defined medium is company information only and not available to the public, but the company has claimed it is based on the formulation determined by Reynolds et al. where NSCs are differentiated with removal of EGF from the

defined proliferation medium and addition of a small amount of serum [234, 235, 279]. In our work within Chapter 3 using adult rat neural stem cells, we prepared our own medium according to these references. However, within this work we chose to focus on testing the ECM scaffolds without varying the soluble chemical factors within the medium and therefore used a commercially available source of medium to be consistent throughout experiments.

The Neurocult medium formulation allows acceptable differentiation of the mNSCs on laminin coated 2D culture dishes, but might not be suitable for use in a 3D configuration as observed within our work. Without the ability to maintain a scaffold entirely composed of laminin, the defined medium used to differentiate the mNSCs might need incorporation of additional soluble components. We have demonstrated that collagen type I, growth factor reduced Matrigel, and HyStem (cross-linked hyaluronic acid) did not allow acceptable attachment of the mNSCs onto the 2D substrates or attachment onto the 3D hydrogel from the neurospheres into the scaffold in order to properly differentiate without the incorporation of additional soluble factors. The HyStem hydrogel allowed substantial 3D structure formation with cells migrating from the neurospheres throughout the gel within the perfused bioreactor chamber only when placed horizontally inline with the chamber containing Matrigel of experiment MNS-3. Chambers horizontally next to each other within this bioreactor have the same perfusion fibers running directly from one chamber to the other allowing secreted soluble factors to be exchanged before dilution into the entire tubing circuit volume. Therefore, mNSC structure formation and increased neuronal differentiation within the HyStem gel of MNS-3 and not of MNS-5, most likely is attributed to soluble factors released from the Matrigel.

The medium perfusion fibers of the bioreactor have a molecular weight cutoff of 400 kD (kiloDaltons). Glycosan Biosystems Inc. claims the cross-linked HyStem gel has a pore size

allowing diffusion of molecules under 70 kD in size. There are many active ECM components and growth factors within Matrigel, as described above. TGF- β has been demonstrated to drive glial differentiation in human NSCs [306]. bFGF and EGF are the growth factors used to prevent differentiation of NSCs to maintain expansion of the cells. Nerve growth factor (NGF) is an active neurotrophic factor able to modulate axonal processes in primary neurons. However, results of culturing the mNSCs in Matrigel directly resulted in increased astrocyte differentiation from the cells. If one of these soluble growth factors released from the Matrigel containing chamber of bioreactor experiment MNS-3 were responsible for increased neuronal differentiation in the neighboring HyStem containing chamber, there must be a non-soluble component to the Matrigel that prevents this same neuronal differentiation that is blocked by the molecular weight cutoff of the perfusion fibers or HyStem pore size. It is possible that TGF- β , bFGF, or EGF present within the Matrigel could have prevented the neuronal differentiation within the Matrigel, but of interest that the same results did not occur within the neighboring HyStem chamber.

The migration of cells from the neurospheres within the HyStem chamber of bioreactor experiment MNS-3 occurred within the first 12 hours after seeding the neurospheres within the bioreactor as opposed to very little migration from the neurospheres within HyStem of experiment MNS-5. There was an immediate response of the neurospheres within the chamber next to the Matrigel containing chamber instead of a delayed response due to degradation of large ECM molecule components of the Matrigel. Laminin within Matrigel is of the form laminin-1 with three chains, designated α 1, β 1, β 2 (or γ 1) [298]. The β 1 and β 2 chains coil around the α 1 chain creating a four-armed tertiary protein structure that allows multiple binding domains with the other basement membrane protein components [307]. The molecular weights

of the separate chains are $\alpha 1 = 400$ kD, $\beta 1 = 222$ kD, and $\beta 2 = 210$ kD [294]. The type IV collagen within Matrigel is composed of two chains in the form $\alpha 1(IV)_2\alpha 2(IV)$ [298]. The molecular weights of these two chains are 185 kD and 170 kD. These high molecular weights render these ECM components unlikely candidates in their ability to perfuse from one chamber to the other in the 4 chamber bioreactor as well as through the HyStem gel pores [308]. It is possible that later degradation of these ECM components are able to perfuse into the circulation, but the response of the mNSC structure formation within the HyStem chamber next to the Matrigel was immediate. Also, the mNSCs within the chamber containing HyStem plus 100 $\mu\text{g}/\text{mL}$ laminin within experiment MNS-5 achieved morphologies within the first culture day different to that seen in the MNS-3 chamber. The cells in the HyStem chamber next to the Matrigel chamber of MNS-3 had a migratory response out from the neurospheres into the surrounding hydrogel allowing structure formation between spheres within the first culture day. The cells within the HyStem chamber containing laminin of MNS-5 instead appeared to have a more flattened morphology with increased attachment and spreading of the cells in the neurospheres to the surrounding hydrogel within the first culture day.

Within this work we chose to focus on analysis of the neuronal and astrocytic differentiation of the mouse neural stem cells within the different cultures. Immunostaining for O4, an early oligodendrocyte marker, was initially performed on laminin coated 2D control cultures, but resulted in low detection of cells possibly differentiating towards the oligodendrocyte lineage. Additionally, quantification of gene expression for MBP, an oligodendrocyte marker, was performed with qRT-PCR with mRNA collected from the mouse neural stem cells differentiated with collagen and Matrigel as substrates or 3D hydrogels. These results showed very low expression levels of MBP and oligodendrocyte presence of cells at the

end of the differentiation period. However, it is important to further analyze differentiation of neural stem cells into oligodendrocytes. These cells are the more desired cell types able to be obtained from neural stem cells for therapies specifically in myelin-associated diseases. For example, multiple sclerosis is an auto-immune disorder where the immune system specifically attacks the myelin sheaths provided by oligodendrocytes that maintain insulation of signaling neurons preventing neurons from properly signaling and communicating and controlling functions. Conditions and environments useful in driving oligodendrocyte differentiation of neural stem cells are therefore of great interest in achieving these cell types for possible cell therapies and creating models of myelinated neurons in developing therapeutic strategies for diseases involving these cells. Also, a proper *in vitro* culture model of a neuronal network of cells with signaling neurons within the bioreactor devices will require a mixed population of cells including myelination of neurons by oligodendrocytes. Further work could investigate the oligodendrocyte differentiation of these cells resulting from differentiation within different ECM hydrogel scaffolds.

Further experiments are necessary to reproduce the increased structure formation and neuronal differentiation of the mNSCs within the HyStem hydrogels due to soluble Matrigel factor perfusion within the four chamber bioreactor. Experiments can be performed to both test the effects soluble components released from Matrigel hydrogels within surrounding medium and separately test effects of individual Matrigel components on mNSC cultures to determine which factors are inhibitory or permissive for cell attachment or neuronal differentiation. Also, it is possible that the inhibitory factor of Matrigel preventing it from being a suitable hydrogel useful in NSC cultures could be the density of this hydrogel. Within experiment MNS-3, the cells of the Matrigel containing chamber remained as neurospheres with no changes in

morphology until culture day 6. It was only after the six days of culture that the cells began to extend processes from the neurospheres into the hydrogel. However, within the statically cultured 3D Matrigel cultures, the neurospheres extended processes within the first day of culture and therefore opposes this theory. Thonhoff et al. have also demonstrated increased astrocyte differentiation from human fetal neural stem cells cultured within 3D Matrigel hydrogels [309]. The aspect of the cross-linked HyStem hydrogel providing a longer lasting hydrogel makes it a more acceptable matrix useful for scaffolds for neural stem cells in long term dynamic cultures. The HyStem hydrogel has the ability to last within long term cultures, but improvements to the culture medium used for the mNSCs to be effective within the HyStem hydrogels must be improved upon.

3.5 CONCLUSION

It is likely that *in vitro* regulation of neurosphere attachment, proliferation, migration, and differentiation is as complex as the *in vivo* regulation by coordination of temporal and spacial changes in cell surface receptors responding to different growth factors and extracellular matrix molecules. Our results have provided a first step in describing mouse neural stem cell differentiation in a 3D organization with varying the ECM components. The HyStem 3D ECM hydrogel matrix provides a stable scaffold allowing neural stem cell structure formation and differentiation under 3D dynamic conditions *in vitro* within the bioreactor device with the appropriate additive soluble factors and should continue to be used for establishing these cultures. Optimization of neural stem cell cultures within our hollow fiber-based bioreactor devices could allow multiple investigations into the mechanisms of neural stem cell expansion,

migration, and differentiation. The next experiments should focus on the soluble factors necessary for enhanced neuronal differentiation of the NSCs within the HyStem hydrogels in the 3D dynamic environment. The bioreactor system allows easy manipulation of the culture environment in order to more accurately study the properties of the neural stem cells due to the variations within the culture environment. The study of neural stem cell expansion and differentiation under 3D dynamic conditions could help to more accurately predict the outcome of methods used with *in vivo* studies using NSCs as a cell therapy. Additionally, human neural stem cells could be cultured within the bioreactor devices to directly describe the abilities of NSCs to be delivered into a dynamic three-dimensional environment similar to the body.

4.0 LASER MODIFIED HOLLOW FIBER SCAFFOLDS TO COMPARTMENTALIZE *IN VITRO* NEURONAL CELL CULTURE SYSTEMS FOR 3D DIRECTED AXONAL OUTGROWTH

4.1 INTRODUCTION

4.1.1 Significance of compartmentalization of axons from cell bodies *in vitro*

The objective of the work within this chapter was to further advance the ability to achieve a superior *in vitro* neuronal cell culture model. The above chapters discuss the ability of the hollow fiber-based bioreactors to allow high density 3D neuronal cell growth, but the work here demonstrates our ability to fabricate a scaffold useful for bioreactor designs to control and direct neuronal axon growth within the *in vitro* 3D dynamic culture model. The scaffold designed here can allow neuronal cell bodies to be separated from their axons inducing compartmentalization for controlled signaling interactions among neurons. This compartmentalization will allow unique environments to be applied both to the neuronal cell bodies cultured within the cell compartment of the culture model and to the process/axon growth within the scaffolds, simultaneously. This differential growth could be useful for analyzing axonal regeneration from neuronal cell bodies. Most importantly this aspect of the proposed culture models will allow controlled growth of the configuration of the neuronal cells and specifically the direction of the

axon growth and synapse formation with other axons for controlled signaling. Separation of neuronal cell axons from their bodies through a cylindrical 3D scaffold mimics axonal growth *in vivo* from the brain through the spinal column. Testing therapeutic reagents for extending axonal regeneration within *in vitro* culture models integrating this same configuration for neuronal cell cultures might prove very valuable for more accurate assessment of the effects of these reagents.

4.1.2 Excimer laser ablation in tissue engineering

We have developed this scaffold for controlling specific neuronal cell body and axonal process outgrowth *in vitro* by performing excimer laser ablation modifications to microporous polyethersulfone (PES) hollow fibers. Excimer laser ablation for tissue engineering applications was performed in 1994 by Nakayama and Matsuda to create pores in polymer scaffolds for cardiovascular tissue engineering [310]. Further work has been performed by Tiaw et al. to produce porous poly(caprolactone) sheets with excimer laser ablation for a possible skin substitute [311]. There have been other reports on the use of excimer laser ablation on polymer scaffolds to manipulate cell growth, but none for controlling neuronal cell growth [312-315].

Excimer laser ablation was utilized to generate specifically sized channels within the walls of PES hollow fibers in order to compartmentalize growth of neuronal cell bodies from their axonal processes and further facilitate directed process growth into the 3-D space of the fiber lumens. Compartmentalization of neuronal cell bodies from their axons may lead to controlled synaptic networking between cell bodies within a 3D space. Further incorporation of these scaffolds into a hollow fiber-based bioreactor to establish high-density 3-D *in vitro* neuronal cell culture models with defined axonal pathways in the directions of the lumens of the scaffolds will allow creation of a tool for studying 3-D neuronal networking *in vitro*. The growth

of only the neuronal axons into the fiber scaffolds allows a direct method of analyzing directed neurite outgrowth within a 3-D space at high densities that more accurately mimics the *in vivo* environment.

Figure 61 is a diagram describing this proposed advanced *in vitro* neuronal cell culture model with a hollow fiber-based bioreactor foundation including incorporation of excimer laser modified hollow fiber scaffolds able to direct axonal growth throughout the system. The picture on the left describes the overall design concept of the bioreactor where multiple cell compartments can be connected using the modified hollow fiber scaffolds permitting axonal growth from one compartment to another. The picture on the top right describes the 3D neuronal process outgrowth within the hollow fiber-based bioreactor cell compartment achieved within the previous chapters. The picture on the bottom right describes the concept of the desired objective for the laser modified hollow fiber scaffold used to compartmentalize neuronal cell body growth from directed axon growth through the lumen of the scaffold. Figure 62 is a diagram of a simplified version of this design concept based on the 4 chambered analytical bioreactor. This design would allow high density 3D neurite outgrowth from neurons within each of the two cell compartment chambers. These two chambers would be connected only via the lumen of a single hollow fiber scaffold able to direct axonal growth from one compartment to the other through first through the laser created channels of the scaffold. Reagents having the potential to affect axonal outgrowth into the scaffold could be applied as gradients to the upper cell compartment by perfusion through the separate hollow fiber bundle of the lower cell compartment and through the lumen of the scaffold fiber. This design would enable testing of chemotropic factor gradients on high density tissue-like neuronal cell cultures in 3D assessing the ability to enhance nerve regeneration by directed axonal outgrowth.

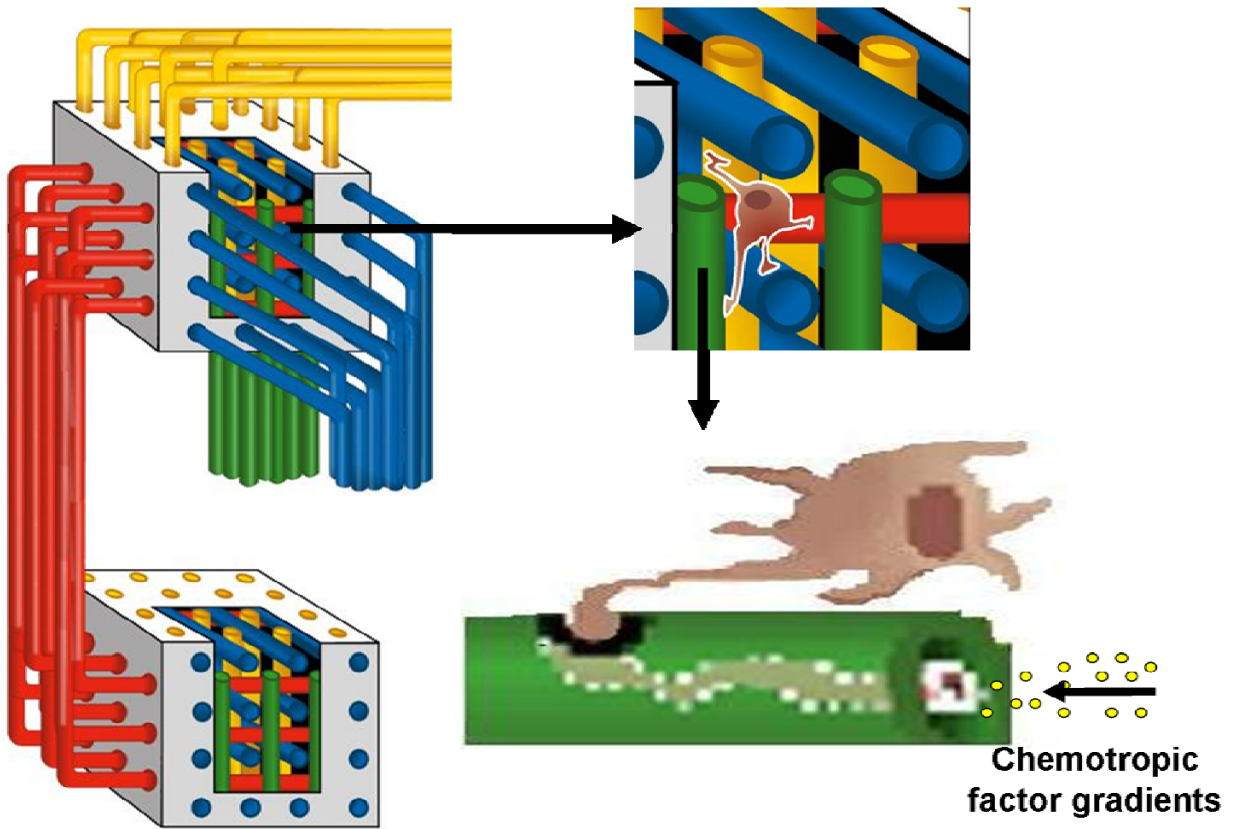


Figure 61. Diagram describing design concept of advanced *in vitro* neuronal cell culture model with a hollow fiber-based bioreactor foundation and incorporation of the laser modified hollow fiber scaffolds for directed axonal growth.

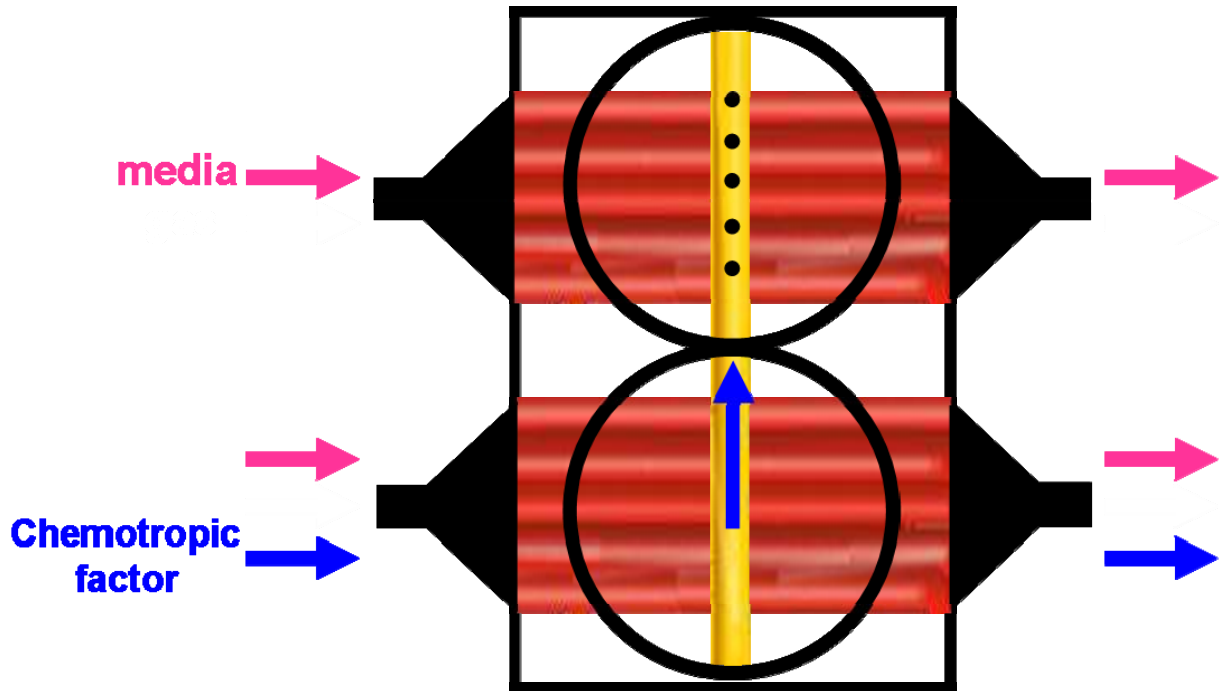


Figure 62. Diagram of design concept for simplified neuronal cell bioreactor *in vitro* culture model utilizing a single laser modified hollow fiber scaffold for directed axonal growth from one compartment to the other.

4.2 METHODS

4.2.1 Laser modification of PES flat sheet membranes and hollow fibers

Ultrafiltration microporous polyethersulfone hollow fibers (MicroPES TF10, Membrana, Wuppertal, Germany) with inner diameter of $300 \pm 40 \mu\text{m}$, wall thickness of $100 \pm 25 \mu\text{m}$, and maximum pore size of $0.5 \mu\text{m}$ were used. PES flat sheet membrane counterparts (Membrana, Wuppertal, Germany) to these fibers with similar pore structure were also used to enable characterization of laser modifications on 2D surfaces. All laser modifications were performed with a KrF 248 nm nanosecond excimer laser (Lambda-Physik EMG-202) with a full-width-half-

maximum pulse duration of 25 ns at a pulse frequency of 2Hz, at room temperature in an open air atmosphere. The laser beam path through the mask projection system to the sample stage is shown in Figure 63. Laser pulse energy was controlled at position Figure 63(a) by rotation of a variable attenuator plate (JPSA Laser UM-VA) and measured with a Molecron JD-100 pyroelectric joulemeter.

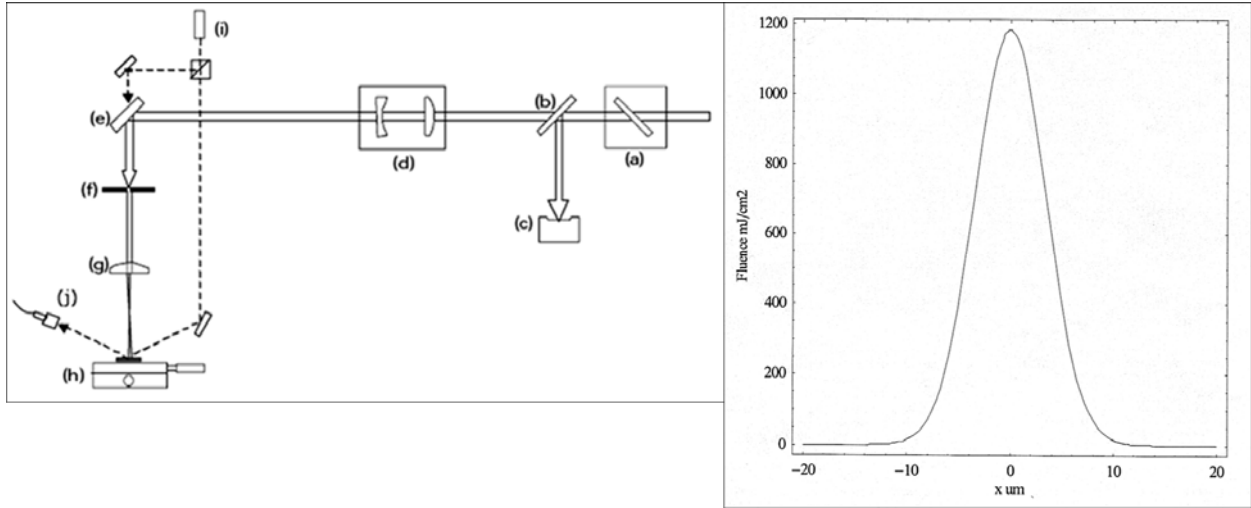


Figure 63. Schematic view of excimer projection irradiation system and Gaussian fluence profile using 25 μm copper mask and unattenuated beam (peak surface fluence at 1,200 mJ/cm^2). a) Variable attenuator, b) fused silica plate, c) joulemeter, d) adjustable field lens, e) turning mirror, f) copper mask, g) singlet lens, uncoated $f = 100\text{mm}$, h) X-Y sample stage, i) diode laser, j) fiber optic line to photodetector.

Circular channels were created in PES fibers by laser beam projection through a prefabricated copper mask with a 25 μm diameter pinhole at position (f) in Figure 63 and singlet projection lens at positioned at (g) for 5X demagnification. This resulted in a circular beam 5 μm in diameter incident the side of the PES fiber. Channel creation was optimized by varying each laser setting of pulse number, placement of the projection lens, and laser fluence, or energy density, independently. Single rows of 5 μm diameter channels were patterned onto PES fiber walls using 35-50 pulses ($N = 35-50$) at a peak surface fluence of 1,200 mJ/cm^2 .

For comparison, large area PES flat sheet membrane surfaces were modified without a mask at laser fluence values used in channel creation. Fluence calibration in both cases was obtained with a series of single shots on silicon and SiO₂ multilayer thin film wafers under flood irradiation (without mask) and with the 25 μm copper mask at known pulse energies. Using a technique described elsewhere [316], the absolute fluence under flood irradiation as well as the spatial fluence variation in the projected beam with the 25 μm mask could be determined. This was used to laser modify a continuous area on the PES flat sheet membranes with different fluences under flood irradiation that mimicked the surfaces cells would see along channel walls. The PES flat sheet membranes were modified under flood irradiation with rows of single laser pulses overlapping to have 5 pulses within one beam diameter in order to correct for the Gaussian beam profile. Fluences used were similar to those using the 25 μm mask. These surfaces considerably approximates the fiber channel walls because only a small fraction of the 50 pulses used to create the channels modifies the final wall surface due to the narrow Gaussian beam profile. These flat sheet membranes allowed surface characterization of the laser modifications to the PES surfaces.

4.2.2 Surface characterization of laser modified PES flat sheet membranes

4.2.2.1 Contact angle measurements

To analyze changes in surface chemistry after laser modification, advancing and receding contact angle measurements were performed on unmodified PES flat sheet membranes and membranes modified with peak surface fluences of 300, 600, 900, and 1200 mJ/cm². These measurements were performed by placing a 3 μl ultrapure water droplet on sample surface, adding 1 μl to

existing droplet for advancing angle, capturing image with VCA2000 video contact angle system (goniometer, Advanced Surface Technology Inc.), then removing 1 μ l for receding angle, and capturing another image of this droplet. Computer software calculated the angle of contact between surface and adjacent droplet edge. Ten independent measurements were performed per each sample resulting in two angle measurements per droplet.

4.2.2.2 Quantification of laminin adsorption on PES flat sheet membranes

PES flat sheet membranes both unmodified and modified with a peak laser surface fluence of 1,200 mJ/cm^2 were cut into disks (n=5 of each) fitting the wells of 48-well plates (BD and Co., Franklin Lakes, NJ), sterilized for cell culture by ethylene oxide, and subsequently washed with phosphate buffered saline (PBS; Gibco/Invitrogen Corp., Grand Island, NY). Each of the PES disks and n=5 TCPS control wells were incubated at 37 $^{\circ}\text{C}$ in a humidified incubator with atmosphere of 5% CO_2 for 12 hours with 10 $\mu\text{g}/\text{ml}$ laminin in 400 μl PBS (total 4 μg laminin per disk). The supernatants from each well were removed and collected. The non-adsorbed laminin from each disk was detected using a Micro BCATM Protein Assay Kit (Pierce, Rockford, IL) [317]. For this assay, 200 μl of each of the supernatants were added to 200 μl of the BCA working reagent in a 48 well plate (only half of the supernatant was analyzed). A standard was made with known amounts of laminin diluted in PBS in separate wells with same volume of working reagent and total volume. These plates were incubated for 2 hours in 5% CO_2 humidified incubator. Solutions were then measured with Fluorometer (SpectraFluor Plus; Tecan Group Ltd., Mannedorf, Switzerland) at 560 nm. Total μg adsorbed laminin was calculated by doubling the amount measured to get the total amount of non-adsorbed laminin and then subtracted from the total 4 μg amount added.

4.2.2.3 PC12 cell adhesion assay on PES flat sheet membranes

PES flat sheet membranes both unmodified and modified with peak laser surface fluences of 300, 600, 900, and 1200 mJ/cm² (n=5 of each) were cut into disks fitting the wells of 48-well plates as performed above for the laminin adsorption study. Laminin adsorption to n = 5 disks of each group was performed as above with n = 5 of the unmodified disks incubated with only PBS for 12 hours. The neuronal-like rat pheochromocytoma cell line (PC12; ATCC, Manassas, VA) was used to allow easy plating and quantification of cells attached to modified disk surfaces. 4x10⁴ PC12 cells were plated onto each sample surface with DMEM/F-12 media (Gibco/Invitrogen Corp.) including 10% horse serum (Gibco/Invitrogen Corp.), 5% fetal bovine serum (Gibco/Invitrogen Corp.), and 1000 IU/ml penicillin/1000 µg/ml streptomycin (Gibco/Invitrogen Corp.) and allowed to attach for 12 hours at 37 °C in humidified incubator with atmosphere of 5% CO₂. Disks were then washed with PBS and transferred to new wells and plates were stored at -80°C at least 4 hours to freeze kill adhered cells. Adhered cells to surfaces of different laser modified PES membrane disks were quantified using CyQUANT-GR™ nucleic acid fluorescence assay kit (Molecular Probes/Invitrogen Corp., Eugene, OR). Fluorescent measurements of CyQUANT-GR™ reagent were taken with a Fluorometer (SpectraFluor Plus; Tecan Group Ltd., Mannedorf, Switzerland) after 15 minute incubation on disks. A calibration curve with known cell amounts translated the fluorescence readings into cell numbers.

4.2.3 Primary rat neural progenitor cell differentiation on modified hollow fibers

Interactions of a neuronal cell type on PES hollow fibers with laser created channels were assayed by culturing adult rat neural progenitor cells (NPCs) isolated from the subventricular

zone of adult rat brains (generously donated by Dr. Glenn Gobbel, University of Pittsburgh) [295]. Single fibers with a single row of 5 μm diameter laser created channels were coated first with poly-ornithine and then 10 $\mu\text{g}/\text{ml}$ laminin. Undifferentiated neurospheres were plated at a density of 1×10^5 cells/ml onto fibers along with differentiation media consisting of DMEM/F12 (Gibco/Invitrogen Corp.) with an additional 3 mM D-glucose, 1.2 mM sodium bicarbonate, 0.46 mM HEPES, 2% B27 (Gibco/Invitrogen Corp.), 0.1 mg/ml apo-transferrin, 23 $\mu\text{g}/\text{ml}$ insulin, 55 μM putrescine, 20 nM progesterone, 30 nM sodium selenite, 1000 IU/ml penicillin/1000 $\mu\text{g}/\text{ml}$ streptomycin (Gibco/Invitrogen Corp.), 20 ng/ml bFGF, and 3% fetal calf serum (FCS; Gibco/Invitrogen Corp.). These cultures were maintained for 1 week with media replacement every 2 days.

Results of these cell cultures were analyzed by fluorescent immunocytochemistry staining of β -III-tubulin and Hoechst counterstaining along with SEM. Fiber samples for immunocytochemistry were first fixed by washing with PBS, fixed in 4% paraformaldehyde for 30 minutes, and finally rinsed two times in PBS. Samples were then prepared for staining by permeabilization in 0.3% Triton-X, washed in PBS, and blocked with goat serum. β -III-tubulin (TUJ1) primary monoclonal antibody (dilution 1:750; Covance, Princeton, NJ) in 3% goat serum/PBS was added for 1 hour and then washed with PBS. Secondary antibody used was Alexa Flour 594 anti-mouse (dilution 1:1000; Molecular Probes/Invitrogen Corp.) in 3% goat serum/PBS for 1 hour. Samples were then washed twice with PBS and counterstained with Hoechst dye (dilution 1:500).

4.2.4 Scanning electron microscopy

The topographies of laser modified PES flat sheet membranes and PES fibers with laser created channels were examined using field emission SEM (Philips XL-30; FEI Company, Hillsboro, OR) after samples were sputter coated with Au/Pd layer using a Cressington 108 Auto (Cressington, Watford, UK). For fiber samples including rat neural progenitor cells, the SEM preparation procedure involved fixing the cells with a 2.5% solution of glutaraldehyde, treatment with osmium tetroxide, and alcohol dehydration followed by critical point drying.

4.2.5 Statistical analysis

Statistical analyses of experiments included first a one-way ANOVA using Statistical Analysis Software. To compare two groups within an experiment, variance ratios were compared to corresponding F-values to statistically validate either equal or unequal variances. Finally, to determine statistical significance between means of two groups within an experiment, two-tailed Fisher's protected *t*-tests with either the validated equal or unequal variances was performed with a confidence interval of 95%. All data points are expressed as mean \pm standard deviation.

4.3 RESULTS

4.3.1 Peak fluence of KrF excimer laser pulse at PES surface

The multilayer silicon/SiO₂ thin film wafer measurements under flood irradiation and mask projection irradiation combined with a numerical model allowed determination of the absolute fluence profile of the beam at the sample surface [316]. The fluence profile of the beam using the 25 μm mask is shown in Figure 63. The x-axis shows the maximum diameter of the beam at the sample surface to be 5 μm , enabling creation of channels somewhat less than 5 μm using this mask. Successful calibration also permitted matching of the peak surface fluence in the projected beam to the flood irradiation experiments using PES flat sheet membranes, by adjusting the overall laser attenuator settings.

4.3.2 Optimization of laser created channels in PES hollow fibers

The three major variable settings on our KrF excimer laser system are the number of pulses to the sample (N), the position of the projection lens, and the fluence of the beam (F in mJ/cm^2). A series of tests were run in order to determine the individual effects of each setting on the creation of channels within the PES fiber walls (results shown in Figure 64). The number of laser pulses to the PES surface was able to change the amount of material removed from the channel and hence its depth. Figure 64(a-c) depicts the results with SEM images of channels in PES fiber walls with increasing the pulse number on the PES fiber surface with constant $F = 1,200 \text{ mJ}/\text{cm}^2$ from (a) $N = 10$ to (b) $N = 20$ and (c) $N = 40$. At this fluence it was found that with $N = 50$ a channel can be created that extends through the entire wall thickness of the fibers (channels used

in experiments with these settings are shown in Figure 65). Next, the position of the projection lens was varied while holding constant an $F = 1,200 \text{ mJ/cm}^2$ and $N = 50$. This enabled changing the focus of the projected beam image and led to altering the contour and slope of the edges of the channels created within the PES fiber walls. Figure 64(d-e) shows representative SEM images of channels created with two different lens positions. The channel in Figure 64(d) was created with the projected beam image in focus to produce steeper, more precise edges. Figure 64(e) depicts a channel formed with the lens position raised to result in the beam being slightly out of focus. This results in more sloped edges of the channels towards the outer surface of fibers while still keeping the smaller $5 \text{ }\mu\text{m}$ diameters at the inner surface. Finally, tests were performed varying the beam fluence with an attenuator plate within the beam path (Figure 63a). Other settings were held at $N = 50$ and lens position at the above mentioned setting to create the sloped edges. Results of SEM images of channels created with three representative fluences are shown in Figure 64(f-k). The effect of varying laser fluence was on the intensity of the beam being projected onto the PES fiber sample. Decreasing the fluence led to decreasing the diameter of the channel created within the PES fiber wall. It was not possible to create channels through the entire wall thicknesses of the fibers below $F = 600 \text{ mJ/cm}^2$ as shown in Figure 64(f).

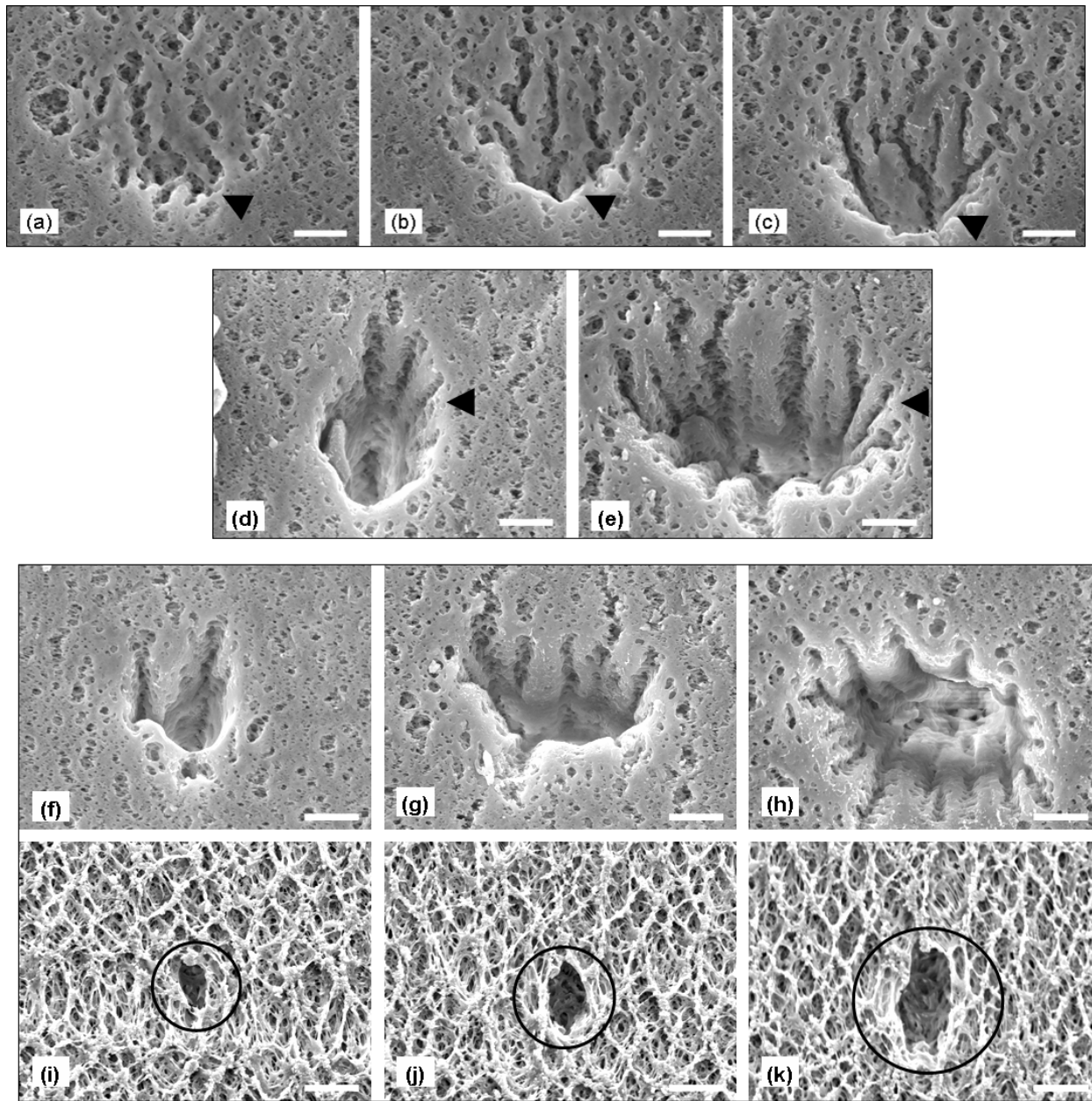


Figure 64. SEM images of channel creation in PES fiber with the following settings: $F = 1,200 \text{ mJ/cm}^2$ and (a) $N = 10$, (b) $N = 20$, (c) $N = 40$ (arrowheads highlight different channel depths); $F = 1,200 \text{ mJ/cm}^2$ and $N = 50$ with demagnifying singlet lens positions (d) in focus and (e) out of focus (arrowheads highlight edge differences); and $N = 50$, singlet lens out of focus, and fluences of (f,i) 600 mJ/cm^2 , (g,j) 900 mJ/cm^2 , and (h,k) $1,200 \text{ mJ/cm}^2$ ((f-h) outer fiber surface and (i-k) inside luminal fiber surface (created channels circled to distinguish between natural pores); scale bars = $5 \mu\text{m}$).

The optimal settings for reproducibly creating 5 μm diameter channels with smooth sloped edges leading to the inner lumens of the PES fibers are using an $F = 1,200 \text{ mJ/cm}^2$, $N = 50$, and a lens position to make the beam slightly out of focus. SEM images of channels with these settings are shown in Figure 65. The arrangement of these channels on the PES fibers that have further been used in the cell culture experiments are shown in Figure 65c. However, any desired channel pattern could easily be created in the fiber walls with this system.

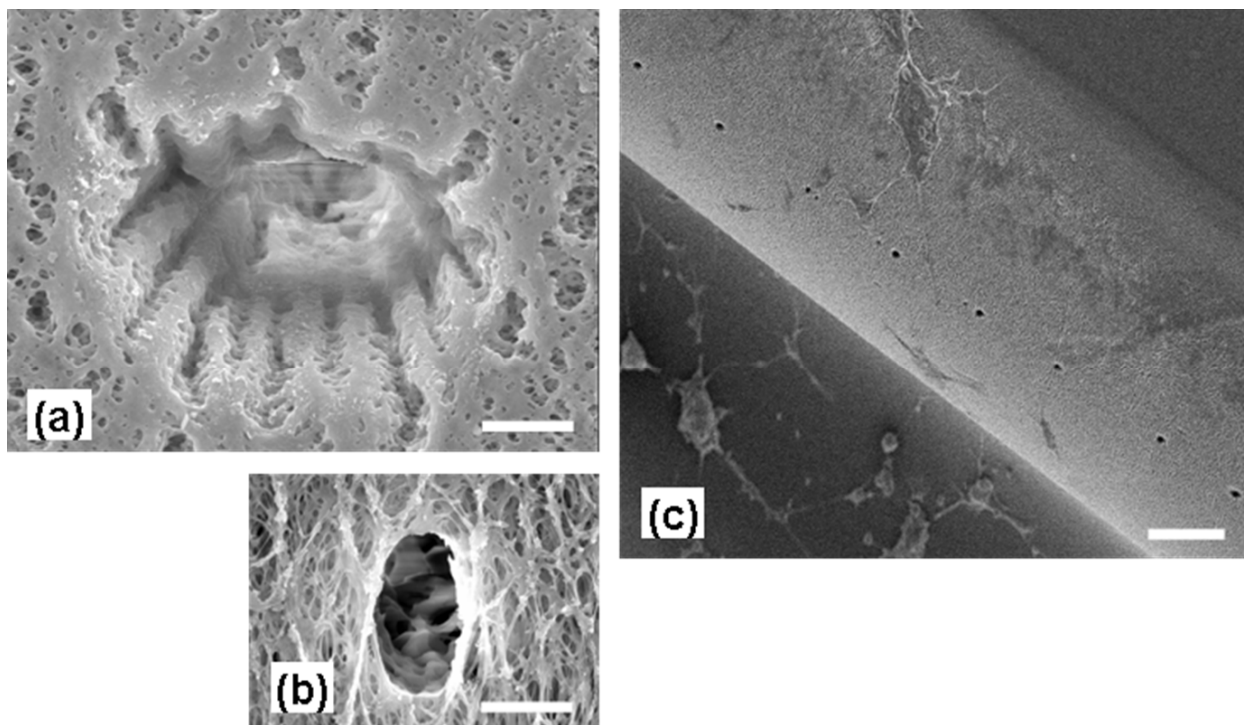


Figure 65. SEM images of channels in PES fibers further used in cell culture experiments viewed from (a) outer fiber surface and (b) inside luminal fiber surface (scale bars = 5 μm). Pattern of channels used in cell culture experiments shown in (c) single row arrangement along axis of fiber (scale bar = 100 μm). Laser settings used are 1,200 mJ/cm^2 , 50 pulses at 2 Hz, and demagnifying lens position out of focus.

4.3.3 PES flat sheet membrane surface wettability varying laser fluence

SEM images of these flat sheet membranes modified with different laser fluences producing surfaces similar to the walls of the channels created within the fibers revealed no major microstructural/topographical differences (images not shown). In order to determine any changes in the surface hydrophilicity with laser modification that could possibly affect cell interactions with the channels, contact angle measurements were taken. The results of the measured contact angles on these different PES flat sheet membranes are listed in Table 4. The unmodified PES flat sheet membrane surfaces are extremely hydrophilic consistent with these fibers being used mainly for ultrafiltration. The contact angles of droplets on these unmodified surfaces were next to zero due to the membrane almost completely absorbing the droplet. However, as the fluence of the laser beam is increased the contact angles of droplets on the modified surfaces increases significantly resulting in very hydrophobic surfaces with contact angles over 100°. The higher fluence of 1,200 mJ/cm² that is used in creating channels in the fiber walls results in an extremely hydrophobic surface with advancing and receding angles of 125° ± 1.5° and 110° ± 5.2° respectively.

Table 4. Contact angle measurements on PES flat sheet membrane surfaces modified with varying laser fluences (n=10 droplets per surface).

Table 1.	Contact Angle Measurements (degrees, Mean \pm SD)	
Fluence (mJ/cm ²)	Advancing angle ^a	Receding angle ^a
1. unmodified	<10	<10
2. 300	101.71 \pm 7.01 ¹	79.96 \pm 9.22 ¹
3. 600	118.06 \pm 2.62 ^{1,2}	106.97 \pm 7.23 ^{1,2}
4. 900	126.04 \pm 3.82 ^{1,2,3}	111.20 \pm 5.87 ^{1,2,3}
5. 1,200	125.13 \pm 1.51 ^{1,2,3}	110.94 \pm 5.23 ^{1,2}

a = Superscript indicates p-value < 0.05 with group indicated by the number of the superscript.

4.3.4 Laminin adsorption on laser modified PES flat sheet membrane surfaces

In order to determine protein adsorption changes to the surfaces of laser modified MicroPES fibers from unmodified surfaces, counterpart flat sheet membrane disks were coated with 10 μ g/ml laminin (total of 4 μ g) for 12 hours. A MicroBCA assay kit was used to measure total amounts of non-adsorbed laminin within the supernatants of the laminin added to the PES disks after the 12 hours. The results of n=5 disks of each of TCPS surfaces, unmodified PES, and laser modified PES disks using F = 1,200 mJ/cm² are shown in Figure 66. The means of the total adsorbed laminin quantities for the TCPS, unmodified, and laser modified disks were 0.433 μ g \pm 0.148, 0.044 μ g \pm 0.035, and 0.522 μ g \pm 0.189, respectively. The laminin adsorbed to the TCPS surfaces and the laser modified PES surfaces with F = 1,200 mJ/cm² were significantly higher compared to the unmodified PES surfaces (p-value < 0.01).

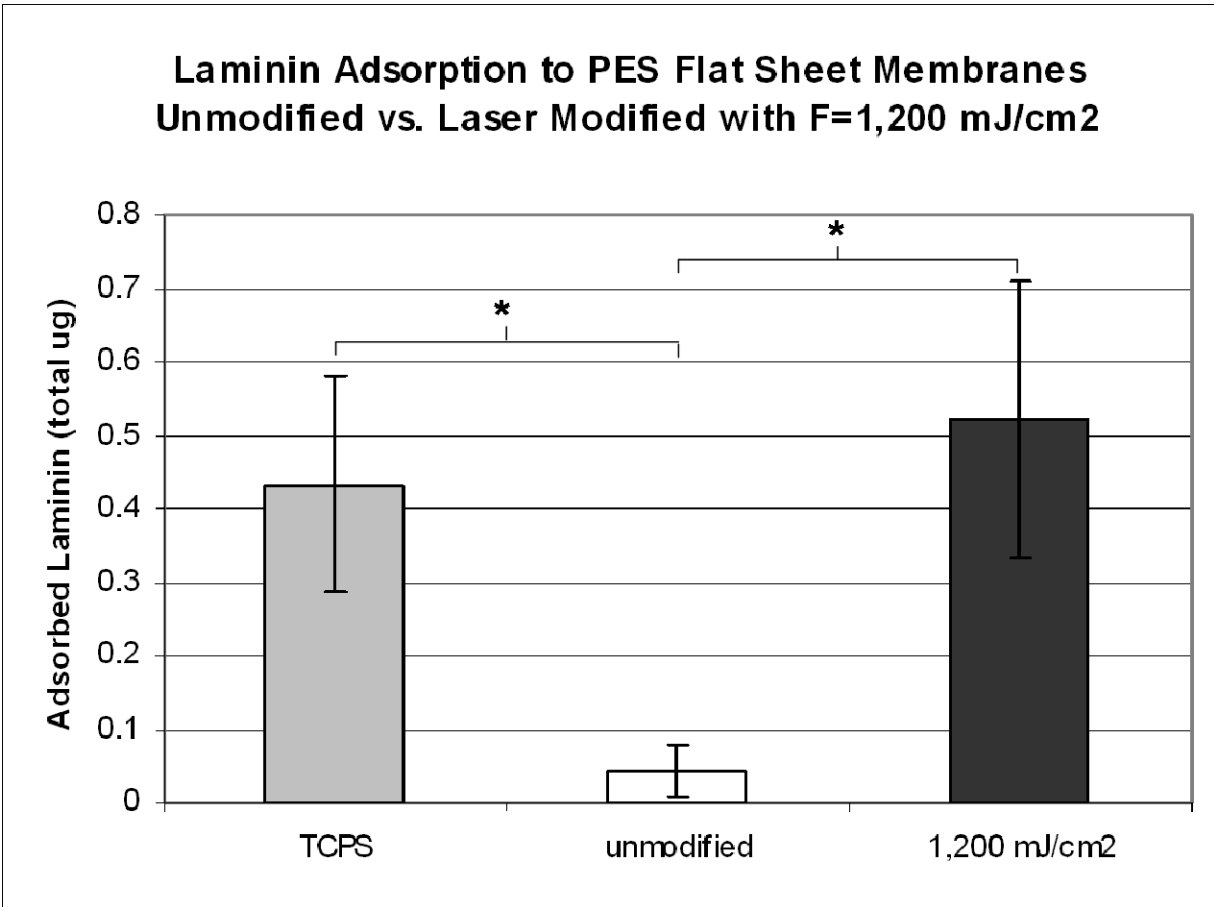


Figure 66. Quantification of laminin after adsorption of 10 $\mu\text{g/ml}$ for 12 hours to TCPS and PES flat sheet membranes unmodified and laser modified with $F = 1,200 \text{ mJ/cm}^2$ (bars = mean \pm SD, $n = 5$, and * = p -value < 0.01).

4.3.5 PC12 cell adhesion to PES flat sheet membrane surfaces varying laser fluence

Rat PC12 neuron-like cells were seeded onto the different PES flat sheet membrane surfaces modified with the same laser fluences as tested for contact angle measurements to see correlations between wettability of the surface and cell adhesion. The results quantifying the percentage of PC12 cells that adhered to the different surfaces normalized to the control tissue culture treated polystyrene (TCPS) surfaces are shown in Figure 67. Groups included the

completely unmodified PES surface, unmodified PES surface coated with 10 $\mu\text{g/ml}$ laminin, and laser modified PES disks coated with 10 $\mu\text{g/ml}$ laminin. First, PC12 cell attachment on the unmodified PES surfaces was increased significantly by coating with laminin compared to the completely unmodified surface ($p\text{-value} < 0.001$) demonstrating the reason for coating the total fiber surface with laminin for further cell culture use. Within the laminin coated surfaces, the results showed a significant increase in PC12 cell attachment to PES membranes with a laser modification at a fluence of 1,200 mJ/cm^2 compared to the unmodified coated membranes ($p\text{-value} < 0.05$). Overall, the results in Figure 67 show the trend of increasingly enhanced PC12 cell adhesion by modifying the PES surface with increasing laser fluences up to 1,200 mJ/cm^2 , which is used in creating the actual channels in the PES fibers.

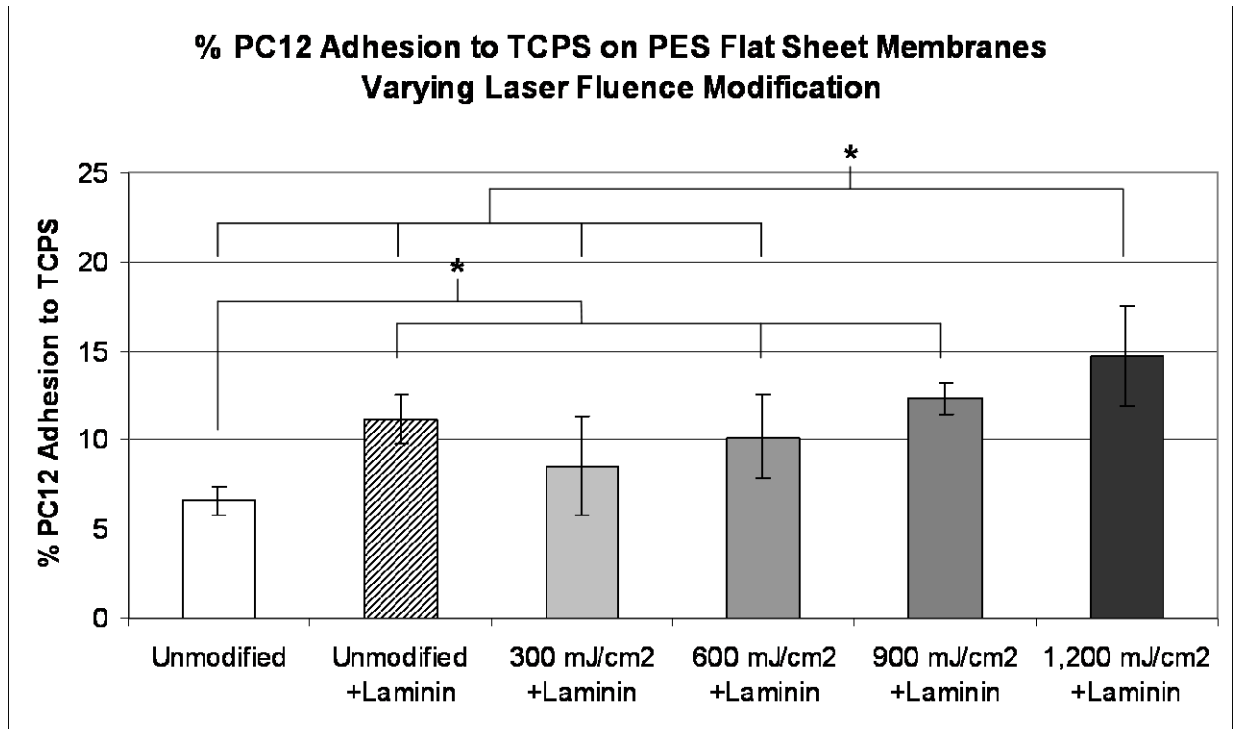


Figure 67. PC12 cell adhesion on PES flat sheet membrane surfaces modified with varying laser fluences followed by EtO sterilization and coating with 10 $\mu\text{g/ml}$ laminin with the exception of the first group being the completely unmodified membrane surface (data normalized to tissue culture treated polystyrene (TCPS) control surfaces, bars = mean \pm SD, $n = 5$, and * = p -value < 0.05).

4.3.6 Primary rat NPC differentiation on laser modified PES hollow fibers

With the aim of proving the laser modified PES fibers to be biocompatible we cultured and differentiated adult rat NPCs on their outer surfaces. Fluorescent immunocytochemistry staining and SEM images representing the growth of the differentiated neurons on these fiber surfaces including the laser channels are shown in Figure 68. Figure 68a shows β -III-tubulin/Alexa 594 in processes of NPCs differentiated along the neuronal lineage (all cell nuclei counterstained with Hoechst dye). The staining shows substantial process growth across the PES fiber surfaces. Figure 68b illustrates the growth of the differentiated neural progenitor cells on the outer fiber

surface including a single row of evenly spaced 5 μm laser created channels. Some channels are not seen due to covering cell body clusters. Figure 68c depicts the growth of two cell body clusters around two laser created channels and their process connections between each other and to the channels. Figure 68d shows a higher magnification of one neuronal process leading from a multiple cell body cluster growing down into the laser created channel towards the inner lumen of the PES fiber. These laser-created channels within the PES fiber walls appear compatible for adult rat NPC growth and prove conducive to cell process outgrowth across them.

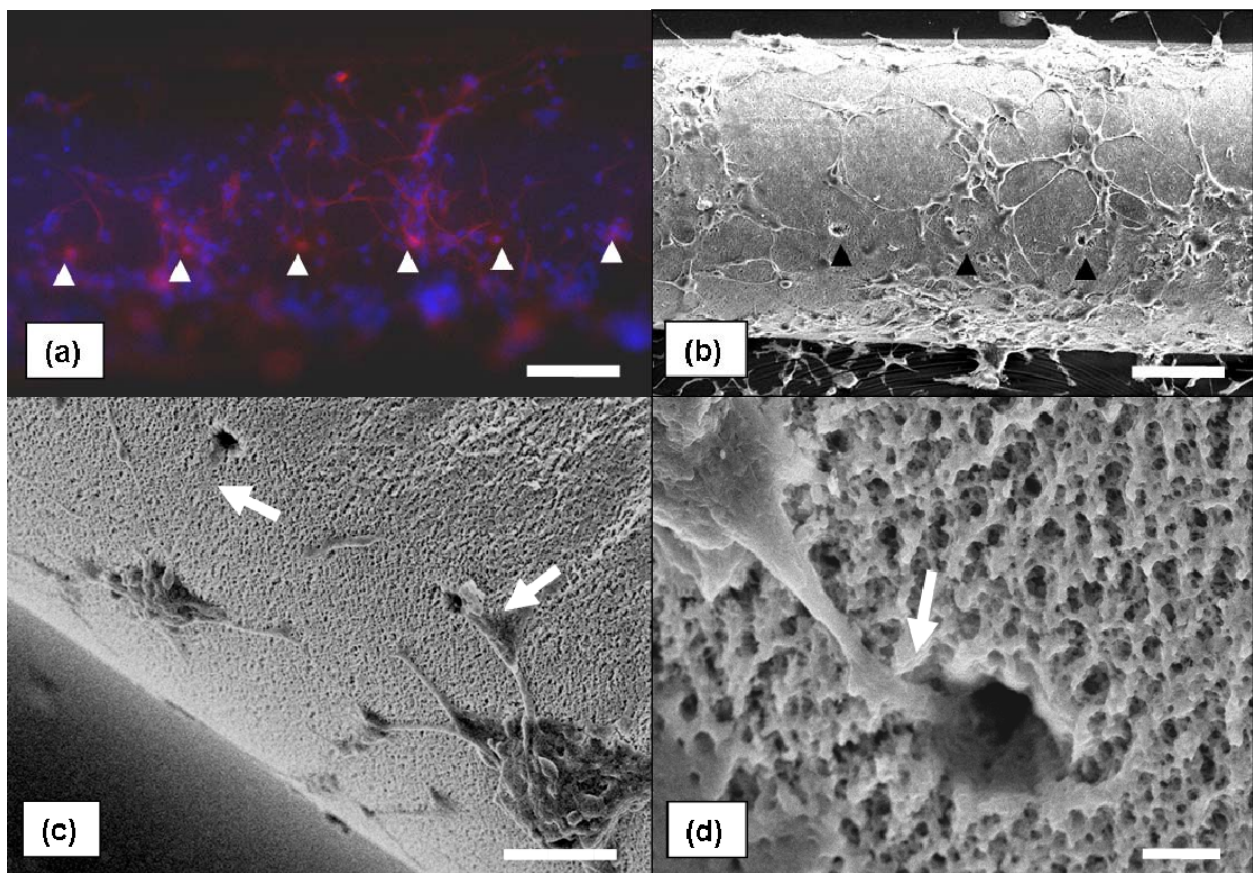


Figure 68. Images of primary adult rat neural stem cells differentiated on laser modified PES fiber including channels (arrowheads point to laser channels and white arrows point to process growth into laser created channels). (a) β -III-tubulin/Alexa Flour 594 stained neuronal processes with Hoechst nuclei counterstain, scale bar = 100 μm ; (b) SEM image, scale bar = 100 μm ; (c) SEM image, scale bar = 50 μm ; and (d) SEM image, scale bar = 5 μm .

4.4 DISCUSSION

4.4.1 Channel creation in PES hollow fibers via excimer laser ablation

A series of investigations varying different parameters within the KrF excimer laser system has established an optimal combination of settings in order to generate 5 μm diameter channels through the walls of PES hollow fibers. To facilitate the ablation of sufficient material to create a channel passing entirely through the 100 μm wall to the inner lumen of the fiber, a pulse number of $N = 50$ was necessary when using a fluence of $F = 1,200 \text{ mJ/cm}^2$. The etch depth per pulse with excimer laser ablation of polyethersulfone films has been reported to be from 0.32-0.50 μm with $F = 1,000 \text{ mJ/cm}^2$ [318-320], but is it possible that we achieved a much greater etch depth per pulse due to the highly porous nature of our PES fibers and membranes. Small changes in the projection lens position (Figure 1g) in the vertical direction allowed control over the focus of the beam. It is possible that creation of channels using a slightly unfocused beam having larger diameters at the fiber surface forms larger areas for the neuronal cell processes to notice the channels and can better facilitate continued growth into the fiber lumen. Martele et al. reported detrimental structural debris formation on polyurethanes with excimer laser ablation [321], but we have not seen any fragment deposition of this kind using polyethersulfone that would hinder cell growth. Therefore, the optimal settings used in our laser system in creating channels suitable for our neuronal cell/axonal process compartmentalization were with $F = 1,200 \text{ mJ/cm}^2$, $N = 50$, and the projection lens position set slightly out of focus. Using a 25 μm pinhole mask along with the 5X demagnifying projection lens at the settings mentioned above we are reproducibly able to generate smoother sloped edged channels that taper in diameter towards the

luminal fiber side down to approximately 5 μm in diameter. Lower fluences and/or a smaller pinhole in the mask projection can allow even smaller diameter channels.

Polyethersulfone (PES) is a non-degradable, biocompatible polymer typically utilized as hollow fiber membranes in medical applications such as ultrafiltration and hemodialysis devices due to its biocompatibility, excellent thermal stability, and chemical resistance [322-325]. Yu and Bellamkonda have demonstrated significant sciatic nerve regeneration using a nerve guide conduit based on semi-permeable polysulfone tubes [326]. Recently, Unger et al. have demonstrated good cell attachment and growth of different cell types on PES hollow fiber membranes [327]. We use similar commercially available PES hollow fibers with unproblematic laser modification as scaffolds for directing neuronal cell and axon growth *in vitro*. The cell studies reported here have demonstrated compartmentalization of the neuronal cell bodies of the differentiated adult rat neuronal cell bodies from the processes via the 5 μm diameter laser created channels. Observation of these cell cultures on the laser modified PES hollow fibers revealed spontaneous growth of the processes into the channels proving good biocompatibility of the laser modified surface.

Use of these modified PES ultrafiltration hollow fiber membranes as scaffolds will allow incorporation into a 3-D hollow fiber-based bioreactor utilizing the same PES fiber membranes as the integral perfusion system for delivering nutrients to the cell compartment along with integral oxygenation fibers. These bioreactors will be constructed based on the technology previously developed by our group [116-118, 137, 222]. The purpose of separating the cell bodies from the axonal processes lies in the ability of the lumens of the fibers to further direct axonal process growth in a 3-D space at high tissue density by using the bioreactor device to provide gradients of neurotrophic factors, such as nerve growth factor (NGF), through the

lumens of the fibers. Use of multiple hollow fibers with these laser created channels could allow a 3D space for neuronal cultures with specific axonal growth and signaling, enabling a system for superior testing of directed neurite outgrowth and behavior in three dimensions. Many researchers investigate neural networks *in vitro* on two-dimensional surfaces such as microelectrode arrays (MEAs). Maher et al. have created a micromachined silicon chip with wells to hold neurons for controlled cell positions contacting electrodes [328]. Recently, Suzuki et al. have layered a patterned agarose gel film on an MEA to control cell positions on the chip [79]. These systems allow specific neuronal signaling and recordings from low-density cultures. Heron et al. have recently developed an *in vitro* method of co-culturing neurons with astrocytes in Matrigel to determine effects of protein gradients on axonal outgrowth within a cellular environment. These authors believe the higher density cell environment to be a crucial part of *in vitro* neuronal culture investigations instead of the more typical neuronal monolayer culture on synthetic biomaterials [329]. Our laser modified PES hollow fiber scaffolds incorporated into a hollow fiber-based bioreactor as discussed here will allow the high-density 3-D neuronal and possibly co-culture growth and organization, which hopefully will lead to either more accurate or representative responses from the cells when stimulated.

The device can more specifically be used to culture neural stem cells at high densities to assess the effect of different drug or therapeutic protein stimulation on their abilities to direct axonal growth from these cultures. The device configuration with the laser modified scaffolds compartmentalizing the neuronal cell bodies from the axons will recreate an *in vitro* model of the spinal cord and can be used to test different reagents on the ability of the high density nerve tissue to grow throughout the fiber scaffolds. The other intended use of the device would be to control networking of high density neuronal cultures *in vitro*. The cell bodies of one

compartment can be connected to another cell body compartment using the laser modified fiber scaffolds where the axons of the cells from one compartment grow throughout the scaffold fiber lumens and form synapses with the cell bodies of the other connecting cell body compartment.

4.4.2 Significance of laser modification to PES hollow fiber/membrane surface

Surface characterization of the laser modified PES surfaces was performed via contact angle measurements, quantification of laminin adsorption, quantification of PC12 cell adhesion, and assessment of rat neural progenitor cell interactions. These experiments, with the exception of the NPC cultures, were accomplished using laser modified flat sheet PES membranes with laser fluence matched to the peak fluence of the channel experiments. The results with the PES membranes demonstrated increased hydrophobicity, increased laminin adsorption, and enhanced PC12 cell adhesion in the high fluence laser modified surfaces compared to the unmodified PES surface. Previous laser modification of polyethersulfone with the intent to control cell interactions has included either CO₂ laser plasma treatment or UV-assisted graft polymerization in order to increase the membrane permeability and hydrophilicity to prevent fouling [330, 331]. However, our results show that KrF excimer laser modification of PES with the high peak surface fluences necessary to create the channels resulted in ablation of the polymer with possible re-deposition of broken polymer chain molecules back onto the surface that created a hydrophobic surface that is more favorable for cell growth after coating with the laminin protein. Others have also reported an increased hydrophobicity of a polymer surface after excimer laser ablation [332, 333].

It is hypothesized that excimer laser ablation in polyethersulfone is due to the photothermal ablation model where random polymer chain scission occurs and fragments are

ejected from the surface with some re-deposition back onto the surface and reacting with the surface radicals created [334]. Duncan et al. reported XPS results of excimer laser ablation of certain polymers to have decreased O/C ratio with high fluences possibly due to the higher energies creating an increased volume expansion and fragment velocity preventing oxygen radicals from forming [313]. Analysis with TOF mass spectrometry of ejected and re-deposited fragments of excimer laser ablation on polysulfone films by Kokai et al. resulted in increased deposition of hydrocarbon species with higher laser fluences [334, 335].

The increasingly hydrophobic surface observed with the higher fluence of $F = 1,200 \text{ mJ/cm}^2$ most likely permits the observed increase in laminin adsorption onto the areas surrounding and inside the laser created channels within the PES fibers leading to increased cell attachment. Hernández et al. have recently analyzed laminin molecule adsorption and conformation onto surfaces with varying -OH group densities using the phase signal of AFM [336]. This work demonstrated the most laminin molecules adsorbed to the more hydrophobic surfaces with the fewest -OH groups. The excimer laser modification works similarly with decreasing the O/C ratio as reported by Duncan et al. and allows the increase in laminin adsorption. Laminin is known to enhance neuronal cell adhesion and neurite extension [73, 280, 337-339]. Dertinger et al. have demonstrated axon orientation from rat hippocampal neurons in the direction of increasing surface density of laminin [340]. The spontaneous process outgrowth of the differentiated rat NPCs toward the laser channels on the fiber scaffolds demonstrated here might be due to the increased density of laminin molecules surrounding these channels due to the laser surface modification. Therefore, the laser modification leading to structured channels able to direct axon processes into the scaffold wall also creates an enhanced region around the

channels that the neuronal cell processes might attach and be influenced to grow across further leading them down into the lumens of the fibers as desired.

4.5 CONCLUSIONS

KrF excimer laser ablation was successfully conducted to reproducibly generate tapered 5 μm diameter channels within PES hollow fiber walls. This laser modification resulted in channel wall surfaces compatible and even beneficial to neuronal process growth through the walls of the PES fibers. The 5 μm diameter channels are able to allow process growth into the fiber walls while preventing entrance of the neuronal cell bodies into the fiber scaffold. These channels within the PES fibers comprise a scaffold allowing compartmentalization of the neuronal cell bodies from the axonal processes in order to further control and direct axonal growth for 3D *in vitro* neural tissue engineering.

5.0 FUTURE EXPERIMENTS

5.1 MOUSE NEURAL STEM CELL 4 CHAMBER BIOREACTORS

The experiments performed in Chapter 3 lead to a basic understanding of behavior of mouse neural stem cell differentiation within different 3D ECM matrices and the effects of dynamic culture conditions. These experiments have also brought about a multitude of further questions regarding the behavior of these cells within a 3D matrix. The work presented here focused on the differentiation of the mouse neural stem cells. However, it would also be of interest to investigate expansion of the stem cell population within a controlled scalable system like the hollow fiber-based bioreactors on their ability to expand large quantities of the stem cells. This feature would be necessary in providing these cells as a commercially available product used in clinical cell therapies were very large quantities of the stem cells are desired.

The most significant future experiments would include further investigation of the results obtained within the 4 chamber bioreactor of experiment MNS-3 containing superior structure formation with increased neuronal differentiation within the HyStem hydrogel chamber adjacent to the Matrigel containing chamber. First, control 3D hydrogels of Matrigel excluding cells could be maintained under static conditions within a 12 well tissue culture plate with Neurocult Differentiation medium. This system could be maintained under normal static cell culture conditions over time in order for the medium to be conditioned with the factors released from the

Matrigel hydrogel. The medium could be collected at different time points throughout this culture with further hydrolytic degradation of the Matrigel with longer time points. The collected medium could be tested on the differentiation of the mouse neurospheres plated on 2D laminin coated dishes. This experiment could prove the hypothesis that it was soluble components released from the Matrigel hydrogels that lead to the increased neuronal differentiation within the HyStem chamber of bioreactor experiment MNS-3. Further experiments could be employed to individually test the known components of Matrigel separately on the differentiation of the mouse neurospheres. Addition of these factors, such as soluble laminin, TGF- β , NGF, PDGF, IGF-1, could be separately added to the differentiation and tested on control cultures to see which factors affect the differentiation. Also, plates coated with adsorbed collagen IV and entactin could also be tested on the neurosphere differentiation because these are also components of Matrigel.

We have been able to demonstrate with the presented results that optimal neuronal cell differentiation and survival from the mouse neural stem cells is dependent upon more than just the ECM scaffold the cells are encapsulated within. It is equally important to improve the differentiation medium formulation for achieving neuronal differentiation from the neurospheres within 3D dynamic culture conditions. The experiments described above provide an initial framework for improving the medium formulation testing Matrigel components, however, other growth factors useful in natural nervous system development in vivo could be tested such as BDNF and GDNF.

Also, the neurospheres within the chamber of bioreactor MNS-5 containing HyStem with 100 $\mu\text{g}/\text{mL}$ laminin appeared to have initial migration and spreading of cells within the first few days, but then deteriorated after culture day 5. It is possible that this deterioration was due to

loss of the laminin within the HyStem hydrogel since the laminin was only encapsulated within the hydrogel and not covalently linked. Dynamic perfusion of this hydrogel within the bioreactor most likely lead to the release of laminin into the circulating medium where it is diluted within the large 75 mL volume. Experiments testing methods for long-term incorporation of laminin within the system could prove very useful in achieving superior neuronal differentiation and survival from neural stem cells. Also, custom hydrogels could be developed for achieving such a scaffold and could be investigated within the hollow fiber-based bioreactor. Stabenfelt et al. have fabricated such a hydrogel made of methylcellulose functionalized with covalently linked laminin molecules [341]. Tysseling-Mattiace et al. have developed a scaffold of self-assembling nanofibers displaying a surface of IKVAV sequences derived from laminin.

Further definition of an injectable scaffold used to enhance neuronal differentiation of neural stem cells is particularly useful in clinical applications using these cells, but could also be used to accomplish further use of the hollow fiber-based bioreactor devices as tools for testing further control and manipulation of neural stem cells. The enhanced culture of these cells within the devices could allow experiments testing the control over the migration of these cells throughout the 3D space of the bioreactor. Results of these experiments could prove useful in developing strategies for enhancing the roles of endogenous neural stem cells in regenerating nervous system tissue destroyed by disease or trauma. Also, the bioreactor could be useful in circulating defined culture medium including factors such as tumor necrosis factor-alpha (TNF- α) which is present in the inflammatory conditions found after nervous system trauma in order to synthetically mimick the inflammatory environment while still attempting to control neural stem cell behavior under these conditions. Other factors possibly tested such as this could be the

inhibitor molecules found within the adult CNS after spinal cord injuries preventing nerve regeneration in order to develop strategies allowing the neural stem cells to overcome these molecules and continue nerve regeneration.

5.2 PRIMARY RAT CORTICAL NEURON BIOREACTORS

Use of the PC12 cell line was able to demonstrate that neurite outgrowth within 3D could be enhanced by culture within the dynamic perfusion of the hollow fiber-based bioreactors. However, this cell line could not be used to analyze synapsin I as a marker only for synaptic transmission able to definitively prove that the bioreactor enhances the ability of neuronal cells to form superior synapse formation. The contact inhibition of the cells used did not allow tissue formation and therefore possibly prevented superior neuronal networking capable within the bioreactor devices. Further experiments would move from cell lines to primary neurons. Neuroscience research often utilizes cultures of embryonic day E17-E18 rat cortical neurons dissociated from cortical rat brain tissue.

Experiments within this work initially used the PC12 cell line because it is an accepted cell line for modeling neuronal behavior especially directed neurite outgrowth. The benefit of using a cell line is that the cells can easily be expanded to obtain the large number of cells required for bioreactor culture. Past experiments using the 8 mL hollow fiber-based bioreactor typically has required a minimum of 1×10^8 cells for initial inoculation in order to have a successful outcome for any tissue formation. The PC12 cell line was easily expanded to achieve these quantities. We continued with experiments using mouse neural stem cells because data on culture of these cells in a 3D dynamic environment is valuable in developing clinical strategies

using these cells, but also because stem cells have the capability to be expanded. The 8 mL hollow fiber-based bioreactor experiments for culture of mouse neural stem cells took approximately 8 weeks for expansion of the mNSCs from passage 1 to passage 8 in order to obtain $>1 \times 10^8$ cells needed for the bioreactor experiment plus control cultures. These experiments allowed us to demonstrate culture of primary neuronal cells within the bioreactors.

Adult mature neurons derived from the rat brain cortex are often used in cell culture experiments in the field of neuroscience, but mature neurons are post-mitotic and cannot be expanded. There are approximately 1×10^8 neurons within a single rat brain [342]. However, isolation of these cells from rat brains results in substantially fewer numbers useful for cell culture. BrainBits LLC is a company specializing in the commercial dissection and isolation of animal nervous system tissue obtaining neuronal cell populations available for sale making it easier to obtain primary neuronal cell cultures without isolating the cells. BrainBits offers approximately 2×10^6 E18 rat cortical neurons for approximately \$120, which is cost effective and prevents the need for maintenance of animals and dissections. However, in order to perform a bioreactor experiment within the 8 mL bioreactor, either too many rats would need to be sacrificed on the same day of bioreactor inoculation or buying the cells from BrainBits would cost at least \$6,000 to obtain 1×10^8 neurons. This has made it undesirable for use to attempt these experiments. It has only been recently that our group has been able to produce and successfully perform experiments using newer bioreactor designs, such as the 4 chambered analytical scale bioreactor, that have cell compartments with smaller volumes than the 8 mL bioreactor requiring fewer cells. Therefore, the successful experiments in Chapter 3 using the 4 chamber bioreactor with cell compartment volumes <1 mL has proved the feasibility of continued experiments using this device with primary rat cortical brain neuron cultures. These

experiments could potentially be used to generate high density 3D neuronal tissue within the bioreactor that achieves superior synaptogenesis and neuronal network formation.

5.3 DESIGN AND DEVELOPMENT OF NEURONAL CELL SPECIFIC BIOREACTOR INCLUDING FIBER SCAFFOLDS FOR DIRECTED AXONAL OUTGROWTH

The purpose of this thesis has been to initiate development of a hollow fiber-based bioreactor specific for allowing high density neuronal cell cultures in 3D with control over directed axonal outgrowth. We have achieved demonstrating the ability of the currently used bioreactors within the lab to support neuronal cell cultures. We have also fabricated a scaffold allowing directed axonal growth in 3D useful in these hollow fiber-based bioreactors. The continuation of this work would entail the combination of this modified scaffold into a novel hollow fiber-based bioreactor design allowing compartmentalized neuronal cell body cultures connected with the modified scaffolds fibers directing axonal growth to and from compartments. A possible design scheme was described previously within section 4.1. We have already begun fabrication of a prototype of employing the design described in Figure 62. A photograph of this prototype is shown in Figure 69.

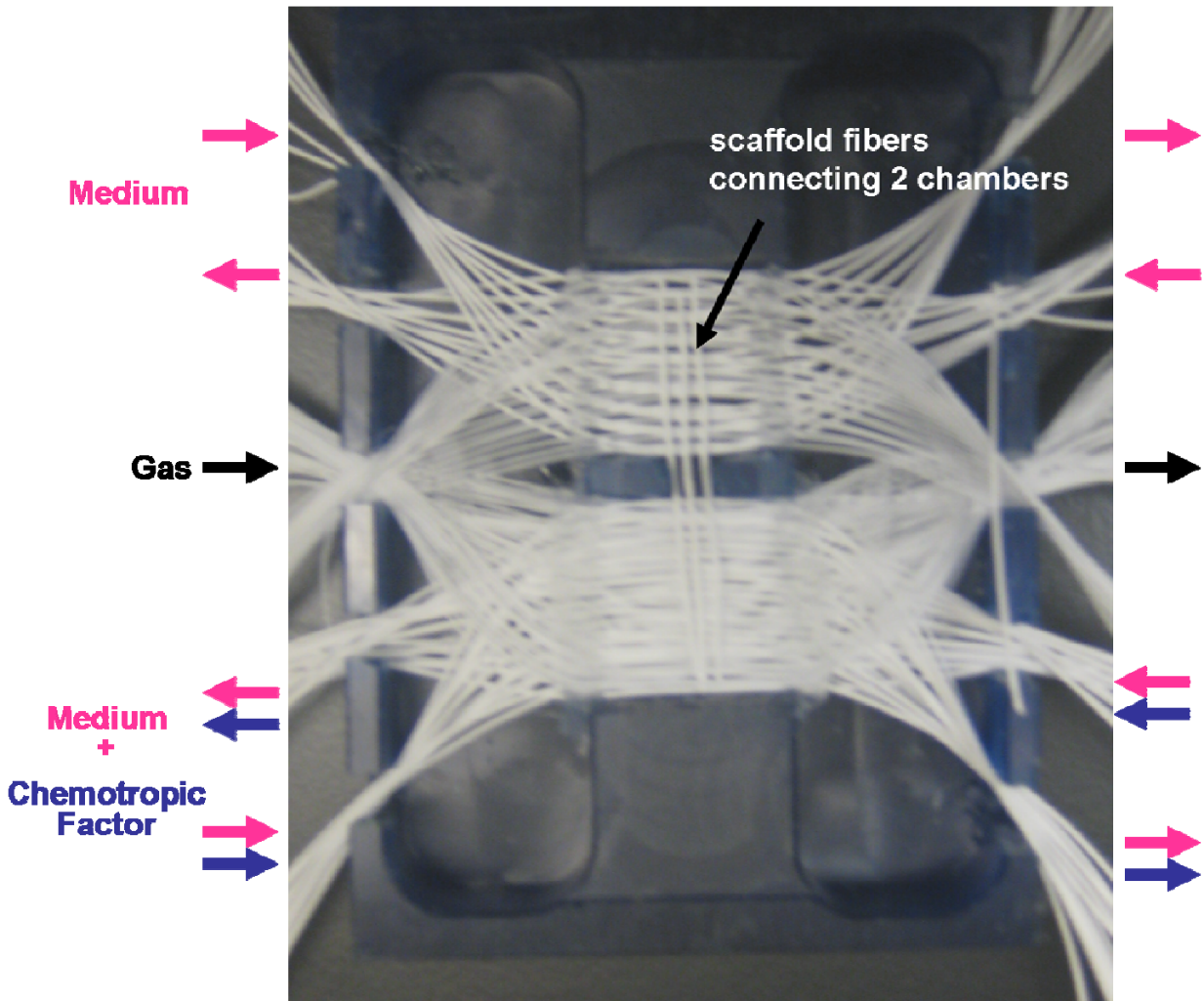


Figure 69. Photograph of first prototype for novel 2 chamber neuronal cell bioreactor incorporating scaffold laser modified PES hollow fibers. This is the bioreactor in development with placement of the gas and medium perfusion fiber bundles. There is a top and bottom chamber like the desired design with their own independent perfusion fibers. They do however share the same gas perfusion bundle, shown in the middle extending to both chambers. Colored arrows depict flow patterns possible with these separate fiber bundles extending from the bioreactor that will further be capped for separate ports, to have separate tubing circuits connected to each chamber. Also, the medium perfusion flow paths allow counter-current flow within each chamber. The separate perfusion circuits allow perfusion of a chemotropic factor of interest to be tested within the device possibly creating a gradient from the bottom chamber through the scaffold fibers to the top chamber for directed axonal outgrowth through the device.

Further completion of this prototype with incorporation of modified scaffold fibers connecting the two cell compartment chambers, will allow testing of this device with its ability to create gradients within the scaffold fibers. Perfusion of fiber bundles through the cell compartments can be separated into two independent tubing circuits. The newer perfusion systems have the capability to pump two tubing circuits, so this is already possible. The medium perfused through the bottom chamber could include a dye used to color the medium through this chamber. Experiments testing this perfusion could determine the transport of this color medium flow from one chamber to the other and how the colored medium becomes diluted in order to investigate gradient formation of the colored medium from one compartment to the other. This would be the first step in testing this device to be used as a neuronal cell specific bioreactor able to provide chemotropic factor gradients within a 3D space to high density neuronal cell cultures for testing factors enhancing nerve regeneration.

After the optimization of the design of this novel device, multiple experiments could finally be performed in using the device as the intended tool. Primary neuronal cultures could be used within this smaller scale bioreactor for screening drugs or proteins useful for enhancing nerve regeneration. Also, further experiments could be performed varying other bioreactor parameters such as flow rates and oxygen levels on their effects of neuronal cell cultures and axonal outgrowth. It is likely that optimal clinical strategies for achieving functional recovery with nerve regeneration require combination therapies. This novel bioreactor device could easily provide the model for testing these therapies in combination. It is possible that chemotropic factors enhancing nerve regeneration are particularly useful only at specific concentrations and combinations. This device would allow testing of the multiple protocols necessary in investigating the proper protocol of combination of these factors.

APPENDIX A

ORIGINAL PC12 CELL LINE BIOREACTOR EXPERIMENTS

PC12 Bioreactor Cultures. Two separate hollow fiber-based bioreactors were inoculated with PC12 cells in a collagen type I gel solution (BD Bioscience). One bioreactor was inoculated with a 3ml cell pellet suspended in a 1 mg/ml collagen solution. The other was inoculated with a 1.5ml cell pellet in a 1.5 mg/ml collagen solution. Both cultures were kept for 6 days with perfusion of 75 ng/ml NGF supplemented media. Collagen gels with same initial cell densities were kept in parallel for each experiment in Petri dishes for same time period with NGF media exchange every other day. Tissue/fiber samples were removed from the bioreactor for histological and confocal fluorescence microscopy analysis.

Results and Discussion. Glucose consumption and lactate production increased at least two fold by end of bioreactor cultures. Bioreactor opening revealed macroscopic tissue formation in both experiments. Histological analysis qualitatively showed a higher density of cells than control Petri dish gels. Masson's trichrome staining (Figure 1a) showed presence of injected collagen between fibers for use as cell matrix. Stacked confocal fluorescence images of Alexa488-Phalloidin/DAPI stained bioreactor tissue samples showed high density 3D cell aggregates with some 3D neurite outgrowth between aggregates (single image shown in Figure 70). PC12 cell

cultures in our bioreactor system showed high density tissue formation, but neurite outgrowth in 3D from individual cells was prevented due to this tissue formation.

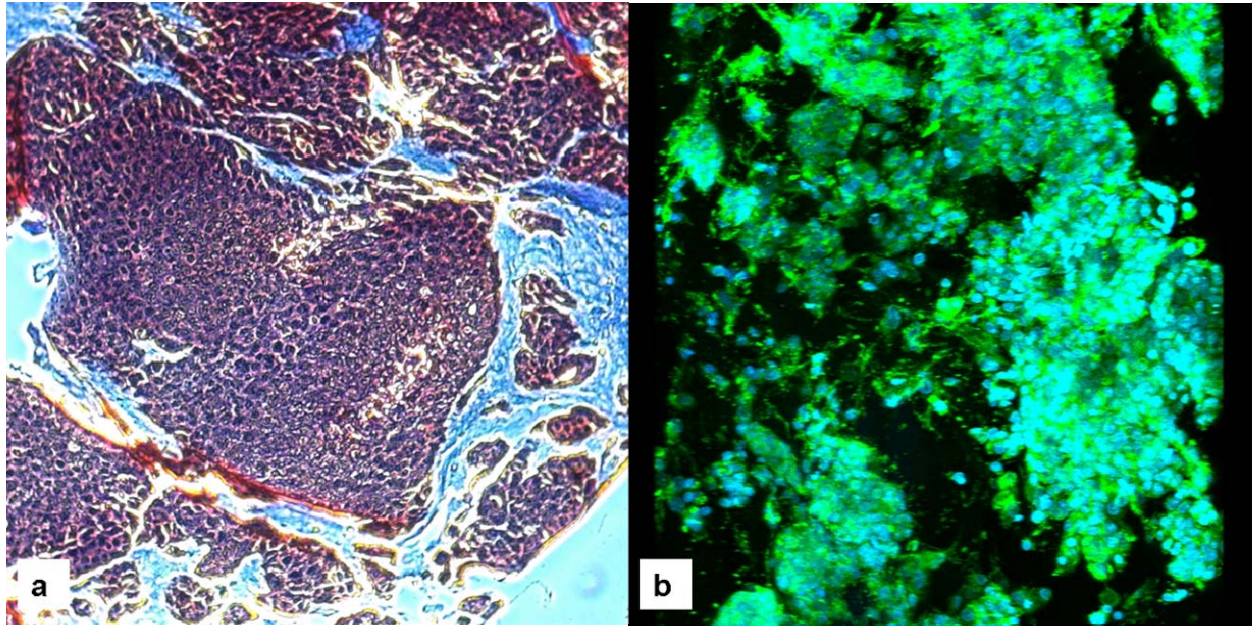


Figure 70. a) Masson's Trichrome stained section of higher density PC12 cell bioreactor (20X), b) confocal fluorescence of Alexa488-Phalloidin/DAPI stained block from lower density PC12 cell bioreactor (20X).

APPENDIX B

COMPATIBILITY OF INJECTABLE HYDROGELS IN HOLLOW FIBER-BASED BIOREACTORS

Use of bioreactor test chamber to analyze compatibility of collagen gel with perfusion system. A test chamber device was used to test the compatibility of the collagen gel matrix surrounding the PES microporous hollow fibers within the cell compartment space. This chamber is seen in Figure 71. Pre- and post-bioreactor perfusion pressures were monitored via pressure transducers in order to assess any problems with fluid flow through the perfusion circuit due to collagen gel incorporation. It will be necessary for pressures across perfusion fibers through cell chamber to remain stable to ensure constant flow through cell compartment. To assess this, sterile H₂O was pumped through the feed and recirculation tubing of the circuit volume to first fill the test chamber at flow rates giving similar pre- and post-bioreactor pressure measurements as that of the 8 ml bioreactors. A heating element maintained test chamber at 37°C to ensure proper gelation of collagen after injection. Then flow was completely turned off to prevent the possibility of perfused H₂O diluting or disrupting collagen gel formation. A collagen solution at room temperature brought to pH 7.0-7.4 at a final concentration of 1 mg/mL was injected by two syringes each through the two cell compartment ports. The viscous collagen solution filled the

chamber by forcing the H₂O out through the PES fiber pores into the recirculation tubing. Once in the test chamber the collagen gelled completely after 30 minutes and H₂O flow was resumed. Pressure transducers connected to circuit were then used to measure any pressure changes across the test chamber due to collagen incorporation by comparison to previously measured values. The pressure levels remained stable compared to before and after collagen injection into the cell compartment with flow through the fibers. This proved the compatibility of use of the collagen gel matrix within the bioreactor perfusion devices. Also, perfusion fibers were then fixed in 10% buffered formalin at end of experiment and stained with aniline blue in order to observe any collagen deposition within fiber lumens to check for fiber membrane fouling. The images of this staining of perfusion fibers is shown in Figure 72. Collagen was only detected within the gel surrounding the extra-capillary space around the fibers, whereas no collagen was detected within the lumens of the perfusion fibers again proving compatibility of the use of collagen gel within the cell compartments of the bioreactors as an ECM scaffold enhancing cell behavior within the compartment.

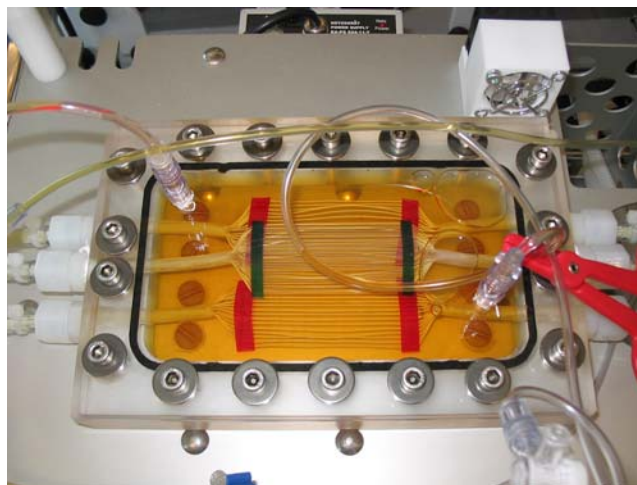


Figure 71. Bioreactor test chamber used for testing compatibility of collagen gel with perfusion fibers after inoculation into cell compartment within extra-capillary space.



**Collagen
surrounding
outside of PES
fiber bundle**



**Outside surface
of PES fiber
with stained
collagen**

**Open inside luminal
surface of PES fiber
with no collagen
staining**

Figure 72. Photographs of PES perfusion fibers taken from test chamber with compatibility testing of collagen gel formation around fibers within cell compartment. Fibers were stained with aniline blue to detect collagen. Cut fiber revealed aniline blue collagen staining only on outer surface of fibers, with no staining within lumen of fibers demonstrating collagen gel does not clog fiber lumens interfering with perfusion.

APPENDIX C

STATIC SINGLE FIBER CULTURE MODEL

We have also constructed a small scale *in vitro* compartmentalized culture model with a single laser-modified PES hollow fiber in order to apply chemotropic gradients for attracting neuronal axons into the fiber scaffold under static conditions. The model design was based on a modified 35 mm diameter polystyrene Petri dish. The dish includes a middle divider to form two compartments. A single PES microporous hollow fiber was sealed with compatible polyurethane along the diameter of the bottom of the Petri dish. A plastic divider piece fitting the dimensions of the Petri dish with a slit to fit over the fiber was sealed perpendicularly across the top of the fiber in order to divide the dish into two separate compartments. Movement of fluid and factors can only move from one compartment to the other via diffusion into fiber, through length of the fiber lumen, and out of the fiber. The fiber in one compartment, termed the “cell compartment”, can be modified to include the laser generated channels (left side Figure 73). The other compartment, termed the “factor compartment” can be used to apply chemotropic factor gradients by diffusion through the fiber to the cell compartment (right side Figure 73).

This model can be used for testing compatibility of a single PES hollow fiber including laser channels with different neuronal cell types. The compartmentalized configuration allows

application of chemotropic factor gradients by diffusion from one compartment to the other. The purpose of these factor gradients is to attract the neuronal cell axons to grow into the laser channels and further down the lumen of the fiber scaffold. To prepare for gradient applications to cell cultures within the models, a modified Petri dish top including two ports and reinforced with silicone is pressed firmly onto the top of the model in order to seal the two model compartments. Then a 10 ml syringe was connected to one port to flush sterile PBS from one compartment to the other in order to wet the fiber lumen. The PBS is then removed and cell media is replaced into both compartments and incubated overnight to allow media incorporation into the fiber lumen before cell seeding. All single fiber culture experiments can be prepared by these methods.

Bioactivity of NGF after gradient application to single fiber culture models was assessed by collection of cell compartment media from models at different time points and placement onto separately cultured PC12 cells on laminin coated 12 well plates (three models used for each time point). Models used had either laser modification to include a single row of laser created channels (Figure 74: 5 μ m) or were normal fibers without channels (Figure 74: none). Time points of media collection after NGF application to factor compartment were 6, 24, and 48 hours. PC12 cell % differentiation and number of neurites per cell was quantified from ten cells of each five high powered images taken after 24 hour treatment from each collected mediums. Control known amounts of NGF were also applied to other PC12 cell wells and neurite outgrowth was quantified. Figure 74 shows the results of these two measurements. All time point measured levels of PC12 neurite outgrowth after model media treatments show levels significant from 0 ng/ml of known NGF stimulation and are in the range of at least the active 25 ng/ml NGF stimulation (Figure 74). NGF after diffusion in the single fiber culture models through the

modified PES fibers is confirmed to be bioactive and able to stimulate neuronal cells growing on the fiber scaffolds in the cell side compartment.

This single fiber culture model allows testing of chemotropic factor gradients under static conditions, however we believe the culture was not reproducible in creating effective gradients for testing. The gradients within the design system here are created by diffusion only due to concentration gradients. However, any movement of the Petri dish creates a convective flow within the system disturbing the diffusion. Also, the gradient would change significantly with the need for medium replacement in order to feed the cultured cells. This does not allow a steady gradient through the fiber of the chemotropic factor being investigated. Therefore, we believe continuation of testing gradients of factors for enhancing nerve regeneration through our laser modified hollow fiber scaffolds would be more accurately tested within a dynamic system where the gradients are controlled by the bioreactor perfusion systems. We therefore did not continue further experiments using static single fiber culture model.

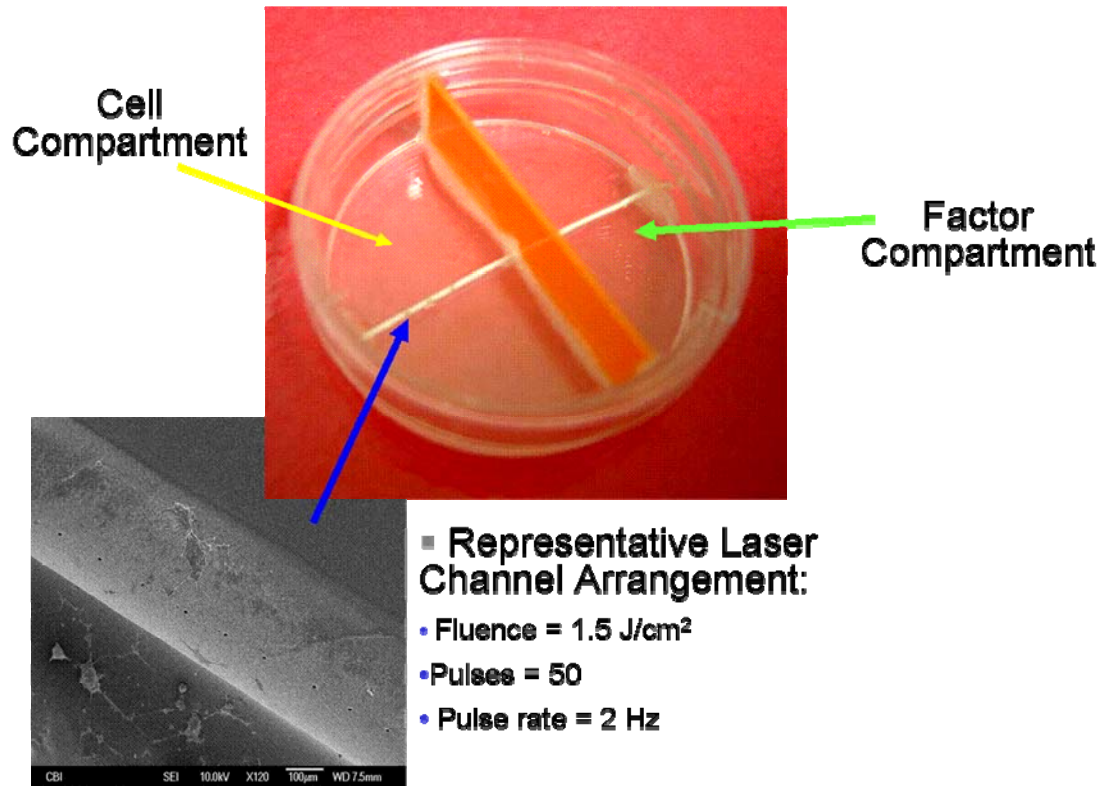


Figure 73. Single fiber culture model showing compartmentalized 35 mm Petri dish connected by laser modified scaffold PES hollow fiber for diffusion of chemotropic factors from right compartment to left cell containing compartment.

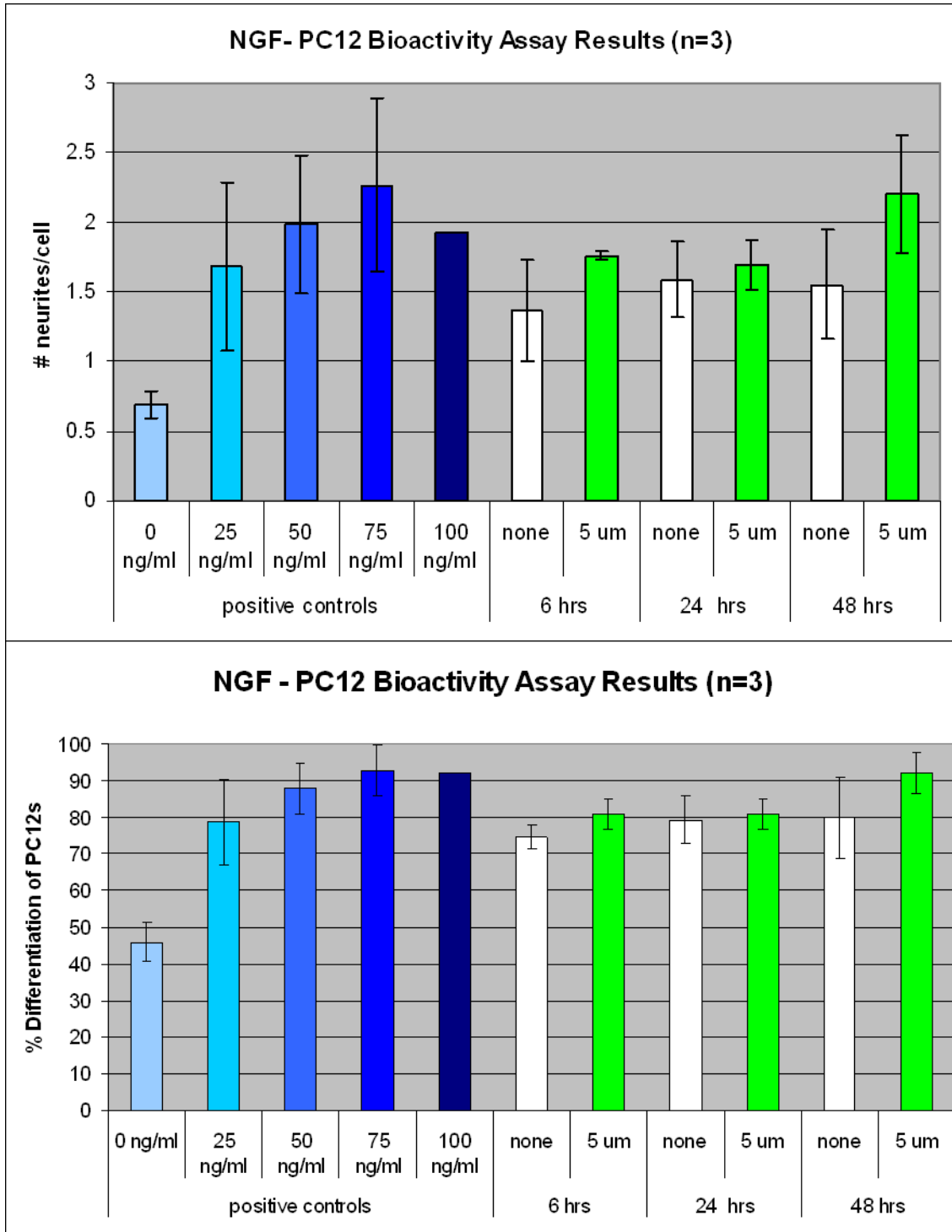


Figure 74. Bioactivity of NGF after diffusion through single fiber culture models compared to positive control fresh NGF; samples collected from opposite compartment after time listed for diffusion through fiber within model and then placed on test PC12 cultures (neurites counted after 24 hrs medium stimulation).

BIBLIOGRAPHY

- [1] Aguayo AJ, David S, Bray JM. Influences of the glial environment on the elongation of axons after injury: transplantation studies in adult rodents. *J Exp Biol* 1981;95:231-240.
- [2] Bray GM, Vidal-Sanz M, Aguayo AJ. Regeneration of axons from the central nervous system of adult rats. *Prog Brain Res* 1987;71:373-379.
- [3] Disorder Information Pages. vol. 2008: National Institute of Neurological Disorders and Stroke, 2008.
- [4] Stroke National Institute of Neurological Disorders and. Disorder Information Pages. 2008.
- [5] Health US National Institutes of. Alzheimer's Information. In: Aging NIO, editor, 2008.
- [6] Neyer JR, Greenlund KJ, Denny CH, Keenan NL, Casper M, Labarthe DR, Croft JB. Prevalence of Stroke--- United States, 2005. *CDC MMWR Weekly*, vol. 56, 2007. p.469-474.
- [7] Roitberg B. Transplantation for stroke. *Neurological Research* 2004;26:256-264.
- [8] American Cancer Society Inc. *Cancer Facts & Figures 2007*. vol. 2007: Surveillance Research, 2007.
- [9] Shannon KM. Long-term outcome in Parkinson disease: no advantage to initiating therapy with dopamine agonists. *Nat Clin Pract Neurol* 2008;Epub ahead of print.
- [10] Morrisette DA, Parachikova A, Green KN, Laferla FM. Relevance of transgenic mouse models to human Alzheimer disease. *J Biol Chem* 2008;Epub ahead of print.
- [11] Major ongoing stroke trials. *Stroke* 2008;39:e154-162.
- [12] Cooper JD. Moving towards therapies for juvenile Batten disease? *Exp Neurol* 2008;211:329-331.
- [13] Taupin P. HuCNS-SC (StemCells). *Curr Opin Mol Ther* 2006;8:156-163.

- [14] Weinstock-Guttman B, Ramanathan M, Zivadinov R. Interferon-beta treatment for relapsing multiple sclerosis. *Expert Opin Biol Ther* 2008;8:1435-1447.
- [15] Linker RA, Kieseier BC, Gold R. Identification and development of new therapeutics for multiple sclerosis. *Trends Pharmacol Sci* 2008;Epub ahead of print.
- [16] Bartt RE. Multiple sclerosis, natalizumab therapy, and progressive multifocal leukoencephalopathy. *Curr Opin Neurol* 2006;19:341-349.
- [17] www.spinalcord.uab.edu National SCI Statistical Center. Facts and Figures at a Glance. National Spinal Cord Injury Statistical Center (NSCISC), June 2005.
- [18] Reier PJ. Cellular Transplantation Strategies for Spinal Cord Injury and Translational Neurobiology. *NeuroRx: Journal of the American Society for Experimental NeuroTherapeutics* 2004;1:424-451.
- [19] Becker D, Sadowsky CL, McDonald JW. Restoring function after spinal cord injury. *Neurologist* 2003;9:1-15.
- [20] Nayak MS, Kim YS, Goldman M, Keirstead HS, Kerr DA. Cellular therapies in motor neuron diseases. *Biochimica et Biophysica Acta* 2006;article in press (available online).
- [21] Pearse DD, Bunge MB. Designing cell- and gene-based regeneration strategies to repair the injured spinal cord. *J Neurotrauma* 2006;23:438-452.
- [22] Knoller N, Auerbach G, Fulga V, Zelig G, Attias J, Bakimer R, Mardner JB, Yoles E, Belkin M, Schwartz M, Hadani M. Clinical experience using incubated autologous macrophages as a treatment for complete spinal cord injury: Phase I study results. *J Neurosurg: Spine* 2005;3:173-181.
- [23] Guenard V, Aebischer P, Bunge RP. The astrocyte inhibition of peripheral nerve regeneration is reversed by Schwann cells. *Exp Neurol* 1994;126:44-60.
- [24] Schlosshauer B, Dreesmann L, Schaller HE, Sinis N. Synthetic nerve guide implants in humans: a comprehensive survey. *Neurosurgery* 2006;59:740-748.
- [25] Meek MF, Coert JH. US Food and Drug Administration/Conformit Europe-Approved absorbable nerve conduits for clinical repair of peripheral and cranial nerves. *Ann Plast Surg* 2008;60:466-472.
- [26] Yang DP, Zhang DP, Mak KS, Bonder DE, Pomeroy SL, Kim HA. Schwann cell proliferation during Wallerian degeneration is not necessary for regeneration and remyelination of the peripheral nerves: axon-dependent removal of newly generated Schwann cells by apoptosis. *Mol Cell Neurosci* 2008;38:80-88.

- [27] Lundborg G, Dahlin LB, Danielsen N, Gelberman RH, Longo FM, Varon S. Nerve regeneration in silicone chambers; influence of gap length and of distal stump components. *Exp Neurol* 1982;76:361-375.
- [28] Shine HD, Harcourt PG, Sidman RL. Cultured peripheral nervous system cells support peripheral nerve regeneration through tubes in the absence of a distal nerve stump. *J Neurosci Res* 1985;14:393-401.
- [29] Aebischer P, Guenard V, Brace S. Peripheral nerve regeneration through blind-ended semipermeable guidance channels: effect of the molecular weight cutoff. *J Neurosci* 1989;9:3590-3595.
- [30] Diaz-Flores L, Gutierrez R, Varela H, Evora P, Valladares F, Rodrigues M, Rancel N, Alvarez-Arguelles H. Contribution of the proximal and distal nerve stumps to peripheral nerve regeneration in silicone chambers. *Histol Histopathol* 1995;10:937-946.
- [31] Weis J, May R, Schroder JM. Fine structural and immunohistochemical identification of perineurial cells connecting proximal and distal stumps of transected peripheral nerves at early stages of regeneration in silicone tubes. *Acta Neuropathol* 1994;88:159-165.
- [32] Williams LR, Azzam NA, Zalewski AA, Assam RN. Regenerating axons are not required to induce the formation of a Schwann cell cable in a silicone chamber. *Exp Neurol* 1993;120:49-59.
- [33] Johnson EO, Charchanti A, Soucacos PN. Nerve repair: experimental and clinical evaluation of neurotrophic factors in peripheral nerve regeneration. *Injury* 2008;39:S37-42.
- [34] Frostick SP, Yin ZQ, Kemp GJ. Schwann cells, neurotrophic factors, and peripheral nerve regeneration. *Microsurgery* 1998;18:397-405.
- [35] Lykissas MG, Batistatou AK, Charalabopoulos KA, Beris AE. The role of neurotrophins in axonal growth, guidance, and regeneration. *Curr Neurovasc Res* 2007;4:143-151.
- [36] Tang F, Shang K, Wang X, Gu J. Differentiation of embryonic stem cell to astrocytes visualized by green fluorescent protein. *Cell Mol Neurobiol* 2002;22:95-101.
- [37] Martino G, Pluchino S. The therapeutic potential of neural stem cells. *Nature Reviews: Neuroscience* 2006;7:395-406.
- [38] Billon N, Jolicoeur C, Ying QL, Smith A, Raff M. Normal timing of oligodendrocyte development from genetically engineered, lineage-selectable mouse ES cells. *J Cell Sci* 2002;115:3657-3665.
- [39] Liu S, Qu Y, Stewart TJ, Howard MJ, Chakraborty S, Holekamp TF, McDonald JW. Embryonic stem cells differentiate into oligodendrocytes and myelinate in culture and after spinal cord transplantation. *PNAS* 2000;97:6126-6131.

- [40] McDonald JW, Liu XZ, Qu Y, Liu S, Mickey SK, Turetsky D, Gottlieb DI, Choi DQ. Transplanted embryonic stem cells survive, differentiate and promote recovery in injured rat spinal cord. *Nature Medicine* 1999;5:1410-1412.
- [41] Deshpande DM, Kim YS, Martinez T, Carmen J, Dike S, Shats I, Rubin LL, Drummond J, Krishnan C, Hoke A, Maragakis N, Shefner J, Rothstein JD, Kerr DA. Recovery from paralysis in adult rats using embryonic stem cells. *Ann Neurol* 2006;60:32-44.
- [42] Barnett SC, Riddell JS. Olfactory ensheathing cells (OECs) and the treatment of CNS injury: advantages and possible caveats. *J Anat* 2004;204:57-67.
- [43] Plachez C, Richards LJ. Mechanisms of axon guidance in the developing nervous system. *Curr Top Dev Biol* 2005;69:267-346.
- [44] Paves H, Saarma M. Neurotrophins as in vitro growth cone guidance molecules for embryonic sensory neurons. *Cell Tissue Res* 1997;290:285-297.
- [45] Crone SA, Lee KF. The bound leading the bound: target-derived receptors act as guidance cues. *Neuron* 2002;36:333-335.
- [46] Schulte-Herbruggen O, Braun A, Rochlitzer S, Jockers-Scherubl MC, Hellweg R. Neurotrophic factors-- a tool for therapeutic strategies in neurological, neuropsychiatric and neuroimmunological diseases? *Curr Med Chem* 2007;14:2318-2329.
- [47] Allen SJ, Dawbarn D. Clinical relevance of the neurotrophins and their receptors. *Clin Sci (Lond)* 2006;110:175-191.
- [48] Dickson BJ. Molecular mechanisms of axon guidance. *Science* 2002;298:1959-1964.
- [49] Mueller BK, Yamashita T, Schaffar G, Mueller R. The role of repulsive guidance molecules in the embryonic and adult vertebrate central nervous system. *Philos Trans R Soc Lond B Biol Sci* 2006;361:1513-1529.
- [50] Sahenk Z, Nagaraja HN, McCracken BS, King WM, Freimer ML, Cedarbaum JM, Mendell JR. NT-3 promotes nerve regeneration and sensory improvement in CMT1A mouse models and in patients. *Neurology* 2005;65:681-689.
- [51] Hirono T, Torimitsu K, Kawana A, Fukuda J. Recognition of artificial microstructures by sensory nerve fibers in culture. *Brain Res* 1988;446:189-194.
- [52] Rutkowski GE, Miller CA, Jeftinija S, Mallapragada SK. Synergistic effects of micropatterned biodegradable conduits and Schwann cells on sciatic nerve regeneration. *J Neur Eng* 2004;1:151-157.
- [53] Dowell-Mesfin NM, Abdul-Karim MA, Turner AMP, Schanz S, Craighead HG, Roysam B, Shain JN Turner

W. Topographically modified surfaces affect orientation and growth of hippocampal neurons. *Journal of Neural Engineering* 2004;1:78-90.

[54] Claverol-Tinture E, Ghirardi M, Fiumara F, Rosell X, Cabestany J. Multielectrode arrays with elastomeric microstructured overlays for extracellular recordings from patterned neurons. *Journal of Neural Engineering* 2005;2:L1-L7.

[55] Mahoney MJ, Chen RR, Tan J, Saltzman WM. The influence of microchannels on neurite growth and architecture. *Biomaterials* 2005;26:771-778.

[56] Goldner JS, Bruder JM, Li G, Gazzola D, Hoffman-Kim D. Neurite bridging across micropatterned grooves. *Biomaterials* 2006;27:460-472.

[57] Wheeler BC, Corey JM, Brewer GJ, Branch DW. Microcontact printing for precise control of nerve cell growth in culture. *J Biomech Engineering* 1999;121:73-78.

[58] Faid K, Voicu R, Bani-Yaghoub M, Tremblay R, Mealing G, Py C, Barjovanu R. Rapid fabrication and chemical patterning of polymer microstructures and their applications as a platform for cell cultures. *Biomed Microdevices* 2005;7:179-184.

[59] Kam L, Shain W, Turner JN, Bizios R. Axonal outgrowth of hippocampal neurons on micro-scale networks of polylysine-conjugated laminin. *Biomaterials* 2001;22:1049-1054.

[60] Oliva Jr AA, James CD, Kingman CE, Craighead HG, Banker GA. Patterning axonal guidance molecules using a novel strategy for microcontact printing. *Neurochem Res* 2003;28:1639-1648.

[61] Schmalenberg KE, Uhrich KE. Micropatterned polymer substrates control alignment of proliferating Schwann cells to direct neuronal regeneration. *Biomaterials* 2005;26:1423-1430.

[62] Heller DA, Garga V, Kelleher KJ, Lee TC, Mahubani S, Sigworth LA, Lee TR, Rea MA. Patterned networks of mouse hippocampal neurons on peptide-coated gold surfaces. *Biomaterials* 2005;26:883-889.

[63] Thiebaud P, Lauer L, Knoll W, Offenhausser A. PDMS device for patterned application of microfluids to neuronal cells arranged by microcontact printing. *Biosensors & Bioelectronics* 2002;17:87-93.

[64] Bettinger C, Orrick B, Misra A, Langer R, Borenstein J. Microfabrication of poly(glycerol-sebacate) for contact guidance applications. *Biomaterials* 2006;27:2558-2565.

[65] Wu H, Odom TW, Chiu DT, Whitesides GM. Fabrication of complex three-dimensional microchannel systems in PDMS. *J Am Chem Soc* 2003;125:554-559.

- [66] Turcu F, Tratsk-Nitz K, Thanos S, Schuhmann W, Heiduschka P. Ink-jet printing for micropattern generation of laminin for neuronal adhesion. *J Neuroscience Methods* 2003;131:141-148.
- [67] Aebischer P, Guenard V, Valentini RF. The morphology of regenerating peripheral nerves is modulated by the surface microgeometry of polymeric guidance channels. *Brain Res* 1990;53:211-128.
- [68] Evans GRD. Challenges to nerve regeneration. *Seminars in Surgical Oncology* 2000;19:312-318.
- [69] Evans GRD, Brandt K, MS MS Widmer, Lu L, Meszlenyi RK, Gupta PK, Mikos AG, Hodges J, Williams J, Gurlek A, Nabawi A, Lohman R, Patrick CW. *In vivo* evaluation of poly(L-lactic acid) porous conduits for peripheral nerve regeneration. *Biomaterials* 1999;20:1109-1115.
- [70] Flynn L, Dalton PD, Shoichet MS. Fiber templating of poly(2-hydroxyethyl methacrylate) for neural tissue engineering. *Biomaterials* 2003;24:4265-4272.
- [71] Blacher S, Maquet V, Schils F, Martin D, Schoenen J, Moonen G, Jerome R, Pirard JP. Image analysis of the axonal ingrowth into poly(D,L-lactide) porous scaffolds in relation to the 3-D porous structure. *Biomaterials* 2003;24:1033-1040.
- [72] Smith CL. Cytoskeletal movements and substrate interactions during initiation of neurite outgrowth by sympathetic neurons *in vitro*. *J Neurosci* 1994;14:384-398.
- [73] Dodla M, Bellamkonda R. Anisotropic scaffolds facilitate enhanced neurite extension *in vitro*. *J Biomed Mater Res A* 2006;78:213-221.
- [74] Cai J, Peng X, Nelson KD, Eberhart R, Smith GM. Permeable guidance channels containing microfilament scaffolds enhance axon growth and maturation. *J Biomed Mater Res A* 2005;75:374-386.
- [75] Kapur TA, Shoichet MS. Immobilized concentration gradients of nerve growth factor guide neurite outgrowth. *J Biomed Mater Res* 2004;68A:235-243.
- [76] Bender MD, Bennett JM, Waddell RL, Doctor JS, Marra KG. Multi-channeled biodegradable polymer/Cultisphere composite nerve guides. *Biomaterials* 2004;25:1269-1278.
- [77] Itoh S, Yamaguchi I, Suzuki M, Ichinose S, Takakuda K, Kobayashi H, Shinomiya K, Tanaka J. Hydroxyapatite-coated tendon chitosan tubes with adsorbed laminin peptides facilitate nerve regeneration *in vivo*. *Brain Res* 2003;993:111-123.
- [78] Suzuki M, Itoh S, Yamaguchi I, Takakuda K, Kobayashi H, Shinomiya K, Tanaka J. Tendon chitosan tubes covalently coupled with synthesized laminin peptides facilitate nerve regeneration *in vivo*. *J Neurosci Res* 2003;72:646-659.

- [79] Suzuki I, Sugio Y, Jimbo Y, Yasuda K. Stepwise pattern modification of neuronal network in photo-thermally-etched agarose architecture on multi-electrode array chip for individual-cell-based electrophysiological measurement. *Lab Chip* 2005;5:241-247.
- [80] Williams LR, Varon S. Modification of fibrin matrix formation in situ enhances nerve regeneration in silicone chambers. *J Comparative Neurology* 1985;231:209-220.
- [81] Valentini RF, Sabatini AM, Dario P, Aebischer P. Polymer electret guidance channels enhance peripheral nerve regeneration in mice. *Brain Res* 1989;480:300-304.
- [82] Ahmed MR, Jayakumar R. Peripheral nerve regeneration in cell adhesive peptide incorporated collagen tubes in rat sciatic nerve -- early and better functional regain. *J Peripher Nerv Syst* 2005;10:390-391.
- [83] Ahmed M Rafiuddin, Jayakumar R. Peripheral nerve regeneration in RGD peptide incorporated collagen tubes. *Brain Res* 2003;993:208-216.
- [84] Matsumoto K, Ohnishi K, Kyotani T, Sekine T, Ueda H, Nakamura T, Endo K, Shimizu Y. Peripheral nerve regeneration across an 80-mm gap bridged by a polyglycolic acid (PGA)-collagen tube filled with laminin-coated collagen fibers: a histological and electrophysiological evaluation of regenerated nerves. *Brain Res* 2000;868:315-328.
- [85] Schense JC, Block J, Aebischer P, Hubbell JA. Enzymatic incorporation of bioactive peptides into fibrin matrices enhances neurite extension. *Nature Biotech* 2000;18:415-419.
- [86] Waddell RL, Marra KG, Collins KL, Leung JT, Doctor JS. Using PC12 cells to evaluate poly(caprolactone) and collagenous microcarriers for applications in nerve guide fabrication. *Biotechnol. Prog.* 2003;19:1767-1774.
- [87] Chavez-Delgado ME, Mora-Galindo J, Gomez-Pinedo U, Feria-Velasco A, Castro-Castaneda S, Toral FA Lopez-Dellamary, Anda S Luquin-De, Garcia-Segura LM, Garcia-Estrada J. Facial nerve regeneration through progesterone-loaded chitosan prosthesis. A preliminary report. *J Biomed Mater Res* 2003;67B:702-711.
- [88] Hudson TW, Evans GRD, Schmidt CE. Engineering strategies for peripheral nerve repair. *Orthopedic Clinics of North America* 2000;31.
- [89] Cao X, Shoichet MS. Defining the concentration gradient of nerve growth factor for guided neurite outgrowth. *Neuroscience* 2001;103:831-840.
- [90] Kotwal A, Schmidt CE. Electrical stimulation alters protein adsorption and nerve cell interactions with electrically conducting biomaterials. *Biomaterials* 2001;22:1055-1064.
- [91] Kruse PF, Myhr BC, Johnson JE, White PB. Perfusion system for replicate mammalian cell cultured in T-60 flasks. *J Natl Cancer Inst.* 1963;31:109-123.

- [92] Kruse PF, Miedema E. Production and characterization of multiple-layered populations of animal cells. *J Cell Biol* 1965;27:273-279.
- [93] Butler M, Imamura T, Thomas J, Thilly WG. High yields from microcarrier cultures by medium perfusion. *J Cell Sci* 1983;61:351-363.
- [94] Olivier V, Hivart P, Descamps M, Hardouin P. In vitro culture of large bone substitutes in a new bioreactor: importance of the flow direction. *Biomed Mater* 2007;2:174-180.
- [95] Wang L, Hu YY, Wang Z, Li X, Li DC, Lu BH, Xu SF. Flow perfusion culture of human fetal bone cells in large beta-tricalcium phosphate scaffolds with controlled architecture. *J Biomed Mater Res A* 2008;Epub ahead of print.
- [96] Jaasma MJ, Plunkett NA, O'Brien FJ. Design and validation of a dynamic flow perfusion bioreactor for use with compliant tissue engineering scaffolds. *J Biotechnol* 2008;133:490-496.
- [97] Holtorf HL, Jansen JA, Mikos AG. Modulation of cell differentiation in bone tissue engineering constructs cultured in a bioreactor. *Adv Exp Med Biol* 2006;585:225-241.
- [98] Niklason LE, Gao J, Abbott WM, Hirschi KK, Houser S, Marini R, Langer R. Functional arteries grown in vitro. *Science* 1999;284:489-493.
- [99] Freed LE, Vunjak-Novakovic G. Spaceflight bioreactor studies of cells and tissues. *Adv Space Biol Med* 2002;8:177-195.
- [100] Saini S, Wick TM. Effect of low oxygen tension on tissue-engineered cartilage construct development in the concentric cylinder bioreactor. *Tissue Eng* 2004;10:825-832.
- [101] Saini S, Wick TM. Concentric cylinder bioreactor for production of tissue engineered cartilage: effect of seeding density and hydrodynamic loading on construct development. *Biotechnol Prog* 2003;19:510-521.
- [102] Griffith LG, Tannenbaum S, Powers MJ, Domansky K, Thompson CD. Vascularized Perfused Microtissue/Micro-Organ Arrays. US Patent, vol. Patent No. US 6,197,575 B1, 2001.
- [103] Sivaraman A, Leach JK, Townsend S, Iida T, Hogan BJ, Stolz DB, Fry R, Samson LD, Tannenbaum SR, Griffith LG. A microscale in vitro physiological model of the liver: predictive screens for drug metabolism and enzyme induction. *Curr Drug Metab* 2005;6:569-591.
- [104] Kim SS, Utzunomiya H, Koski JA, Wu BM, Cima MJ, Sohn J, Mukai K, Griffith LG, Vacanti JP. Survival and function of hepatocytes on a novel three-dimensional synthetic biodegradable polymer scaffold with an intrinsic network of channels. *Ann Surg* 1998;228:8-13.
- [105] Potter K, Butler J, Adams C, Fishbein K, McFarland E, Horton W. Cartilage formation in a hollow fiber bioreactor studied by proton magnetic resonance microscopy. *Matrix Biol* 1998;17:513-523.

- [106] Sussman NL, Kelly JH. Improved liver function following treatment with an extracorporeal liver assist device. *Artif Organs* 1993;17:27-30.
- [107] Watanabe FD, Mullon CJ, Hewitt WR, Arkadopoulos N, Kahaku E, Eguchi S, Khalili T, Arnaout W, Shackleton CR, Rozga J, Soloman B, Demetriou AA. Clinical experience with a bioartificial liver in the treatment of severe liver failure. A phase I clinical trial. *Ann Surg* 1997;225:484-491.
- [108] Martin Y, Vermette P. Bioreactors for tissue mass culture: Design, characterization, and recent advances. *Biomaterials* 2005;26:7481-7503.
- [109] Meng Q, Zhang G, Wu D. Hepatocyte culture in bioartificial livers with different membrane characteristics. *Biotechnol Lett* 2004;26:1407-1412.
- [110] Dixit V. Development of a bioartificial liver using isolated hepatocytes. *Artif Organs* 1994;18:371-384.
- [111] Saito A. Research into the development of a wearable bioartificial kidney with a continuous hemofilter and a bioartificial tubule device using tubular epithelial cells. *Artif Organs* 2004;28:58-63.
- [112] Humes HD, Weitzel WF, Bartlett RH, Swaniker FC, Paganini EP, Luderer JR, Sobota J. Initial clinical results of the bioartificial kidney containing human cells in ICU patients with acute renal failure. *Kidney Int* 2004;66:1578-1588.
- [113] Patzer JF II, Lopez RC, Zhu Y, Wang ZF, Mazariegos GV, Fung JJ. Bioartificial liver assist devices in support of patients with liver failure. *Hepatobiliary Pancreat Dis Int* 2002;1:18-25.
- [114] Sauer IM, Kardassis D, Zeillinger K, Pascher A, Gruenwald A, Pless G, Irgang M, Kraemer M, Puhl G, Frank J, Muller AR, Steinmuller T, Denner J, Neuhaus P, Gerlach JC. Clinical extracorporeal hybrid liver support--phase I study with primary porcine liver cells. *Xenotransplantation* 2003;10:460-469.
- [115] Chen CT, Fishbein KW, Torzilli PA, Hilger A, Spencer RG, Jr, Horton WE. Matrix fixed-charge density as determined by magnetic resonance microscopy of bioreactor-derived hyaline cartilage correlates with biochemical and biomechanical properties. *Arthritis Rheum* 2003;48:1047-1056.
- [116] Gerlach J, Kloppel K, Muller C, Schnoy N, Smith M, Neuhaus P. Hepatocyte aggregate culture technique for bioreactors in hybrid liver support systems. *Int J Art Org* 1993;16:843-846.
- [117] Gerlach J, Schnoy N, Smith M, Neuhaus P. Hepatocyte culture between woven capillary networks - a microscopic study. *Artif Organs* 1994;18:226-230.

- [118] Gerlach J, Zeilinger K, Holland G, Muller C, Neuhaus P. Recovery of primary human hepatocytes and nonparenchymal cells from preservation injury to tissue-like structures in large-scale bioreactors for liver support: An initial TEM study. *J Investig Surg* 2003;16:83-92.
- [119] Hager JC, Carman R, Porter LE. Neonatal hepatocyte culture on artificial capillaries: a model for drug metabolism and the artificial liver. *ASAIO Journal* 1983;6:26-35.
- [120] Aastrom Biosciences Inc. Ann Arbor, MA USA.
- [121] Limited Diagnostic Chemicals. Prince Edward Island, Canada.
- [122] Christiansen GS, Danes B, Allen L, Leinfelder PJ. A culture chamber for the continuous biochemical and morphological study of living cells in tissue culture. *Exp Cell Res* 1953;5:10-15.
- [123] Rose G. A separable and multipurpose tissue culture chamber. *Tex Rep Biol Med* 1954;12:1074-1083.
- [124] Freed JJ. Cell culture perfusion chamber: Adaptation for microscopy of clonal growth. *Science* 1963;140:1334-1335.
- [125] Katinger H. Principles of animal cell fermentation. *Dev Biol Stand* 1987;66:195-209.
- [126] GmbH. Minucells and Minutissue Vertriebs. Bad Abbach, Germany.
- [127] Synthecon Inc. Houston, TX USA.
- [128] LLC Wave Biotech. Bridgewater, NJ USA.
- [129] AG Integra Biosciences. Chur, Switzerland.
- [130] AG Sartorius. Goettingen, Germany.
- [131] Spectrum Laboratories Inc. Rancho Dominguez, CA USA.
- [132] Knazek RA, Gullino PM, Kohler PO, Dedrick RL. Cell culture on artificial capillaries: An approach to tissue growth in vitro. *Science* 1972;178:65-66.
- [133] Wolf CF, Munkelt BE. Bilirubin conjugation by an artificial liver composed of cultured cells and synthetic capillaries. *Trans Am Soc Artif Intern Organs* 1975;21:16-27.
- [134] Hager JC, Carman R, Stoller R, Panol G, Leduc EH, Thayer WR, Porter LE, Galletti PM, Calabresi P. A prototype for a hybrid artificial liver. *Trans Am Soc Artif Intern Organs* 1978;24:250-253.

- [135] Gloeckner H, Lemke HD. New miniaturized hollow-fiber bioreactor for in vivo like cell culture, cell expansion, and production of cell-derived products. *Biotechnol Prog* 2001;17:828-831.
- [136] MacDonald JM, Wolfe SP, Roy-Chowdhury I, Kubota H, Reid LM. Effect of flow configuration and membrane characteristics on membrane fouling in a novel multicoaxial hollow-fiber bioartificial liver. *Ann N Y Acad Sci* 2001;944:334-343.
- [137] Gerlach J, Encke J, Hole O, Muller C, Ryan CJ, Neuhaus P. Bioreactor for larger scale hepatocyte in vitro perfusion. *Transplantation* 1994;58:984-988.
- [138] Gerlach JC, Fuchs M, Smith MD, Bornemann R, Encke J, Neuhaus P, Riedel E. Is a clinical application of hybrid liver support systems limited by an initial disorder in cellular amino acid and alpha-keto acid metabolism, rather than by later gradual loss of primary hepatocyte function? *Transplantation* 1996;62:224-228.
- [139] Gerlach JC, Zeilinger K, Grebe A, Puhl G, Pless G, Sauer I, Grunwald A, Schnoy N, Muller C, Neuhaus P. Recovery of preservation-injured primary human hepatocytes and non-parenchymal cells to tissuelike structures in larger-scale bioreactors for liver support: An initial transmission electron microscopy study. *J Investig Surg* 2003;16:83-92.
- [140] Gerlach JC, Mutig K, Sauer IM, Schrade P, Efimova E, Mieder T, Naumann G, Grunwald A, Pless G, Mas A, Bachmann S, Neuhaus P, Zeilinger K. Use of primary human liver cells originating from discarded grafts in a bioreactor for liver support therapy and the prospects of culturing adult liver stem cells in bioreactors: A morphological study. *Transplantation* 2003;76:781-786.
- [141] Sauer IM, Zeilinger K, Obermayer N, Pless G, Grunwald A, Pascher A, Mieder T, Roth S, Goetz M, Kardassis D, Mas A, Neuhaus P, Gerlach JC. Primary human liver cells as source for modular extracorporeal liver support-- a preliminary report. *Int J Artif Organs* 2002;25:1001-1005.
- [142] Flendrig LM, IaSoe JW, Jorning GG, Steenbeek A, Karlsen OT, Bovee WM, Ladiges NC, teVelde AA, Chamuleau RA. In vitro evaluation of a novel bioreactor based on an integral oxygenator and a spirally wound nonwoven polyester matrix for hepatocyte culture as small aggregates. *J Hepatol* 1997;26:1379-1392.
- [143] Humes HD, MacKay SM, Funke AJ, Buffington DA. Tissue engineering of a bioartificial renal tubule assist device: In vitro transport and metabolic characteristics. *Kidney Int* 1999;55:2502-2514.
- [144] DeBartolog L, Jarosch-VonSchweder G, Haverich A, Bader A. A novel full-scale flat membrane bioreactor utilizing porcine hepatocytes: Cell viability and tissue-specific functions. *Biotechnol Prog* 2000;16:102-108.

- [145] Shito M, Kim NH, Baskaran H, Tilles AW, Tompkins RG, Yarmush ML, Toner M. In vitro and in vivo evaluation of albumin synthesis rate of porcine hepatocytes in a flat-plate bioreactor. *Artif Organs* 2001;25:571-578.
- [146] Bhatia SN, Yarmush ML, Toner M. Controlling cell interactions by micropatterning in co-cultures: Hepatocytes and 3T3 fibroblasts. *J Biomed Mater Res* 1997;34:189-199.
- [147] Powers MJ, Janigian DM, Wack KE, Baker CS, Stolz D Beer, Griffith LG. Functional behavior of primary rat liver cells in a three-dimensional perfused microarray bioreactor. *Tissue Eng* 2002;8:499-513.
- [148] Powers MJ, Domansky K, Kaazempur-Mofrad MR, Kalezi A, Capitano A, Upadhyaya A, Kurzawski P, Wack KE, Stolz DB, Kamm R, Griffith LG. A microfabricated array bioreactor for perfused 3D liver culture. *Biotechnol Bioeng* 2002;78:257-269.
- [149] Bancroft GN, Sikavitsas VI, Mikos AG. Design of a flow perfusion bioreactor system for bone tissue-engineering applications. *Tissue Eng* 2003;9:549-554.
- [150] Ambrosino G, Varotto S, Basso S, Galavotti D, Cecchetto A, Carraro P, Naso A, DeSilvestro G, Plebani M, Giron G, Abatangelo G, Donato D, Braga GP, Cestroni A, Marrelli L, trombetta M, Lorenzelli V, Picardi A, Valente ML, Palu G, Colantoni A, VanThiel D, Ricordi C, D'Amico DF. Alex (artificial liver for extracorporeal xenoassistance): A new bioreactor containing a porcine autologous biomatrix as hepatocyte support. Preliminary results in an ex vivo experimental model. *Int J Art Org* 2002;25:960-965.
- [151] Linti C, Zipfel A, Schenk M, Dauner M, Doser M, Viebahn R, Becker HD, Planck H. Cultivation of porcine hepatocytes in polyurethane nonwovens as part of a biohybrid liver support system. *Int J Art Org* 2002;25:994-1000.
- [152] Humes HD, Fissell WH, Weitzel WF. The bioartificial kidney in the treatment of acute renal failure. *Kidney Int Suppl* 2002;61:121-125.
- [153] Sussman NL, Chong MG, Koussayer T, He DE, Shang TA, Whisennand HH, Kelly JH. Reversal of fulminant hepatic failure using an extracorporeal liver assist device. *Hepatology* 1992;16:60-65.
- [154] Mazariegos GV, Patzer JF, Lopez RC, Giraldo M, Devera ME, Grogan TA, Zhu Y, Fulmer ML, Amiot BP, Kramer DJ. First clinical use of a novel bioartificial liver support system (BLSS). *Am J Transplant* 2002;2:260-266.
- [155] Mundt A, Puhl G, Muller A, Sauer I, Muller C, Richard R, Fotopoulou C, Doll R, Gabelein G, Hohn W, Hofbauer R, Neuhaus P, Gerlach J. *Int J Artif Organs*. A method to assess biochemical activity of liver cells during clinical application of extracorporeal hybrid liver support. 2002;25:542-548.

- [156] Irgang M, Sauer IM, Karlas A, Zeilinger K, Gerlach JC, Kurth R, Neuhaus P, Denner J. Porcine endogenous retroviruses: No infection in patients treated with a bioreactor based on porcine liver cells. *J Clin Virol* 2003;28.
- [157] Sauer IM, Zeilinger K, Pless G, Kardassis D, Theruvath T, Pascher A, Goetz M, Neuhaus P, Gerlach JC. Extracorporeal liver support based on primary human liver cells and albumin dialysis - treatment of a patient with primary graft non-function. *J Hepatol* 2003;39:649-653.
- [158] VandeKerkhove MP, DiFlorio E, Scuderi V, Mancini A, Belli A, Bracco A, Scala S, Zeuli L, DiNicuolo G, Amoroso P, Calise F, Chamuleau RA. Bridging a patient with acute liver failure to liver transplantation by the AMC-bioartificial liver. *Cell Transplant* 2003;12:563-568.
- [159] Low HP, Savarese TM, Schwartz WJ. Neural precursor cells form rudimentary tissue-like structures in a rotating-wall vessel bioreactor. *In Vitro Cell Dev Biol Anim* 2001;37:141-147.
- [160] Dutt K, Harris-Hooker S, Ellerson D, Layne D, Kumar R, Hunt R. Generation of 3D retina-like structures from a human retinal cell line in a NASA bioreactor. *Cell Transplant* 2003;12:717-731.
- [161] Wang SS, Good TA. Effect of culture in a rotating wall bioreactor on the physiology of differentiated neuron-like PC12 and SH-SY5Y cells. *Journal of Cellular Biochemistry* 2001;83:574-584.
- [162] Lelkes PI, Galvan DL, Hayman GT, Goodwin TJ, Chatman DY, Cherian S, Garcia RM, Unsworth BR. Simulated microgravity conditions enhance differentiation of cultured PC12 cells towards the neuroendocrine phenotype. *In Vitro Cell Dev Biol Anim* 1998;34:316-325.
- [163] Lin HJ, O'Shaughnessy TJ, Kelly J, Ma W. Neural stem cell differentiation in a cell-collagen-bioreactor culture system. *Develop Brain Res* 2004;153:163-173.
- [164] Sen A, Kallos MS, Behie LA. Expansion of mammalian neural stem cells in bioreactors: effect of power input and medium viscosity. *Developmental Brain Research* 2002;134:103-113.
- [165] Gerecht-Nir S, Cohen S, Itskovitz-Eldor J. Bioreactor cultivation enhances the efficiency of human embryoid body (hEB) formation and differentiation. *Biotechnol Bioeng* 2004;86.
- [166] Ahmed Z, Underwood S, Brown RA. Nerve guide material made from fibronectin: Assessment of *in vitro* properties. *Tissue Engineering* 2003;9:219-231.
- [167] Pearson RG, Molino Y, Williams PM, Tandler SJ, Davies MC, Roberts CJ, Shakesheff KM. Spatial confinement of neurite regrowth from dorsal root ganglia within nonporous microconduits. *Tissue Engineering* 2003;9:201-207.
- [168] Rutkowski GE, Heath CA. Development of a bioartificial nerve graft. II. Nerve regeneration *in vitro*. *Biotechnol. Prog.*

2002;18:373-379.

[169] Luo Y, Shoichet MS. A photolabile hydrogel for guided three-dimensional cell growth and migration. *Nature Materials* **2004**;3:249-253.

[170] Chiu DT, Jeon NL, Huang S, Kane RS, Wargo CJ, Choi IS, Ingber DE, Whitesides GM. Patterned deposition of cells and proteins onto surfaces by using three-dimensional microfluidic systems. *Proc Natl Acad Sci U S A* 2000;97:2408-2413.

[171] Peterman MC, Mehenti NZ, Bilbao KV, Leng CJ Lee

T, Noolandi J, Bent SF, MS MS Blumenkranz, Fishman HA. The Artificial Synapse Chip: a flexible retinal interface based on directed retinal cell growth and neurotransmitter stimulation. *Artif Organs* 2003;27:975-985.

[172] O'Shaughnessy TJ, Lin HJ, Ma W. Functional synapse formation among rat cortical neurons grown on three-dimensional collagen gels. *Neuroscience Letters* 2003;340:169-172.

[173] Rosoff WJ, Urbach JS, Esrick MA, McAllister RG, Richards LJ, Goodhill GJ. A new chemotaxis assay shows the extreme sensitivity of axons to molecular gradients. *Nature Neuroscience* 2004;7:678-785.

[174] Shany B, Vago R, Baranes D. Growth of primary hippocampal neuronal tissue on an aragonite crystalline biomatrix. *Tissue Engineering* 2005;11:585-596.

[175] Akins RE. Cardiac muscle tissue engineering: toward and in vitro model for electrophysiological studies. *Am J Physiol Heart Circ Physiol* 1999;277:H433-H444.

[176] Carrier RL, Papadaki M, Rupnick M, Schoen FJ, Bursac N, Langer R, Freed LE, Vunjak-Novakovic G. Cardiac tissue engineering: cell seeding, cultivation parameters, and tissue construct characterization. *Biotechnol Bioeng* 1999;64:580-589.

[177] Radisic M, Marsano A, Maidhof R, Wang Y, Vunjak-Novakovic G. Cardiac tissue engineering using perfusion bioreactor systems. *Nature Protocols* 2008;3:719-738.

[178] Papadaki M. Tissue engineering of functional cardiac muscle: molecular, structural and electrophysiological studies. *Am J Physiol Heart Circ Physiol* 2001;280:H168-H178.

[179] Zimmermann WH. Three-dimensional engineered heart tissue from neonatal rat cardiac myocytes. *Biotechnol Bioeng* 2000;68:106-114.

[180] Freed LE, Vunjak-Novakovic G, Langer R. Cultivation of cell-polymer cartilage implants in bioreactors. *J Cell Biochem* 1993;51:257-264.

[181] Freed LE, Vunjak-Novakovic G, Marquis JC, Langer R. Kinetics of chondrocyte growth in cell-polymer implants. *Biotechnol Bioeng* 1994;43:597-604.

- [182] Volkmer E, Drosse I, Otto S, Stangelmayer A, Stengele M, Kallukalam BC, Mutschler W, Schieker M. Hypoxia in static and dynamic 3D culture systems for tissue engineering of bone. *Tissue Eng Part A* 2008;14:1331-1340.
- [183] Kim BS, Putnam AJ, Kulik TJ, Mooney DJ. Optimizing seeding and culture methods to engineer smooth muscle tissue on biodegradable polymer matrices. *Biotechnol Bioeng* 1998;57:46-54.
- [184] Buono R Del, Pignatelli M, Bodmer WF, Wright NA. The role of the arginine-glycine-aspartic acid-directed cellular binding to type I collagen and rat mesenchymal cells in colorectal tumour differentiation. *Differentiation* 1991;46:97-103.
- [185] Wang R, Xu J, Juliette L, Castilleja A, Love J, Sung SY, Zhau HE, Goodwin TJ, Chung LW. Three-dimensional co-culture models to study prostate cancer growth, progression, and metastasis to bone. *Semin Cancer Biol* 2005;15:353-364.
- [186] Sakiyama SE, Schense JC, Hubbell JA. Incorporation of heparin-binding peptides into fibrin gels enhances neurite extension: an example of designer matrices in tissue engineering. *FASEB J* 1999;13:2214-2224.
- [187] Schense JC, Hubbell JA. Three-dimensional migration of neurites is mediated by adhesion site density and affinity. *Journal of Biological Chemistry* 2000;275:6813-6818.
- [188] Herbert CB, Bittner GD, Hubbell JA. Effects of fibrinolysis on neurite growth from dorsal root ganglia cultured in two- and three-dimensional fibrin gels. *J Comp Neurol* 1996;365:380-391.
- [189] Herbert CB, Nagaswami C, Bittner GD, Hubbell JA, Weisel JW. Effects of fibrin micromorphology on neurite growth from dorsal root ganglia cultured in three-dimensional fibrin gels. *J Biomed Mater Res* 1998;40:551-559.
- [190] Lin PW, Wu CC, Chen CH, Ho HO, Chen YC, Sheu MT. Characterization of cortical neuron outgrowth in two- and three-dimensional culture systems. *J Biomed Mater Res B Appl Biomater* 2005;75:146-157.
- [191] Greene LA, AS Tischler. Establishment of a noradrenergic clonal line of rat adrenal pheochromocytoma cells which respond to nerve growth factor. *Proc Natl Acad Sci U S A* 1976;73:2424-2428.
- [192] Greene LA, Aletta JM, Rukenstein A, Green SH. PC12 pheochromocytoma cells: culture, nerve growth factor treatment, and experimental exploitation. *Methods Enzymol* 1987;147:207-216.
- [193] Dichter MA, Tischler AS, Greene LA. Nerve growth factor-induced change in electrical excitability and acetylcholine sensitivity of a rat pheochromocytoma cell line. *Nature* 1977;268:501-504.

- [194] Rudy B, Kirschenbaum B, Rukenstein A, Greene LA. Nerve growth factor increases the number of functional Na channels and induces TTX-resistant Na channels in PC12 pheochromocytoma cells. *J Neurosci* 1987;7:1613-1625.
- [195] Tischler AS. Chromaffin cells as models of endocrine cells and neurons. *Ann N Y Acad Sci* 2002;971:366-370.
- [196] Gopalakrishnan SM, Teusch N, Imhof C, Bakker MH, Schurdak M, Burns DJ, Warrior U. Role of Rho kinase pathway in chondroitin sulfate proteoglycan-mediated inhibition of neurite outgrowth in PC12 cells. *J Neurosci Res* 2008;86:2214-2226.
- [197] Voegelzang M, Forster UB, Han J, Ginsberg MH, French-Constant C. Neurite outgrowth on a fibronectin isoform expressed during peripheral nerve regeneration is mediated by the interaction of paxillin with alpha4beta1 integrins. *BMC Neurosci* 2007;8:44.
- [198] Hausott B, Schlick B, Vallant N, Dorn R, Klimaschewski L. Promotion of neurite outgrowth by fibroblast growth factor receptor 1 overexpression and lysosomal inhibition of receptor degradation in pheochromocytoma cells and adult sensory neurons. *Neuroscience* 2008;153:461-473.
- [199] Radio NM, Breier JM, Shafer TJ, Mundy WR. Assessment of chemical effects on neurite outgrowth in PC12 cells using high content screening. *Toxicol Sci* 2008;105:106-118.
- [200] Crumpton T, Atkins DS, Zawia NH, Jr, Barone S. Lead exposure in pheochromocytoma (PC12) cells alters neural differentiation and Sp1 DNA-binding. *Neurotoxicology* 2001;22.
- [201] Koh HS, Yong T, Chan CK, Ramakrishna S. Enhancement of neurite outgrowth using nano-structured scaffolds coupled with laminin. *Biomaterials* 2008;29:3574-3582.
- [202] Castro F de. Chemotropic molecules: guides for axonal pathfinding and cell migration during CNS development. *News Physiol Sci*. 2003;18:130-136.
- [203] Goodhill GJ, Baier H. Axon guidance: stretching gradients to the limit. *Neural Comput* 1998;10:521-527.
- [204] Tse TH, Chan BP, Chan CM, Lam J. Mathematical modeling of guided neurite extension in an engineered conduit with multiple concentration gradients of nerve growth factor (NGF). *Ann Biomed Eng* 2007;35:1561-1572.
- [205] Jovanovic JN, Sihra TS, Nairn AC, Jr, Hemmings HC, Greengard P, Czernik AJ. Opposing changes in phosphorylation of specific sites in synapsin I during Ca²⁺-dependent glutamate release in isolated nerve terminals. *J Neurosci* 2001;21:7944-7953.
- [206] Hosaka M, Hammer RE, Sudhof TC. A phospho-switch controls the dynamic association of synapsins with synaptic vesicles. *Neuron* 1999;24:377-387.

- [207] Bloom O, Evergren E, Tomilin N, Kjaerulff O, Low P, Brodin L, Pieribone VA, Greengard P, Shupliakov O. Colocalization of synapsin and actin during synaptic vesicle recycling. *J Cell Bio* 2003;161:737-747.
- [208] Kao HT, Song HJ, Porton B, Ming GL, Hoh J, Abraham M, Czernik AJ, Pieribone VA, Poo MM, Greengard P. A protein kinase A-dependent molecular switch in synapsins regulates neurite outgrowth. *Nature Neuroscience* 2002;5:431-437.
- [209] Romano C, Nichols RA, Greengard P. Synapsin I in PC12 cells. II. Evidence for regulation by NGF of phosphorylation at a novel site. *J Neurosci* 1987;7:1300-1306.
- [210] Sudhof TC, Czernik AJ, Kao HT, Takei JK, Johnston PA, Horiuchi A, Kanazir SD, Wagner MA, Perin MS, Camilli P De, Greengard P. Synapsins: Mosaics of shared and individual domains in a family of synaptic vesicle phosphoproteins. *Science* 1989;245:1474-1480.
- [211] Hilfiker S, Benfenati F, Doussau F, Nairn AC, Czernik AJ, Augustine GJ, Greengard P. Structural domains involved in the regulation of transmitter release by synapsins. *J Neurosci* 2005;25:2658-2669.
- [212] Gitler D, Xu Y, Kao HT, Lin D, Lim S, Feng J, Greengard P, Augustine GJ. Molecular determinants of synapsin targeting to presynaptic terminals. *J Neurosci* 2004;24:3711-3720.
- [213] DeCamilli P, Cameron R, Greengard P. Synapsin I (Protein I), a nerve terminal-specific phosphoprotein. I. Its general distribution in synapses of the central and peripheral nervous system demonstrated by immunofluorescence in frozen and plastic sections. *J Cell Bio* 1983;96:1337-1354.
- [214] Romano C, Nichols RA, Greengard P, Greene LA. Synapsin I in PC12 cells. I. Characterization of the phosphoprotein and effect of chronic NGF treatment. *J Neurosci* 1987;7:1294-1299.
- [215] Lu B. Expression of synapsin I correlates with maturation of the neuromuscular synapse. *Neuroscience* 1996;74:1087-1097.
- [216] Ferreira A, Han HQ, Greengard P, Kosik KS. Suppression of synapsin II inhibits the formation and maintenance of synapses in hippocampal culture. *Proc Natl Acad Sci U S A* 1995;92:9225-9229.
- [217] Chin LS, Li L, Ferreira A, Kosik KS, Greengard P. Impairment of axonal development and of synaptogenesis in hippocampal neurons of synapsin I-deficient mice. *Proc Natl Acad Sci U S A* 1995;92:9230-9234.
- [218] Ferreira A, Kao HT, Feng J, Rapoport M, Greengard P. Synapsin III: developmental expression, subcellular localization, and role in axon formation. *J Neurosci* 2000;20:3736-3744.

- [219] Vawter MP, Thatcher L, Usen N, Hyde MTM, Kleinman JE, Freed WJ. Reduction of synapsin in the hippocampus of patients with bipolar disorder and schizophrenia. *Molecular Psychiatry* 2002;7:571-578.
- [220] Das KP, Freudenrich TM, Mundy WR. Assessment of PC12 cell differentiation and neurite growth: a comparison of morphological and neurochemical measures. *Neurotoxicol Teratol.* 2004;26:397-406.
- [221] Gerlach JC, Botsch M, Kardassis D, Lemmens P, Schon M, Janke J, Puhl G, Unger J, Kreamer M, Busse B, Bohmer C, Belal R, Ingenlath M, Kosan M, Kosan B, Sultmann J, Patzold A, Teitze S, Rossaint R, Muller C, Monch E, Sauer IM, Neuhaus P. Experimental evaluation of a cell module for hybrid liver support. *Int J Art Org* 2001;24:793-798.
- [222] Gerlach J, Neuhaus P. Culture model for primary hepatocytes. *in Vitro Cell Dev Biol* 1994;30A:640-642.
- [223] Monga SP, Hout MS, Baun MJ, Micsenyi A, Muller P, Tummalapalli L, Ranade AR, Luo JH, Strom SC, Gerlach JC. Mouse fetal liver cells in artificial capillary beds in three-dimensional four-compartment bioreactors. *Am J Pathol* 2006;167:1279-1292.
- [224] Krewson CE, Chung SW, Dai W, Saltzman MW. Cell aggregation and neurite growth in gels of extracellular matrix molecules. *Biotechnol Bioeng* 1994;43:555-562.
- [225] Cullen DK, Vukasinovic J, Glezer A, LaPlaca MC. Microfluidic engineered high cell density three-dimensional neural cultures. *J Neural Eng* 2007;4:159-172.
- [226] Dichter MA, Tischler AS, Greene LA. Nerve growth factor-induced increase in electrical excitability and acetylcholine sensitivity of a rat pheochromocytoma cell line. *Nature* 1977;268:501-504.
- [227] Fujita K, Lazarovici P, Guroff G. Regulation of the differentiation of PC12 pheochromocytoma cells. *Environ Health Perspect* 1989;80:127-142.
- [228] Eaton MJ, Duplan J. Useful cell lines derived from the adrenal medulla. *Molecular Cellular Endocrinology* 2004;228:39-52.
- [229] Foster-Barber A, Bishop JM. Src interacts with dynamin and synapsin in neuronal cells. *Proc Natl Acad Sci U S A* 1998;95:4673-4677.
- [230] Brigadski T, Hartmann M, Lessmann V. Differential vesicular targeting and time course of synaptic secretion of the mammalian neurotrophins. *J Neurosci* 2005;25:7601-7614.
- [231] Tao-Cheng JH, Dosemeci A, Bressler JP, Brightman MW, Simpson DL. Characterization of synaptic vesicles and related neuronal features in nerve growth factor and ras oncogene differentiated PC12 cells. *J Neurosci Res* 1995;42:323-334.

- [232] Hall FL, Mitchell JP, Vulliet PR. Phosphorylation of synapsin I at a novel site by proline-directed protein kinase. *J Biol Chem* 1990;265:6944-6948.
- [233] Xue JF, Liu ZJ, Hu JF, Chen H, Zhang JT, Chen NH. Ginsenoside Rb1 promotes neurotransmitter release by modulating phosphorylation of synapsins through a cAMP-dependent protein kinase pathway. *Brain Res* 2006;1106:91-98.
- [234] Reynolds BA, Weiss S. Generation of neurons and astrocytes from isolated cells of the adult mammalian central nervous system. *Science* 1992;255:1707-1710.
- [235] Reynolds BA, Tetzlaff W, Weiss S. A multipotent EGF responsive striatal embryonic progenitor cell produces neurons and astrocytes. *J Neurosci* 1992;12:4565-4574.
- [236] Shihabuddin LS, Ray J, Gage FH. FGF-2 is sufficient to isolate progenitors found in the adult mammalian spinal cord. *Exp Neurol* 1997;148:577-586.
- [237] Rietze RL, Reynolds BA. Neural stem cell isolation and characterization. *Methods Enzymol* 2006;419:3-23.
- [238] Lobo MVT, Alonso FJM, Redondo C, Lopez-Toledano MA, Caso E, Herranz AS, Paino CL, Reimers D, Bazan E. Cellular characterization of epidermal growth factor-expanded free-floating neurospheres. *J Histochem & Cytochem* 2003;51:89-103.
- [239] Doetsch F, Caille I, Lim DA, Garcia-Verdugo JM, Alvarez-Buylla A. Subventricular zone astrocytes are neural stem cells in the adult mammalian brain. *Cell Mol Neurobiol* 1999;97:703-716.
- [240] Doetsch F, Petreanu L, Caille I, Garcia-Verdugo JM, Alvarez-Buylla A. EGF converts transit-amplifying neurogenic precursors in the adult brain into multipotent stem cells. *Neuron* 2002;36:1021-1034.
- [241] Doetsch F. A niche for adult neural stem cells. *Curr Opin Genetics Development* 2003;13:543-550.
- [242] He F, Sun YE. Glial cells more than support cells? *Int J Biochem Cell Biol* 2007;39:661-665.
- [243] White RE, Jakeman LB. Don't fence me in: harnessing the beneficial roles of astrocytes for spinal cord repair. *Restor Neurol Neurosci* 2008;26:197-214.
- [244] Davies JE, Proschel C, Zhang N, Noble M, Mayer-Proschel M, Davies SJ. Transplanted astrocytes derived from BMP- or CNTF-treated glial-restricted precursors have opposite effects on recovery and allodynia after spinal cord injury. *J Biol* 2008;7:24.

- [245] Doetsch F, Garcia-Verdugo JM, Alvarez-Buylla A. Cellular composition and three-dimensional organization of the subventricular germinal zone in the adult mammalian brain. *J Neurosci* 1997;17:5046-5061.
- [246] Laywell ED, Rakic P, Kukekov VG, Holland EC, Steindler DA. 2000. Proc Natl Acad Sci U S A Identification of a multipotent astrocytic stem cell in the immature and adult mouse brain.;97:13883-13888.
- [247] Mirzadeh Z, Merkle FT, Soriano-Navarro M, Garcia-Verdugo JM, Alvarez-Buylla A. Neural stem cells confer unique pinwheel architecture to the ventricular surface in neurogenic regions of the adult brain. *Cell Stem Cell* 2008;3:265-278.
- [248] Capela A, Temple S. LeX/ssea-1 is expressed by adult mouse CNS stem cells, identifying them as non-ependymal. *Neuron* 2002;35:865-875.
- [249] Mercier F, Kitasako JT, Hatton GI. Anatomy of the brain neurogenic zones revisited: Fractones and the fibroblast/macrophage network. *J Comp Neurol* 2002;451:170-188.
- [250] Mercier F, Kitasako JT, Hatton GI. Fractones and other basal laminae in the hypothalamus. *J Comp Neurol* 2003;455:324-340.
- [251] Kerever A, Schnack J, Vellinga D, Ichikawa N, Moon C, Arikawa-Hirasawa E, Efrid JT, Mercier F. Novel extracellular matrix structures in the neural stem cell niche capture the neurogenic factor fibroblast growth factor 2 from the extracellular milieu. *Stem Cells* 2007;25:2146-2157.
- [252] Shen Q, Wang Y, Kokovay K, Lin G, Chuang SM, Goderie SK, Roysam B, Temple S. Adult SVZ stem cells lie in a vascular niche: a quantitative analysis of niche cell-cell interactions. *Cell Stem Cell* 2008;3:289-300.
- [253] Tavazoie M, Veken L Van der, Silva-Vargas V, Louissaint M, Colonna L, Zaidi B, Garcia-Verdugo JM, Doetsch F. A specialized vascular niche for adult neural stem cells. *Cell Stem Cell* 2008;3:279-288.
- [254] Saghatelian A, Chevigny A de, Schachner M, Lledo PM. Tenascin-R mediates activity-dependent recruitment of neuroblasts in the adult mouse forebrain. *Nature Neuroscience* 2004;7:347-356.
- [255] Huang W, Zhang L, Niu R, Liao H. Tenascin-R domains modulate migration of neural stem/progenitor cells in vitro. *In Vitro Cell Dev Biol Anim* 2008;Epub ahead of print.
- [256] Leone DP, Relvas JB, Campos LS, Hemmi S, Brakebusch C, Fassler R, French-Constant C, Suter U. Regulation of neural progenitor proliferation and survival by beta1 integrins. *J Cell Sci* 2005;118:2589-2599.

- [257] Lathia JD, Patton B, Eckley DM, Magnus T, Mughal MR, Sasaki T, Caldwell MA, Rao MS, Mattson MP, French-Constant C. Patterns of laminins and integrins in the embryonic ventricular zone of the CNS. *J Comp Neurol* 2007;505:630-643.
- [258] Campos LS. β 1 integrins and neural stem cells: making sense of the extracellular environment. *BioEssays* 2005;27:698-707.
- [259] Tate MC, Garcia AJ, Keselowsky BG, Schumm MA, Archer DR, LaPlaca M. Specific β 1 integrins mediate adhesion, migration, and differentiation of neural progenitors derived from the embryonic striatum. *Mol Cell Neurosci* 2004;27:22-31.
- [260] Yoshida N, Hishiyama S, Yamaguchi M, Hashiguchi M, Miyamoto Y. Decrease in expression of α 5 β 1 integrin during neuronal differentiation of cortical progenitor cells. *Exp Cell Res* 2003;287:262-271.
- [261] Yu RK, Yanagisawa M. Glycosignaling in neural stem cells: involvement of glycoconjugates in signal transduction modulating the neural stem cell fate. *J Neurochemistry* 2007;103:39-46.
- [262] Sherman LS, Back ST. A 'GAG' reflex prevents repair of the damaged CNS. *TRENDS in Neuroscience* 2007;31:44-52.
- [263] Kabos P, Matundan H, Zandian M, Bertolotto C, Robinson ML, Davy BE, Yu JS, Jr. RC Krueger. Neural precursors express multiple chondroitin sulfate proteoglycans, including the lectican family. *Biochem and Biophys Res Communications* 2004;318:955-963.
- [264] Cao QL, Howard RM, Dennison JB, Whittemore SR. Differentiation of engrafted neuronal-restricted precursor cells is inhibited in the traumatically injured spinal cord. *Experimental Neurology* 2002;177:349-359.
- [265] Ao Q, Wang AJ, Chen GQ, Wang SJ, Zuo HC, Zhang XF. Combined transplantation of neural stem cells and olfactory ensheathing cells for the repair of spinal cord injuries. *Med Hypotheses* 2007;69:123401237.
- [266] Cummings BJ, Uchida N, Tamaki SJ, Salazar DL, Hooshmand M, Summers R, Gage FH, Anderson AJ. Human neural stem cells differentiate and promote locomotor recovery in spinal cord-injured mice. *PNAS* 2005;102:14069-14074.
- [267] Ricci-Vitiani L, Casalbore P, Petrucci G, Lauretti L, Montano N, Larocca LM, Falchetti ML, Lombardi DG, Gerevini VDG, Cenciarelli C, D'Alessandris QG, Fernandez E, Maria R De, Maira G, Peschle C, Parati E, Pallini R. Influence of local environment on the differentiation of neural stem cells engrafted onto the injured spinal cord. *Neurological Research* 2006;28:488-492.

- [268] Fujiwara Y. Intravenously injected neural progenitor cells of transgenic rats can migrate to the injured spinal cord and differentiate into neurons, astrocytes, and oligodendrocytes. *Neuroscience Letters* 2004;366:287-291.
- [269] Teng YD, Lavik EB, Qu X, Park KI, Ourednik J, Zurakowski D, Langer R, Snyder EY. Functional recovery following traumatic spinal cord injury mediated by a unique polymer scaffold seeded with neural stem cells. *Proc Natl Acad Sci U S A* 2002;99:3024-3029.
- [270] Hofstetter C. Allodynia limits the usefulness of intraspinal neural stem cell grafts; directed differentiation improves outcome. *Nature Neuroscience* 2005;8:346-353.
- [271] Lu P, Jones LL, Snyder YE, Tuszynski MH. Neural stem cells constitutively secrete neurotrophic factors and promote extensive host axonal growth after spinal cord injury. *Exp Neurol* 2003;181:115-129.
- [272] Pluchino S, Quattrini A, Brambilla E, Gritti A, Salani G, Dina G, Galli R, Carro U Del, Amadio S, Bergami A, Furlan R, Comi G, Vescovi AL, Martino G. Injection of adult neurospheres induces recovery in a chronic model of multiple sclerosis. *Nature* 2003;422:688-694.
- [273] Jeong SW. Human neural stem cell transplantation promotes functional recovery in rats with experimental intracerebral hemorrhage. *Stroke* 2003;34:2258-2263.
- [274] Zhang R. Stroke transiently increases subventricular zone cell division from asymmetric to symmetric and increases neuronal differentiation in the adult rat. *J Neurosci* 2004;24:5810-5815.
- [275] Rafuse VF, Soundararajan P, Leopold C, Robertson HA. Neuroprotective properties of cultured neural progenitor cells are associated with the production of sonic hedgehog. *Neuroscience* 2005;131:899-916.
- [276] Richardson RM, Broaddus WC, Holloway KL, Fillmore HL. Grafts of adult subependymal zone neuronal progenitor cells rescue hemiparkinsonian behavioral decline. *Brain Res* 2005;1032:11-22.
- [277] Ourednik J, Ourednik V, Lynch WP, Schachner M, Snyder EY. Neural stem cells display an inherent mechanism for rescuing dysfunctional neurons. *Nature Biotechnol* 2002;20:1103-1110.
- [278] Svendsen CN. Long-term survival of human central nervous system progenitor cells transplanted into a rat model of Parkinson's disease. *Exp Neurol* 1997;148:135-146.
- [279] Reynolds BA, Weiss S. Clonal and population analyses demonstrate that an EGF-responsive mammalian embryonic CNS precursor is a stem cell. *Dev Biol* 1996;175:1-13.

- [280] Luckenbill-Edds L. Laminin and the mechanism of neuronal outgrowth. *Brain Res Rev* 1997;23:1-27.
- [281] Powell SK, Kleinman HK. Neuronal laminins and their cellular receptors. *Int J Biochem Cell Biol* 1997;29:401-414.
- [282] Martinez-Ramos C, Lainez S, Sancho F, Garcia-Esparza MA, Planells-Cases R, Garcia-Verdugo JM, Gomez-Ribelles JL, Salmeron-Sanchez M, Monleon-Pradas M, Barcia JA, Soria JM. Differentiation of postnatal neural stem cells into glia and functional neurons on laminin-coated polymeric substrates. *Tissue Eng Part A* 2008;14:1365-1375.
- [283] Ma W, Fitzgerald W, Liu QY, O'Shaughnessy TJ, Maric D, Lin HJ, Alkon DL, Barker JL. CNS stem and progenitor cell differentiation into functional neuronal circuits in three-dimensional collagen gels. *Exp Neurol* 2004;190:276-288.
- [284] Ma W, Tavakoli T, Chen S, Maric D, Liu JL, O'Shaughnessy TJ, Barker JL. Reconstruction of functional cortical-like tissues from neural stem and progenitor cells. *Tissue Eng Part A* 2008;14:1673-1686.
- [285] Nakajima M, Ishimuro T, Kato K, Ko I, Hirata I, Arima Y, Iwata H. *Biomaterials* 2007;28:1048-1060.
- [286] Prang P, Muller R, Eljaouhari A, Heckmann K, Kunz W, Weber T, Faber C, Vroemen M, Bogdahn U, Weidner N. The promotion of oriented axonal regrowth in the injured spinal cord by alginate-based anisotropic capillary hydrogels. *Biomaterials* 2006;27:3560-3569.
- [287] Wu S, Suzuki Y, Kitada M, Kitaura M, Kataoka K, Takahashi J, Ide C, Nishimura Y. *Neurosci Letters* 2001;312:173-176.
- [288] Vacanti MP, Leonard JL, Dore B, Bonassar LJ, Cao Y, Stachelek SJ, Vacanti JP, O'Connell F, Yu CS, Farwell AP, Vacanti CA. Tissue-engineered spinal cord. *Transplat Proc* 2001;33:592-598.
- [289] Little L, Healy KE, Schaffer D. Engineering biomaterials for synthetic neural stem cell microenvironments. *Chem Rev* 2008;108:1787-1796.
- [290] Hotta T. Dermal fillers. The next generation. *Plast Surg Nurs* 2004;24:14-19.
- [291] Tezel A, Fredrickson GH. The science of hyaluronic acid dermal fillers. *J Cosmet Laser Ther* 2008;10:35-42.
- [292] Baumann LS, Shamban AT, Lupo MP, Monheit GD, Thomas JA, Murphy DK, Walker PS, Group JUVEDERM vs. ZYPLAST Nasolabial Fold Study. Comparison of smooth-gel hyaluronic acid dermal fillers with cross-linked bovine collagen: a multicenter, double-masked, randomized, within-subject study. *Dermatol Surg* 2007;33:S128-S135.

- [293] Conrozier T, Chevalier X. Long-term experience with hylan GF-20 in the treatment of knee osteoarthritis. *Expert Opin Pharmacother*. 2008;9:1797-1804.
- [294] Sasaki M, Kleinman HK, Huber H, Deutzmann R, Yamada Y. Laminin, a multidomain protein. The A chain has a unique globular domain and homology with the basement membrane proteoglycan and the laminin B chains. *J Biol Chem* 1988;263:16536-16544.
- [295] Gobbel GT, Choi SJ, Niranjan S, Beier A. Long-term cultivation of multipotential neural stem cells from adult rat subependyma. *Brain Res* 2003;980:221-232.
- [296] Pluchino S. Neurosphere-derived multipotent precursors promote neuroprotection by an immunomodulatory mechanism. *Nature* 2005;436:266-271.
- [297] Guarnieri D, Battista S, Borzacchiello A, Mayol L, DeRosa E, Keene DR, Muscariello L, Barbarisi A, Netti PA. Effects of fibronectin and laminin on structural, mechanical, and transport properties of 3D collagenous network. *J Mat Sci Mat Med* 2007;18:245-253.
- [298] Kleinman HK. Preparation of basement membrane components from EHS tumors. *Current Protocols in Cell Biology* 1998;10.2.1-10.2.10.
- [299] Biederer T, Scheiffele PA. Mixed-culture assays for analyzing neuronal synapse formation. *Nature Protocols* 2007;2:670.
- [300] Li Y. Essential role of TRPC channels in the guidance of nerve growth cones by brain-derived neurotrophic factor. *Nature* 2005;434:894.
- [301] Palmer TD, Ray J, Gage FH. FGF-2 responsive neuronal progenitors reside in proliferative and quiescent regions of the adult rodent brain. *Mol Cell Neurosci* 1995;6:474-486.
- [302] Kuhn HG, Winkler J, Kempermann G. Epidermal growth factor and fibroblast growth factor-2 have different effects on neural progenitors in the adult rat brain. *J Neurosci* 1997;17:5820-5827.
- [303] Pencea V, Bingaman KD, Wiegand SH. Infusion of brain derived neurotrophic growth factor into the lateral ventricle of the adult rat leads to new neurons in the parenchyma of the striatum, septum, thalamus, and hypothalamus. *J Neurosci* 2001;21:6706-6717.
- [304] Falk A, Frisen J. Amphiregulin is a mitogen for adult neural stem cells. *J Neurosci Res* 2002;69:757-762.
- [305] Hienola A, Pekkanen M, Raulo E. HB-GAM inhibits proliferation and enhances differentiation of neural stem cells. *Mol Cell Neurosci* 2004;26:75-88.
- [306] Soen Y, Mori A, Palmer TD, Brown PO. *Mol Syst Biol* 2006;2:37.

- [307] Beck K, Hunter I, Engel J. Structure and function of laminin: Anatomy of a multidomain glycoprotein. *FASEB J* 1990;4:148-160.
- [308] Kleinman HK, McGarvey ML, Liotta LA, Robey PG, Tryggvason K, Martin GR. Isolation and characterization of type IV procollagen, laminin, and heparan sulfate proteoglycan from the EHS sarcoma. *Biochemistry* 1982;21:6188-6193.
- [309] Thonhoff JR, Lou DI, Jordan PM, Zhao X, Wu P. Compatibility of human fetal neural stem cells with hydrogel biomaterials in vitro. *Brain Res* 2008;1187:42-51.
- [310] Nakayama Y, Matsuda T. Microporous polymer surfaces prepared by an excimer laser ablation technique. *ASAIO Journal* 1994;40:M590-M593.
- [311] Tiaw KS, Goh SW, Hong M, Wang Z, Lan B, Teoh SH. Laser surface modification of poly(epsilon-caprolactone) (PCL) membrane for tissue engineering applications. *Biomaterials* 2005;26:763-769.
- [312] Mello A Prina, Bari MA, Prendergast PJ. A comparison of excimer laser etching and dry etching process for surface fabrication of biomaterials. *Journal of Materials Processing Technology* 2002;124:284-292.
- [313] Duncan AC, Weisbuch F, Rouais F, Lazare S, Baquey Ch. Laser microfabricated model surfaces for controlled cell growth. *Biosensors & Bioelectronics* 2002;17:413-426.
- [314] Iwanaga S, Akiyama Y, Kikuchi A, Yamato M, Sakai K, Okano T. Fabrication of a cell array on ultrathin hydrophilic polymer gels utilizing electron beam irradiation and UV excimer laser ablation. *Biomaterials* 2005;26:5395-5404.
- [315] Aguilar CA, Lu Y, Mao S, Chen S. Direct micro-patterning of biodegradable polymers using ultraviolet and femtosecond lasers. *Biomaterials* 2005;26:7642-7649.
- [316] Leonard JP. Determination of the absolute fluence profile in pulsed laser processing using melt-induced phase changes in an amorphous silicon thin film. *Rev Sci Instrum* 2006;77:153101.
- [317] Smith PK, Krohn RI, Hermanson GT, Mallia AK, Gartner FH, Provenzano MD, Fujimoto EK, Goeke NM, Olson BJ, Klenk DC. Measurement of protein using bicinchoninic acid. *Analytical Biochemistry* 1985;150:76-85.
- [318] Laude LD, Martinez D, Dicara CI, Hanus FR, Kolev K. The ablation of polymers under excimer laser irradiation: the physics of the process and the polymer structure. *Nuclear Instruments and Methods in Physics Research B* 2001;185:147-155.
- [319] Niino H, Nakano M, Nagano S, Yabe A. Periodic morphological modification developed on the surface of polyethersulfone by XeCl excimer laser photoablation. *Appl Phys Lett* 1989;55:510-512.

- [320] D' Couto GC, Babu SV. Heat transfer and material removal in pulsed excimer-laser-induced ablation: Pulsewidth dependence. *Journal of Applied Physics* 1994;76:3052-3058.
- [321] Martele Y, Callewaert K, Swennen I, Naessens K, Baets R, Speybroeck V Van, Waroquier M, Aaert H Van, P P Dierickx, Schacht E. Micropatterning of polyurethanes with lasers. *Polymer International* 2002;51:1172-1177.
- [322] David S, Gerra D, Nitti CD, Bussolati B, Teatini U, Longhena G, Guastoni C, Bellotti N, Combarnous F, Tetta C. Hemodiafiltration and high-flux hemodialysis with polyethersulfone membranes. *Contrib Nephrol* 2003;43-54.
- [323] Locatelli F, Filippo SD, Manzoni C. Efficiency in hemodialysis with polyethersulfone membrane (DIAPES). *J Virol Methods* 2003;109:99-101.
- [324] Huang Q, Paul D, Seibig B. Advances in solvent-free manufacturing of polymer membranes. *Desalination* 2002;14:1-3.
- [325] Vienken J, Diamantoglou M, Henne W, Nederlof B. Artificial dialysis membranes: from concept to large scale production. *Am J Nephrol* 1999;19:355-362.
- [326] Yu X, Bellamkonda RV. Tissue engineering scaffolds are effective alternatives to autografts for bridging peripheral nerve gaps. *Tissue Engineering* 2003;9.
- [327] Unger R, Huang Q, Peters K, Protzer D, Paul D, Kirkpatrick C. Growth of human cells on polyethersulfone (PES) hollow fiber membranes. *Biomaterials* 2005;26:1877-1884.
- [328] Maher MP, Dvorak-Carbone H, Pine J, Wright JA, Tai YC. Microstructures for studies of cultured neural networks. *Med Biol Eng Comput* 1999;37:110-118.
- [329] Heron PM, Sutton BM, Curinga GM, Smith GM, Snow DM. Localized gene expression of axon guidance molecules in neuronal co-cultures. *J Neurosci Methods* 2007;159:203-214.
- [330] Wavhal DS, Fisher ER. Modification of porous poly(ether sulfone) membranes by low-temperature CO₂-plasma treatment. *Journal of Polymer Science: Part B: Polymer Physics* 2002;40:2473-2488.
- [331] Pieracci J, Crivello JV, Belfort G. Increasing membrane permeability of UV-modified poly(ether sulfone) ultrafiltration membranes. *Journal of Membrane Science* 2002;202:1-16.
- [332] Heitz J, Svorcik V, Bacakova K, Ratajova E, Gumpenberger T, Bauerle D, Dvorankova B, Kahr H, Graz I, Romanin C. Cell adhesion on polytetrafluoroethylene modified by UV-irradiation in an ammonia atmosphere. *J Biomed Mater Res A* 2003;67:130-137.
- [333] Yip J, Chan K, Sin KM, Lau KS. Comprehensive study of polymer fiber surface modifications Part 1: high-fluence UV-excimer-laser-induced structures. *Polymer International* 2004;53:627-633.

- [334] Kokai F, Niino H, Yabe A. Laser ablation of polysulfone films: a laser ionization TOF mass spectrometric study. *Applied Physics A (Materials Science Processing)* 1998;A67:607-612.
- [335] Kokai F, Niino H, Yabe A. Laser ablation of polyethersulfone films: The decomposition of the chain structure and the expansion of neutral species studied by laser ionization mass spectrometry. *J Phys Chem B* 1998;102:8400-8408.
- [336] Hernandez JC, Sanchez M Salmeron, Soria JM, Ribelles JL Gomez, Pradas M Monleon. Substrate chemistry-dependent conformations of single laminin molecules on polymer surfaces are revealed by the phase signal of atomic force microscopy. *Biophys J* 2007;93:202-207.
- [337] Yamada Y, Kleinman HK. Functional domains of cell adhesion molecules. *Curr Opin Cell Biol* 1992;4:819-823.
- [338] Ruoslahti E. Fibronectin and its receptors. *Ann Rev Biochem* 1988;57:375-413.
- [339] Jucker M, Kleinman HK. Fetal rat septal cells adhere to and extend processes on basement membrane, laminin, and a synthetic peptide from the laminin A chain sequence. *J Neurosci Res* 1991;28:507-517.
- [340] Dertinger SK, Jiang X, Li Z, Murthy VN, Whitesides GM. Gradients of substrate-bound laminin orient axonal specification of neurons. *Proc Natl Acad Sci U S A* 2002;99:12542-12547.
- [341] Stabenfeldt SE, Garcia AJ, LaPlaca MC. Thermoreversible laminin-functionalized hydrogel for neural tissue engineering. *J Biomed Mater Res Part A* 2005;77A:718-725.
- [342] Braitenberg V. Brain size and number of neurons: An exercise in synthetic neuroanatomy. *J Comp Neurosci* 2000;10:71-77.